UNCLASSIFIED

AD NUMBER
ADB012018
LIMITATION CHANGES
TO: **Approved for public release; distribution is unlimited.**
FROM: **Distribution authorized to U.S. Gov't. agencies only; Test and Evaluation; APR 1976. Other requests shall be referred to Army Materials and Mechanics Research Center, Attn: AMXMR-PL, Watertown, MA 02172.**
AUTHORITY
AMMRC ltr, 8 Jun 1978

THIS PAGE IS UNCLASSIFIED

THIS REPORT HAS BEEN DELIMITED
AND CLEARED FOR PUBLIC RELEASE
UNDER DOD DIRECTIVE 5200.20 AND
NO RESTRICTIONS ARE IMPOSED UPON
ITS USE AND DISCLOSURE,

DISTRIBUTION STATEMENT A

APPROVED FOR PUBLIC RELEASE;
DISTRIBUTION UNLIMITED.

AD

①

ADB012018

AMMRC CTR 76-12

BRITTLE MATERIALS DESIGN, HIGH TEMPERATURE GAS TURBINE

Technical Report By:

Arthur F. McLean, Ford Motor Company, Dearborn, Michigan 48121
Robert R. Baker, Ford Motor Company, Dearborn, Michigan 48121
Raymond J. Bratton, Westinghouse Electric Corporation, Pittsburgh, Pennsylvania 15235
Donald G. Miller, Westinghouse Electric Corporation, Pittsburgh, Pennsylvania 15235

April, 1976

Interim Report Number 9, July 1, 1975 to December 31, 1975

Contract Number DAAG 46-71-C-0162

Sponsored by the Advanced Research Projects Agency

ARPA Order Number 1849

Project Code Number 1D10

Agency Accession Number DA OD 4733

D D C
JUL 8 1976
A

97

Distribution limited to U.S. Government agencies, only: Test and Evaluation data; April, 1976. Other requests for this document must be referred to the Director, Army Materials and Mechanics Research Center, ATTN: AMXMR-PL, Watertown, Massachusetts 02172.

Prepared for

ARMY MATERIALS AND MECHANICS RESEARCH CENTER
Watertown, Massachusetts 02172

AD No.
DDC FILE COPY

DISCLAIMER NOTICE

THIS DOCUMENT IS THE BEST QUALITY AVAILABLE.

COPY FURNISHED CONTAINED A SIGNIFICANT NUMBER OF PAGES WHICH DO NOT REPRODUCE LEGIBLY.

B010 248L

The findings in this report are not to be construed as an official Advanced Research Projects Agency, Department of the Army, or U.S. Government position, either expressed or implied, unless so designated by other authorized documents.

Mention of any trade names or manufacturers in this report shall not be construed as advertising nor as an official indorsement or approval of such products or companies by the United States Government.

DISPOSITION INSTRUCTIONS

Destroy this report when it is no longer needed. Do not return it to the originator.

(18) (19)

AMMRC CTR-76- 12

(6)

BRITTLE MATERIALS DESIGN, HIGH TEMPERATURE GAS TURBINE.

Technical Report By:

(10)
Arthur F. McLean, Ford Motor Company, Dearborn, Michigan 48121
Robert R. Baker, Ford Motor Company, Dearborn, Michigan 48121
Raymond J. Bratton, Westinghouse Electric Corporation, Pittsburgh, Pa 15235
Donald G. Miller, Westinghouse Electric Corporation, Pittsburgh, Pa 15235

(11) Apr[redacted]976 (9) Interim rept. no. 9, 1 Jul - 31 Dec 75,

Interim Report Number 9, July 1, 1975 to December 31, 1975

(15) ~~Contract Number~~ DAAG 46-71-C-0162, ARPA Order-1849

Sponsored by the Advanced Research Projects Agency

ARPA Order Number 1849 (12) 187p.

Project Code Number 1D10

Agency Accession Number DA OD 4733

Distribution limited to U.S. Government agencies only; Test Evaluation data; April, 1976. Other requests for this document must be referred to the Director, Army Materials and Mechanics Research Center, ATTN: AMXMR-PL, Watertown, Massachusetts 02172

Prepared for:

ARMY MATERIALS AND MECHANICS RESEARCH CENTER
Watertown, Massachusetts 02172

141 250

ACCESSION for
NTIS
DDC
UNANNOUNCED
JUSTIFICATION
BY
B

ABSTRACT

The demonstration of uncooled brittle materials in structural applications at 2500°F is the objective of the "Brittle Materials Design, High Temperature Gas Turbine" program. Ford Motor Company, the contractor, will utilize a small vehicular gas turbine while Westinghouse, the subcontractor, will use a large stationary gas turbine. Both companies had in-house research programs in this area prior to this contract.

A significant achievement in the vehicular turbine project was the successful engine test, 175 hours at 1930°F, of a silicon nitride stator. Durability testing on a nose cone was extended to 246 hours, equalling the previously demonstrated durability of 245 hours on 1st and 2nd stage rotor tip shrouds. A "Refel" silicon carbide combustor previously demonstrated 171 hours durability, crack-free, including 20 hours at 2500°F. Two additional combustors of the same material were tested for 10 hours each. Eight hours of testing the stationary ceramic flowpath at 2500°F were accumulated; non-catastrophic cracks occurred in the nosecone and stator after surviving three hours crack-free. Two stator vanes survived 1000 cycles to 2500-2600°F plus 3720 cycles to 2900°F in the thermal shock rig. A poor quality partially bladed duo-density silicon nitride turbine rotor was tested for two hours with excursions to 1920°F and 33,600 rpm before failure. Two ceramic rotors with short blades were successfully proof spun to 64,000 rpm, cold, as part of a program to test ceramic rotors with phased increases in blade height. One of seven hot pressed rotor hubs, spun to determine material strength, achieved 111,800 rpm before failure.

A concentrated effort on turbine rotor fabrication development was initiated. Improvements in the rotor fabrication processes have been made. Reduction of the MgO content increased the hot strength of the hot-pressed silicon nitride rotor hub material. Over 500 rotor blade rings were fabricated using the injection molding process and some high density rotor blade rings were also fabricated by slip-casting. The lower stressed Design D' rotor blade ring injection molding tooling was received and checkout initiated. Improvements in the nitriding cycle and injection molding process produced 2.7 gm/cm^3 test bars with a characteristic 4 point bend strength of 44.3 ksi with a Weibull slope of 6.8; this represents a considerable improvement over the 17,000 psi strength of 2.3 gm/cm^3 silicon nitride developed earlier in the program. A stress rupture test on 2.7 gm/cm^3 injection molded material was suspended without failure after 1159 hours at 2300-2400°F and stresses in 4 point bending of up to 35 ksi. This is a significant improvement over a previous creep test on 2.55 gm/cm^3 material when failure occurred at 35 ksi at 2300°F.

The goal of the stationary turbine project is to demonstrate ceramic stator vanes operating at a maximum temperature of 2500°F for 100 cycles simulating peaking service conditions. The original goal to accomplish this in an advanced gas turbine engine was revised to complete the demonstration in a static test rig. Sixty cycles have been completed in the static test rig with the total time at temperature (2500°F) approaching three hours and three of the original eight vanes remain crack-free. Twenty-eight tapered-twisted silicon nitride airfoils and 24 end caps of the 3rd generation (advanced turbine) design were received for the 2500°F static rig test. Physical properties of the boron nitride insulators are reported. A tensile creep test of NC-132 silicon nitride was suspended without failure after 10,000 hours at 2100°F and 10,000 psi. The effect of static oxidation in the 2000-2500°F range on the high temperature strength of NC-132 was determined. Several CVD coatings were applied to NC-132 to reduce the strength degradation observed due to oxidation; preliminary results are presented. Experimental silicon nitride billets hot-pressed with yttria showed negligible weight gains at 1800 and 2500°F in an oxidizing atmosphere for periods up to 300 hours. High purity alpha silicon nitride powder of low oxygen content can now be produced at the rate of 8-9 kg/month.

FOREWORD

This report is the ninth semi-annual technical report of the "Brittle Materials Design, High Temperature Gas Turbine" program initiated by the Advanced Research Projects Agency, ARPA Order Number 1849, and Contract Number DAAG-46-71-C-0162. This is an incrementally-funded six year program.

Since this is an iterative design and materials development program, design concepts and materials selection and/or properties presented in this report will probably not be those finally utilized. Thus all design and property data contained in the semi-annual reports must be considered tentative, and the reports should be considered to be illustrative of the design, materials, processing, and NDT techniques being developed for brittle materials.

The principal investigator of this program is Mr. A. F. McLean, Ford Motor Company, and the technical monitor is Dr. A. E. Gorum, AMMRC. The authors would like to acknowledge the valuable contributions in the performance of this work by the following people:

Ford Motor Company

N. Arnon, P. Beardmore, J. H. Buechel, D. J. Cassidy, J. C. Caverly D. A. Davis, G. C. DeBell, E. F. Dore, A. Ezis, W. A. Fate, E. A. Fisher, M. U. Goodyear, J. W. Grant, D. L. Hartsock, P. H. Havstad, R. A. Jeryan, C. F. Johnson, K. H. Kinsman, C. A. Knapp, J. G. LaFond, J. A. Mangels, W. E. Meyer, M. E. Milberg, W. M. Miller, T. G. Mohr, P. F. Nicholls, A. Paluszny, G. Peitsch, J. J. Schuldies, J. R. Secord, L. R. Swank, W. Trela, J. Uy, T. J. Whalen, R. M. Williams, W. Wu

Westinghouse Electric Corporation

C. A. Andersson, C. R. Booher, Jr., C. B. Brenneman, E. S. Diaz, F. F. Lange, G. L. Levari, W. Malchman, S. Mumford, A. Scalzo, S. C. Singhal, J. White

Army Material and Mechanics Research Center

G. E. Gazza, E. M. Lenoe, R. N. Katz, H. Priest

TABLE OF CONTENTS

Page No.

Title Page i
Abstract ii
Foreward iii
Table of Contents iv
List of Illustrations v
List of Tables xii

1. Introduction 1
2. Introduction and Summary-Vehicular Turbine Project 3
  2.1 Vehicular Turbine Project Plan 5
  2.2 Progress and Cumulative Status Summary-Vehicular Turbine Project 7
    2.2.1 Ceramic Component Development 7
    2.2.2 Materials Technology 14
  2.3 Future Plans 16
3. Progress on Ceramic Component Development-Vehicular Turbine Project 19
  3.1 Ceramic Rotor Development 19
    3.1.1 Design and Analysis 21
    3.1.2 Materials and Fabrication 29
    3.1.3 Rotor Testing 39
  3.2 Ceramic Stator, Nose Cone and Combustor Development 47
    3.2.1 Design and Analysis 48
    3.2.2 Materials and Fabrication 50
    3.2.3 Testing 52
4. Progress on Materials Technology-Vehicular Turbine Project 61
  4.1 Properties of Hot Pressed Si_3N_4 62
  4.2 Properties of Injection Molded Reaction Sintered Si_3N_4 67
  4.3 Properties of Slip Cast Reaction Sintered Si_3N_4 72
  4.4 Silicon Milling Studies 74
  4.5 Reactions of Ceramics to Leaded-Fuel Turbine Exhaust 78
  4.6 High Temperature Fracture Behavior of Ceramic Materials 95
  4.7 Non-Destructive Evaluation of Ceramic Components 100
5. Progress on the Stationary Turbine Project 103
  5.1 Stationary Turbine Project Plan 104
  5.2 Status Summary -- Stationary Turbine Project 106
    5.2.1 Component Development 107
    5.2.2 Materials Technology 111
  5.3 Future Plans 115
6. Progress on Ceramic Component Development - Stationary Turbine Project 117
  6.1 Stator Vane Development 117
    6.1.1 Static Rig Testing 118
    6.1.2 Vane Fabrication 138
7. Progress on Material Technology - Stationary Turbine Project 141
  7.1 Material Engineering Data 141
    7.1.1 Properties of Boron Nitride Insulator Material 142
    7.1.2 Long Term Tensile Creep Properties of Hot-Pressed Si_3N_4 152
  7.2 Improved Silicon Nitride Materials 153
    7.2.1 Silicon Nitride Powder 154
    7.2.2 The Si_3N_4 - Si_3N_4 - SiO_2 - $Y_2O_3 \cdot 2\ SiO_2$ System 156
  7.3 Oxidation of Hot-Pressed Silicon Nitride 159
    7.3.1 Oxidation Behavior of Experimental Si_3N_4 Hot-Pressed with Y_2O_3 and SiO_2 159
    7.3.2 Effect of Long-Term Oxidation on the Strength of Commercial Hot-Pressed Si_3N_4 161
    7.3.3 Evaluation of Chemical-Vapor-Deposited Si_3N_4 Coatings on Hot-Pressed Silicon Nitride 163
8. References 167

LIST OF ILLUSTRATIONS

		Page No.
Figure 2.1	Schematic View of the Vehicular Gas Turbine Engine Flowpath	5
Figure 2.2	ARPA/Ford Ceramic Turbine Program-Major Project and Development Loops	6
Figure 3.1	First Stage Turbine Disk Temperature (^{o}F) at 55% Speed	22
Figure 3.2	Second Stage Turbine Disk Temperatures (^{o}F) at 55% Speed	23
Figure 3.3	Maximum Principal Tensile Stresses (psi) First Stage Turbine Disk at 55% Speed	24
Figure 3.4	Maximum Principal Tensile Stresses (psi) Second Stage Turbine Disk at 55% Speed	25
Figure 3.5	Slip Casting Mold for Gear Model	29
Figure 3.6	Slip Cast Turbine Rotor Blade Ring	31
Figure 3.7	Schematic of Vacuum Addition to Rotor Tooling	31
Figure 3.8	Gating Modifications to Rotor Tooling	33
Figure 3.9	Hot Press Bonding Assembly for Simultaneous Forming and Bonding a Silicon Nitride Rotor Hub to a Blade Ring	34
Figure 3.10	Duo-Density Rotors Number 808 High Density Curvic Region and 766 Lower Density Curvic Region	35
Figure 3.11	Exaggerated Schematic of Duo-Density Rotor During Hot Press Bonding	37
Figure 3.12	Blade Bend Testing Fixture	40
Figure 3.13	Ceramic Rotor Hub Failure at 111,800 rpm	42
Figure 3.14	Duo-Density Rotor Failure at 60,290 rpm	43
Figure 3.15	Hot Spin Test Rig	44
Figure 3.16	Proposed and Actual Speed and Temperature Schedules	46
Figure 3.17	Maximum Principal Stress (At Element Centroids) vs Time for Selected Points in 1st Stator	49
Figure 3.18	Weibull Distributions of Stator Vane Failure Loads	52

LIST OF ILLUSTRATIONS

		Page No.
Figure 3.19	Combustor Test Rig	53
Figure 3.20	Thick-Wall Silicon Carbide "REFEL" Combustor	54
Figure 3.21	Thin-Wall Silicon Carbide "REFEL" Combustor	55
Figure 3.22	Silicon Nitride Stator After 175 Hours of Durability Testing	58
Figure 4.1	Mean Measured MOR vs Temperature for Several Grades of Si_3N_4	62
Figure 4.2	Elastic Moduli vs Temperature for Press-Bonded, 2% MgO Si_3N_4	64
Figure 4.3	Elastic Moduli vs Temperature for Press-Bonded, 5% MgO Si_3N_4	65
Figure 4.4	Average Coefficient of Thermal Expansion for Several Grades of Si_3N_4	66
Figure 4.5	Attritor Mill vs Ball Mill Particle Size Distribution	74
Figure 4.6	Effect of Wet Grind vs Dry Grind on Silicon From Attritor Mill (550 rpm)	75
Figure 4.7	Effect of Attritor Mill Speed on Particle Size of Silicon (30 Minute Dry Grind)	75
Figure 4.8	Effect of Attritor Milling Time on Particle Size of Silicon (300 rpm Dry)	76
Figure 4.9	Effect of Fast Silicon Removal From Attritor Mill vs Regular Removal (550 rpm Dry)	77
Figure 4.10	Scanning Electron Micrograph of Fracture Surface of Corning 9458 LAS After Exposure to Lead-Containing Exhaust Gases (210x)	79
Figure 4.11	Surface Appearance of Four Sides of Norton NC-203 Hot-Pressed SiC, Specimen 1	81
Figure 4.12	Surface Appearance of Four Sides of Norton HS-130 Hot-Pressed Si_3N_4, Specimen 2	82
Figure 4.13	Surface Appearance of Four Sides of Norton NC-132 Hot-Pressed Si_3N_4, Specimen 3	83
Figure 4.14	Four Views of Ford Reaction Sintered Si_3N_4, Specimen 4	84
Figure 4.15	Four Views of Ford Reaction Sintered Si_3N_4, Specimen 5	85

LIST OF ILLUSTRATIONS

Page No.

Figure 4.16 Four Views of Owens-Illinois C-140 LAS, Specimen 6 86

Figure 4.17 Four Views of Owens-Illinois C-140 LAS, Specimen 7 87

Figure 4.18 Surface Appearance of Four Sides of Corning 9458 LAS, Specimen 8 88

Figure 4.19 Surface Appearance of Four Sides of Corning 9458 LAS, Specimen 9 89

Figure 4.20 SEM of Upstream Surface of Sample 1 Norton NC 203 SiC (1000x) 91

Figure 4.21 SEM of Upstream Surface of Sample 2 Norton HS 130 Si N (1000x) 91

Figure 4.22 SEM of Upstream Surface of Sample 5 Ford Reaction Sintered Si_3N_4 (1000x) 91

Figure 4.23 SEM of Upstream Surface of Sample 6 O-I C-140 LAS (1000x) 91

Figure 4.24 SEM of Upstream Surface of Sample 8 Corning 9458 LAS (1000x) 92

Figure 4.25 X-Ray Diffraction Map of Polished Cross-Section of Sample 8, Corning 9458 LAS. SEM 1000x 93

Figure 4.26 X-Ray Diffraction Map of Polished Cross-Section of Sample 1 Norton NC 203 SiC. SEM 1000x 94

Figure 4.27 Optical Micrograph of a Section Through the As-Pressed Surface of REFEL SiC, Illustrating the Disposition of the Silicon Phase in Proximity to the Surface 96

Figure 4.28 Temperature Dependence of Flexural Strength of REFEL SiC. Range Over Which Subcritical Crack Growth Was Observed is Indicated 96

Figure 4.29 (a) SEM Micrograph of Crack Extension Around an Indented Surface Under Load at 1300°C. (b) Optical Micrograph of Area Indicated in (a) Illustrating the Disposition of the Silicon Phase and the Fracture Path. (c) SEM Micrograph of Area Marked in (b) 97

Figure 4.30 Temperature Dependence of Fracture Strength in Selected Yttria Containing Sialon Type of Materials 98

Figure 4.31 Temperature Dependence of the Extent of Subcritical Crack Growth in a 60% Si_3N_4 - 40% Al_2O_3 + 6% Y_2O_3 Sialon Material. Top Insets Are High Magnification Micrographs of the Fracture Utilizing Flaws Indicated by Arrow 98

LIST OF ILLUSTRATIONS

Page No.

Figure 4.32 Crack Blunting Through Microcrack Formation in a 64.4% Si_3N_4 - 35.6% Al_2O_3 + 16.1% Y_2O_3 Sialon 99

Figure 4.33 Longitudinal (V_1) and Transverse (V_t) Sonic Velocity vs Density of Silicon Nitride 101

Figure 4.34 Acoustic Impedance vs Modulus of Elasticity of Silicon Nitride 102

Figure 5.1 Plan View of 2500°F Static Test Rig 104

Figure 5.2 Stator Vane Design Iterations 106
  I. Parallel Sided Airfoil
  II. Tapered-Twisted Airfoil with Full Cavity Filling Tenons
  III. Tapered-Twisted Airfoil

Figure 5.3 Stator Vane Test Assembly with Si_3N_4 - 3 Piece Stator Vanes and LAS Insulator at the Completion of 2200°F Static Rig Tests (105 cycles) 109

Figure 5.4 Results of Initial 2500°F Static Rig Test - Abortive Combustion Failure After 5 Cycles 110

Figure 5.5 The Interactions between Material Properties and Design 111

Figure 6.1 Longitudinal View of the Ceramic Vane 2500°F Static Rig Test Article 118

Figure 6.2 Inner and Outer Boron Nitride Insulators from 2500°F Static Rig 119

Figure 6.3 Hot Pressed Silicon Nitride Stator Vanes (Norton NC 132) for 2500°F Static Rig Testing - Airfoils 3 and 6 (from left) Were Preoxided 103 hours in an Alumina Lined Muffle Furnace at 2500°F (Static Air) 120

Figure 6.4 2500°F Static Rig Test Assembly in Place Showing Aspirating Thermocouple Rakes 120

Figure 6.5 Gas Temperature Profile Under Steady State Conditions at 1400°F (Idle Temperature) 121

Figure 6.6 Gas Temperature Profile Under Steady State Conditions at 2000°F (Mid Load Temperature) 122

Figure 6.7 Gas Temperature Profile Under Steady State Conditions at 2300°F (Thermocouple Rake Temperature Limitation) 122

Figure 6.8 Extrapolated Gas Temperature Profile Under Steady State Conditions at 2500°F (Peak Load Temperature) 123

LIST OF ILLUSTRATIONS

		Page No.
Figure 6.9	Gas Temperature vs Percent Airfoil Height (Leading Edge) for Extrapolation of Peak Load Gas Temperature Profile	124
Figure 6.10	Combustor Wall Temperature Under Peak Load Conditions at 2500°F	125
Figure 6.11	Planned Stator Vane Transient Thermal Cycle For 2500°F Tests	126
Figure 6.12	Typical Transient Thermal Cycles as Recorded from Static Rig Testing at 2500°F (Cycles 1-25 and 26-60, respectively)	126
Figure 6.13	Stator Vane Test Assembly as It Appeared in the Static Rig After 25 Cycles of Testing to 2500°F	127
Figure 6.14	Typical Example of Airfoil-End Cap Edge Loading Resulting from the Shift in Outer End Cap Position (Cycles 1-25:2500°F Static Rig Test)	128
Figure 6.15	Illustration of Outer End Cap Position Shift During Static Rig Tests at 2500°F (Cycles 1-25)	128
Figure 6.16	Silicon Nitride Stator Vane Components as they Appeared After 25 Cycles of Testing in the Static Rig at 2500°F	129
Figure 6.17	Failure Indications in Silicon Nitride Stator Vane Components After 25 Cycles of Transient Testing in the Static Rig at 2500°F	130
Figure 6.18	Typical Example of Chipping at the Inner End Cap-Airfoil Tenon Interface (Cycles 1-25 Static Rig Test at 2500°F)	130
Figure 6.19	End Cap Failure (Outer 1) from 2500°F Static Rig Test (Cycles 1-25)	131
Figure 6.20	Silicon Nitride Stator Vane Components for Static-Rig Testing at 2500°F (Outer End Cap 1 Together With Airfoils 3, 5-8 Represent Replacement Hardware)	132
Figure 6.21	Silicon Nitride Stator Vanes Installed in Static Rig for Continuation of 2500°F Tests- Airfoils 3 and 6 were Preoxided for 100 hours in an Alumina Lined Muffle Furnace at 2500°F.	133
Figure 6.22	Failure Indications in Silicon Nitride Stator Vane Airfoils (Cycles 26-60 Static Rig Testing at 2500°F)	134
Figure 6.23	Trailing Edge View of Si_3N_4 Components After 2500°F Static Rig Test (Cycles 26-60) Note End Cap Alignment	134
Figure 6.24	Stator Vane Components and Insulators from Static Rig Testing at 2500°F (Cycles 26-60).	135

LIST OF ILLUSTRATIONS

		Page No.
Figure 6.25	Contact Areas on Outer Airfoil Tenons Defined Along Machine Chatter Marks	135
Figure 6.26	Ultraviolet macrographs of Vane 5 Showing Cracks as Revealed by Dye Penetrant	136
Figure 6.27	Ultraviolet Macrographs of Vane 6 (Preoxided) Showing Cracks as Revealed by Dye Penetrant	137
Figure 7.1	Specimen Orientation in Boron Nitride Insulator Materials	143
Figure 7.2	Flexural Specimen "B" Direction	143
Figure 7.3	Flexural Specimen "A" Direction	143
Figure 7.4	The Effect of Temperature on the Flexured Strength of Boron Nitride Insulator Material	145
Figure 7.5	Flexural Specimen for Stress-Strain Determinations	145
Figure 7.6	Typical Load Deflection Curve for Boron Nitride Insulator Material	146
Figure 7.7	Compression Specimen	147
Figure 7.8	Flexural Creep in Boron Nitride Insulator Material	148
Figure 7.9	Thermal Expansion and Sonic Velocity Test Specimens	148
Figure 7.10	Thermal Expansion of Boron Nitride Insulator Material Parallel to the Hot Press Direction "A" (Across Insulator)	149
Figure 7.11	Thermal Expansion of Boron Nitride Insulator Material Perpendicular to the Hot Press Direction "B" (Through the Insulator)	150
Figure 7.12	Thermal Expansion of Boron Nitride Insulator Material Perpendicular to the Hot Press Direction "B" (Repeat Determination)	150
Figure 7.13	Thermal Conductivity Specimen	151
Figure 7.14	Creep Life of Si_3N_4 (NC 132) at 2100°F	152
Figure 7.15	Particle Size Distribution In Screened Silicon Metal Powder	155
Figure 7.16	Effect of Oxidation On the Strength of Hot-Pressed Si_3N_4 - 2000°F	161

LIST OF ILLUSTRATIONS

Page No.

Figure 7.17 Effect of Static Oxidation On the Strength of Hot-Pressed Si_3N_4 - 2200°F 162

Figure 7.18 Schematic Representation of Surface Oxidation of Hot-Pressed Si_3N_4 162

Figure 7.19 CVD Si_3N_4 Coating On Hot-Pressed Si_3N_4 (Deposited by Materials Technology Corp.) 200X 164

Figure 7.20 CVD Si_3N_4 Coating On Hot-Pressed Si_3N_4 (Deposited by Westinghouse Research Laboratories) 500X 165

LIST OF TABLES

Page No.

Table 3.1 Design Constraints for Design E Duo-Density Si_3N_4 Turbines 28

Table 3.2 Slip Cast Blade Bend Test Data 41

Table 3.3 ARPA Durability Test Cycle for Ceramic Combustors 54

Table 3.4 Summary of Nose Cone Testing 56

Table 3.5 Summary of Stator Testing 56

Table 3.6 Summary of Shroud Testing 57

Table 3.7 Test History of Components at 2500°F 59

Table 4.1 Weibull Slope of Hot Pressed Silicon Nitride at Various Temperatures 63

Table 4.2 Properties of Silicon Nitride Injection Molding Compositions 68

Table 4.3 Nitriding Schedules 68

Table 4.4 Effect of Nitriding Cycle on the MOR of Injection Molded Si_3N_4 - 2.72 gm/cm^3 - 75P1 Composition 69

Table 4.5 Effect of Nitriding Cycle on the MOR of Injection Molded Si_3N_4 - 2.82 gm/cm^3 - 92GP Composition 69

Table 4.6 Oxidation Results of 2.7 gm/cm^3 Injection Molded Si_3N_4 70

Table 4.7 Stress Rupture Test of 2.7 gm/cm^3 Injection Molded Si_3N_4 71

Table 4.8 Modulus of Rupture of Slip Cast Si_3N_4 (2.82 gm/cm^3 Density) 72

Table 4.9 Strength of Slip Cast Si_3N_4 For Various Nitriding Cycles 73

Table 4.10 Oxygen and Iron Analysis of Attritor Milled Silicon 77

Table 4.11 Spiral Flow Test on Attritor Milled and 140 Hour Grind Injection Molding Compositions 77

Table 4.12 Weight Gain Data on Second Set of Test Bars 80

Table 4.13 Properties of Nitrided Rotor Shrouds 100

LIST OF TABLES

Page No.

Table 6.1 Airfoil Certification Data 139

Table 7.1 Flexure Strength of Hot-Pressed Boron Nitride "A" Direction 144

Table 7.2 Flexure Strength of Hot-Pressed Boron Nitride "B" Direction 144

Table 7.3 Elastic Modulus Measurements From Flexure Tests 146

Table 7.4 Compression Results For Hot-Pressed Boron Nitride 147

Table 7.5 Spectrochemical Analysis 154

Table 7.6 Characteristics of Experimental Hot-Pressed Discs 156

1. INTRODUCTION

As stipulated by the Advanced Research Projects Agency of the Department of Defense at the outset of this program, the major purpose is to demonstrate that brittle materials can be successfully utilized in demanding high temperature structural applications. ARPA's major program goal is to prove by a practical demonstration that efforts in ceramic design, materials, fabrication, testing and evaluation can be drawn together and developed to establish the usefulness of brittle materials for engineering applications.

The gas turbine engine, utilizing uncooled ceramic components in the hot flow path, was chosen as the vehicle for this demonstration. The progress of the gas turbine engine has been and continues to be closely related to the development of materials capable of withstanding the engine's environment at high operating temperature. Since the early days of the jet engine, new metals have been developed which have allowed a gradual increase in operating temperatures. Today's nickelchrome superalloys are in use, without cooling, at turbine inlet gas temperatures of 1800° to 1900°F. However, there is considerable incentive to further increase turbine inlet temperature in order to improve specific air and fuel consumptions. The use of ceramics in the gas turbine engine promises to make a major step in increasing turbine inlet temperature to 2500°F. Such an engine offers significant advances in efficiency, power per unit weight, cost, exhaust emissions, materials utilization and fuel utilization. Successful application of ceramics to the gas turbine would therefore not only have military significance, but would also greatly influence our national concerns of air pollution, utilization of material resources, and the energy crisis.

From the program beginning, two gas turbine engines of greatly different size were chosen for the application of ceramics. One is a small vehicular turbine of about 200 hp (contractor Ford) and the other is a large stationary turbine of about 30 MW (sub-contractor Westinghouse). One difference in philosophy between the projects is worth noting. Because the ceramic materials, fabrication processes, and designs are not fully developed, the vehicular turbine engine was designed as an experimental unit and features ease of replacement of ceramic components. Iterative developments in a component's ceramic material, process, or design can therefore be engine-evaluated fairly rapidly. This work can then parallel and augment the time-consuming efforts on material and component characterization, stress analysis, heat transfer analysis, etc. Some risk of damage to other components is present when following this approach, but this is considered out-weighed by the more rapid acquisition of actual test information. On the other hand, the stationary turbine engine is so large, so expensive to test, and contains such costly and long lead-time components which could be damaged or lost by premature failure, that very careful material and design work must be performed to minimize the possibility of expensive, time-consuming failures.

It should be noted that both the contractor and sub-contractor had in-house research programs in this area prior to initiation of this program.

Silicon nitride and silicon carbide had been selected as the primary material candidates. Preliminary design concepts were in existence and, in the case of the vehicular engine, hardware had been built and testing had been initiated.

At the out-set, the program was considered to be both highly innovative and risky. However, it showed promise of large scale financial and technological payoff as well as stimulation of the pertinent technical communities. This reporting period is in the fifth year of the program and major accomplishments have been achieved, including the first 100 hour durability demonstration of stationary ceramic hot flowpath components (a nose cone and stator, two shrouds and a spacer) in an engine completely coupled with a control system and producing power.

This is the 9th semi-annual report of progress. The format is the same as the last report, in that it is organized into two major sections. This was done because the technology is rather specifically related to the objectives of each project. In addition, the widespread interest from the turbine technology community centers on either the vehicular turbine project or the stationary turbine project. Each section will be complete in itself and will include its own introduction, to be of more help to the reader. The two sections are titled:

- Vehicular Turbine Project
- Stationary Turbine Project

2. INTRODUCTION AND SUMMARY-VEHICULAR TURBINE PROJECT

The principal objective of the Vehicular Turbine Project is to develop ceramic components and demonstrate them in a 200-HP size high temperature vehicular gas turbine engine. The entire hot flow path will comprise uncooled parts. The attainment of this objective will be demonstrated by 200 hours of operation over a representative duty cycle at turbine inlet temperatures of up to 2500°F. Successful completion of this program objective demonstrates that ceramics are viable structural engineering materials, but will also represent a significant breakthrough by removing the temperature barrier which has for so long held back more widespread use of the small gas turbine engine.

Development of the small vehicular regenerative gas turbine engine using superalloy materials has been motivated by its potentially superior characteristics when compared with the piston engine. These include:

- Continuous combustion with inherently low exhaust emissions
- Multi-fuel capability
- Simple machine - fewer moving parts
- Potentially very reliable and durable
- Low maintenance
- Smooth, vibration-free production of power
- Low oil consumption
- Good cold starting capabilities
- Rapid warm-up time

With such impressive potential, the small gas turbine engine using superalloys has been under investigation by every major on-highway and off-highway vehicle manufacturer in the world

In addition, the small gas turbine engine without exhaust heat recovery (i.e. non-regenerative) is an existing, proven type of power plant widely used for auxiliary power generation, emergency standby and continuous power for generator sets, pump and compressor drives, air supply units, industrial power plants, aircraft turboprops, helicopter engines, aircraft jet engines, marine engines, small portable power plants, total energy systems, and hydrofoil craft engines. While this variety of applications of the small gas turbine using superalloys is impressive, more widespread use of this type engine has been hampered by two major barriers, efficiency and cost. This is particularly so in the case of high volume automotive applications.

Since the gas turbine is a heat engine, efficiency is directly related to cycle temperature. In current small gas turbines, maximum temperature is limited not by combustion, which at stoichiometric fuel/air ratios could produce temperatures well in excess of 3500°F, but by the capabilities of the hot component materials.

Today, nickel-chrome superalloys are used in small gas turbines where blade cooling is impractical, and this limits maximum turbine inlet gas temperature to about 1800°F. At this temperature limit, and considering state-of-the-art component efficiencies, the potential overall efficiency of the small regenerative gas turbine is not significantly better than that of the gasoline engine and not as good as the Diesel. On the other hand a ceramic gas turbine engine operating at 2500°F will have fuel economies superior to the Diesel at significant weight savings.

The other major barrier is cost and this too is strongly related to the hot component materials. Nickel-chrome superalloys, and more significantly cobalt based superalloys which meet typical turbine engine specifications, contain strategic materials not found in this country and cost well over $5/lb.; this is excessively costly with respect to high volume applications such as trucks or automobiles. High temperature ceramics such as silicon nitride or silicon carbide, on the other hand, are made from readily available and vastly abundant raw materials and show promise of significantly reduced cost compared to superalloys, probably by at least an order of magnitude.

Thus, successful application of ceramics to the small gas turbine engine, with an associated quantum jump to 2500°F would not only offer all of the attributes listed earlier, but in addition offer superior fuel economy and less weight at competitive cost with the piston engine.

2.1 VEHICULAR TURBINE PROJECT PLAN

The vehicular turbine project is organized to design and develop an entire ceramic hot flow path for a high temperature, vehicular gas turbine engine. Figure 2.1 shows a schematic of this regenerative engine. Air is induced through an intake silencer and filter into a radial compressor, and then is compressed and ducted through one side of each of two rotary regenerators. The hot compressed air is then supplied to a combustion chamber where fuel is added and combustion takes place.

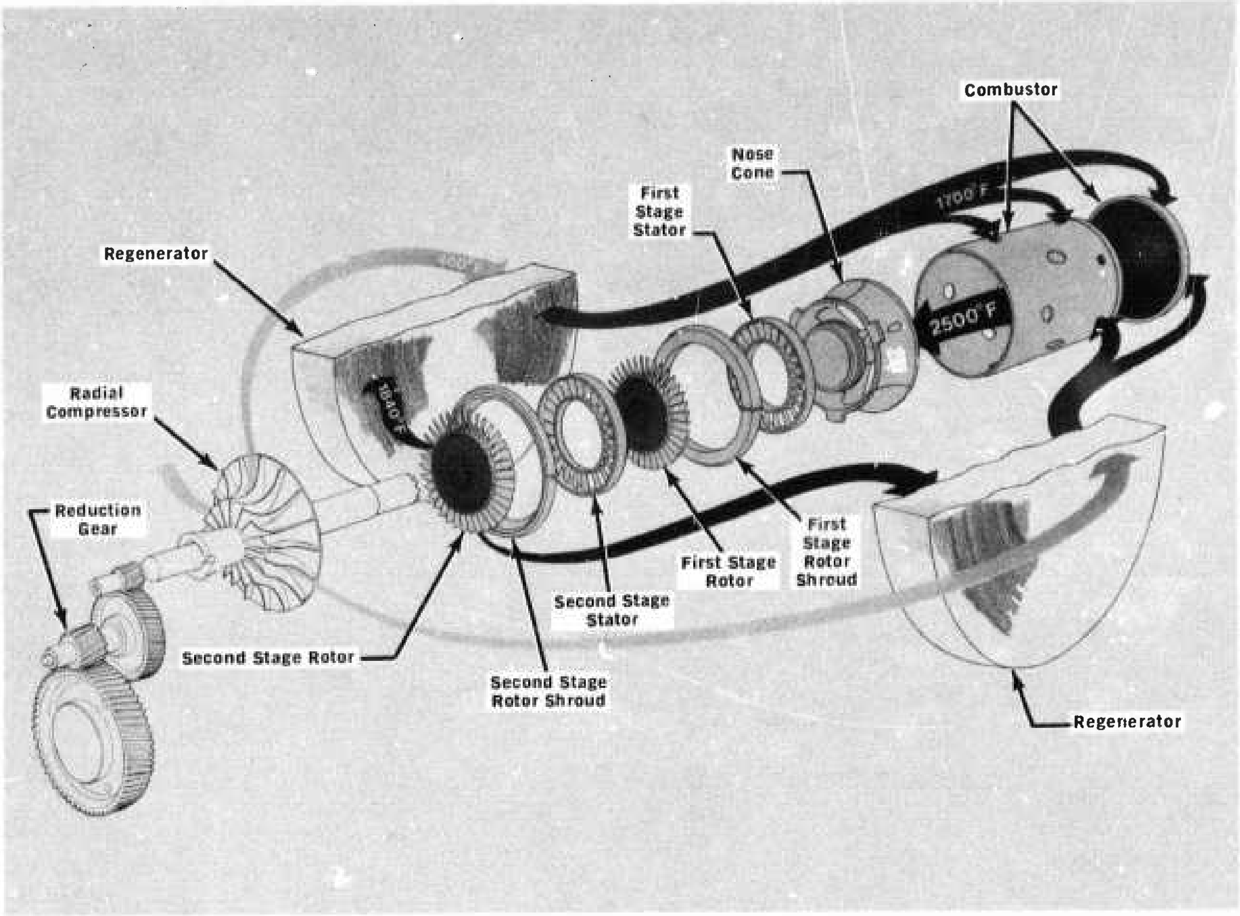
Combustor
Nose Cone
First Stage Stator
1700°F
Regenerator
2500°F
Radial Compressor
1840°F
Reduction Gear
First Stage Rotor
First Stage Rotor Shroud
Second Stage Stator
Second Stage Rotor
Second Stage Rotor Shroud
Regenerator

Figure 2.1 Schematic View of the Vehicular Gas Turbine Engine Flowpath

The hot gas discharging from the combustor is then directed into the turbine stages by a turbine inlet nose cone. The gas then passes through the turbine stages which comprise two turbine stators, each having stationary airfoil blades which direct the gas onto each corresponding turbine rotor. In passing through the turbine, the gas expands and generates work to drive the compressor and supply useful power. The expanded turbine exhaust gas is then ducted through the hot side of each of the two regenerators which, to conserve fuel, transfer much of the exhaust heat back into the compressed air. The hot flow path components, subject to peak cycle temperature and made out of superalloys in today's gas turbine, are the combustor, the turbine inlet nose cone, the turbine stators, the turbine tip shrouds, and the turbine rotors. These are areas where the use of ceramics could result in the greatest benefits, therefore these components have been selected for application in the vehicular turbine project.

Successful development of the entire ceramic flow path, as demonstrated in a high temperature vehicular gas turbine engine, will involve a complex iterative development. Figure 2.2 shows a block diagram flow chart, including the feedback loops, of the major factors involved, and serves to illustrate the magnitude of this complex and comprehensive iterative development program. Of particular importance is the inter-relationship of design, materials development, ceramic processes, component rig testing, engine testing, non-destructive evaluation and failure analysis. One cannot divorce the development of ceramic materials from processes for making parts; no more so can one isolate the design of those parts from how they are made or from what they are made. Likewise, the design of mountings and attachments between metal and ceramic parts within the engine are equally important. Innovation in the control of the environment of critical engine components is another link in the chain. Each of these factors has a relationship with the others, and to obtain success in any one may involve compromises in the others. Testing plays an important role during the iterative development since it provides a positive, objective way of evaluating the various combinations of factors involved. If successful, the test yields the credibility to move on to the next link in the development chain. If unsuccessful the test flags a warning and prompts feedback to earlier developments to seek out and solve the problem which has resulted in failure. Finally, all of the links in the chain are evaluated by a complete engine test, by which means the ultimate objective of the program will be demonstrated. It is important then to recognize that this is a systems development program--no single area is independent, but each one feeds into the total iterative system.

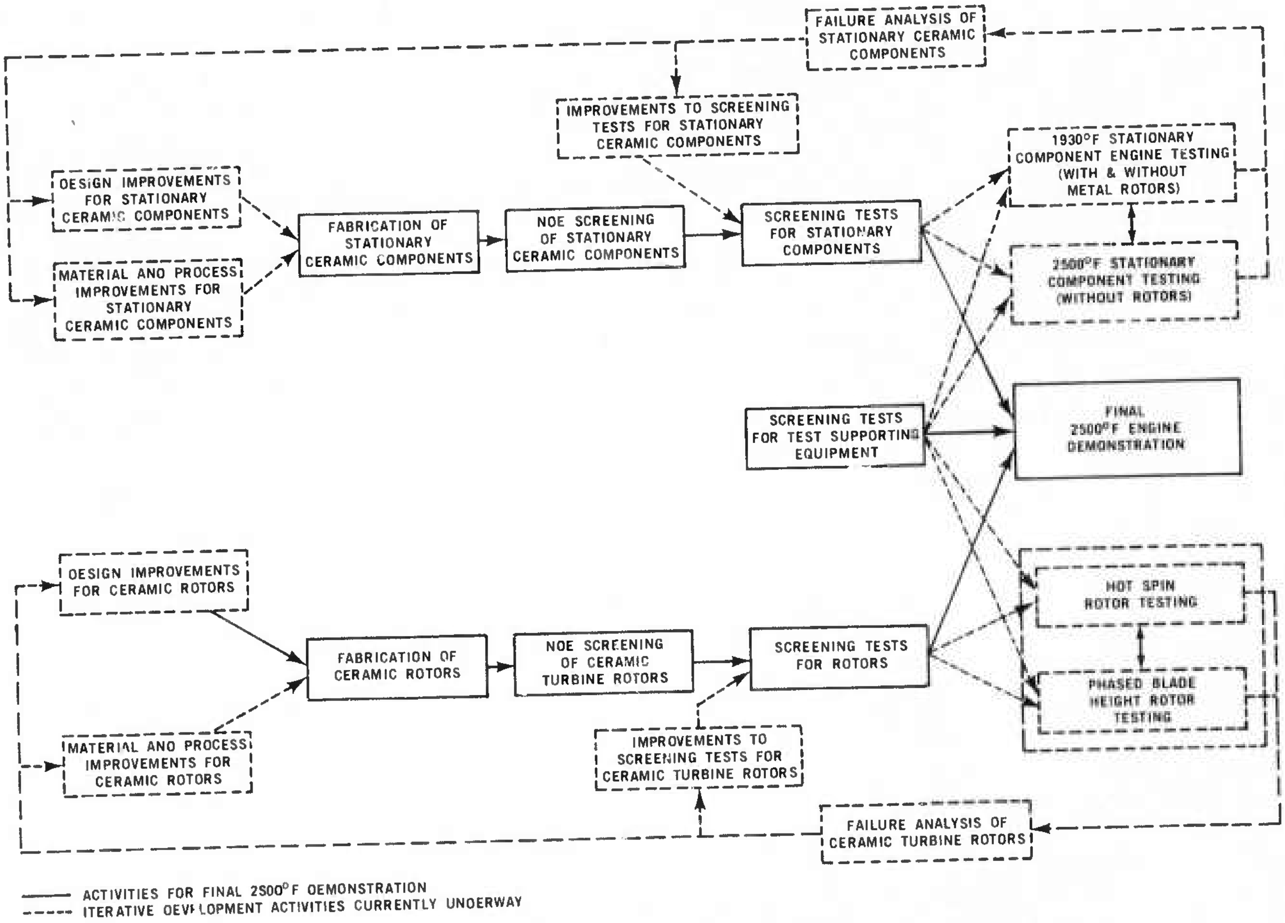
FAILURE ANALYSIS OF STATIONARY CERAMIC COMPONENTS
IMPROVEMENTS TO SCREENING TESTS FOR STATIONARY CERAMIC COMPONENTS
DESIGN IMPROVEMENTS FOR STATIONARY CERAMIC COMPONENTS
MATERIAL AND PROCESS IMPROVEMENTS FOR STATIONARY CERAMIC COMPONENTS
FABRICATION OF STATIONARY CERAMIC COMPONENTS
NDE SCREENING OF STATIONARY CERAMIC COMPONENTS
SCREENING TESTS FOR STATIONARY COMPONENTS
1930°F STATIONARY COMPONENT ENGINE TESTING (WITH & WITHOUT METAL ROTORS)
2500°F STATIONARY COMPONENT TESTING (WITHOUT ROTORS)
SCREENING TESTS FOR TEST SUPPORTING EQUIPMENT
FINAL 2500°F ENGINE DEMONSTRATION
DESIGN IMPROVEMENTS FOR CERAMIC ROTORS
MATERIAL AND PROCESS IMPROVEMENTS FOR CERAMIC ROTORS
FABRICATION OF CERAMIC ROTORS
NDE SCREENING OF CERAMIC TURBINE ROTORS
SCREENING TESTS FOR ROTORS
IMPROVEMENTS TO SCREENING TESTS FOR CERAMIC TURBINE ROTORS
HOT SPIN ROTOR TESTING
PHASED BLADE HEIGHT ROTOR TESTING
FAILURE ANALYSIS OF CERAMIC TURBINE ROTORS
ACTIVITIES FOR FINAL 2500°F DEMONSTRATION
ITERATIVE DEVELOPMENT ACTIVITIES CURRENTLY UNDERWAY

Figure 2.2 ARPA/Ford Ceramic Turbine Program-Major Project and Development Loops

2.2 PROGRESS AND CUMULATIVE STATUS SUMMARY - VEHICULAR TURBINE PROJECT

To meet the program objectives, the work has been divided into two major tasks:

1. Ceramic Component Development
2. Materials Technology

The progress and present status in each of these is summarized in Section 2.2.1 and 2.2.2.

2.2.1 CERAMIC COMPONENT DEVELOPMENT

Two categories of ceramic components are under development: rotating parts (i.e. ceramic rotors), and stationary parts (i.e. ceramic stators, rotor shrouds, nose cones, and combustors). In this iterative development, each component will pass through various phases comprising design and analysis, materials and fabrication, and testing.

Ceramic Rotors

The development of the ceramic turbine rotors is by far the most difficult task in the ARPA program. This is because of:

- the very complex shape of the turbine rotor forcing the development of new and unique fabrication capabilities.
- the high centrifugal stresses associated with maximum rotor speeds of 64,240 rpm.
- the high thermal stresses and associated thermal fatigue resulting from both steady state and transient high temperature gradients from the rotor rim to the rotor hub.
- the hostile environment associated with the products of combustion from the combustor.
- the high temperature of the uncooled blades resulting from turbine inlet gas temperatures of 2500°F.

The fabrication of flaw-free ceramic turbine rotors is a formidable task which must be accomplished before durability testing can be initiated with a reasonable chance of success. Section 2.3 (8) ("Future Plans" in the last report), indicated the necessity of emphasizing and increasing the effort on rotor materials development and rotor process development. The duo-density rotor concept is a complex fabrication process involving a multiplicity of operations and considerable time. Therefore a Turbine Rotor Task Force was established in October, 1975, to maximize the effort on duo-density Si_3N_4 turbine rotor fabrication by deferring all work on stationary ceramic component fabrication and material problems. The goal of the Task Force is to develop a repeatable process for the successful fabrication of duo-density turbine rotors which are, by best available NDT techniques, flaw free.

Note: Numbers in parentheses refer to references listed in Section 8.

Progress and Status

.Fully dense Si_3N_4 first and second stage integral rotors were designed and analyzed (1,2,3,4).

.A method of attaching rotors was conceived and designed (1,2).

.The following approaches for making integral rotors were investigated but discontinued:

-Direct hot pressing of an integral Si_3N_4 rotor (1).

-Ultrasonic machining of a rotor from a hot pressed Si_3N_4 billet (1,2,3).

-Hot pressing an assembly of individually hot pressed Si_3N_4 blades (1,2).

-Pseudo-isostatic hot pressing of an injection molded Si_3N_4 preform (1,2,3).

-Hot pressing using comformable tooling of preformed Si_3N_4 blades and hub (2,3,4).

-Fabrication of a dense SiC blade ring by chemical vapor deposition (1,2,3,4).

-Electric discharge machining of a rotor from a hot pressed SiC billet (2,3,4).

.A "duo-density" Si_3N_4 ceramic rotor was conceived and designed (3).

.Tooling to injection mold Si_3N_4 blade rings was designed and procured (3).

.Over 305 hot press bonding of duo-density rotors were carried out (9).

These have progressed from rotors with flat-sided hubs to current fully-contoured hubs made simultaneously with the hot press bonding operation. Prior severe blade ring distortion problems have been solved by using a double blade fill to support the blade ring during bonding. In addition, the diffusion bond has been improved to its current excellent quality as evidenced by microstructural examination. New experiments were conducted using magnesium nitrate instead of magnesium oxide as a densification aid. Excellent bonding and density were achieved but strength was deficient. Successful modifications were made to the graphite wedge system to reduce blade ring cracking and tearing problems. Problems which remain are occasional blade ring and rim cracking (4,5,6,7,8).

.Over 110 cold spin tests resulted in blade failures over a range of speeds, some of which exceeded full speed requirements of the new Design D' blading. However, an improvement in consistency is required if a reasonable yield from the blade ring fabrication process is to be achieved. This emphasizes the need for three-dimensional blade stress analysis as well as development of a higher strength, better quality blade material. Cold spin testing of rotor hubs of hot pressed Si_3N_4 showed a characteristic failure speed of 115,965 rpm with a Weibull rpm slope of 17.66 (7). Several hot pressed hubs, made by the hot press bonding process, were cold spun to destruction, and showed results consistent with the hot pressed hubs. A high speed motion picture study (3000 frames/sec) was conducted of a turbine rotor failure in the cold spin pit.

.A three dimensional model of the rotor blade along with heat transfer coefficients has been generated for three dimensional thermal and stress analysis (5,6,8).

.Development of better quality blade rings continues. X-ray radiography of green parts has proved effective in detecting major flaws. Slip cast Si_3N_4 test bars having a density of 2.7 gm/cm^3 show four point MOR of 40,000 psi therefore, processes to slip cast a rotor blade ring are under investigation as are methods of achieving 2.7 gm/cm^3 density with injection molded material (6,7,8).

.Thermal shock testing simulating the engine light-off condition was conducted on rotor blade rings for approximately 2,500 cycles without damage (5,6).

.A technique to evaluate probability of failure using Weibull's theories was developed and applied to ceramic rotors (5).

.A test rig was designed and built to simulate the engine for hot spin testing of ceramic rotors (3,4,5). A set of low quality duo-density rotors was spin tested to 20% speed and 1950°F for a short time before failure, believed due to an axial rub (7).

.A revised rotor design (Design D) was conceived, using common rotors at both first and second stage locations (7).

.A lower stress version of the Design D rotor, designated Design D', has been designed using radially stacked blade sections. Blade centrifugal stresses were reduced from 21,000 psi in Design D to 13,180 psi in Design D' (8).

.The rotor test rig was rebuilt and testing initiated to evaluate the rotor attachment mechanism and the curvic coupling mounting design. Hot-pressed Si_3N_4 rotor hubs were subjected to 10 operating cycles from 900 to 1950°F, during a 3-3/4 hour test, without damage (8).

.Design codes for ceramics were refined to include nonlinear thermal properties of materials and to allow for the specification of the MOR-strength and Weibull "m" requirements for a given failure at a specified loading and reliability level (9).

.Rotor hubs were successfully densified and press bonded at both 2% and 3-1/2% MgO levels, resulting in elimination of MgO migration into the blade ring and improved high temperature strength over previous pressings with 5% MgO (9).

.A Design C duo-density rotor with a few obvious flawed blades removed was cold spin tested after static oxidation at 1900°F for 200 hours. A single half-blade failure occurred at 53,710 rpm, which corrects to 68,000 rpm or 105% speed for the present shorter bladed Design D configuration. The results of a number of spin tests of slip cast Si_3N_4 blade segments were combined to yield a median failure speed of 64,000 rpm (9).

.Over five hundred blade rings were injection molded for press bonding experiments, cold spin tests, and hot tests (9).

.New tooling to injection mold lower stressed Design D' rotor blade rings was received and trial moldings to establish molding parameters were initiated (9).

.Progress has been made in several aspects of the press-bonding step of duo-density rotor fabrication. A problem of excessive deflection of the graphite support structure beneath the rotor assemlby, permitting bending and subsequent blade fracture, was solved by the substitution of high modulus hot pressed SiC for the low modulus graphite. Increasing the rate of pressure application also improved the quality of the hub sections (9).

.A new hot spin test rig, designed to improve the turn-around-time in testing turbine rotors, has been constructed, and is currently in the shakedown testing phase. Using gas burners instead of a gas turbine combustion system, this rig simulates the engine environment and was designed to be quickly rebuilt following rotor failures (9).

.In the program to engine evaluate ceramic rotors having reduced blade length (and less risk of catastrophic failure), two duo-density Si_3N_4 rotors with the blades shortened to 10% of the design length have been selected and cold spun to 64,000 rpm (9).

.The aerodynamic design of the increased efficiency Design E turbine was initiated. Flowpath optimization, a one dimensional stress analysis, and preliminary detailed blade section definition were completed for both the first and second stage turbine stators and rotors (9).

.A process has been developed to slip cast turbine rotor blade rings (9).

Ceramic Stators, Rotor Shrouds, Nose Cones, and Combustors

While development of the ceramic turbine rotor is the most difficult task, development of the stationary ceramic flow path components is also necessary to meet the objective of running an uncooled 2500°F vehicular turbine engine. In addition, success in designing, making, and testing these ceramic components will have an important impact on the many current applications of the small gas turbine where stationary ceramics alone can be extremely beneficial. The progress and status of these developments is summarized below, taking each component in turn.

Progress and Status

CERAMIC STATORS

.Early Design A first stage stators incorporating the turbine tip shrouds had been designed, made by assembling individual injection molded Si_3N_4 vanes, and tested, revealing short time thermal stress vane failures at the vane root (1).

.Investigations of a number of modified designs led to Design B where the rotor shroud was separated from the stator. Short time thermal stress vane failures at the vane root were eliminated (1).

.In the fabrication of stators, the starting silicon powder, the molding mixture and the nitriding cycle were optimized for 2.2 gm/cm^3 density (18 ksi-MOR) material (2,3).

.Engine and thermal shock testing of first stage Design B stators revealed a longer term vane cracking problem at the vane mid-span. This led to modification of the vane cord, designated the Design C configuration, which solved the vane mid-span cracking problem.

.A remaining problem in first and second stage Design B stators was cracking of outer shrouds, believed due to the notch effect between adjacent vanes. To solve this, tooling for a one-piece first stage Design C stator was procured (4,5).

.The Design B second stage stator could not be made in one piece due to vane overlap, so an "inverted channel" design was investigated to eliminate notches at the stator outside diameter. However, engine testing showed that axial cracking of the outer shroud remained a problem (3,4,5,6).

.A 50 hour duty-cycle engine test of the hot flow path components to 1930°F was completed. The assembled first stage Design C stator was in excellent condition, some vanes in the second stage inverted channel stator had developed fine cracks (6).

.A 100 hour duty-cycle engine test of the hot flow path components (without a second stage stator) to 1930°F was completed. The one piece first stage Design C stator successfully survived this test (7).

.Improvements in materials and processing resulted in the fabrication of flaw free one piece stators of 2.55 gm/cm^3 density (8).

.A test was devised for mechanically loading stator vanes to failure which provided useful information for material and process development (8).

.Thermal shock testing of 2.7 gm/cm^3 density stator vanes revealed no detectable cracking and negligible strength degradation after 9000 cycles of heating to 2700°F and cooling in the thermal shock rig (8).

.Processing of 2.55 gm/cm^3 density injection molded stators continued. Consistently high weight gains (61-62%) have been obtained using the Brew all-metal furnace employing a slow, gradual rate-of-rise cycle, 4% H_2- 96% N_2 gas under static pressure, and Si_3N_4 setters and muffles (9).

.An injection molded stator of 2.55 gm/cm^3 density Si_3N_4 survived static testing (no rotors) for 175 hours at 1930°F steady state. Weight gain of the stator was less than 1%, which stabilized after 10 hours of testing. The stator is in excellent condition (9).

.Testing of stators up to 2500°F in the Flow Path Qualification Test Rig was initiated with over eight hours of testing accumulated at 2500°F (9).

CERAMIC ROTOR SHROUDS

.Separate first and second stage ceramic rotor shrouds, which are essentially split rings, evolved in the stator change from Design A to Design B (1).

.As a result of rig and engine testing, rotor shrouds made of cold pressed, reaction sintered Si_3N_4 were modified to have flat rather than conical side faces (2).

.Because of occasional cracking, cold pressing was replaced with slip casting for making higher density rotor shrouds, resulting in 2-3 times increase in strength (3).

.Slip casting of rotor shrouds solved the cracking problem but revealed a dimensional change problem as a function of operating time. This was solved by incorporation of nitriding aids and heat treatment cycles and other changes in the fabrication process which reduced instability to acceptable levels (4,5,6).

.A 50 hour duty cycle engine test of the hot flow path components to 1930°F was completed, after which both first and second stage rotor shrouds were in excellent condition (6).

.A 100 hour duty-cycle engine test of the hot flow path components to 1930°F was completed, after which both first and second stage rotor shrouds were in excellent condition (7).

.Further testing of rotor shrouds to 245 hours and over 100 lights showed them to remain crack free and in excellent condition (7).

CERAMIC NOSE CONES (with integral transition duct)

.Early Design A nose cones had been designed, made from injection molded reaction sintered Si_3N_4, and tested (1).

.The nose cone was modified to Design B to accommodate the Design B first Stage stator. Several Design B nose cones were made and tested in rigs and engines (2).

.Voids in molding nose cones were minimized by preferentially heating the tooling during molding (5).

.Circumferential cracking and axial cracking problems led to preslotted, scalloped nose cones designated Design C (3,4,5,6).

.A 50 hour duty-cycle engine test of the hot flow path components to 1930°F was completed, after which the Design C nose cone was in excellent condition (7).

.A 100 hour duty-cycle engine test of the hot flow path components to 1930°F was completed, after which the Design C nose cone was in excellent condition (7).

.Further such testing of the nose cone to 221 hours showed it to remain crack free and in excellent condition (7).

.Improvements in materials and processing resulted in the fabrication of flaw free nose cones of 2.55 gm/cm^3 density (8).

.Processing of 2.55 gm/cm^3 density injection molded nose cones continued. Consistently high weight gains (61-62%) have been obtained using the Brew all-metal furnace employing a slow, gradual rate-of-rise cycle, 4% H - 96% N gas under static pressure and Si_3N_4 setters and muffles (9).

.Testing of nose cones up to 2500°F in the Flow Path Qualification Test Rig was initiated with over eight hours of testing accumulated at 2500°F (9).

CERAMIC COMBUSTOR

.Combustor tubes made of slip cast Si_3N_4 and various grades of recrystallized SiC (Crystar) cracked during light off tests in the combustor rig (4).

.A combustor tube made of reaction sintered SiC (REFEL) seccessfully survived 171 hours of rig testing simulating the engine duty cycle with 20 hours at 2500°F combustor outlet temperature (7). This combustor was also successfully tested in an engine (8).

.Two additional "REFEL" silicon carbide combustors were successfully qualified over a 10 hour portion of the ARPA durability cycle (9).

2.2.2 MATERIALS TECHNOLOGY

Materials technology forms the basis for component development including component design, component fabrication, material quality in the component as-made, and evaluation by testing. There are three major categories under materials technology---materials engineering data, materials science, and non-destructive evaluation. Progress and present status in each of these areas is summarized below:

Materials Engineering Data

.Techniques were developed and applied for correlating the strength of simple ceramic disks with bend test specimens using Weibull probability theories (5).

.Elastic property data as a function of temperature was determined for various grades of silicon nitride and silicon carbide (2,3,4,5,6,7,9).

.The flexural strength vs temperature of several grades of SiC and Si_3N_4 was determined (3,4,5,6,9).

.The compressive strength vs temperature of hot pressed SiC and hot pressed Si_3N_4 was determined (4).

.Creep in bending at several conditions of stress and temperature was determined for various grades of reaction sintered silicon nitride (4,5,6,9).

.The specific heat vs temperature of 2.23 gm/cm^3 reaction sintered Si_3N_4 was measured, as were thermal conductivity and thermal diffusivity vs temperature for both 2.23 gm/cm^3 and 2.68 gm/cm^3 reaction sintered Si_3N_4 (4).

.Stress-rupture data was obtained for reaction sintered silicon nitride under several conditions of load and temperature (6,9).

.A group of 31 2.7 gm/cm^3 density injection molded Si_3N_4 test bars, made using the best current nitriding cycle and an atmosphere of 4% H_2, 96% N_2, resulted in a Weibull characteristic strength of 44.3 ksi and an m value of 6.8. Additional material development work is aimed at obtaining a higher m value (9).

Materials Science

.A technique was developed and applied to perform quantitative x-ray diffraction analyses of the phases in silicon nitride (2).

.An etching technique was developed and used for the study of the microstructure of several types of reaction sintered Si_3N_4 (2).

.The relationship of some processing parameters upon the properties of reaction sintered Si_3N_4 were evaluated (3,4,5,6).

.The oxidation behavior of 2.2 gm/cm^3 density Si_3N_4 was determined at several different temperatures. The effect of oxidation was found to be reduced when the density of reaction sintered Si_3N_4 increased (3,7).

.The relationship of impurities to strength and creep of reaction sintered silicon nitride was studied, and material was developed having considerably improved creep resistance (4,5,6,9).

- Fractography and slow crack growth studies were performed on reaction sintered SiC (5) and hot pressed Si_3N_4 (6,7).

- The development of sintered Sialon-type materials was initiated (7). The effects of Yttria additives are being studied especially as it relates to the formation of glassy phases (8).

- A higher density (2.72 gm/cm^3) molded Si_3N_4 has been developed which will be used for component fabrication. Four point bend strengths of 43 ksi at room temperature were measured (8).

- An experimental study showed that high pressures did not facilitate nitriding of relatively dense silicon compacts. A parallel theoretical study showed that to store sufficient nitrogen within the pores and avoid diffusion an impractically high pressure would be needed (8).

- Three techniques to improve the oxidation resistance of 2.7 gm/cm^3 injection molded Si_3N_4 were evaluated (9).

Non-Destructive Evaluation

- Ultrasonic C-scan techniques were developed and applied for the measurement of internal flaws in turbine ceramics (1,2,3,4).

- Sonic velocity measurements were utilized as a means of quality determination of hot pressed Si_3N_4 (2,3,5,9).

- A computer-aided-ultrasonic system was used to enhance the sensitivity of defect analysis in hot pressed Si_3N_4 (3,4,6).

- Acoustic emission was applied for the detection of crack propagation and the onset of catastrophic failure in ceramic materials (1,2,5,6).

- A method was developed and applied for the detection of small surface cracks in hot pressed Si_3N_4 combining laser scanning with acoustic emission (4).

- X-ray radiography was applied for the detection of internal defects in turbine ceramics (2,3,4,5).

- Hidden flaws in as-molded stators and rotor blade rings were located by x-ray radiography (5,6,7). Such NDE of as-molded parts has been used to develop processes to make flaw free components (8).

- A dye penetrant has been used to detect surface cracks in components made of the 2.55 gm/cm^3 Si_3N_4 (8).

- A state-of-the-art summary of NDE methods as applied to the ceramic turbine programs was compiled (6).

2.3 FUTURE PLANS

Considerable progress has been made on developing ceramics for high temperature applications in the small vehicular gas turbine engine. However, difficult problems must be overcome before achieving the successful demonstration of stationary flow path components and ceramic turbine rotors. The development of the process to fabricate flaw free turbine rotors encountered many problems, necessitating the establishment of the Turbine Rotor Task Force mentioned in Section 2.2.1. When flaw free rotors can be made consistently, the fabrication development of the stationary components will resume.

Component Development

The Turbine Rotor Fabrication Task Force will represent the major effort of the vehicular turbine project with the goal of developing a successful and repeatable fabrication process to make duo-density Si_3N_4 turbine rotors. Part of this effort will be devoted towards simplifying the turbine rotor fabrication process. Fabrication development of injection molded blade rings, aimed at increasing the yield of acceptable parts, will continue. Back-up injection molding tooling, to supplement existing tooling to make Design D' rotor blade rings, will be delivered in the first quarter of 1976. Hot-press bonding experiments will continue to concentrate on densifying the hub without producing flaws in the blade ring.

Evaluation and improvement of the hot-press bonded rotor hub and blade ring materials will be carried out in order to update the reliability analysis of the rotors utilizing the latest 3-D probabilistic design codes. This evaluation is also a valuable part of the feedback to the blade ring and hot-press fabrication processes.

Test rigs to evaluate ceramic rotors are being developed. Cold spinning, static thermal stress testing, and hot spin testing will all form a part of the proof testing sequence employed to screen candidate rotors prior to testing in the turbine rotor test rig. The final engine configuration will be checked out by using duo-density rotors of reduced blade length which will use the same turbine rotor mounting system and surrounding stationary components as will be needed for full bladed ceramic rotors.

Durability development of the stationary flow path components at up to 2500°F will continue on a limited basis until the termination of the Turbine Rotor Task Force. when the fabrication of stationary components will resume.

Material Technology

Work is continuing to improve the room temperature strength, the high temperature strength, and the Weibull "m" value of hot-pressed Si_3N_4 used for duo-density rotor hubs. Principal approaches include the use of high purity Si_3N_4 starting powders plus improvements in powder processing and handling to remove large particles and contaminants.

Feedback from engine and rig testing of stationary components made from reaction sintered Si_3N_4 indicates that improved durability could be expected if improvements in strength and oxidation resistance could be obtained. Therefore, increased emphasis will be placed on the development of improved oxidation resistance of 2.7 gm/cm^3 reaction sintered material. Another area receiving major emphasis will be processing improvements aimed at increasing the yield of acceptable parts and reducing the risk of testing unacceptable parts in both molded and slip cast reaction sintered Si_3N_4. Integral with this effort will be the application and continued development of non-destructive evaluation techniques to assist in the elimination of flaws, in particular, those flaws which are found by testing to have a critical effect upon component life.

3. PROGRESS ON CERAMIC COMPONENT DEVELOPMENT-VEHICULAR TURBINE PROJECT

3.1 DUO-DENSITY CERAMIC ROTOR DEVELOPMENT

SUMMARY

During this report period, mechanical analysis of Design D' rotor configuration continued. At 55% speed condition, the effective heat transfer coefficients were calculated at the rim of the disk, and radiant heat transfer to the cooled mounting bolt was included in the analysis. Plots of the isotherms and maximum principal tensile stresses were prepared.

Using relations derived in the preceeding report(8) for determination of statistical strength, analytical techniques were developed for prediction of strength requirements of specific elements within a structure. This technique allows for trade-off compromises in elemental strength to be assessed without necessarily changing the total structure reliability.

Design of an improved efficiency, low stress, ceramic turbine was initiated. Designated Design E, the design is based upon material and fabrication criteria considered achievable by the end of the vehicular turbine project. Optimization of the flowpath to achieve maximum aerodynamic efficiency, within the constraints imposed, has been completed. Detail design of individual blade sections of rotors and stators is in process.

A slip-casting mold system was developed utilizing a non-porous removable organic material for the mold which is positioned on a plaster base which extracts the water. The consolidated casting is immersed in toluene for removal of the mold.

Injection molding of rotor blade rings continued with substantial quantities of sound moldings made from 2.55 and 2.7 gm/cm^3 Si_3N_4 material. The injection molding die was reworked to allow evacuation of the die cavity to improve material flow, and shorten the cycle time. Parametric studies established optimum molding parameters.

Development of the fabrication process for duo-density rotors continued with refinement of the graphite wedge hot pressing system to eliminate cracking of the rim and blades during hot-press bonding. The MgO content in the Si_3N_4 powder was reduced from 5 w/o to 2 w/o to improve material hot strength and reduce MgO migration into the blade ring rim. It was necessary to increase hot pressing pressure for adequate densification to 4000 psi. In addition, it was discovered that the low elastic modulus of ATJ graphite, used as the support base under the turbine rotor, was deforming during press-bonding and contributing to blade ring damage. Substitution of hot-pressed SiC for the support base produced improved rotor quality.

Thermal shock tests were conducted on blades from three duo-density turbine rotors which showed no erosion degradation in 1324 cycles. A blade bend test fixture was designed and developed to obtain information on blade strength. Agreement was excellent between stresses predicted by a three-dimensional finite-element stress analysis and stresses measured in a strain gauged test blade.

PRECEDING PAGE BLANK NOT FILMED

Cold spin test evaluation of turbine rotors and components continued. Seven press bonded rotors were tested at speeds up to 64,240 rpm. Seven hot pressed rotor hubs were spun to determine material strength and failures occurred from 64,370 to 111,800 rpm. Sixty blade rings or blade ring segments were spun in the program to develop an adequate epoxy cement for attachment of blade rings to ceramic spin arbors. An epoxy capable of over 60,000 rpm was demonstrated.

A test rig was designed and built to test the bore of a fabricated turbine rotor by application of heat to the blade area of a stationary turbine rotor while flowing cooling air through the bore. This produces a thermal stress in the hub with a maximum value at the bore. Development of this test rig will continue.

A simpler hot spin test rig has been designed, built, and installed in the test cell. The purpose of this test rig is to provide for relatively quick turn-around after a turbine rotor failure. Initial shakedown testing has commenced.

A hot spin test of a non-fully-bladed rotor resulted in failure after two hours of testing with excursions to 1920°F and 33,600 rpm. This led to revisions of the turbine rotor test rig. A planned engine test of ceramic rotors with 10% blade height was delayed due to balancing problems; these have been resolved and testing of rotors in a complete engine is expected in the next reporting period.

3.1.1 DESIGN AND ANALYSIS

Introduction

The D' duo-density Si_3N_4 rotor configuration(8) was analyzed with the calculation of temperature and stress distributions at the 55% speed point. A probabilistic approach to the determination of statistical strength requirements was developed and computerized. Salient features of the analysis are discussed and its use demonstrated on a ceramic turbine rotor. Increased efficiency turbines, designated Design E, are being optimized for aerodynamic efficiency consistent with design constraints associated with a small ceramic axial turbine.

Mechanical Analysis

The Design D' rotor configuration, described in Reference 8, was analyzed at the 55% speed condition using a 2-D axisymmetric finite element analysis. The effective heat transfer coefficients at the rim of the disk were calculated from a 3-D thermal analysis (TAP) of the blade. The radiant heat flow from the bore of the disk to the cooled mounting bolt was also included. This additional heat loss was shown(8) to increase the temperature gradient within the rotor disk, and therefore, it was deemed necessary to include it in any future calculations.

The results of the analysis are shown in Figures 3.1 through 3.4. Figures 3.1 and 3.2 are plots of the isotherms for the first and second turbine stages respectively and Figures 3.3 and 3.4 are the contour plots of the corresponding maximum principal tensile stresses. In comparison to the 100% power point(8) both the temperature levels and the stress magnitudes are considerably reduced. Consequently, since the majority of the ARPA duty cycle involves reduced power operation, (lower temperature and speeds), the susceptibility of the rotors to time-dependent failure modes is also reduced.

Strength and Reliability Considerations

Reference 5 showed the application of Weibull's weakest link model and his uniaxial treatment of brittle strength of the ceramic materials used in this program. The governing relations of Weibull analysis and the analytical methods were discussed and the computation of component reliability as a function of statistical material parameters was demonstrated on turbine rotor structures.

In the last report(8), the basic relations were derived for the determination of statistical strength requirements. Using the turbine blade as an example, it was shown that, given a desired survival probability for a component or its element in question, the required strength level and associated allowable variability (slope 'm') can be specified on the basis of Weibull strength analysis. By so defining the strength requirements at the element level, i.e., as function of location in the structure, this type of information can be useful for fabrication development as it will identify the areas within the structure where compromises in strength would be permissible without jeopardizing the overall reliability of the total structure.

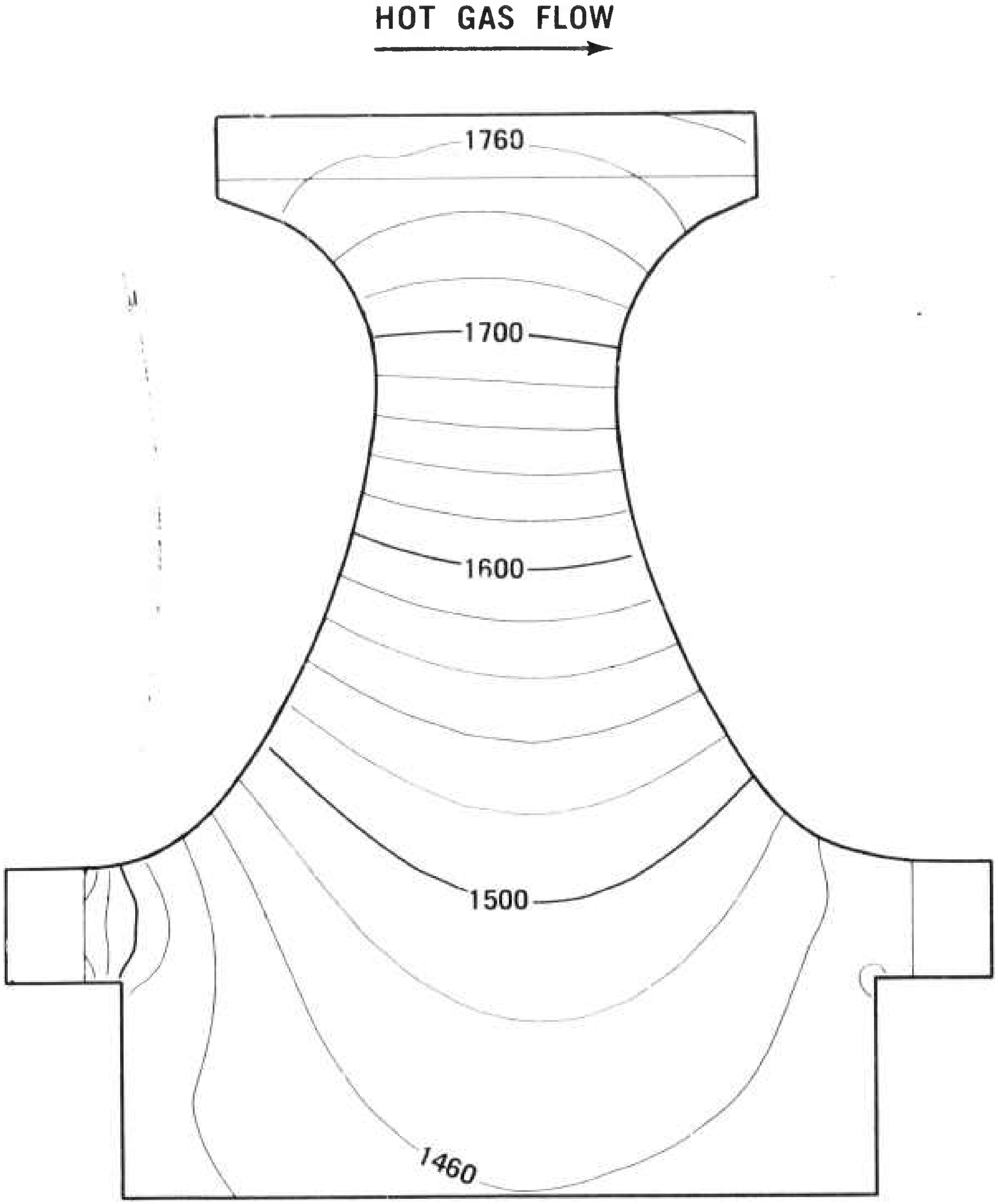
HOT GAS FLOW
1760
1700
1600
1500
1460

Figure 3.1 First Stage Turbine Disk Temperature (°F) at 55% Speed

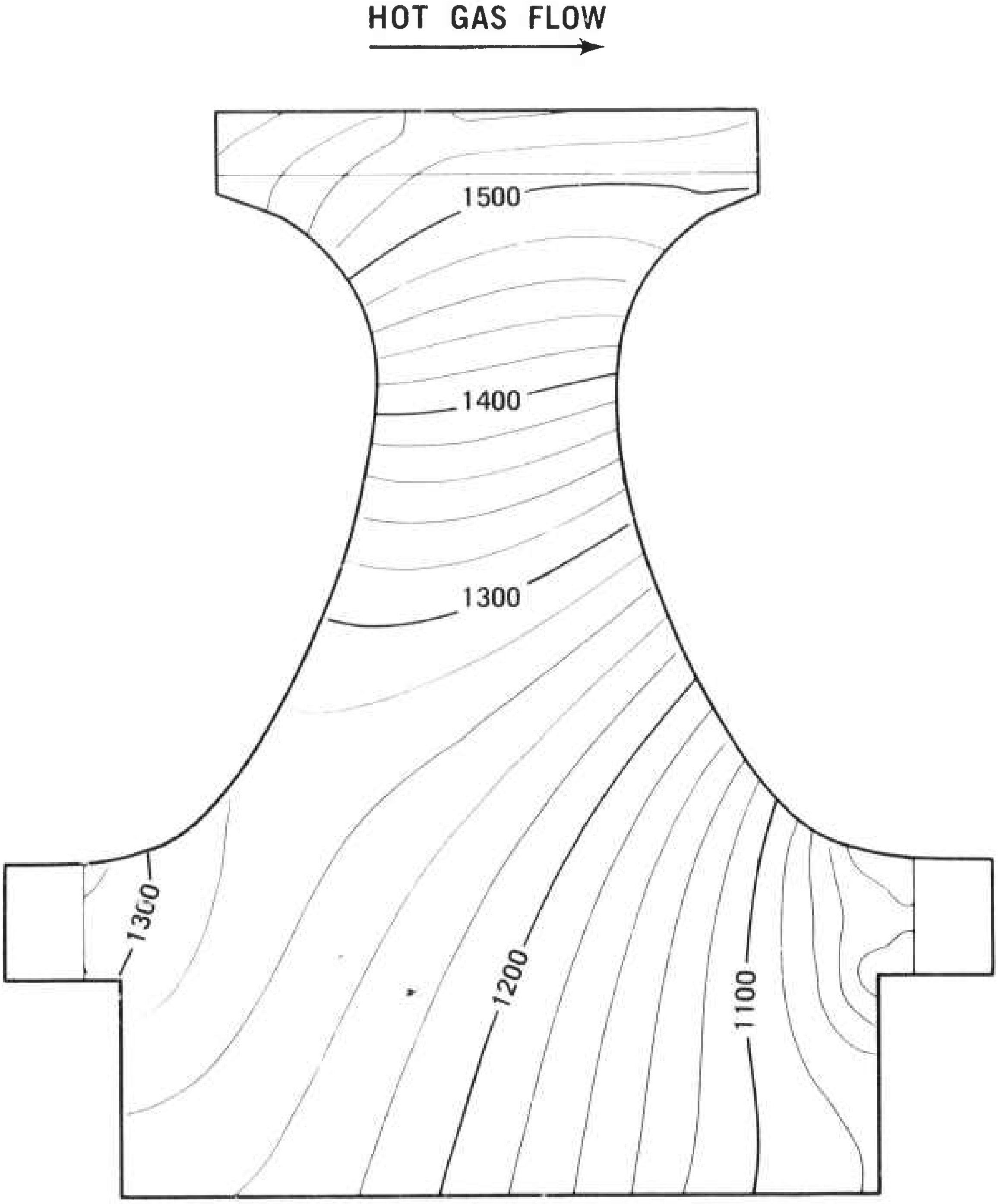
HOT GAS FLOW
1500
1400
1300
1300
1200
1100

Figure 3.2 Second Stage Turbine Disk Temperatures ($^{\circ}$F) at 55% Speed

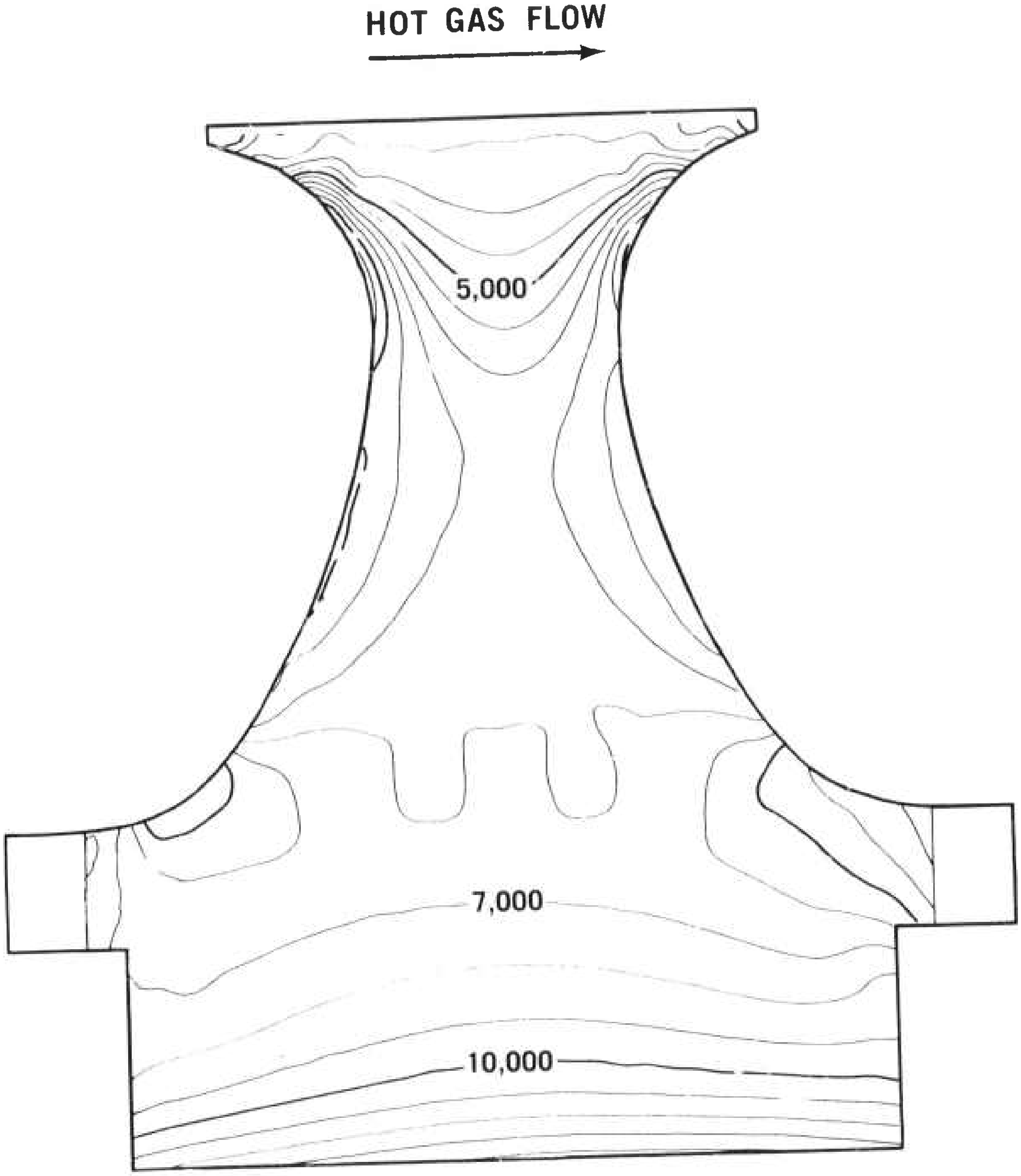
HOT GAS FLOW
5,000
7,000
10,000

Figure 3.3 Maximum Principal Tensile Stresses (psi) First Stage Turbine Disk at 55% Speed

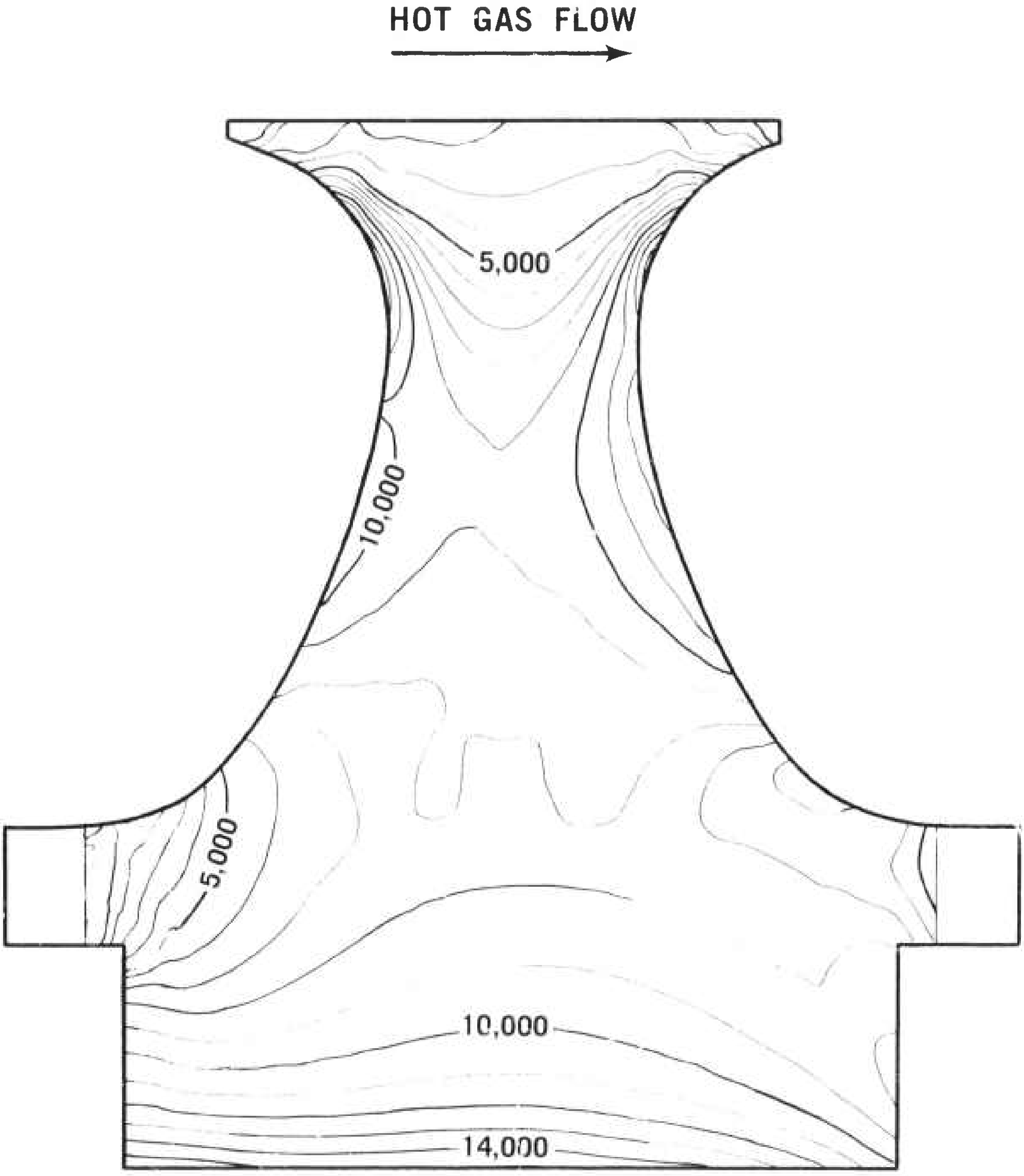
HOT GAS FLOW
5,000
10,000
5,000
10,000
14,000

Figure 3.4 Maximum Principal Tensile Stresses (psi) Second Stage Turbine Disk at 55% Speed

Assuming the structure to be subdivided into "N" uniformly stressed elements and for simplicity, (this is not a necessary prerequisite) a uniform reliability or survival probability throughout the structure, the survival probability of each individual element (i) is given by:

$$R_i = \sqrt[N]{R}$$

where R is the overall reliability of the structure.

From Equation 11 of Reference 8, the mean strength requirement for the i-th element is simply

$$\begin{aligned}\left(\bar{\sigma}_{MOR}\right)_i &= \sigma_i\,\Gamma\left(1 + \frac{1}{m_i}\right)\left[\frac{V_{eff_{MOR_i}}}{V_{eff_i}}\ \ln\ \frac{1}{R_i}\right]^{-\frac{1}{m_i}} \qquad (1)\\ &= \sigma_i\,\Gamma\left(1 + \frac{1}{m_i}\right)\left[\frac{V_{eff_{MOR_i}}}{V_{eff_i}}\ \ln\ \frac{1}{\sqrt[N]{R}}\right]^{-\frac{1}{m_i}}\end{aligned}$$

σ_i is the maximum principal tensile stress in the element.

m_i is the Weibull shape parameter (slope) which may vary with temperature and therefore will be a function of location.

Γ is the Gamma function

$V_{eff_{MOR_i}}$, V_{eff_i} are the effective volumes obtained from Weibull analysis for the MOR bar and the i-th element respectively, both are functions of the local m-value.

Equation 1 can be expressed more conveniently in terms of the characteristic strength. The characteristic strength in a Weibull distribution is that value of stress at which the risk of rupture becomes unity, i.e. for which the probability of failure is 63.2%.

$$P_\Theta = 1 - e^{-1} = 0.632$$

The characteristic strength is related to the Weibull parameter σ_o (characteristic strength per unit effective volume) by

$$\sigma_\Theta = \frac{\sigma_o}{(V_{eff})^{1/m}} \qquad (2)$$

and to the mean strength $\bar{\sigma}$ by

$$\sigma_\Theta = \frac{\bar{\sigma}}{\Gamma(1 + \frac{1}{m})} \qquad (3)$$

substituting equation 3 into 1

$$(\sigma_{\Theta_{MOR_i}}) = \sigma_i \left[\frac{V_{eff_{MOR_i}}}{V_{eff_i}} \ln \sqrt[N]{\frac{1}{R}} \right]^{-\frac{1}{m_i}} \quad (4)$$

The above relations have been incorporated into the design codes and appropriate computer routines were developed to facilitate pointwise specification of strength requirements in the form of contour plots for a given Weibull slope 'm' and the overall component reliability 'R'.

These techniques are being applied to the analysis of the design D' silicon nitride turbine rotors. Preliminary results indicate a need for materials of significantly higher characteristic strength and/or Weibull slope, (in the 1600°F - 2100°F range), than is currently being used in rotors, if high reliability is to be attained.

Confirmation of this analysis and investigation of possible corrective actions are high priority items for the next report period. Possible actions may include, proof testing to eliminate poor samples, applications of potentially better material (strength and/or 'm' value) such as Westinghouse's high strength Si_3N_4 or Norton's NC-132, and possible design improvements to reduce stresses.

Aerodynamic Design of Ceramic Turbines

Design Analysis

Two previously reported turbine design configurations, D(7) and D'(8) exhibited aerodynamic performance deficiencies as compared to the preceeding Design C. Design D differed from C in that common stators and rotors were used for both stages. This facilitated component development efforts, but resulted in a decrease in aerodynamic efficiency. The Design D' decreased efficiency further in relation to D principally because the constraints imposed for low stresses virtually eliminated the aerodynamically desirable "twist" in the rotor blade. To project the near term efficiency potential of a low stress ceramic axial turbine, an analytical design for an improved efficiency (Design E) turbine was initiated during this reporting period. The design criteria used was based on assumptions of material and fabrication capabilities at the conclusion of the vehicular turbine project as listed in Table 3.1.

Aerodynamic analysis of the Design E turbine was composed of two main efforts; optimization of the flowpath, and detailed design of the individual blades. In the first effort, a parametric study was performed to establish preliminary turbine flow area dimensions and gas and blade angles which were optimum in terms of aerodynamic efficiency. In the second effort, individual blade sections at various radii were designed and drawn to conform to the criteria established in the flowpath optimization. Both efforts are conducted to insure that the final blade design is in accordance with the constraints listed in Table 3.1.

TABLE 3.1

DESIGN CONSTRAINTS FOR DESIGN E DUO-DENSITY Si_3N_4 TURBINES

- Compatability with current engine cycle (speed, pressure level, mass flow, temperature).

Rotors

- Helical and centroidally stacked blades
- One dimensional blade stress $\leq$18,000 psi tension. (provisional)
- Two dimensional disk stress $\leq$30,000 psi tension. (provisional)
- Trailing edge thickness = 0.022 tip, 0.029 mean, 0.036 hub.
- Material density in blades of 2.7 gm/cm^3.
- Radial draw fabrication.

Stators

- Axial draw fabrication
- Trailing edge thickness = 0.030.
- Strength requirement is less than that for rotors.

Flowpath optimization was performed using an in-house computer program to calculate multi-stage turbine performance and gas properties at the inter-component planes within the turbine. The program utilizes a modification of the basic Ainley-Matheson(10) method. Loss coefficients were modified in accordance with the correlation of Dunham and Came(11). Gas properties at the inter-component planes were calculated to satisfy radial flow equilibrium with radial variation of total enthalpy using a second order Runge-Kutta integration method.

Detailed design of individual blade sections is currently being carried out to provide stator and rotor blades which conform, as closely as possible, to the criteria established in the flowpath optimization analysis. Both rotor and stator blades have parabolic camberlines. The camberlines are of a single family, for each rotor, so as to provide the helical blade stacking necessary to achieve low stress. To reduce bending stresses, the blade sections have their centroids radially stacked. The stator blade designs will permit axial draw in molding, while the rotor designs will allow radial draw.

Preliminary designs of both the first and second stage rotor blades have been completed, and design of the stators is underway. A detailed analysis of blade surface velocity distributions will be performed to determine if flow separation occurs and the need of any further refinements.

3.1.2 MATERIALS AND FABRICATION

Introduction

The primary in-house effort on fabrication of ceramic turbine rotors continues to be directed at the silicon nitride duo-density concept. Blade rings of reaction sintered Si_3N_4 were fabricated by both a newly-developed disposable mold slip-casting technique and by injection molding using a new 2.7 gm/cm^3 density Si_3N_4. In the press-bonding operation of simultaneously forming the hot pressed Si_3N_4 hub and bonding it to the reaction-sintered blade ring, a number of changes were made in the graphite components and in the stiffness of the support structure in order to solve problems. While quality improvements were made, additional work is needed to improve alignment and load distribution during press-bonding.

Slip Cast Blade Ring Fabrication

A prior report reviewed slip casting as a means of producing reaction sintered silicon nitride parts(5). In the case of slip casting a turbine rotor blade ring for use with the duo-density silicon nitride turbine rotor concept, problems were encountered primarily because of the complex shape involved. The presence of some drying shrinkage coupled with the weakness of the green slip makes it very difficult to remove complex shapes from a conventional plaster mold. As an alternative, a technique was investigated to remove the mold from the complex-shaped casting using a 3-3/4 inch diameter gear-shape having 36 teeth as shown in Figure 3.5.

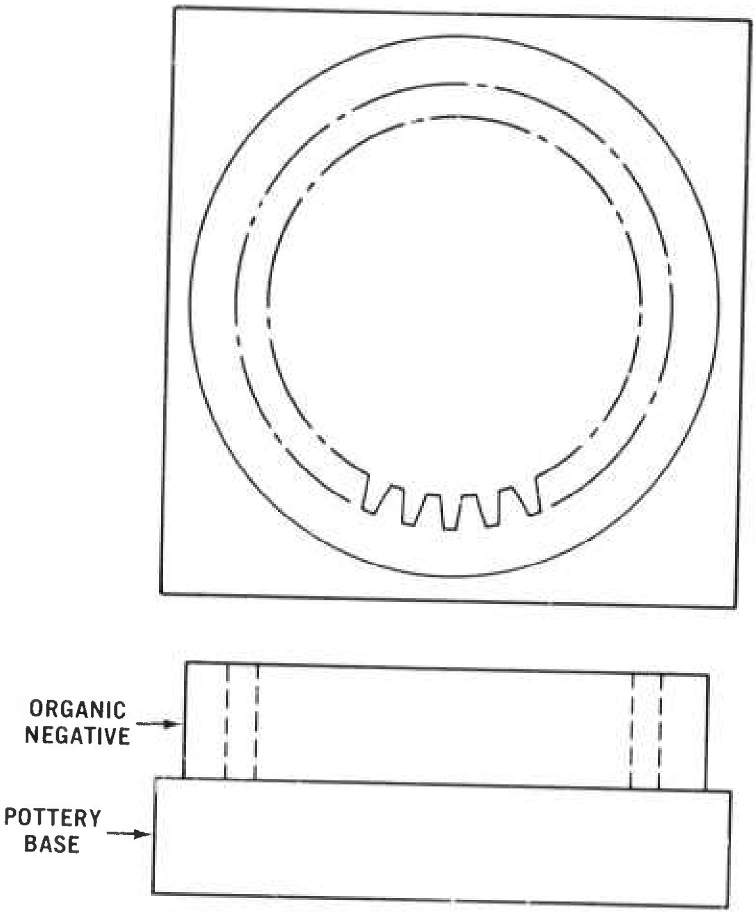

Figure 3.5 Slip Casting Mold for Gear Model

An organic mold representing the negative of the complex teeth portion of the required gear was formed from a soluble, disposable organic, P-dichlorobenzene. A number of techniques could be used to form this mold such as injection molding or casting into a flexible (rubber) pattern.

Some of the reasons which led to P-dichlorobenzene as the mold material are as follows:

1. The organic material must not react with the intended slip.
2. The organic material must provide a smooth surface against which the slip will be cast.
3. The material must be soluble in a solvent which is not miscible with water. The solvent must disolve the organic mold in a reasonable period of time, and not attack the casting material.

Having produced the negative of the complex surface of the ring gear, the base portion of the complete casting mold was made using conventional pottery plaster. The two portions of the mold (i.e. organic and plaster) were mated to form a casting cavity as shown in Figure 3.5. with the pottery base positioned below the organic negative. A suitable aqueous silicon metal slip(5) was then poured into the mold. The plaster portion of the mold extracts the slip vehicle by capillary action, resulting in a consolidated silicon casting. When consolidation was completed the plaster plate was removed. The combined organic negative and the consolidated casting were then immersed in a toluene solvent bath. Toluene is not miscible with the water in the casting and is effective in dissolving the P-dichlorobenzene mold portion. Since the casting is essentially "frozen" during the organic mold removal no green shrinkage was experienced. Once the P-dichlorobenzene was totally dissolved, the casting was removed from the bath and allowed to dry. Having formed the green shape, subsequent processing conforms to accepted practice for the manufacture of reaction sintered silicon nitride components.

The above techniques have been successful in producing complex silicon metal castings and have been applied to turbine rotors, and turbine stators. Figure 3.6 shows a silicon metal turbine rotor casting produced using the above mentioned process.

The original motivation to utilize the slip casting process, as opposed to injection molding, was to produce a more dense reaction sintered silicon nitride and therefore one of higher strength. While it has been demonstrated that high density green silicon slips can be prepared, more development is required to learn how to completely reaction sinter such dense material. At present, injection molding can generally produce as dense a part as slip casting in the fully nitrided state even though slip casting is able to produce denser green bodies. For this reason it has been decided to continue to concentrate on injection molding for the day-to-day fabrication of experimental components and in parallel continue research to investigate the reaction sintering process.

Injection Molded Blade Ring Fabrication

During this reporting period molding of 2.55 gm/cm^3 density Si_3N_4 rotor blade rings was emphasized. A new molding composition of 2.7 gm/cm^3 density Si_3N_4 was also successfully molded into rotor blade rings. Over 400 blade rings were injection molded during this period. Various tooling and molding parameter changes were made to improve rotor blade ring quality.

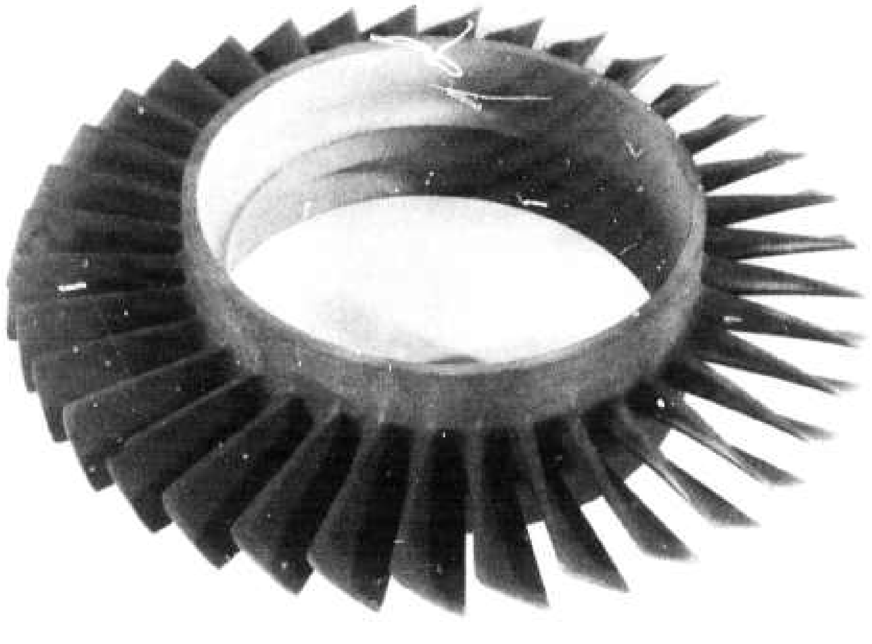

Figure 3.6 Slip Cast Turbine Rotor Blade Ring

The Design C second stage rotor tooling was reworked to obtain a molded blade ring with a smaller blade tip diameter equal to the Design D rotor. While this rework was in process vacuum capability was also added to the die cavity as shown in Figure 3.7. Previous experience with the stator die indicated the advantages associated with die evacuation just prior to material injection(8). Vacuum was supplied through the stationary die half and entered the cavity through the blade tips. A 0.002 inch gap was used to obtain a vacuum while retaining injected material in the die cavity.

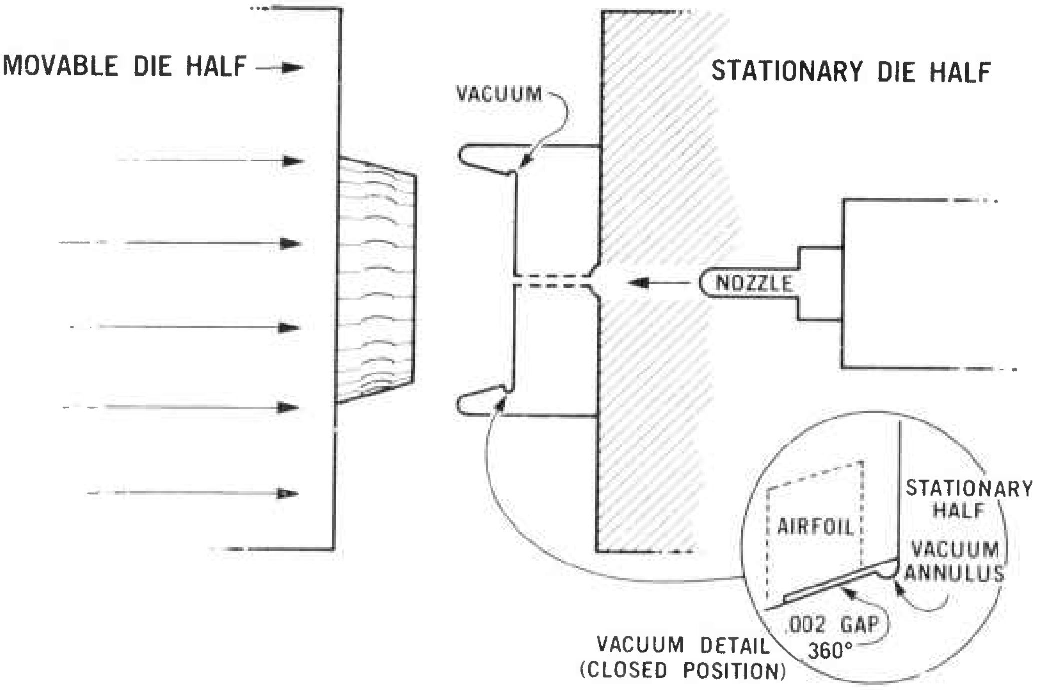
MOVABLE DIE HALF
VACUUM
STATIONARY DIE HALF
NOZZLE
AIRFOIL
STATIONARY HALF
VACUUM ANNULUS
.002 GAP 360°
VACUUM DETAIL (CLOSED POSITION)

Figure 3.7 Schematic of Vacuum Addition to Rotor Tooling

A positive shutoff type nozzle, used for vacuum operation of the stator tooling, proved unacceptable in initial rotor trials. A nozzle with a less positive reverse taper shutoff was required to reduce flow restriction and fill the rotor die cavity completely. This nozzle allowed some material to be pulled from the barrel during die evacuation, thus evacuation time was limited to prevent this material from solidifying prematurely. A new positive shutoff type nozzle will be designed with less flow restriction. This will allow longer evacuation time resulting in a higher cavity vacuum.

Utilizing the reworked die, rotors were molded from 2.55 gm/cm^3 Si_3N_4 material which were both visually and X-ray flaw free in the as-molded state. Evacuation was observed to reduce the incidence of small void type flaws detected by X-ray. Molding parameters, such as die temperature and pressure, used for injection molding of rotors, using vacuum, remained unchanged from Table 3.1 of Reference 6. The material temperature, however, was reduced from 230°F to 210°F. The use of vacuum also permitted faster cycle times since the material was cooler initially and required less cool down time. The absence of entrapped gas pockets eliminated blistering previously encountered with short cycle times.

A new 2.7 gm/cm^3 density Si_3N_4 material, 92FP composition (see Section 4.2 for details), was introduced for injection molded rotors during this report period. A preliminary parametric evaluation was made to determine time, temperature and pressure values required for this system. Die temperatures were raised 5°F to 85°F. Material temperature was set at 210°F for vacuum and 240°F without vacuum, and the holding pressure was set at 8000 psi. Cycle time was 30 seconds total. A program to optimize these parameters was undertaken after which rotors of 2.7 gm/cm^3 density could be molded. Approximately 70% of the rotors molded were visually flaw-free in the as molded condition. This compares favorably with the 80% level of visually flaw-free rotors molded from the 2.55 gm/cm^3 material. Radiographic evaluation of the 2.7 gm/cm^3 blade rings revealed a higher incidence of flawed blades when compared to the 2.55 gm/cm^3 material. The reject level was not unrealistically high, however, and the new Design D' rotor tooling should reduce the level of NDE rejects.

The tooling for D' rotor molding was received and installed on the injection molding machine. Trial moldings to establish parameters using the 2.7 gm/cm^3 material were initiated.

The D' tooling has been designed to be a highly automated tool with a higher level of material flow control. Heating and cooling of the tool has been improved to yield greater temperature control sensitivity. Cooling capacity has been increased to overcome a cooling deficiency in previous tooling which limited molding cycle time. Vacuum capability has been included with the vacuum entering through a 0.002 inch flash ring at the blade tips. The tool has straight (ground) parting lines on the airfoil inserts resulting in a tighter fit and increased vacuum levels over those previously obtained. Airfoil inserts now withdraw on a simple angle which will reduce the loads applied to blades during tool opening. Hydraulic actuation on the die scroll will allow the die opening cycle to be automated. This will also provide smoother, more consistent insert release and allow faster cycle times when used in conjunction with the automatic injection molding cycle. Faster cycle times provide greater flexibility in molding compound formulation and higher shrinkage materials can be molded using faster cycle times.

Material flow appears to have been improved in the D' tooling. The tendency for material to jet and swirl into blades causing a trailing edge knit line near the airfoil base was reduced by gating modifications shown in Figure 3.8. The material is gated to one end of the rotor platform and forced to turn a 90° corner. This right angle causes the material to form an even front advancing to fill the blades uniformly from base to tip. Preliminary tests with short fills show the technique to be successful. Molding of 2.7 gm/cm^3 Si_3N_4 rotors with this tooling will begin once parametric studies are completed.

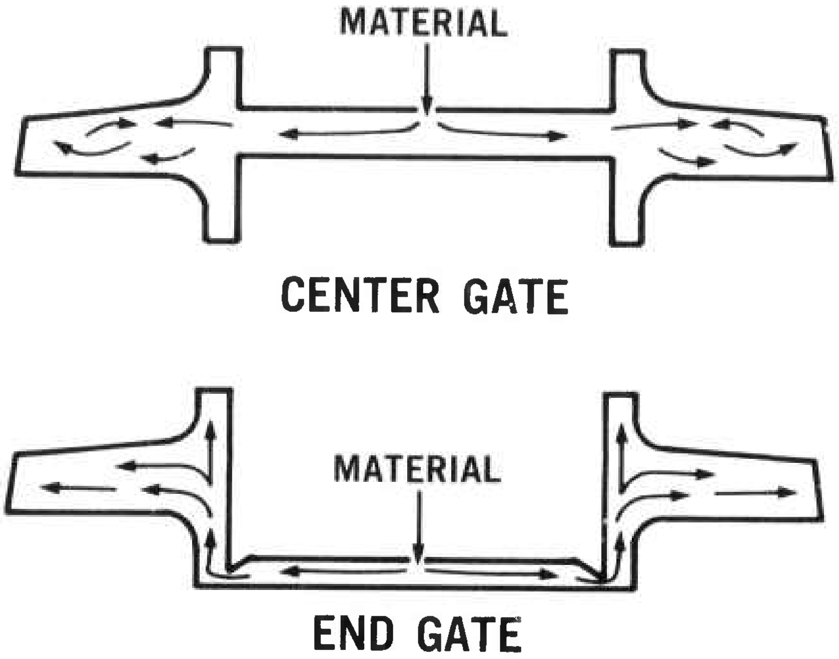

Figure 3.8 Gating Modifications to Rotor Tooling

Duo-Density Rotor Fabrication

The duo-density rotor is the primary approach being developed for fabricating a ceramic turbine rotor. This concept utilizes the high strength of hot-pressed Si_3N_4 in the hub region where stresses are highest but temperatures are moderate and, therefore, creep resulting from the use of an MgO densification aid is minimized. Reaction-sintered Si_3N_4, which can be formed into complex airfoil shapes by injection molding or slip casting, is utilized for the blade rings. Although the reaction-sintered material is of lower strength, it is adequate for the turbine blades because stress levels in this region are lower than in the hub. This concept relies on the ability to bond the two Si_3N_4 components (blade ring and hub) by hot-pressing techniques into an integral turbine rotor.

Work on developing duo-density rotors, during this reporting period, was directed toward further refinement of the graphite wedge hot-pressing system(7),(8) for bonding a theoretically dense Si_3N_4 hub to a reaction-sintered Si_3N_4 blade ring. The procedure for fabricating duo-density turbine rotors involves hot-pressing Si_3N_4 powder to theoretical density for the hub component while simultaneously bonding it to an encapsulated(6) blade ring. The special graphite assembly used for fabrication is illustrated in Figure 3.9. Prior to this period, the Si_3N_4 powder contained 5 w/o MgO as a densification aid and typical hot-pressing parameters used were 1750°C and 2500 psi for 2 hours. Although the

5 w/o MgO Si_3N_4 powder composition enabled the fabrication of duo-density turbine rotors at low pressures of 2500 psi, several problems existed. The high MgO content reduced the high temperature strength of the hub material and in addition, caused magnesium migration into the blade ring rim during hot-press bonding, permitting densification and deformation of the rim of the blade ring.

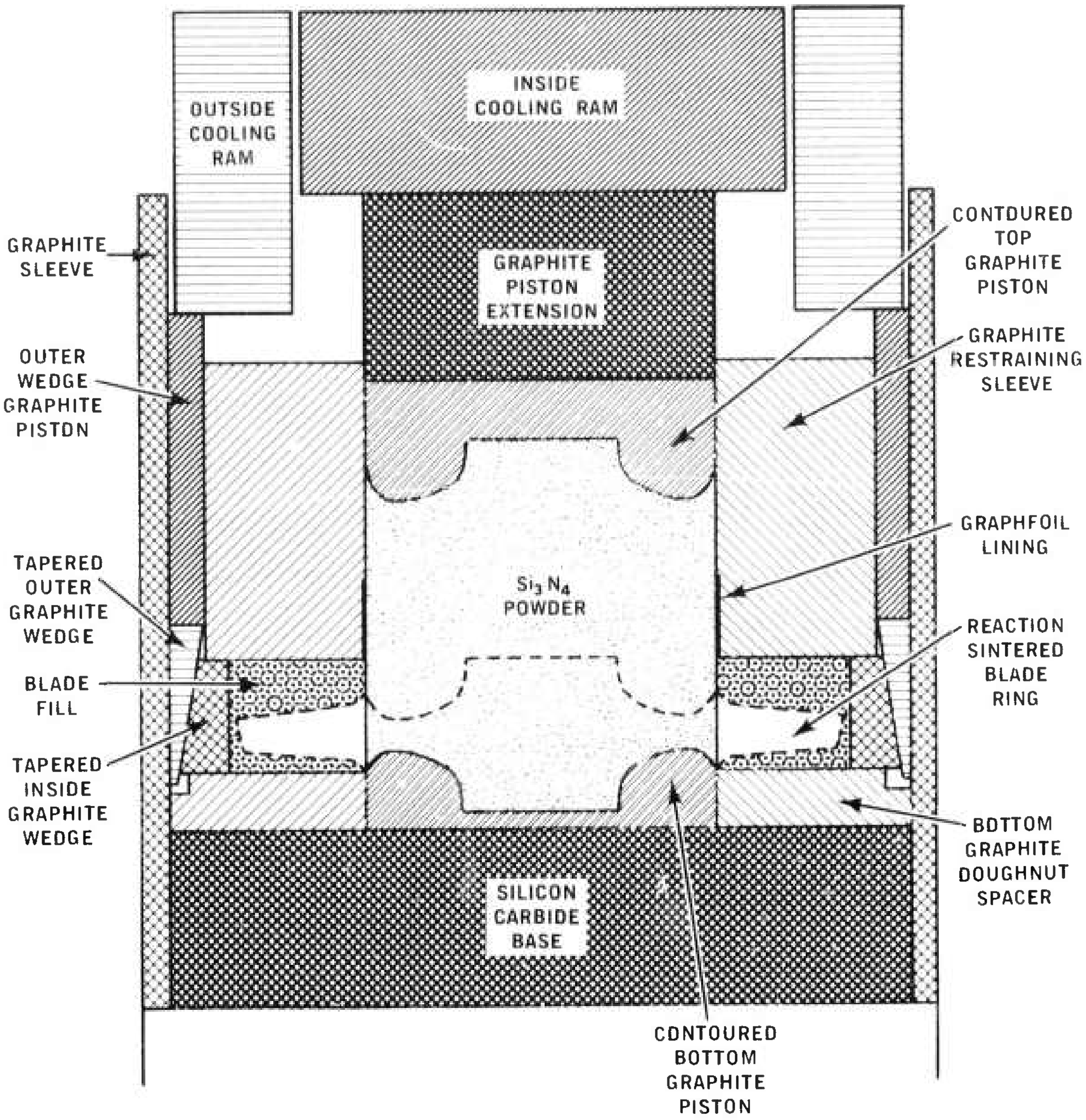

OUTSIDE COOLING RAM
INSIDE COOLING RAM
GRAPHITE SLEEVE
GRAPHITE PISTON EXTENSION
CONTOURED TOP GRAPHITE PISTON
OUTER WEDGE GRAPHITE PISTON
GRAPHITE RESTRAINING SLEEVE
GRAPHFOIL LINING
Si_3N_4 POWDER
TAPERED OUTER GRAPHITE WEDGE
REACTION SINTERED BLADE RING
BLADE FILL
TAPERED INSIDE GRAPHITE WEDGE
BOTTOM GRAPHITE DOUGHNUT SPACER
SILICON CARBIDE BASE
CONTOURED BOTTOM GRAPHITE PISTON

Figure 3.9 Hot Press Bonding Assembly for Simultaneous Forming and Bonding a Silicon Nitride Rotor Hub to a Blade Ring

Fracture of the blade ring during hot-press bonding has been classified into two types. The first type is the severe fracture of the blade ring in which the rim cracks in several places and the majority of the blades are severed. This type of fracture occurs inconsistently and appears to be related to drag(8) of the Si_3N_4 powder on the I.D. of the graphite retaining sleeve which creates large variations in the load distribution. The other class of cracks involve smaller blade root cracks and circumferential rim cracks of the blade ring. This latter class of cracks are believed related to alignment and inadequate support of the graphite wedge system.

Since the higher MgO content (5 w/o) in the Si_3N_4 powder created both material strength and blade ring rim deformation problems, the MgO content was reduced to 2 w/O. This reduced the magnesium migration without sacrificing bond quality, however, complete densification of the Si_3N_4 powder was more difficult. To overcome this problem, the hot-pressing pressure on the hub component was increased from 2500 to 4000 psi.

The higher pressure on the hub component created piston drag and some bonding of the Si_3N_4 powder to the lower edge of the retaining sleeve. A bending moment in the retaining sleeve resulted causing severe fracture of the graphite retaining sleeve and subsequent severe fracture of the blade ring. Several assembly modifications were made to eliminate the drag on the retaining sleeve. The modification most successful was lining the I.D. of the retaining sleeve with graphfoil. Other techniques were less effective in reducing drag or created other problems.

The graphite retaining sleeve was modified to enable the I.D. to be lined with graphfoil as illustrated in Figure 3.9. The I.D. of the retaining sleeve was opened to 3.085 inches (an increase of 0.035 inches) to a height of 2 inches from the end adjacent to the blade ring. This recess was lined with 0.015 inch thick graphfoil. This procedure eliminated all fracture of the graphite retaining sleeve by minimizing drag and bonding of Si_3N_4 powder on the I.D. of the retaining sleeve. In addition, this procedure enabled the rate of application of pressure on the hub component to be increased. Approximately 700 psi pressure is maintained to 1500°C then the pressure is increased to full pressure (4000 psi) within 5 minutes and prior to 1750°C. This earlier application of pressure reduced the SiC reaction and achieved full density throughout the hub as indicated by the dark curvic region in Figure 3.10.

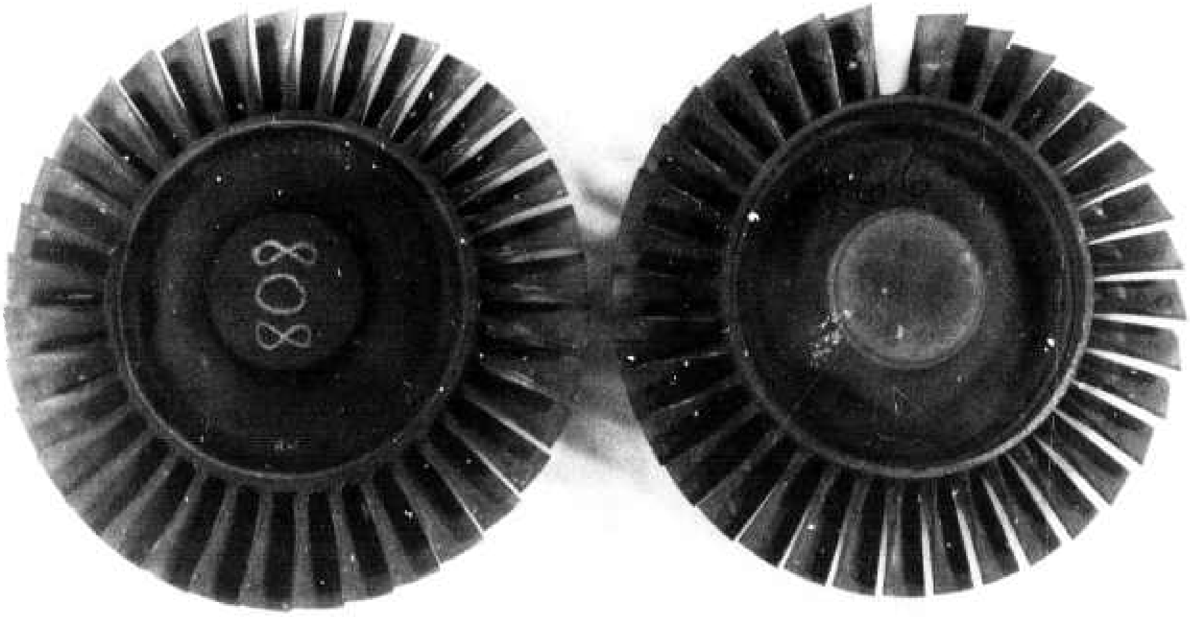

Figure 3.10 Duo-Density Rotors Number 808 High Density Curvic Region and 766 Lower Density Curvic Region

Other less effective modifications involved positioning a graphite washer between the Si_3N_4 blade ring and graphite retaining sleeve, and holding the rotor assembly longer at lower pressures at 1750°C to eliminate drag. A graphite washer 0.25 inches thick was placed between the blade ring and bottom of the graphite retaining sleeve. The intent was to produce a pre-cracked condition in the retaining sleeve to relieve stresses in the retaining sleeve and minimize forces exerted on the blade ring if the washer fractured during hot-press bonding. This technique reduced the severity of the fractures of both the graphite retaining sleeve and Si_3N_4 blade ring, but did not eliminate them on a consistent basis.

The other approach involved maintaining a low pressure (700 psi) on the hub component for longer times at 1750°C prior to applying 4000 psi pressure. This reduced drag and eliminated severe fracture of the Si_3N_4 blade ring, however, a decline in hub quality resulted. It was anticipated that some deterioration in the hub component would result but that adequate hub quality could be maintained. The graphite assembly system, with the blade ring and Si_3N_4 powder, was held at 1750°C for 1 hour with minimal pressure (700 psi) on the hub component. After approximately 75% of the densification had occurred, the pressure was increased to 4000 psi. Although this procedure eliminated drag and subsequent severe fracture of the blade ring, other problems associated with the hub component resulted. The Si_3N_4 hub exhibited a severe SiC reaction resulting in rougher surface finishes than obtained with the previous temperature-pressure schedule. In addition, lower average hub densities of approximately 0.5 to 1.0 percent resulted with even lower densification of the curvic region as indicated by the light gray appearance in Figure 3.10. These results were associated with the long hold at 1750°C in which the large surface area of the Si_3N_4 powder particles were exposed to the carbonaceous atmosphere.

Since the graphfoil lined retaining sleeve enabled the rapid application of pressure and eliminated the severe fracture of the Si_3N_4 blade rings, this procedure was incorporated into the standard hot press bonding procedure. However, the smaller blade root cracks and circumferential cracks persisted and seem to be related to alignment and support of the graphite wedge assembly.

An analysis of the hot-press bonding operation was made and revealed deficiencies in the graphite system which contributed to cracking of the blades and rim of the blade ring. These deficiencies are illustrated in an exaggerated manner in Figure 3.11. As shown, deformation of the graphite foundation occurred resulting in a deflection of the blade ring and cracking or hot tearing of the lower blade edges. In addition, the tendency of the inner wedge to roll and split resultedin a loss of wedge load on the upper half of the blade fill. This in turn resulted in flaring and eventual cracking of the upper rim of the blade ring.

Therefore, to avoid overstressing and fracturing the blades and rim in the hot-press bonding operation, the blade ring must be uniformly supported on a surface or foundation which can resist deflections at the furnace temperatures under the applied loads. In addition, the blade ring must be adequately supported at the blade fill periphery.

Prior to the investigation of the blade ring support system, all hot-press bonding experiments were made using Union Carbide ATJ graphite for the foundation between the blade ring and the lower water cooled ram. This material, because of its rather low Young's Modulus at temperature (approximately 2 x 10^6 psi), was incapable of providing uniform support for the blade ring when subjected to non-uniform loads. The non-uniform loading across the foundation, i.e., a higher loading in the hub region (Figure 3.9), produced a dished deflection of the foundation with the largest deflection corresponding to the higher center load. This deflection results in non-uniform support of the Si_3N_4 blade ring. Deflection of the blade ring in this mode overstressed the lower edges of the airfoils near the hub resulting in blade root cracks which were consistently observed.

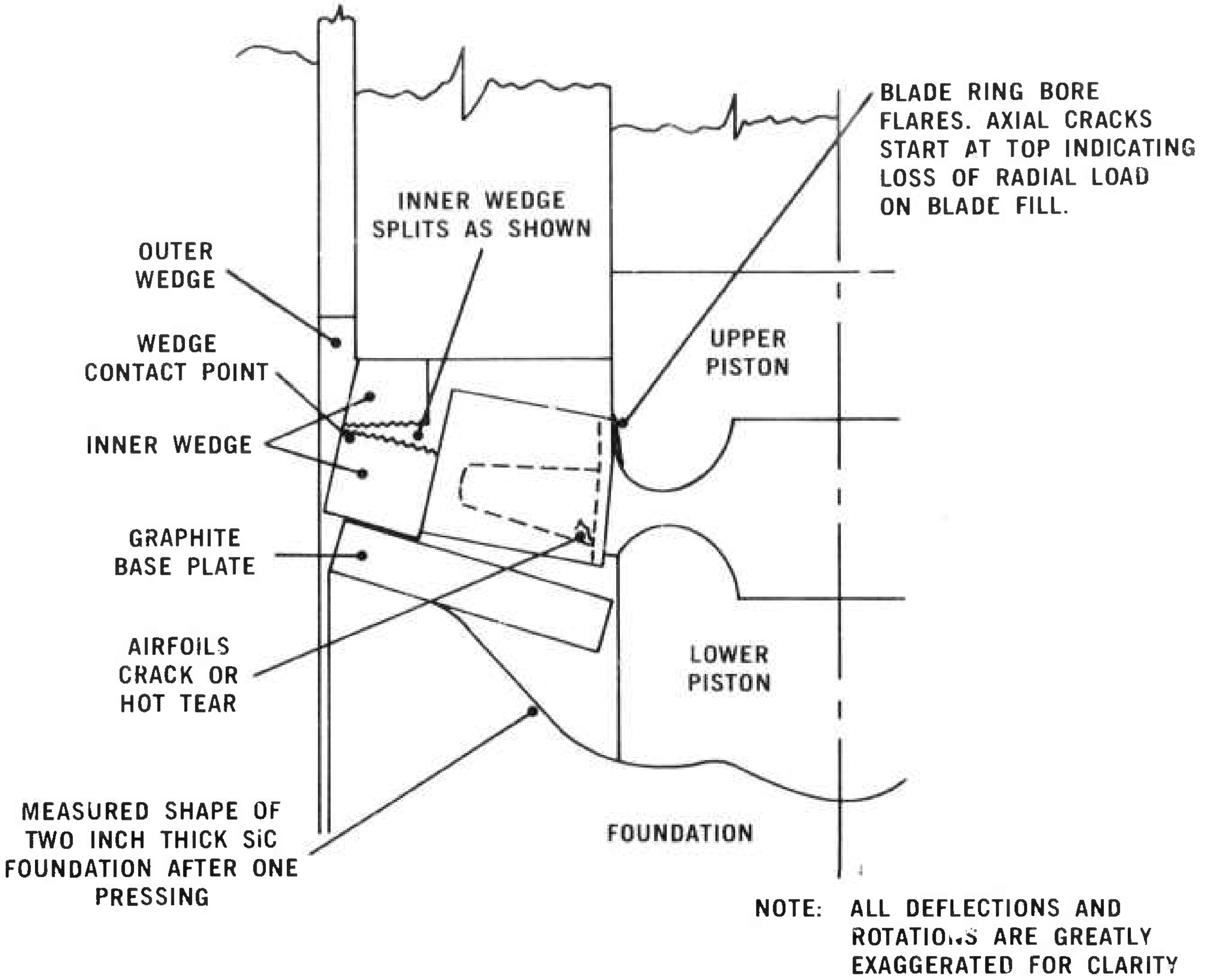
BLADE RING BORE FLARES. AXIAL CRACKS START AT TOP INDICATING LOSS OF RADIAL LOAD ON BLADE FILL.
INNER WEDGE SPLITS AS SHOWN
OUTER WEDGE
WEDGE CONTACT POINT
INNER WEDGE
UPPER PISTON
GRAPHITE BASE PLATE
AIRFOILS CRACK OR HOT TEAR
LOWER PISTON
MEASURED SHAPE OF TWO INCH THICK SiC FOUNDATION AFTER ONE PRESSING
FOUNDATION
NOTE: ALL DEFLECTIONS AND ROTATIONS ARE GREATLY EXAGGERATED FOR CLARITY

Figure 3.11 Exaggerated Schematic of Duo-Density Rotor During Hot Press Bonding

To eliminate bending of the Si_3N_4 blade ring, a stiffer material more resistant to deformation was required. Hot-pressed silicon carbide was selected to replace the graphite as a foundation material. The Young's Modulus of SiC at temperature is approximately 35.0 x 10^6 psi which is significantly higher than the graphite and provided better support for the blade ring. Initial experiments consisted of a one inch thick SiC plate supported by graphite. These experiments indicated that one inch thickness was not sufficient since measurable creep of the SiC plate occurred. A dished deflection of 0.0025 inches was measured after hot-press bonding one turbine rotor. Increasing the thickness of the SiC base to two inches reduced the measurable creep to 0.0006 inches. Several rotors have been hot-pressed using a two inch thick SiC base and results indicate an improvement in rotor quality with respect to blade root cracking, however, cracking has still not been totally eliminated.

The graphite wedge component of the graphite system was modified to improve the support of the blade fill and provide better wedge action during pressing. The graphite wedge system is illustrated in Figure 3.9. The inner wedge ring, cut through at one place, has been used to convert a vertical load to a radial load required for blade-ring backup. The inner wedge had a tendency to roll and crack just above the contact point between the outside and inside wedge resulting in a loss of load on the upper portion of the blade fill and eventually circumferential cracking of the Si_3N_4 blade ring rim. This is illustrated in Figure 3.11. In addition, non-uniform load distributions were produced by inflexibility of the inner graphite wedge cut through at one place.

To provide better support and eliminate the roll of the graphite wedge the contact point was lowered below the centroid of the inner wedge (and the blade fill). To improve the uniformity of the wedge action and thus the applied radial load around the blade fill, the inner graphite wedge was sliced radially into sixteen equal segments increasing its flexibility and load distributing capability. Both of these modifications to the graphite wedge have improved the support and uniformity of the load on the blade filled blade ring.

Investigation and evaluation of the hot-press bonding assembly will continue to improve load distribution and alignments which are critical to the success of this program.

3.1.3 ROTOR TESTING

Introduction

Continued thermal shock rig evaluation of silicon nitride rotor blades was carried out during this period. An additional test which measures the bend strength of finished blades was implemented during this reporting period. This test has been used to evaluate the effects of thermal shock treatment and a 200 hour thermal soak at 1900°F. Room temperature spin pit testing has continued on blade segments, blade rings, rotor hubs and duo-density rotors. A test rig for evaluating rotor hubs using a large radial thermal gradient was designed and built. A simpler hot spin rig to meet the relatively low cost, rapid turn-around requirements of initial hot spin testing has been designed and built. A hot spin test of a non-fully bladed rotor resulted in failure and led to revisions of the turbine rotor testing. A planned engine test of ceramic rotors with 10% blade height was delayed due to balancing problems; these have been resolved and testing of rotors in a complete engine is expected in the next reporting period.

Thermal Shock Rig Testing

The blades of 3 duo-density turbine rotors were thermal shocked with encouraging results. Two rotors, one with slip cast blades and one with injection molded blades showed no erosion or failures after 1324 cycles, of 45 seconds duration, at 2100°F with a thermal down shock of 500°F/second. Another rotor with injection molded blades sustained a failure at the junction of the blade and rotor platform after one cycle. This failure was attributed to a flaw at the blade root as another set of blades from this rotor sustained 1323 cycles, of 45 seconds duration, at 2100°F without failure.

The effect of thermal shocking on the room temperature strength of blade rings was investigated. Two rotor blade rings of 2.8 - 2.84 gm/cm^3 density slip cast Si_3N_4 were tested for 50 cycles on each of eight blades. Maximum temperature was 2500°F for 45 seconds duration and a downshock rate of 800°F/second. There were no failures on the test rig although further blade bending tests revealed a degradation in strength which is described in more detail later in this section.

Blade Bend Testing

A need was recognized for a rotor blade test to supplement the cold spin pit testing. The primary functions of this test were to be:

- Determine individual blade strength
- Determine room temperature material strength degradation as a function of thermal shocking or soaking
- Compare various materials and processes
- Potential use for proof testing blades
- Evaluation of NDE techniques

The test developed is similar to the stator vane load testing described in Reference (8) and Section 3.2.3 of this report. The test setup, shown in Figure 3.12 consists of an 1/8" diameter steel ball which contacts the test blade, an indexing mechanism and a mounting plate. A crosshead speed of 0.02 inches per minute was used with the load graphically recorded. The failure mode is nearly pure bending with an inherent trace of torsien present due to the twisted geometry of the blade. The direction of loading puts the leading and trailing edges of the blade in compression and the back or suction surface in tension.

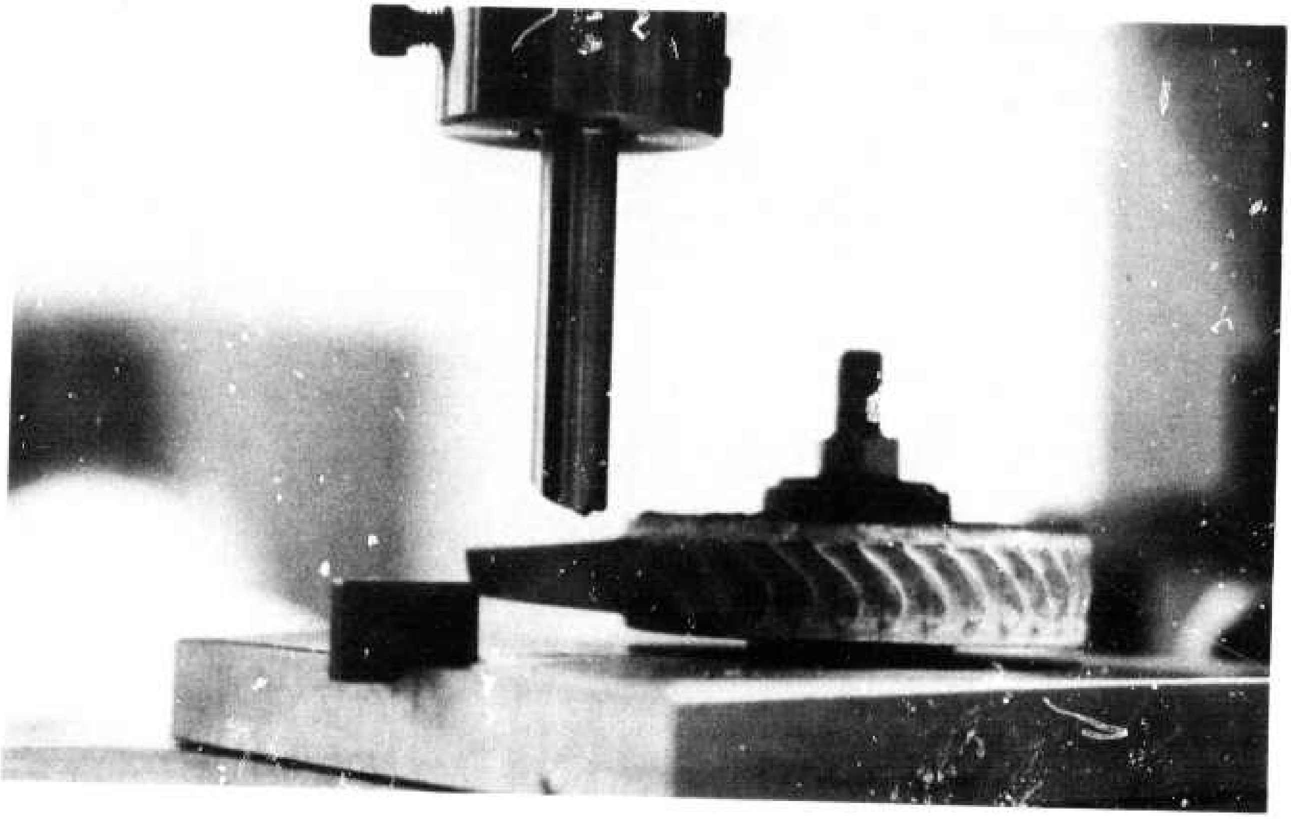

Figure 3.12 Blade Bend Testing Fixture

A three dimensional finite element stress analysis (SAP)[5] of the blade using an analytical model similar to that shown in a previous report(6) was completed for this blade loading configuration. An assumed coefficient of friction of 0.25 between the sperical ended loading rod and the blade surface resulted in a calculated stress of 38,500 psi tension for a 113 pound load.

A rotor blade ring was instrumented with rectangular strain gauges at the back of three blades near the rim of the blade ring. The recorded maximum bending and torsional stresses were in excellent agreement with the predicted values based on the assumed coefficient of friction of 0.25.

Table 3.2 summarizes the test results. The purpose of this series of tests was to establish the strength of slip cast blades without visible flaws. The strengths presented were determined analytically using the relationship that 113 pounds produces 38,500 psi tension.

The results for three slip cast blade rings showed excellent Weibull slopes ranging from 11.6 to 15.6 which are higher than the slope for slip cast test bars (8.18, see Section 4.3 of this report). These Weibull slopes have not been analytically adjusted for the observed radial variation of failure locations and hence are conservative as they include "bench-test" variable not present in the engine.

TABLE 3.2

SLIP CAST BLADE BEND TEST DATA

Condition of Blade Ring	Blade Ring S.N.	Density gm/cm^3	Number of Tests	Strength Range ksi		Weibull Slope 'm'	Characteristic Strength ksi
Baseline*	129	2.8	28	18.5	26.5	15.6	24.2
Baseline*	190	2.82	12	37.9	50.5	13.2	45.9
Baseline*	222	2.8	9	23.6	[illegible]	11.6	28.7
Baseline	92	2.84	14	24.2	37.9	8.7	32.8
Thermal** Shocked	92	2.84	8	16.7	32.5	4.5	27.6
Baseline	204	2.82	19	34.5	42.6	16.8	39.6
Thermal * Soaked**	**204**	**2.82**	**7**	**21.8**	**34.1**	**5.1**	28.9
Baseline	273	2.8	8	32.5	38.2	16.1	36.0
Thermal Shocked	273	2.8	6	16.7	32.5	9.3	32.0
Thermal Soaked	273	2.8	9	23.8	34.5	8.7	31.1

* Baseline = Blades tested as nitrided
** Thermal Shocked = Blades tested after 50 cycles to 2500°F
*** Thermal Soaked = Blades tested after soaking at 1900°F for 200 hours

Three slip cast blade rings were used to evaluate the effects of thermal shocking and thermal soaking on blade strength. Two blade rings were tested after the blades had been subjected to 50 cycles to 2500°F in the thermal shock rig. The nearly 50% decrease in Weibull slope and 1[illegible]5% decrease in characteristic strength was attributed to the presen[illegible] unreacted silicon found in the high density blade rings. A similar stren[illegible] degradation was observed after soaking the blades in air at 1900°F for [illegible] hours and was also attributed to unreacted silicon as no degradation in t[illegible] strength of fully nitrided test bars, after an identical soak, was foun[illegible] see Section 4.2).

Cold Spin Testing

The equipment, techniques and procedures used in cold spin testing of ceramic turbine rotors, hubs and blade rings has been outlined in previous reports (2,7,8). The spin test takes place at room temperature in a partial vacuum with gradually increasing speed (400 rpm/second) to a pre-determined qualification speed or until failure occurs.

Recently the major emphasis was directed toward evaluating the strength of complete rotor blade rings, although other components such as hubs and rotor assemblies were also tested. This cold spin testing phase produces data which is valuable feedback to the fabrication process.

During this reporting period seven press bonded rotors were tested with two Design D rotors attaining qualifying speeds of 53,000 rpm and an additional two rotors, with blades of 100% of designed length, were successfully tested to 64,240 (100% design speed) rpm. Failures of the other rotors tested occurred in the range of 15,710 rpm to 52,140 rpm. These failures were due primarily to blade cracks introduced earlier in the fabrication process.

Seven hot pressed Si_3N_4 rotor hubs were spun to destruction to determine material strength properties. Failure occurred in the range of 64,370 rpm to 111,800 rpm. These hubs were flaw free by visual inspection prior to testing. Figure 3.13 shows a hub failure at 111,800 rpm. The lower range of failure speeds were attributed to incomplete densification in the curvic coupling region. This problem is addressed in Section 3.1.2.

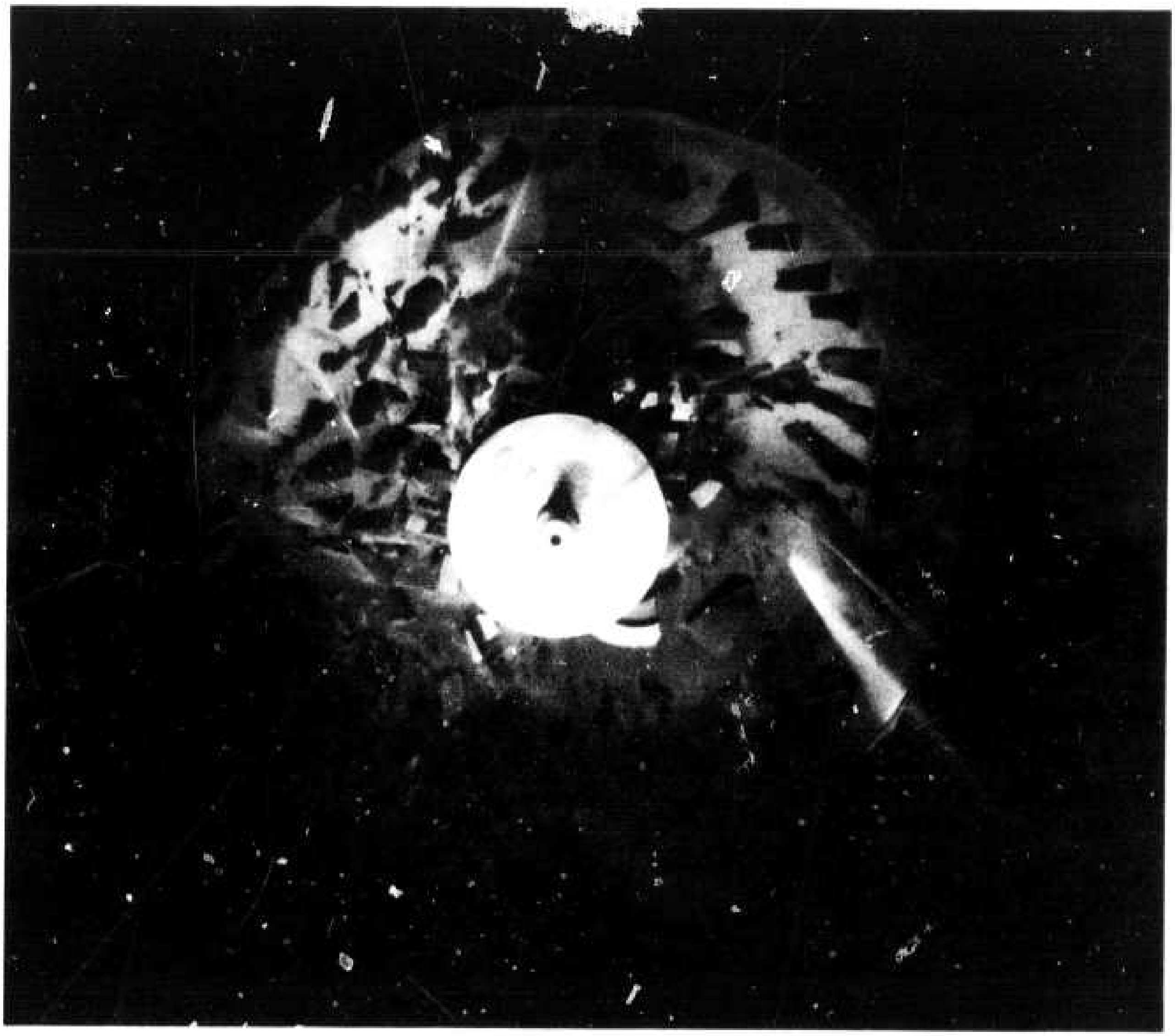

Figure 3.13 Ceramic Rotor Hub Failure at 111,800 rpm

The effort in rotor blade ring and blade segment testing was primarily directed to evaluation of various epoxies used to fasten the blade ring or segments to a hot pressed Si_3N_4 hub. Sixty tests of bonded blade rings or blade segments (two or three blades per segment) were carried out to various speeds. Figure 3.14 shows a hot-pressed hub and epoxy bonded blade ring at the instant of failure at 60,290 rpm showing the epoxy joint still intact.

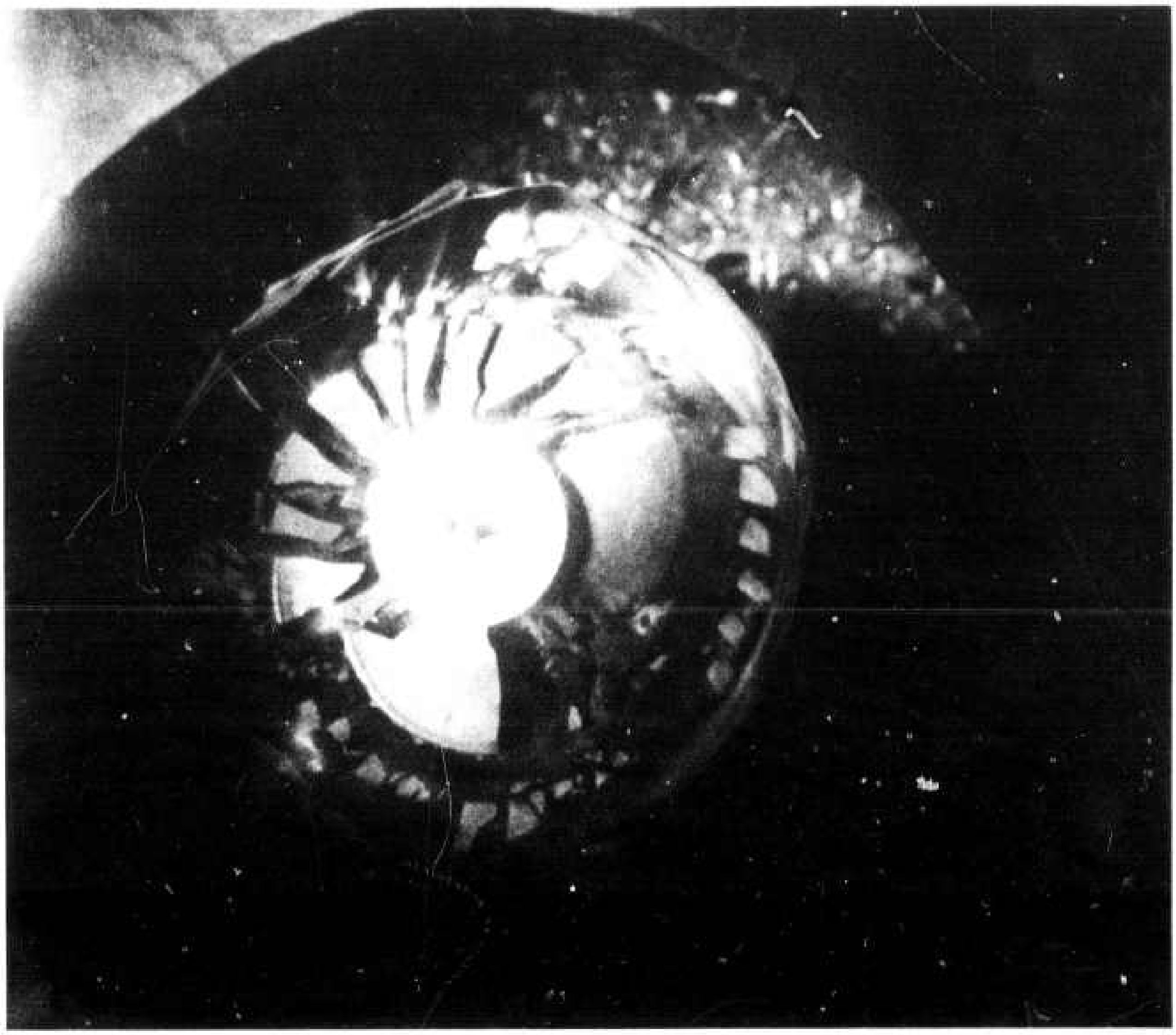

Figure 3.14 Duo-Density Rotor Failure at 60,290 rpm

Thermal Stress Rig Testing

A test rig was designed and built which introduces a radial thermal gradient in the rotor thereby producing a high tensile stress in the bore of the rotor. This rig will be used to supplement the cold spin proof test by proof testing the bore region of the rotor. Cold spinning cannot subject the bore of the rotor to high stresses without over stressing the blades and platform area.

The rig consists of a cylindrical container in which a rotor is placed between two 1000 watt electrical heaters. These heaters raise the temperature of the rotor blades and platform while the bore of the rotor is cooled by a tube delivering shop air. Thermocouples will be used to monitor the rotor and air temperatures and strain gages will be used in the rotor bore to record the strain level reached.

The rig has been built and the associated instrumentation and recorders are in final check out.

Hot Spin Rig

While the existing turbine rotor test rig is suited to long time endurance testing with good simulation of engine operating conditions, it is not ideally suited for the relatively low cost, rapid turn-around, requirements of initial hot spin testing. Therefore, a simpler hot spin rig, as shown in Figure 3.15, was designed and built. This rig permits:

1. Single stage testing without stators and nose cone.
2. A simplified rotor attachment mechanism (a conical pilot).
3. A simple gas-fired nozzle arrangement.
4. A burst ring and pre-cured ceramic fiber insulation.
5. A simplified bolting arrangement, using an air cooled bolt, replacing the engine "folded" bolt.
6. Inclusion of a viewing port for an optical pyrometer to permit measurement of blade temperatures.

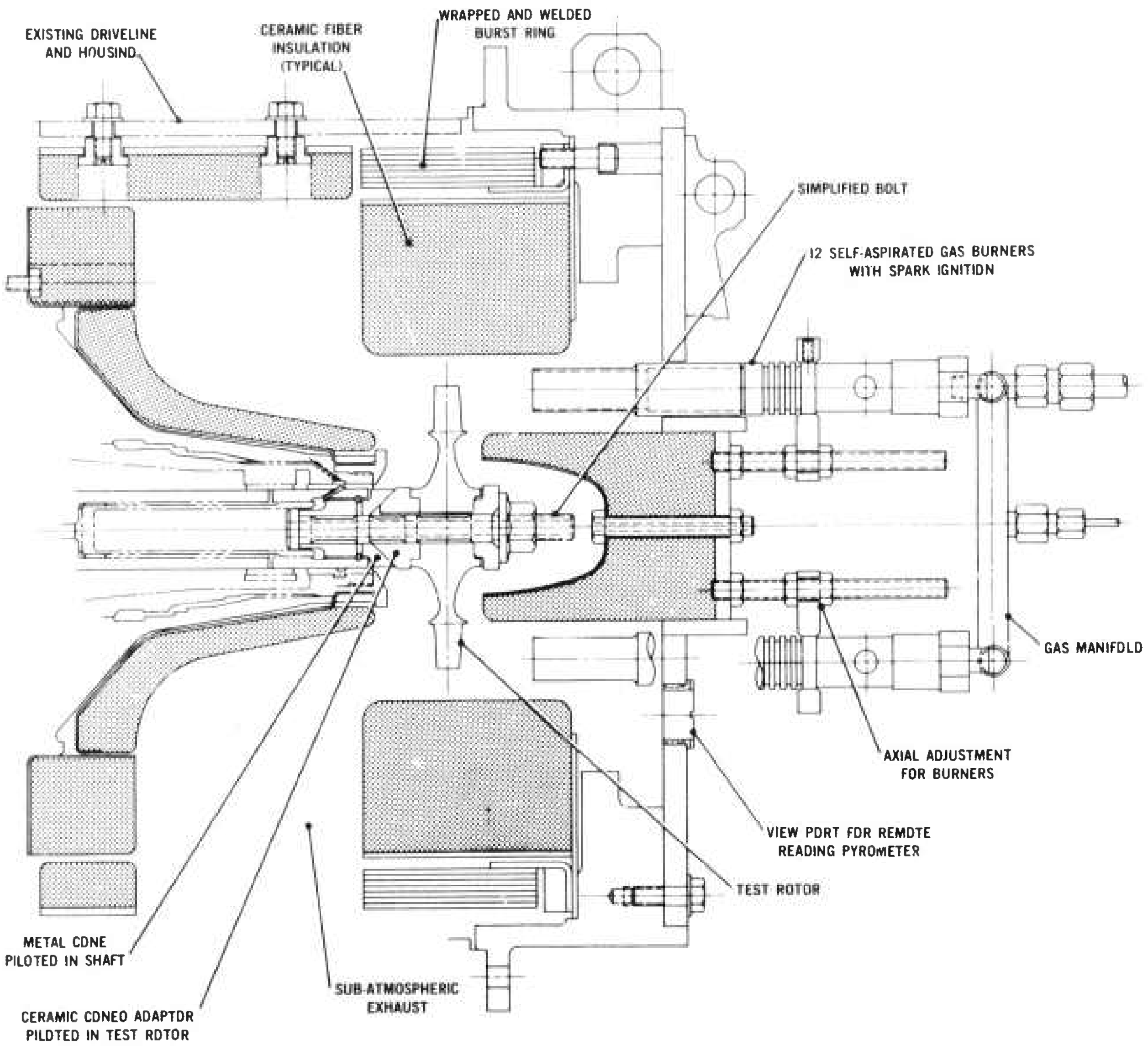
EXISTING DRIVELINE AND HOUSING
CERAMIC FIBER INSULATION (TYPICAL)
WRAPPED AND WELDED BURST RING
SIMPLIFIED BOLT
12 SELF-ASPIRATED GAS BURNERS WITH SPARK IGNITION
GAS MANIFOLD
AXIAL ADJUSTMENT FOR BURNERS
VIEW PORT FOR REMOTE READING PYROMETER
TEST ROTOR
SUB-ATMOSPHERIC EXHAUST
METAL CONE PILOTED IN SHAFT
CERAMIC CONED ADAPTOR PILOTED IN TEST ROTOR

Figure 3.15 Hot Spin Test Rig

The rotor is piloted to a ceramic adaptor mounted to a metal coned shaft insert by the bolt. Torque requirements are furnished by friction supplied by the bolt clamping load. The natural gas jets can be positioned axially relative to the rotor. Adjustment of secondary air is achieved by orifices in the end cover. A slight depression in the exhaust pressure level, (1.0-1.5 inches of water), provides for maintenance of air flow and direction. The twelve gas jets are self aspirating with both gas and air being externally supplied to the rig. Pre-cured ceramic fiber insulation mounted on sheet metal is bolted in place for insulation. An inconel X-750 (spiral wound and welded) burst ring protects the main housing. While this simplified hot spin rig is not intended to simulate aerodynamic loading on the blades, it is capable of subjecting the blades and rotor rim to 2500°F gas temperature and 100% speed.

Initial shakedown testing of the hot spin rig was started in this reporting period and to date all testing has been non-rotational to determine the rig cooling air flow requirements as a function of gas temperature and checkout of instrumentation and rig safety equipment.

Turbine Rotor Test Rig Testing

During this reporting period, a duo-density silicon nitride rotor was selected for initial testing in the turbine rotor test rig even though it was not flaw free. A number of badly flawed blades were deliberately removed leaving 23 reasonable appearing blades. The bond between the hub and the rim appeared sound. Testing of this rotor was considered beneficial for test rig shakedown and development, and for accumulation of ceramic rotor test experience.

Figure 3.16 shows the planned and actual test schedules of rotor speed and turbine inlet temperature. The planned test schedule consisted of the following:

> After a warm-up of the test rig and ceramic hardware, the curvic couplings were to be "run-in" over the two five minute cycles at a temperature of 1950°F and shaft speed of 35,000 rpm. The test rig would then be run at 1950°F and 45,000 rpm for five minutes after which the turbine inlet temperature would be increased in two steps to 2200°F. Maximum time at 2200°F was to be limited because of temperature limitations of the downstream test rig hardware.

The testing actually accomplished is also shown in Figure 3.16. After the initial warm-up period, three short one minute runs were made up to 1920°F and 33,600 rpm after which a catastrophic failure of the rig and ceramic components occurred. Both the duo-density Si_3N_4 turbine rotor and the hot pressed Si_3N_4 spacer hub were completely shattered. Hot turbine exhaust gases had back flowed through the rig melting the aluminum centrifugal compressor. The tensile member of the folded rotor bolt was severely deformed and broken while the compressive member was completely unscrewed from the main rotor shaft.

While the primary cause of the failure was not fully established, it became clear that several modifications to the test rig were needed. Accordingly, the compressor was replaced by a "dummy" wheel and cooling air was re-routed to be supplied from an external source. More extensive instrumentation and recording equipment was installed. Thus, the test rig operation and future failures can be monitored and analyzed more readily.

Finally, an improved method of rotor attachment was implemented. This includes a more positive method of locking the compression member of the "folded bolt" design into the rotor shaft.

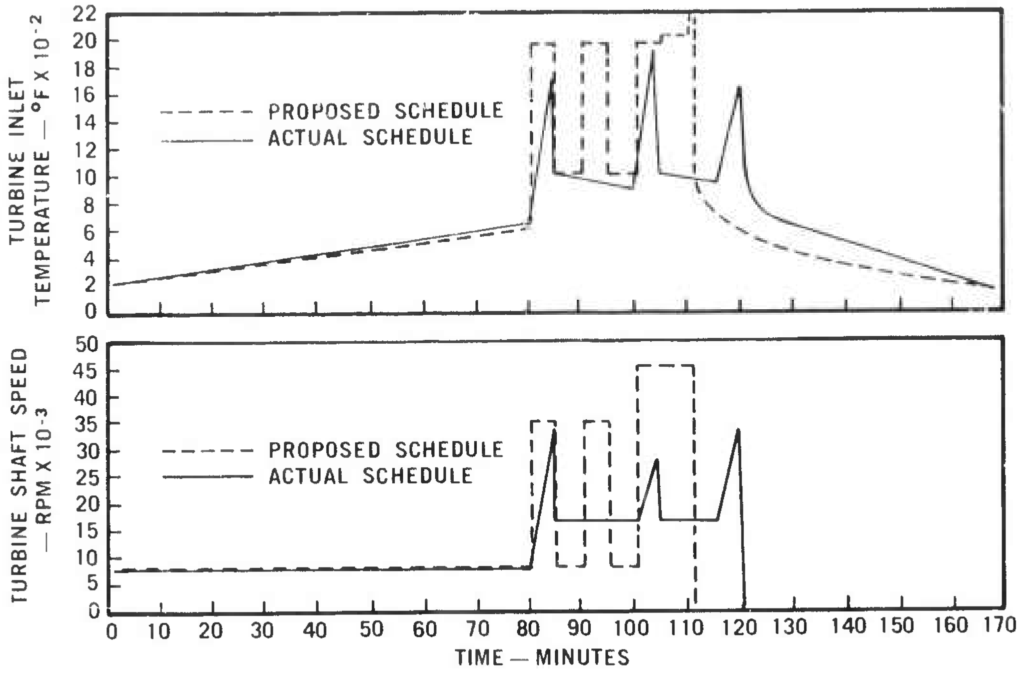

Figure 3.16 Proposed and Actual Speed and Temperature Schedules

Engine Testing of Ceramic Rotors

A set of ceramic rotors with 10% height blades were fabricated from reject parts for testing in a complete engine. The associated ceramic components required for the test were qualified and the rotor bolting system modified to incorporate the latest changes previously described. However, the final build of the main rotor assembly was held up because of problems of balancing and curvic coupling lubrication.

Attempts to balance ceramic wheels using the Nickel Ease (TM) lubricant previously used to reduce friction between metal and ceramic curvic teeth proved to be difficult and non-repeatable. The graphite particles in the lubricant produced minute changes in the meshing of the curvic teeth resulting in changes in unbalance of 0.015-0.020 in-oz (0.005 in-oz is current unbalance limit in the rotor shaft assembly). This value of unbalance was reduced when the parts were clamped and unclamped indicating that a crushing or flattening of the graphite was taking place. The rotors were assembled without balance problems using a lubricant made of 40 micron nickel powder and light oil. This nickel/oil combination, however, resulted in failure of the ceramic curvic coupling when used as the only lubricant in a load and thermal cycle test, which simulated the load and thermal expansion of engine parts. Nickel Ease had previously passed several cycles of this test.

A replacement lubricant, Dow Corning Molykote 321, has been tested which results in repeatable balance, and recoating without disturbing the assembly balance. It has also passed a modified load thermal cycle which included two soaks, one for 1/2 hour at 1075°F and another for 1 hour at 1400°F, without failures in the ceramic teeth. Based on these results the ceramic rotors with 10% height blades will be assembled using the Molykote lubrication for testing in a complete engine.

3.2 CERAMIC STATORS, ROTOR SHROUDS, NOSE CONES, AND COMBUSTOR DEVELOPMENT

SUMMARY

A three-dimensional heat transfer and thermal stress analysis of the first stage stator was conducted by Lawrence Livermore Laboratory (12) for a cold start-up transient. The maximum principal tensile stress of 2600 psi occurs four seconds after light-off and is in the trailing edge of the airfoil near the inner shroud.

Stators of 2.55 gm/cm^3 density were injection molded utilizing die cavity evacuation, a redesigned gating system and an overflow reservoir. These changes along with an improved system of alignment of the die halves resulted in fabricating improved quality stators. Preliminary molding of 2.7 gm/cm^3 stators was initiated. The Design D nose cone injection molding tooling was received. Checkout of this new tooling and fabrication of stationary flow path components has been deferred in order to concentrate on injection molding rotor blade rings as part of the Turbine Rotor Task Force.

Stator vane bend testing confirmed the improvements made in both the material and the fabrication process. Thermal shock rig testing of 2.7 gm/cm^3 vanes resulted in 2 vanes surviving 1000 cycles to 2500-2600°F plus 3720 cycles to 2900°F, however, some glass formation and leading edge erosion occurred.

Fourteen new stators successfully passed the qualification light-off test and, along with two stators which were previously qualified, accumulated 440 hours of hot running. One stator was rig tested at 1930° for 175 hours and is in excellent condition.

Two new designs of the silicon carbide "REFEL" combustor successfully passed the ten hour qualification test for ceramic combustors.

Seven of eleven nose cones passed the light-off qualification test but have subsequently cracked. Internal molding flaws, an interim design modification and removal of bell insulation are the prime suspects. The insulation has been replaced and the design updated.

Eight hours of testing at 2500°F were accumulated in the 2500°F Flowpath Qualification Test Rig, part of this time was on rig checkout. A stator and nose cone survived three hours at 2500°F but were both cracked after four hours and ten minutes.

Development of the stationary flow path components will continue on a limited basis until the termination of the Turbine Rotor Task Force when fabrication of these components will resume.

3.2.1 DESIGN AND ANALYSIS

A three dimensional thermal stress analysis of the first stage stator was conducted by Lawrence Livermore Laboratory (12). The analysis assumed constant material properties as follows:

.Thermal conductivity	$K = 0.418$ BTU/(hr.) (in.) (°F)
.Specific heat capacity	$C_p = 0.269$ BTU/(lb.) (°F)
.Elastic modulus	$E = 17.0 \times 10^6$ psi
.Poisson's ratio	$\nu = 0.25$ in./in.
.Thermal coefficient of expansion	$\alpha = 1.3 \times 10^{-6}$ in./(in.) (°F)
.Density	$\rho = 0.083$ lb./in.^{3}

The thermal boundary conditions used represented a cold start-up transient, starting with the stator at a uniform initial temperature of 60°F and suddenly introducing hot gas at 1970°F through the stator annulus. Heat flow to the structure was predicted using predetermined convection coefficients reported earlier (7). Those surfaces not exposed to hot gas flow were assumed to be insulated.

The mechanical boundary conditions imposed were those required by a repetitive structure, approximated by roller boundaries on the cut faces of the single segment taken from the complete stator ring.

The analysis was conducted using the SAP IV computer code utilizing 424 discrete eight node isoparametric elements and 810 nodal points. The conclusions of the Livermore analysis were as follows:

(1) The critical region in the first stage stator during start-up transient is the trailing edge of the airfoil near the inner shroud (see Figure 3.17).

(2) The maximum principal tensile stress during this transient occurs four seconds after light-off and is about 2600 psi.

(3) The highest stresses are a result of incompatibility of thermal response between the major parts of the component, (i.e. heavy outer and inner shrouds with low thermal response and a delicate airfoil with quick response).

It should be pointed out that there are some significant limitations with this analysis as indicated below:

(1) The material properties were assumed to be temperature independent.

(2) The finite element model was not sufficiently refined in the region of the airfoil root fillet to determine stresses in that area.

(3) Stresses were calculated at element centroids, thus any stresses due to bending were not indicated.

(4) The mechanical boundary constraints utilized were adequate for a repetitive structure under symetrical loads. However, due to thermal gradients and the non-symetrical airfoil, the loading was nonsymetrical.

More detailed information is presented in Reference (12).

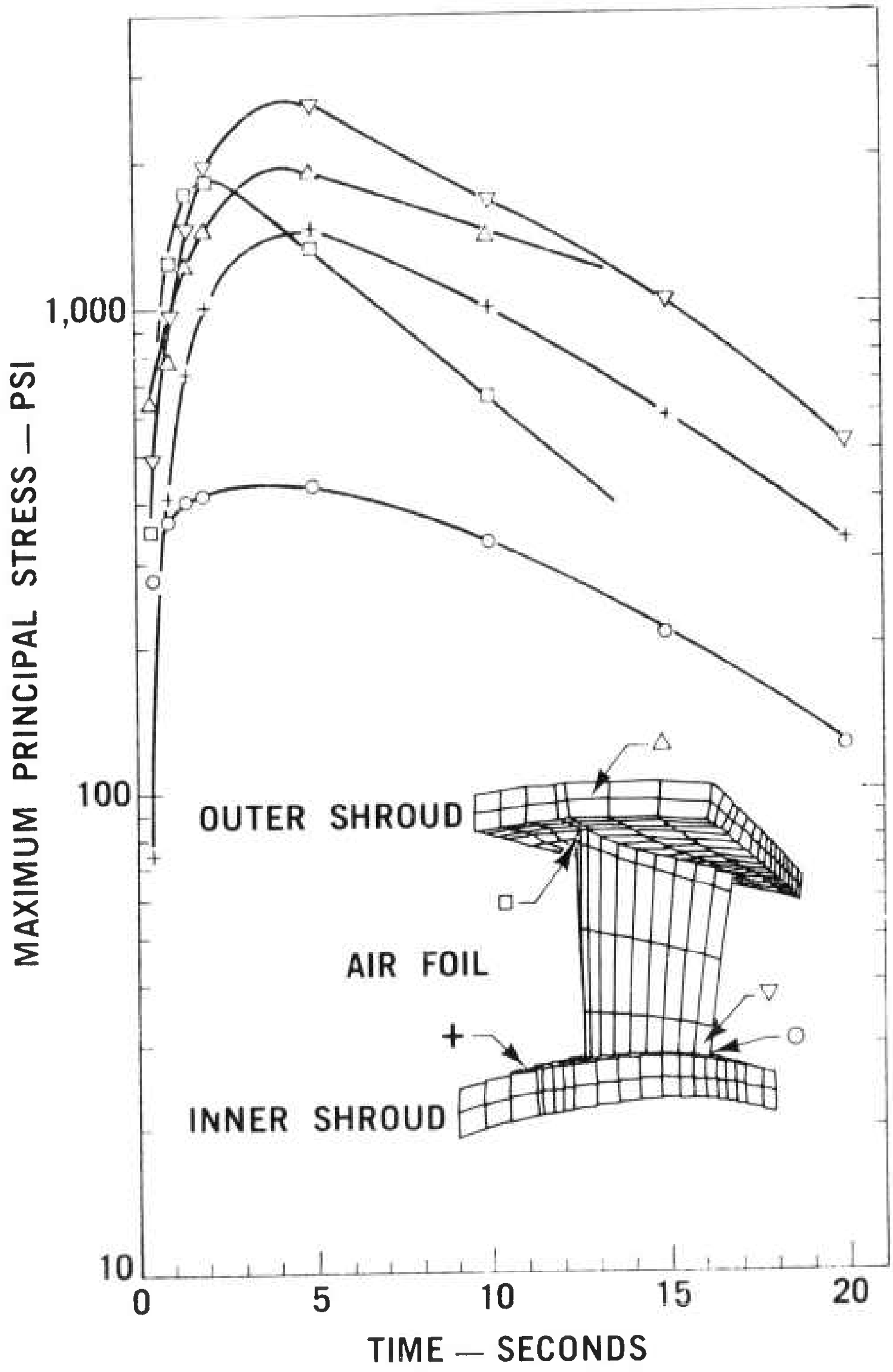

Figure 3.17 Maximum Principal Stress (At Element Centroids) vs Time for Selected Points in 1st Stator

3.2.2 MATERIALS AND FABRICATION

Introduction

Development of molding technology required to fabricate flaw free Si_3N_4 stators of 2.55 and 2.7 gm/cm^3 density continued during this reporting period. Utilization of cavity evacuation, improved material gating, and other die modifications resulted in molded stators which are flaw free by current NDE techniques.

Modifications were made to update the nose cone tooling to the latest flow path configuration. These changes have been completed and the new tooling is ready for molding trials when fabrication of stationary components is resumed at the end of the Turbine Rotor Task Force.

Silicon Nitride Stator Fabrication

As described in the last interim report (8), the use of vacuum was successful in eliminating entrapped gas flaws in stators of 2.55 gm/cm^3 density. This system was developed to a point where previous problems, such as material entry into the vacuum system and vacuum leakage, were eliminated. A positive shutoff nozzle was also installed to prevent material from being drawn into the die during evacuation prior to injection.

Although vacuum eliminated most flaws, some gas bubbles which entered the die with the initial mass of injected material were trapped in a three vane segment which was the last areas to fill (8). A redesigned gate detail was fabricated and installed in the tooling which eliminated these flaws. The material was gated to enter the stator at the six-o'clock position and allowed to exit the stator cavity into an overflow reservoir at the 12-o'clock position. The reservoir volume was set at 20% of the cavity volume. Entrapped gases as well as excess mold release, which tended to be pushed through the die at the front of the flowing material, were effectively flushed into the reservoir.

The occurrence of inner shroud cracks at the fillets between the vanes and inner shrouds due to the inaccuracy of clamping release on the molding machine, have been minimized. [illegible] modifications to the tooling were required to reduce its sensitivity to misalignment in the molding machine.

It was determined that the molding machine has a 0.004 inches/inch inaccuracy in alignment as the clamping force was released and the die opened. Elimination of this inaccuracy is impractical on a large molding machine, thus the die has to be made insensitive to the misalignment. Four shear plates were added to the tooling in an effort to correct the misalignment over a limited range of the die opening cycle. Shear plates are hardened steel plates which guide the die during the opening cycle and restrict its movement in one direction. These plates proved only partially successful as occasional cracking at the the stator inner shroud still occurred.

Adding a taper to the inner shroud inside surface proved effective in eliminating the occasional cracking of 2.55 gm/cm^3 stators. The taper is 0.005 inches/inch, exceeding the misalignment by 0.001 inches/inch. This eliminates the interference condition which occurred between die halves during opening of the press.

Preliminary molding of 2.7 gm/cm^3 material was initiated, however, production of flaw free stators was not accomplished. More development is required to eliminate occasional vane cracking at the vane inner shroud fillet and internal voids. These efforts were interrupted when the Rotor Task Force was formed in order to concentrate on injection molding rotor blade rings.

Silicon Nitride Nose Cone Fabrication

During this reporting period, modifications were made to the nose cone tooling to update it to the latest flow path configuration. New cavity details were fabricated to enable the Design D nose cone to be molded. Interchangeability was maintained so that Design B and C nose cones can still be fabricated if required.

Positive insert locks were added to the tooling to replace the temporary insert locks previously used. These locks will hold the inserts in a closed position until the core pins in the struts have been removed. Movement of the insert prior to pin removal has produced strut cracking.

Silicon Nitride Rotor Shroud Fabrication

No development work was carried out on rotor shroud fabrication during this reporting period. The continued emphasis to use existing nondestructive methods to determine component quality did, however, reveal variations in elastic modulus in specific lots of fabricated shrouds. These differences were detected in the nitrided state using sonic velocity measurements to calculate Young's modulus. The data is reported in Section 4.7 of this report.

3.2.3 TESTING

Introduction

The stationary hot flow path components include the combustor, turbine inlet nose cone, common first and second stage stators, and first and second stage rotor tip shrouds. In order to evaluate these components, five different types of test rigs are employed. The Thermal Shock Test Rig is used to test stator vane design modifications and materials; the Combustor Test Rig is used for combustor evaluation; the 2500°F Flow-path Test Rig is used to evaluate all of the stationary components up to temperatures of 2500°F; Engine Test Rigs are used for light-off qualification and durability testing, and a Stator Vane Load Test is used to monitor quality control of stator fabrication.

Stator Vane Load Testing

Stator vane testing was initiated as a basis for establishing a quality control measure to assess material and process improvements(8). During this report period, stator vane testing was used to monitor changes in material and nitridation cycles for a given lot of stator assemblies which were eliminated as engine test candidates due to flaws at the as-molded stage. Only vanes which were unflawed by stringent visible examination were subjected to load testing.

The statistical results of these vane loading tests are shown in Figure 3.18 The crosshatched area represents Weibull distributions for mechanically tested stators from several independent nitridings. The data indicates that the changes previously made in the fabrication process resulted in producing stator assemblies of much better quality for engine testing.

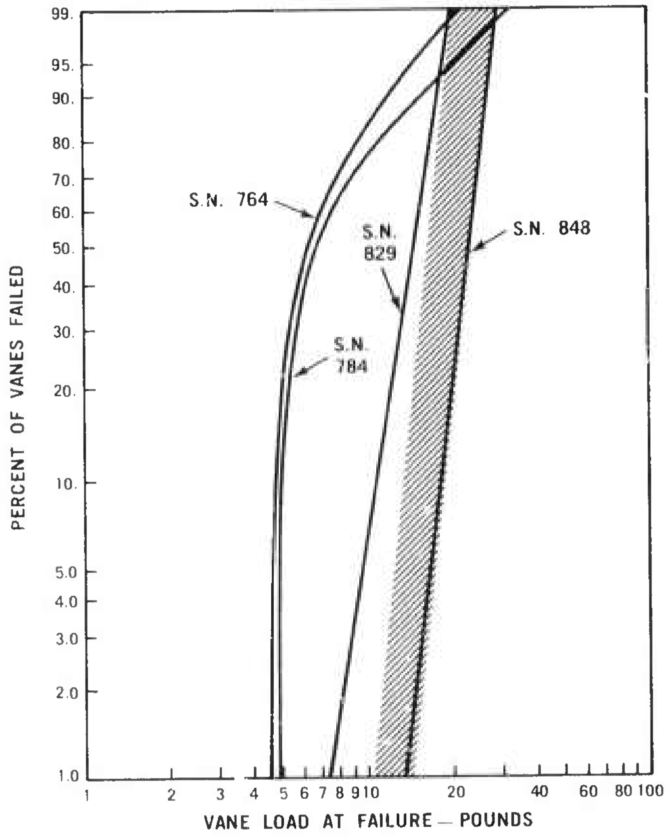

Figure 3.18 Weibull Distributions of Stator Vane Failure Loads

Thermal Shock Rig Testing

Thermal shock testing on 2.7 gm/cm^3 stator segments was continued. Six test segments previously tested to 1000 cycles at 2500 - 2600°F were further subjected to tests at part temperatures of 2900°F. Cycle time was 45 seconds heating, 135 second cooling, and the resulting down shock was 800°F/sec maximum. Two of the six vanes were tested for 3720 cycles without failure. Of the four failures, two were at the midspan of the vanes and two were at the base of the vanes. Failures occurred at 1812 cycles, 2056 cycles, 2800 cycles and 3120 cycles. There was some glass formation and leading edge erosion on all samples.

Ceramic Combustor Testing

Evaluation of ceramic combustors has been conducted by subjecting prototype components to a series of tests simulating engine conditions. During previous reporting periods (4,6,7,8) tests were conducted with dense, high strength, reaction bonded silicon carbide (REFEL), which showed it was a very good candidate for combustor tube material.

The steady-state combustor test rig used is shown in Figure 3.19. This rig provides a simulation of the steady-state operating conditions that a combustor experiences in an engine, and its features were described in some detail in a previous report (6).

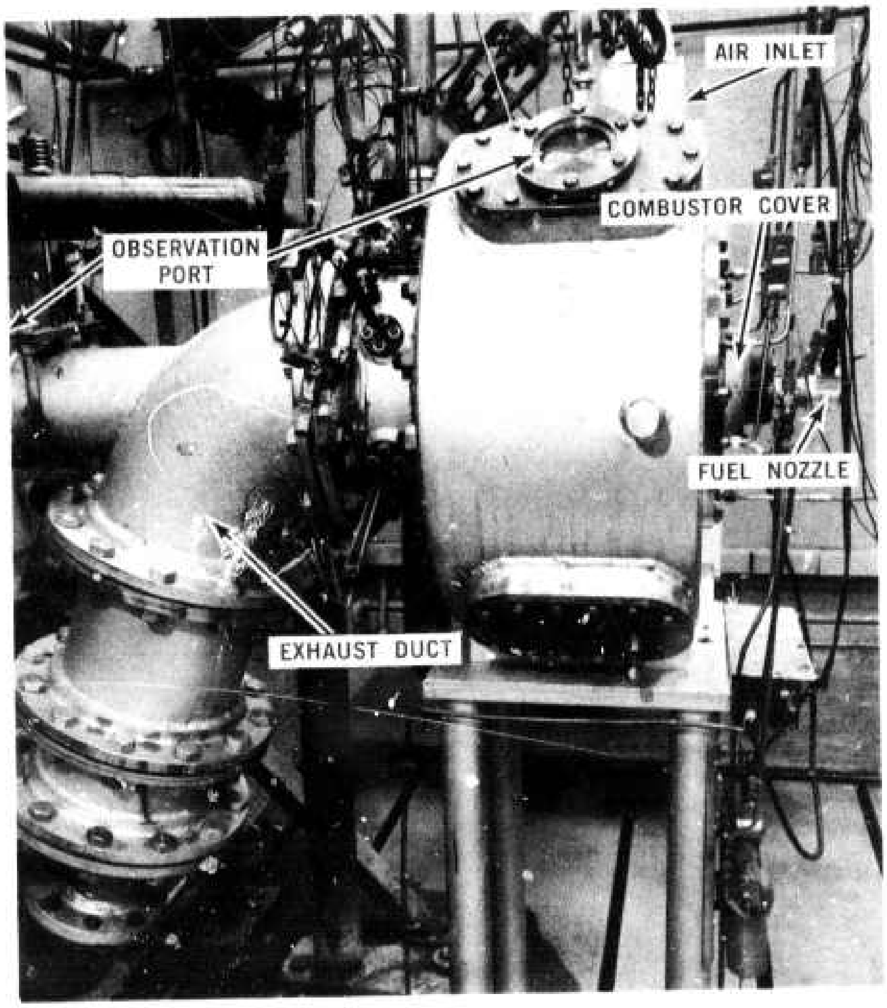

Figure 3.19 Combustor Test Rig

During this reporting period, two new designs of the silicon carbide "Refel" combustor tube were evaluated, each over a 10 hour portion of the ARPA durability cycle. There were no cracks or other visual damage. The conditions and time of the 10 hour durability cycle are listed in Table 3.3, Figures 3.20 and 3.21 are photographs of these combustor tubes. Further 10 hour qualification tests of additional components will be completed to assess the consistency of combustor durability under this test. One of the new designs will then be selected as primary candidate for the 200 hour ARPA cycle durability test.

TABLE 3.3

ARPA DURABILITY TEST CYCLE
FOR CERAMIC COMBUSTORS

Equivalent Engine Speed %	T_6 °F	P_6 psia	W_a PPS	T_7 °F	Time Hours-Minutes
55	1628	24.7	0.63	1930	4 - 30
59	1590	26.9	0.71	1930	2 - 30
69	1495	33.3	0.93	1930	- 40
77.5	1413	40.8	1.15	1930	- 30
86.5	1337	50.1	1.41	1930	- 30
100	1680	70.9	1.95	2500	1 - 20
					10 hours

T_6 - inlet air temperature to the combustor

P_6 - inlet air pressure to the combustor

W_a - combustor airflow (pounds per second)

T_7 - exit gas temperature from the combustor

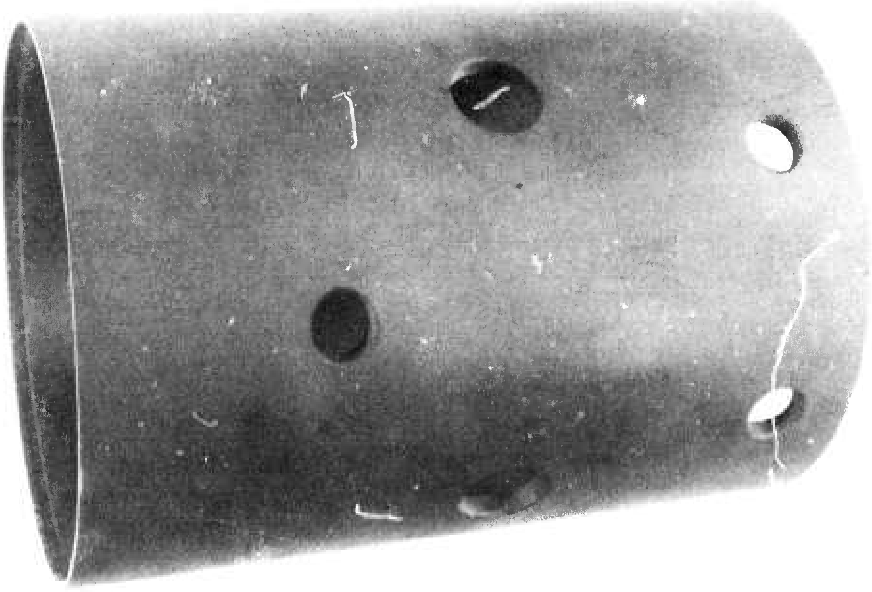

Figure 3.20 Thick-Wall Silicon Carbide "REFEL" Combustor

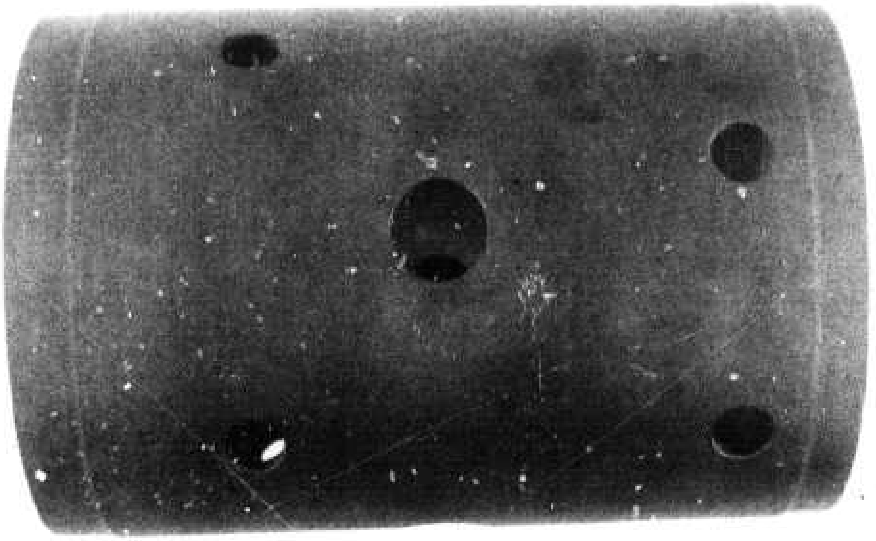

Figure 3.21 Thin-Wall Silicon Carbide "REFEL" Combustor

Engine and Rig Testing

Evaluation of turbine inlet nose cones, first and second stage stators, and first and second stage rotor tip shrouds continued in engine test rigs. Each component was qualified by subjecting it to 10 cold lights followed by immediate engine shutdown prior to any longer time durability testing.

Tables 3.4 to 3.6 show the results of engine testing on silicon nitride ceramic stationary components performed to date, with the top lines indicating the target values established for each component. Testing during this reporting period was concentrated on the light-off qualification test and static engine tests.

The major effort on nose cones has been on the evaluation of higher density (2.55 gm/cm^3) silicon nitride components with a new design modification necessary because of the incorporation of thermocouple holes. Seven of eleven nose cones successfully passed the light-off qualification test. Three of the failed parts cracked through obvious flaws. The remaining 7 components have accumulated over 189 hours of hot running, but all have cracked. Four failed in the inner body, two failed in the outer shroud, and one failed during handling.

There are two probable causes for inner body cracks. First, an interim design modification was incorporated to allow for utilization of on-hand Design B parts in the new Design D configuration and second, an evaluation of reduced inner body insulation was undertaken. Since previous nose cones without these modifications ran successfully, these changes are believed to be the cause of the inner body failures. In order to verify this, two nose cones without these modifications were each tested for over 30 hours without an inner body failure. However, testing was terminated because one nose cone developed an outer shroud crack and the other was broken during handling. Evaluation of this type of nose cone is continuing.

TABLE 3.4

SUMMARY OF NOSE CONE TESTING

Material and Design Identification Number	Static Engine Testing				Cyclic Testing (ARPA)					2500 F Static Testing		Miscellaneous Tests		Component Status	Total Part Time Hours**	Total Part Lights
	Light (Cold)	Shutdowns Cold	Shutdowns Hot	Hours**	Lights Cold	Lights Hot	Shutdowns Cold	Shutdowns Hot	Hours**	Lights	Hours	Lights	Hours**			
Target	10	9	1	0.2	14	26	-	40	200	4	25					
S-73												142	16.75	F	16.75	142
1-102*	25	18	7	24.5	44	36	21	59	221.5					F,B	246.00	105
1-103	19	17	2	0.40	1	2	0	3	50.5					F,O	50.90	22
1-130					5	3	2	6	24.5					F,H	24.50	8
S-202*	10	9	1	0.20	9	2	9	2	6.5	1	5.0	1	18.30	F,C,O,X	30.00	28
2-207*	60	51	9	37.9	6	10		16	42.8			4	9.8	F,B	90.50	80
1-304*	46	42	4	2.00								15	50.3	F,C,O,X	52.3.	61
2-320												10	1.15	F,X	1.15	10
2-321	30	27	3	0.50								29	27.50	F,X	28.00	59
3-806*	27	20	7	18.5	1			1	13.25			6	2.50	F,B	34.25	34
3-807*	64	58	6	1.23										F,C,X	1.23	64
3-814*	19	13	6	33.91										F,C	33.91	19
4-871*	14	9	5	62.25										F,B	62.25	14
4-872*	56	51	5	1.1										F,B	1.10	56
4-875*	10	9	1	0.25						3	4.2	2	1.85	F,B	6.3	15
4-876*	16	9	7	55.50										F,B	55.50	16
4-889*	40	36	4	1.00										F,C	1.00	40
S-890*	19	14	5	32.1										F,H	32.1	19
4-903*	10	9	1	0.25										F,C,X	0.25	10
4-910*	12	11	1	0.25										F,B	0.25	10
4-916	26	18	8	30.90										F,C	30.90	26
4-917*	10	9	1	0.25										F,C,X	0.25	10
4-920*	10	9	1	0.25										F,B,X	0.25	10

*New entry this reporting period **Up to 1930°F

Key to Component Status
F = Failed
O = Failure occurred in other than ARPA duty cycle
H = Part failed during handling
C = Cracked shroud
B = Inner body crack
X = Internal material flaw involved in failure

TABLE 3.5

SUMMARY OF STATOR TESTING

Material and Design Identification Number	Static Engine Testing				Cyclic Testing (ARPA)					2500°F Static Testing		Miscellaneous Tests		Component Status	Total Part Time Hours**	Total Part Lights
	Light (Cold)	Shutdowns Cold	Shutdowns Hot	Hours**	Lights Cold	Lights Hot	Shutdowns Cold	Shutdowns Hot	Hours**	Lights	Hours	Lights	Hours**			
Target	10	9	1	0.2	14	26	-	40	200	4	25					
1-372*	10	9	1	0.20	1	2	0	3	50.5			2	7.9	F,V,I,O	58.60	15
2-421	10	9	1	0.20								3	2.80	C,X	3.00	13
2-424	10	9	1	0.25								9	2.75	C,X	3.00	19
2-428	10	9	1	0.20	17	14	6	25	103					F,C	103.20	41
2-430	10	9	1	0.20	14	13	6	21	61.5					F,C	61.70	37
1-715	10	9	1	0.20								6	0.10	F,V,O	0.30	16
1-751	11	10	1	0.20								2		C,V,O,X	0.20	13
2-817	34	31	3	0.75										S	0.75	34
1-820	14	13	1	0.30										C,X	0.30	14
1-841*	12	11	1	0.20	6	10		16	42.8					F,C	43.00	28
1-848	11	10	1	0.20										F,H	0.20	11
1-852*	23	20	3	1.70										F,O	1.70	23
1-858*	12	11	1	0.20	6	10		16	42.8					F,C	43.00	28
1-865*	12	11	1	0.25								2	9.50	F,V,I,O	10.15	14
1-868*	12	11	1	0.25								2	9.50	F,V,I,O	10.15	14
2-880*	10	9	1	0.25								1	5.00	S	5.25	11
3-889*	43	39	4	17.4										S	17.4	43
3-898*	10	9	1	0.25										S	0.25	10
1-911*	15	9	6	54.25										F,V	54.25	15
2-911A*	11	10	1	0.25						1	.25	11	21.75	F,V,I,O	22.25	23
4-924*	10	9	1	0.25								1	0.50	F,V,X	0.75	11
4-940*	29	15	14	32.75										F,C	32.75	29
4-943*	10	9	1	0.25						3	4.2	1	1.45	F,C	5.9	14
4-954*	19	9	10	175.00										S	175.00	19
3-955*	12	9	3	23.00										F,C	23.00	12

*New entry this reporting period **Up to 1930°F

Key to Component Status
S = Serviceable
F = Failed
O = Failure occurred in other than ARPA duty cycle
H = Part failed during handling
C = Cracked shroud
V = Vane(s) failed
X = Internal material flow involved in failure
I = Impact failure from combustor carbon

TABLE 3.6

SUMMARY OF SHROUD TESTING

Material and Design Identification Number	Static Engine Testing				Cyclic Testing (ARPA)					2500°F Static Testing		Miscellaneous Tests		Component Status	Total Part Time Hours**	Total Part Lights
	Light (Cold)	Shutdowns Cold	Shutdowns Hot	Hours**	Lights Cold	Lights Hot	Shutdowns Cold	Shutdowns Hot	Hours**	Lights	Hours	Lights	Hours**			
Target	10	9	1	0.2	14	26		40	200	4	25					
First Shrouds																
1-24	19	17	2	0.40	1	2	0	3	50.50					S	50.90	22
1-111	13	[illegible]	1	0.20	61	41	34	68	245.00					S	245.20	115
2-119*	15	13	2	0.25										F,C	0.25	15
2-120*	12	11	1	0.25										S	0.25	12
2-124*	10	9	1	0.25										S	0.25	10
Second Shrouds																
3-2*	10	9	1	0.25										F,C	0.25	10
3-3*	12	11	1	0.25										S	0.25	12
3-4*	10	9	1	0.25										F,C	0.25	10
4-6												3	1.75	F	1.75	3
4-38	19	17	2	0.40	1	2	0	3	50.5					S	50.90	22
4-100					1	9	0	10	11.0			30	1.60	S	12.60	40
4-102					1	9	0	10	7.8					S	7.80	10
4-104												75	5.10	S	5.10	75
4-106	10	9	1	0.20	61	41	34	68	245.00					S	245.20	112

*New entry this reporting period **Up to 1930°F

Key to Component Status
S = Serviceable
F = Failed
C = Cracked shroud

Outer shroud cracks were probably due to reduced strength in the outer shroud resulting from slotting modifications incorporated when thermocouple holes were included in the part. In order to strengthen the weakest section, where the cracks had occurred, the slots were angled to increase the section size. One nose cone was made with this modification and was serviceable after 30 hours of test when it was broken in handling. Evaluation of this concept is continuing.

Fourteen new stators successfully passed the light-off qualification test. These stators plus two others accumulated over 440 hours of hot running during this reporting period. Four stators remain serviceable while five others failed, two due to improper processing and four due to carbon impact from an experimental combustor in the 2500°F flow path rig.

The problem of improper processing involved stators 841, 848, and 858. Although these stators were originally thought to be good, as mentioned in the last report (8), it was discovered that the furnace in which they were nitrided was improperly sealed allowing oxygen to be present during the nitriding cycle. After this was discovered, the parts were expected to have a short life span. Subsequent testing verified this since stators 841 and 858 failed after 42 hours of testing. Stator 848 was broken during handling.

This problem has been corrected and in addition, a nitriding cycle change has been incorporated. Using these changes three stators were made for testing. Unfortunately during finish grinding of two of these stators some chipping of the outer shrouds occurred. All three stators were tested. Two failed after 5 and 32 hours, believed due to stresses caused by the poor finish machining. However, the third stator, which had good finish grinding, was tested for 175 hours and is in excellent condition as shown in Figure 3.22. Further stators from this system will be evaluated.

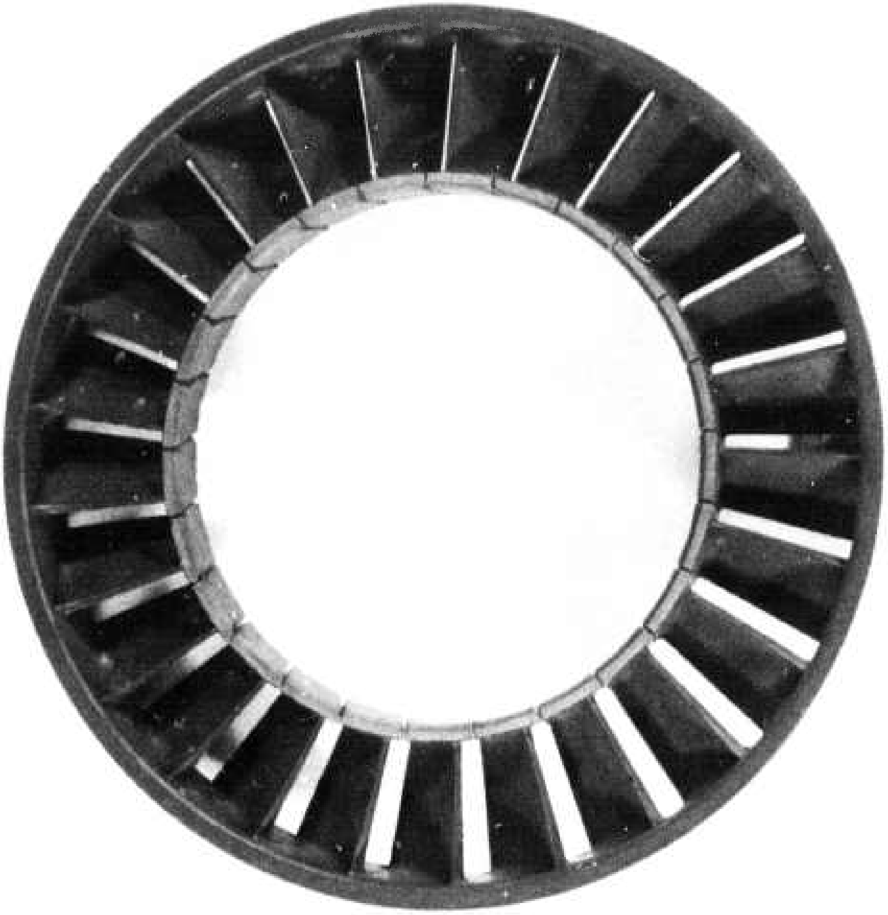

Figure 3.22 Silicon Nitride Stator After 175 Hours of Durability Testing

One piece SiC stators were fabricated (7) and subjected to the normal light-off qualification test (8). During this reporting period, we had planned to conduct further testing on the remaining SiC stators (8), but the specially-machined nosecone used to run SiC stators was broken during handling. A replacement nose cone is being prepared so that further SiC stator testing can start early in the next reporting period.

Three of six shrouds successfully passed the 10 light qualification test while the three that failed were broken due to a failure of the adjacent supporting structure. Evaluation of shrouds is continuing.

2500°F Flow Path Test Rig

The major part of this reporting period was devoted to developing the rig capability to operate at a temperature of 2500°F. This effort involved the following:

1. Development of a metal combustor to operate at a turbine inlet temperature of 2500°F. (Since the 2500°F Flow Path Test Rig is non-regenerative, a special combustor was needed which can be metal. A metal combustor is preferred during early testing in this rig.)

2. Investigate and improve the complete combustion system for operation at various flow conditions.

3. Investigate several alternate temperature sensors to monitor and control turbine inlet temperature.

4. Develop procedures for the control of the rig during starting, transients, steady state, shutdowns, and emergency situations.

5. Monitor performance of rig components and make modifications to correct problem areas.

As of the end of this reporting period, 8 hours of rig running time at 2500°F were accumulated. Approximately half of this time, during rig checkout, previously damaged flow path hardware was used.

A nose cone and a stator each accumulated 4:10 hours of component durability at 2500°F. The test history of these components is shown in Table 3.7. Both were made of injection molded Si_3N_4 with a density of 2.55 gm/cm^3.

TABLE 3.7

TEST HISTORY OF COMPONENTS AT 2500°F

	Accumulated Time (Hrs/Min)	Inspection Results
Nose cone S/N 875	1:30	OK
	3:00	OK
	4:10	Inner body cracked; no parts missing
Stator S/N 943	1:30	OK
	3:00	OK
	4:10	Outer shroud broken in two places; no vane failures; no parts missing

The inspection of the failed parts showed that:

1. No obvious material flaws were found on the broken sections.

2. The insulation on the nose cone shrank away from the inner body, thus losing much of its effectiveness and probably resulted in a higher than normal thermal stress.

3. The stator outer shroud was chipped in several places. The origin of the chipping was traced to a faulty grinding operation which was performed on the stator just prior to the test. Investigation of this failure is continuing.

During the next reporting period, a complete disassembly and rebuild of the rig will be performed in order to replace cracked ducting parts. 2500°F testing of flow path components will resume as soon as the rig is rebuilt.

4. PROGRESS ON MATERIALS TECHNOLOGY - VEHICULAR TURBINE PROJECT

SUMMARY

Materials technology is a very important portion of the systems approach employed in this project for the development of high temperature gas turbine engines. The generation of ceramic material property data, in progress since the beginning of the project, has been instrumental in component design modifications and failure analysis. As testing and fabrication experience was gained, improvements in materials have also been made. The properties of these improved materials are determined and fed back into design modifications and failure analysis, thus closing the loop. The work on determining material properties and on generating material improvements for the vehicular ceramic turbine project is reported in this section.

Initial measurements of strength and Weibull slope at several temperatures were made on different compositions of hot-pressed Si_3N_4, including process variations of contoured hubs from press-bonded duo-density rotors and hot-pressed flat billets. Elastic properties were measured up to 1800°F for press-bonded hubs of 2 and 5 w/o MgO contents, showing slightly lower values with the 5% material. Thermal expansion determinations show a trend of higher expansions as MgO content increases.

Development work was continued on 2.7 gm/cm^3 density injection molded Si_3N_4, and improvements were made in flow and mold release properties. It was also found possible to mold test bars of material with densities as high as 2.82 gm/cm^3. Work on methods for reducing the oxidation of 2.7 gm/cm^3 molded Si_3N_4 has shown that a rapid pre-oxidation at 2660°F, intended to produce a protective oxide surface film without appreciable internal oxidation, improved the weight and thermal expansion changes after oxidation testing. Preliminary stress-rupture tests in bending indicated that the 2.7 gm/cm^3 molded Si_3N_4 had good life at temperatures up to 2400°F and stresses up to 35 ksi.

Short term testing was performed to evaluate the behavior of turbine ceramic materials when exposed to the combustion products resulting when lead-containing gasoline was used as turbine fuel. No deleterious effects were found when these materials were examined.

High temperature fracture characteristics of ceramic turbine materials continue to be investigated. To date, no evidence of subcritical crack growth at temperatures up to 1400°C has been observed in reaction sintered Si_3N_4. Subcritical crack growth was noted in "REFEL" reaction sintered SiC, and appears to be primarily influenced by the silicon phase present in this material.

In the application of non-destructive evaluation techniques to turbine ceramics, it was found that the sonic velocity of reaction sintered Si_3N_4 responds to changes in nitriding parameters. This adds further to the usefulness of this measurement, since it provides a means of evaluating the effects of changes in the fabrication process on actual turbine engine components.

PRECEDING PAGE BLANK-NOT FILMED

4.1 PROPERTIES OF HOT PRESSED SILICON NITRIDE

Introduction

The strength, elastic modulus and thermal expansion properties have been determined for various preliminary grades of Ford hot pressed silicon nitride. The starting powder for hot pressing was A.M.E. CP-85 grade. CP-85 is A.M.E.'s designation for a commercially pure grade of silicon nitride powder for hot pressing. "CP" is the abbreviation for "controlled phase", referring to a content of at least 85% alpha phase material. The calcium content of this material is between 0.3 and 0.7 w/o.

Strength Properties

Four-point bending, at quarter-point loading, was used to evaluate the strength according to the Proposed Military Standards for Testing of Ceramic Materials (13). Top span was 3/8 inch, bottom span 3/4 inch; crosshead speed was 0.02 inch/minute. All samples were tested in the strong direction (perpendicular to pressing). The bend strength data are shown in Figure 4.1. Strength data for Norton's HS-130 hot pressed silicon nitride are also shown in Figure 4.1 for comparison purposes. "HP" refers to hot pressed flat billets while "PB" refers to press bonded rotors with contoured hubs. The rate of pressurization and the maximum pressure used to produce "PB" parts were lower than those used to make "HP" parts.

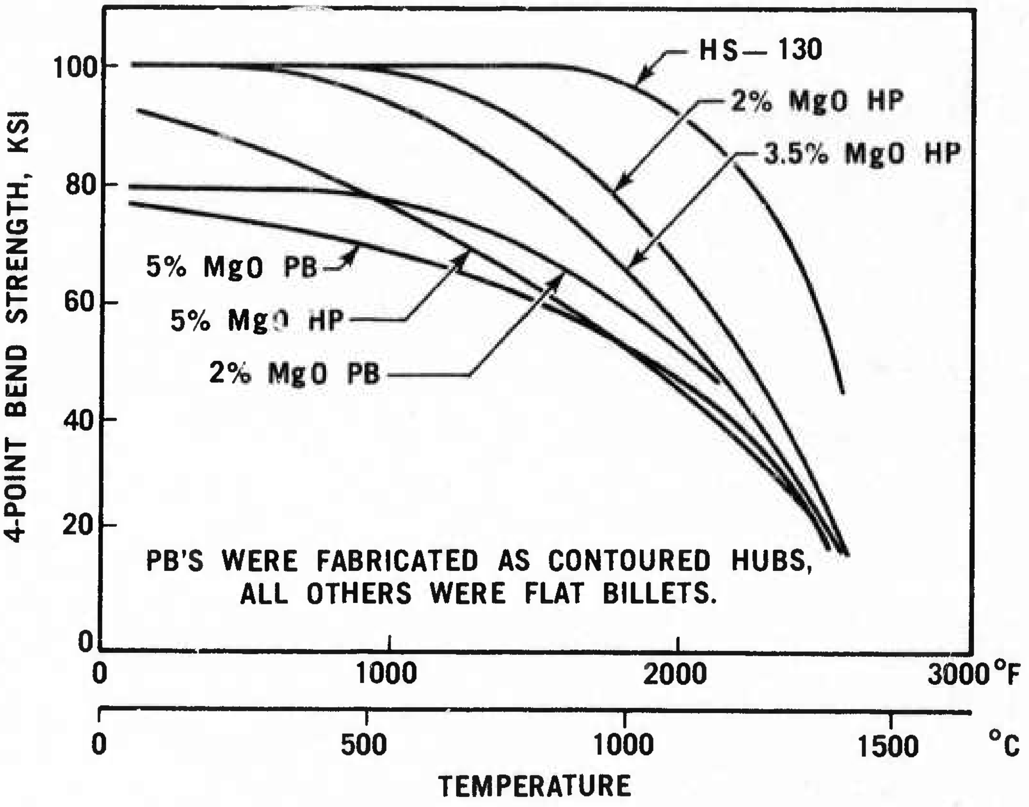

Figure 4.1 Mean Measured MOR vs Temperature for Several Grades of Si_3N_4

Based on the bend strength data, the Weibull slopes were determined using a "Most Likelihood Estimator", (14) (MLE), computer program. These results are tabulated in Table 4.1.

TABLE 4.1

WEIBULL SLOPE OF HOT PRESSED SILICON NITRIDE AT VARIOUS TEMPERATURES

Material	Temperature °F				
	78	1600	1900	2100	2300
2% MgO HP	4.11		10.48		
3.5% MgO HP	12.28		17.04		
5% MgO HP	5.31		11.50		
2% MgO PB	7.74	3.11		5.46	
5% MgO PB	5.90		4.90	6.10	8.80

Plans are underway to improve both the hot strength and the reliability of the hot pressed press bonded material. These include removal of foreign particles in the starting powder, optimization of powder particle size, rigid quality control in processing, reduction of calcium and oxygen contents, and optimization of MgO: SiO_2 molal ratio (15).

Elastic Modulus Measurements in Si_3N_4

Elastic moduli have been measured for two press-bonded Si_3N_4 samples (ρ = 3.17 gm/cm^3) having 2% and 5% concentrations of MgO in the starting Si_3N_4 powders.

Longitudinal and shear moduli data, together with Young's moduli calculated from the measured data, are shown in Figures 4.2 and 4.3.

The shear modulus was found to change only slightly with increasing MgO concentration in the 2-5% range investigated, and is within 5% of shear moduli obtained from measurements on other high density silicon nitrides.

The longitudinal modulus decreases with increasing MgO concentration by about 2% per 1% MgO. Longitudinal moduli of both press bonded samples are higher than for Norton hot pressed Si_3N_4; the 2% press bonded sampled has longitudinal moduli 20% higher than the Norton material.

Thermal Expansion Properties

Thermal expansions of rotor materials have been determined up to 2500°F. The average coefficients of thermal expansion for 5% MgO PBSN, 2% MgO PBSN, and 2.7 gm/cm^3 Slip Cast Silicon Nitride, (SCSN), are shown in Figure 4.4.

It can be seen that, as the MgO content increases from zero, in the slip cast material, to 5 w/o in the hot pressed material, the coefficient of thermal expansion increases. However, the rate of increase in thermal expansion with MgO content does not follow the rule of mixtures for silicon nitride and magnesia because the MgO has reacted to produce another phase or phases. The rule of mixtures can still be applied if the new phases have been identified and their weight fractions, coefficients of thermal expansion, bulk moduli and densities as functions of temperature are known.

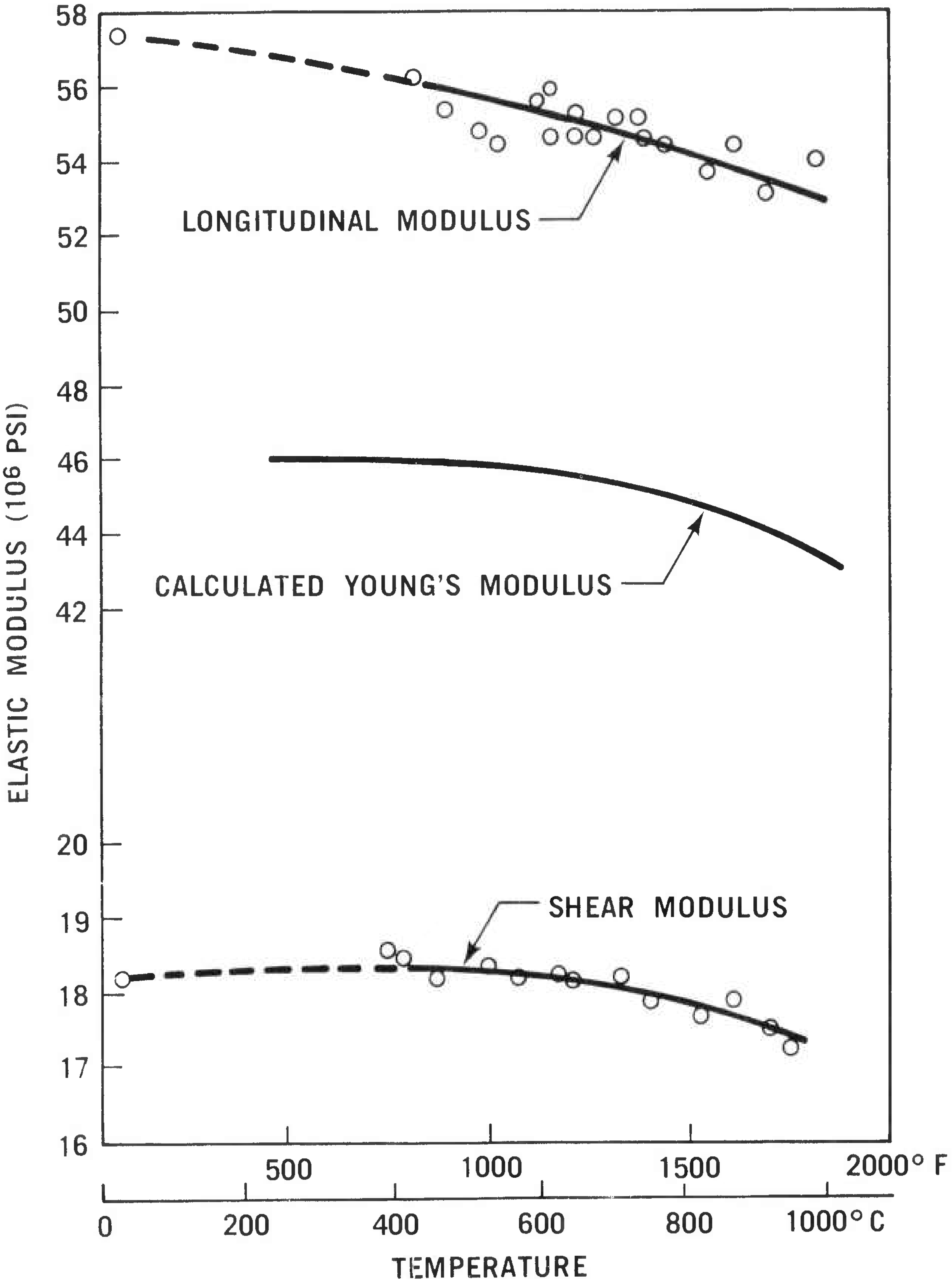

Figure 4.2 Elastic Moduli vs Temperature for Press-Bonded, 2% MgO Si_3N_4

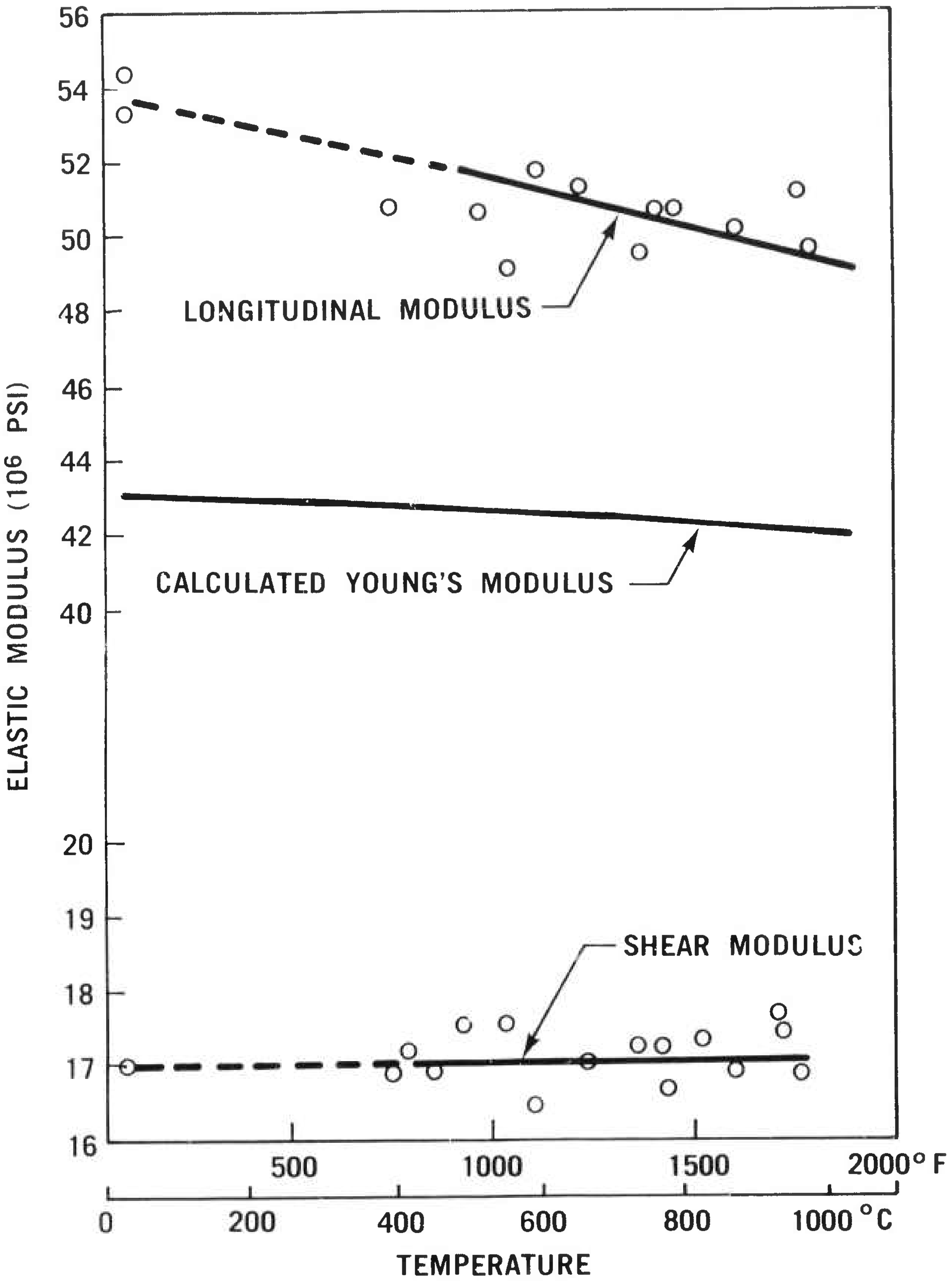

Figure 4.3 Elastic Moduli vs Temperature for Press-Bonded, 5% MgO Si_3N_4

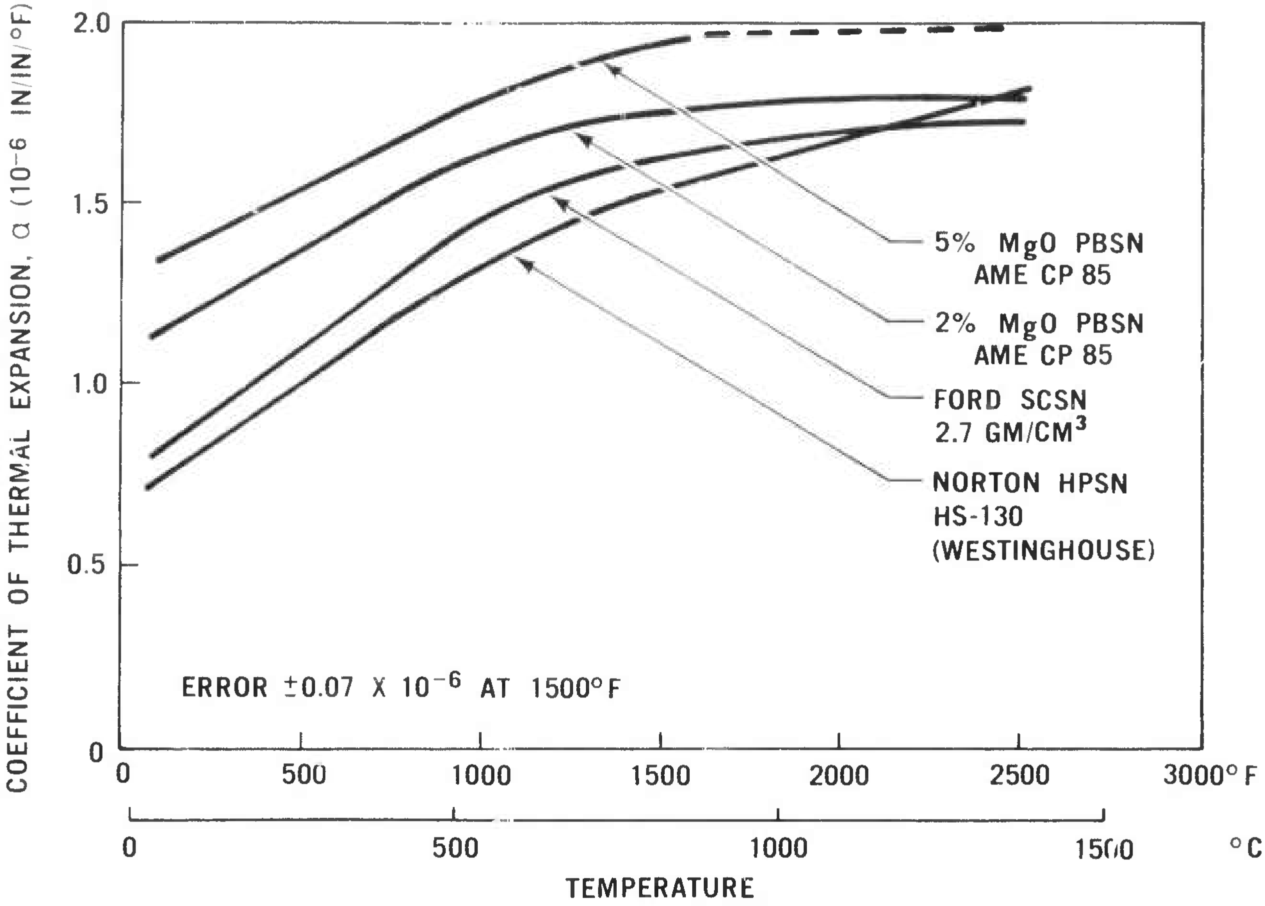

Figure 4.4 Average Coefficient of Thermal Expansion for Several Grades of Si_3N_4

4.2 PROPERTIES OF INJECTION MOLDED REACTION SINTERED SILICON NITRIDE

Introduction

In previous interim reports (7,8), work was presented on the theory of developing a highly loaded silicon-polymer injection molding composition and the implementation of this theory using various particle size distributions of silicon powder. The various molding compositions were quantitatively compared with regard to molding parameters. Nitriding experiments were also described that showed the strength of reaction sintered Si_3N_4 as a function of nitriding cycles.

In this report, molding compositions designed for use in the fabrication of the duo-density turbine rotor blade rings are described. Further experiments to optimize the nitriding of 2.7 gm/cm^3 Si_3N_4 material and initial nitriding experiments on 2.8 gm/gm^3 Si_3N_4 material are described. Preliminary physical property data is presented on early developmental samples of molded 2.7 gm/cm^3 Si_3N_4. These properties include Weibull strength data, oxidation and creep properties.

Molding Properties

In the last interim report (8), the molding properties of various molding compositions were presented. These compositions were adequate for molding stators. However, blade cracking during molding due to the mold release property and low green strength of the 74R and 75P1 compositions precluded their use in the turbine rotor tooling. Minor changes in composition were made to improve both these properties. The resulting compositions, 92HP, 92FP and 92GP, yielded Si_3N_4 densities of 2.6 gm/cm^3, 2.72 gm/cm^3 and 2.82 gm/cm^3 respectively. These are compared in Table 4.2 to the 75P1 composition. The spiral flow distance of 92FP is equal to the 75P1 composition while exhibiting over a 70% increase in green strength. Qualitatively, the mold release of the 92 series composition is better. As discussed in Section 3.1.2 both the 92HP and 92FP compositions produced flaw free rotor blade rings by x-ray.

The change in the organic composition made it possible to injection mold test bars yielding a Si_3N_4 density of 2.82 gm/cm^3 (92GP). The molding properties of this material are also given in Table 4.2.

No attempts have been made to mold rotor blade rings using this composition; however, the properties show that this might be done with some development.

Nitriding Studies

In the last interim report (8), it was shown that the modulus of rupture of the 2.7 gm/cm^3 injection molded Si_3N_4 was strongly dependent on both the nitriding cycle and the atmosphere. The nitriding cycles which had a constant rate temperature increase along with hydrogen/nitrogen atmospheres showed the best results. This section expands these findings by examining cycles utilizing constant rate temperature increases with intermediate holds and investigating the effect of hydrogen/nitrogen compositions. The nitriding studies were also expanded to include the 2.82 gm/cm^3 Si_3N_4 (92GP) described previously.

Table 4.3 shows the nitriding schedules used. The JM4 cycle, which was found to be the best in the last report (8), has a maximum temperature of 2550°F. The JM5 cycle is the same except that the maximum temperature is 2660°F. Cycle

B6C incorporates a step function over the temperature range 2150 to 2335°F followed by a hold at 2335°F. The AMMRC cycle (8) employes all step-hold temperature increases with a maximum at 2550°F.

TABLE 4.2

PROPERTIES OF SILICON NITRIDE INJECTION MOLDING COMPOSITIONS

Property	Test Method	92HP	92FP	92GP	75P1
Density (gm/cm^3)	ASTM C373-56	2.6	2.72	2.82	2.72
Green Strength (psi)	3 Point MOR L = 1-1/8"	3900	> 4000	2900	2300
Molding Shrinkage (%)	Direct Measurement	0.5	0.4	0.35	0.4
Spiral Flow (inches)	ASTM D3123-72 Test Conditions T Material 200 F T Die = 80 F P Injection = 2000 psi	24	10	6.75	10
Rotor Molding Results	See Section 3.1.2 for details	- See Below -			

92HP - Produces rotors flaw free by x-ray.
92FP - Produces rotors flaw free by x-ray.
92GP - No apparent problem molding test specimens. Have not attempted to mold rotors.
75P1 - Release and strength problem in blade area. Blade cracks.

TABLE 4.3

NITRIDING SCHEDULES

Designation	Time at Temperature
JM4	Room temperature - 2150°F furnace rate (500°F/hour), 2150°F hold for 72 hours, 2150-2550°F at 7°F/hour.
JM5	R.T. - 2150°F furnace rate (500°F/hour), 2150°F hold for 72 hours, 2150-2660°F at 7°F/hour.
B6C	R.T. - 2150°F furnace rate (500°F/hour), 2150°F hold for 72 hours, 2150-2335°F at 90°F/hour, 2335°F hold for 24 hours, 2335-2550°F at 7°F/hour.
AMMRC (8)	R.T. to 1300°F furnace rate (≃ 360°F/hour), 1300°F hold for 20 hours, 2282°F hold for 3 hours, 2416°F hold for 20 hours, 2510°F hold for 7 hours, 2552°F hold for 20 hours. (Transitions at 360°F/hour).

Table 4.4 presents the nitriding/strength data for the 75P1 material. The hydrogen/nitrogen composition was varied for the first 3 runs (0%, 1.0%, 4.0% H_2) and shows that 4.0% H_2 produces the best strength. The JM5 cycle also shows superior strength results with 4% H_2 atmosphere. Examination of this material using optical microscopy shows no metallic phase even through the weight gain was only 57%. This nitriding will be repeated to check this anomoly. The B6C cycle with the 2335°F hold offered no improvement.

TABLE 4.4

EFFECT OF NITRIDING CYCLE ON THE MOR OF INJECTION MOLDED Si_3N_4
2.72 gm/cm^3 - 75P1 COMPOSITION

Nitriding Cycle	Nitriding Atmosphere	Average MOR (ksi)*	MOR Range (ksi)	Average Weight Gain (%)
JM4	100% N_2	35.1	39.5-32	58.5
JM4	1%H /99% N_2	37.6	43 -29	58
JM4	4%H /96% N_2	43.2	58 -33	59
JM5	100% N_2	30.6	35.4-25.6	58.5
JM5	4%H /96% N_2	43.4	46.1-41	57**
B6C	4%H /96% N_2	35.3	39.7-30.7	59

* 1/8 x 1/4 x 1-1/2" specimen, 3/8 x 1-1/8" fixture, 0.02 inch/minute load rate.
** No free silicon detected when examined at 250x.

Table 4.5 shows the results of the first attempts at nitriding the 92GP (2.82 gm/cm^3) material. The weight gains were low for the cycles used, and the strength was much below the projected range of 48 to 58 ksi.

TABLE 4.5

EFFECT OF NITRIDING CYCLE ON THE MOR OF INJECTION MOLDED Si_3N_4
2.82 gm/cm^3 - 92GP COMPOSITION

Nitriding Cycle	Nitriding Atmosphere	Average* MOR (ksi)	MOR Range (ksi)	Average Weight Gain (%)
JM4	4% H /96% N_2	41.3	46-37	56.5
JM5	100% N_2	34.7	40-25	58
AMMRC	100% N_2	33	35-30	58
AMMRC	1% H /99% N_2	39.3	43-33	58

*1/8 x 1/4 x 1-1/2" specimen, 3/8 x 1-1/2" fixture, 0.02 inch/minute load rate

Physical Properties

During this reporting period, characterization of the best 2.72 gm/cm^3 injection molded Si_3N_4 as currently developed was started. This characterization was performed to supply preliminary design data and to identify potential problem areas.

The room temperature modulus of rupture values from a number of batches of 75P1 molding material and a number of JM4 - 4% H_2 nitridings were analyzed to obtain Weibull parameters. Results of 31 tests show the material exhibits an "m" value of 6.78 and a characteristic strength of 44.3 ksi (determined by MLE technique.)

A number of oxidation tests were performed on the 2.72 gm/cm^3 Si_3N_4 under two temperature conditions; 1900°F and 2300°F, with both as-nitrided and treated surface conditions. All the data is presented in Table 4.6.

TABLE 4.6

OXIDATION RESULTS ON 2.7 gm/cm^3 INJECTION MOLDED Si_3N_4*

Material Treatment	Temperature (°F)	Exposure Time (Hours)	Δ Weight (%)	Average MOR** (ksi)	Δ MOR (%)	Δ Thermal Expansion*** (ppm)
None	-	0	-	40.0	Baseline	Baseline
	1900	200	+ 0.75	40.1	0	+ 100
	2300	200	+ 0.55	31.3	- 22	+ 150
Flash Oxidized at 2660°F for 1-1/2 hours	1900	200	+ 0.17	39.0	- 2	0
	2300	200	+ 0.19	34.5	- 14	0
CVD Coated with Si_3N_4	-	0	0	30.7	- 23	No data
	1900	200	+ 0.79	28.8	- 28	
	2300	200	+ 0.25	20.6	- 49	
Cr_2O_3 Impregnated	-	0	0	28.4	- 29	No data
	1900	200	- 0.05	23.8	- 41	
	2300	200	- 0.5	23.5	- 41	

* Material code; 75Q, nitrided using JM4 cycle in 4% H_2/96% N_2

** 1/8 x 1/4 x 1-1/2" sample, 3/8 x 1-1/8" test fixture, 0.02 inch/minute load rate, room temperature MOR.

*** Maximum difference in thermal expansion up to 900°C.

The baseline material, with no treatment, exhibits 0.75% weight gain upon oxidation at 1900°F for 200 hours and a slight increase in thermal expansion (100 ppm) when compared to the same material with no oxidation and also shows no degradation in strength. However, when oxidized at 2300°F, a large loss (22%), in strength is noted. The degradation in strength and increase in thermal expansion point out potential problems with this material.

Three techniques, (flash oxidation, Chemical Vapor Deposited Si_3N_4 coatings and Cr_2O_3 impregnation), have been used in an attempt to eliminate both the strength degradation and the increase of thermal expansion. All these techniques concentrate on sealing the surface of the material, thereby preventing oxidation of the bulk material.

The results, presented in Table 4.6 show the flash oxidation technique to be the most promising treatment for improving the oxidation resistance of the 2.7 gm/cm^3 Si_3N_4. With this technique the weight gain was greatly reduced, there was no increase in thermal expansion, and the room temperature strength degradation was reduced to 14%, after 200 hours exposure at 2300°F. The flash oxidation technique will be further developed by exploring the effects of varying both the flash temperature and time.

The other techniques resulted in a large strength degradation before any exposure to oxidizing temperatures. Oxidation testing resulted in further loss in strength. The weight gains with C.V.D. Si_3N_4 coating was the same as the baseline material, while the Cr_2O_3 impregnation technique resulted in weight loss. These test samples changed color, from a dark green to gray, indicating the Cr_2O_3 was unstable.

Creep and Stress Rupture Properties

Only one test was performed to examine the stress rupture properties of the 2.7 gm/cm^3 injection molded Si_3N_4. However, this test was of long duration and consisted of two temperatures and various stress levels as described in Table 4.7. The first 375 hours were run at 2300°F at stresses between 20 and 35 ksi. The remaining 784 hours were run at 2400°F and stresses between 7 and 35 ksi. It should be noted that the last 68 hours of the test were run at 2400°F and 35 ksi (85% of the room temperature Modulus of Rupture) and no failure resulted. This test shows that this material exhibits excellent stress rupture capability.

TABLE 4.7

STRESS RUPTURE TEST OF 2.7 gm/cm^3
INJECTION MOLDED Si_3N_4*

Cumulative Time at Temperature (Hours)	Temperature (°F)	Stress (ksi)	Time At Each Stress Condition (Hours)
0- 90	2300	20	90
90- 212	2300	25	122
212- 277	2300	30	65
277- 375	2300	35	98
375- 467	2400	15	92
467- 542	2400	20	75
542- 656	2400	25	114
656- 779	2400	20	123
779- 896	2400	25	117
896- 952	2400	7	56
952-1091	2400	30	139
1091-1159	2400	35	68

Test concluded without failure

Total strain after 1159 hours was 0.296%

*Material code; 75Q, nitrided using JM4 cycle in 4% H_2/96% N_2

The material exhibited very little creep during the test. At most stress conditions it was impossible to measure any deformation. The overall strain after 1159 hours was only 0.296%, which included the elastic contributions caused by the various stress changes. Even including this error, the steady state creep rate for the entire test is approximately 2.5×10^{-6}/hr.

4.3 PROPERTIES OF SLIP CAST REACTION SINTERED SILICON NITRIDE

Introduction

Section 3.1.2 of this report describes the slip casting process used to fabricate duo-density turbine rotor blade rings. Accordingly, physical property data of slip cast reaction sintered silicon nitride was obtained to aid in the rotor design effort. The material used was of typical slip cast rotor densities (2.8 gm/cm^3), and nitrided using the B6C schedule and 100% N_2 atmosphere.

Test Results

The modulus of rupture data was determined at various temperatures. The average and characteristic strengths along with the Weibull modulus, m, are reported in Table 4.8. The strength values are significantly lower than would be expected for a 2.8 gm/cm^3 density material (estimated strength level should be between 45 and 55 ksi). Very little variation in strength is observed as the test temperature is increased, however, the Weibull modulus does decrease with increasing temperature.

A program was initiated to study the effect of nitriding cycles and atmospheres on the strength of the slip cast Si_3N_4 since it was shown previously that the strength of injection molded Si_3N_4 (7,8,9) is affected by the nitriding cycle. Table 4.9 shows the results obtained to date. The slip cast samples used in this study had been cast previously using different techniques and starting slips. However, neglecting these variations, it seems that the JM5 cycle using 100% N_2 produced the best strength data. These results showed an average MOR of 50.7 ksi at a 2.8 gm/cm^3 density level. Further work is required to optimize the slip cast material and assess its potential.

TABLE 4.8

MODULUS OF RUPTURE OF SLIP CAST SI$_3$N$_4$ (2.82 gm/cc DENSITY)

Temperature °F	Weibull Analysis Method	Average MOR* (ksi)	Characteristic Strength (ksi)	m	Number of Samples
Room Temp.	MLE	29.7	31.2	8.18	19
1300	MLE	32.5	34.5	7.42	20
1700	MLE	34.5	36.9	6.54	20
2100	MLE	33.7	36.0	6.26	18

*1/8 x 1/4 x 1" sample; 3/8 x 3/4" bend fixture, 0.02 in/min load rate.

TABLE 4.9

STRENGTH OF SLIP CAST Si_3N_4 FOR VARIOUS NITRIDING CYCLES

Nitriding* Cycle	Nitriding ATM	Average** MOR (ksi)	MOR Range (ksi)	Density (gm/cm^3)	Δ Weight (%)	Comments
JM4	100 N_2	26 +	25-27	2.67/2.74	60	Chemically adjusted slip to give low density-solid cast
JM4	4% H_2/96 N_2	26 +	25-27	2.67/2.74	60.3	
JM5	100 N_2	37 +	36-40	2.8	60.1	Solid cast
		50.7 +	46-53	2.8	60.4	Centrifugally cast, sample from rotor hub
JM5	4% H_2/96 N_2	43 +	32-50	2.68	59.5	Experimental slip, change in particle size distribution, change in deflocculant
B6C	100 N_2	29.7 ++	25-37	2.82	59	Solid cast
	4% H_2/96% N_2	41 ++	38-46	2.82	59	Centrifugally cast, sample from rotor hub

* See Table 4.3 for description of cycles

** Four point bending 1/8 x 1/4 x 1-1/2" samples, load rate 0.02 in/min

+ 3/8 x 1-1/8" fixture size

++ 3/8 x 3/4" fixture size

4.4 SILICON MILLING STUDIES

Introduction

The material powder used in the injection molded ceramic turbine components is a nominal 325 mesh grade silicon. This material is dry ground using alumina balls for a period of 140 hours in a ball mill. Such a procedure is used to produce the broad particle size distribution as shown in Figure 4.5.

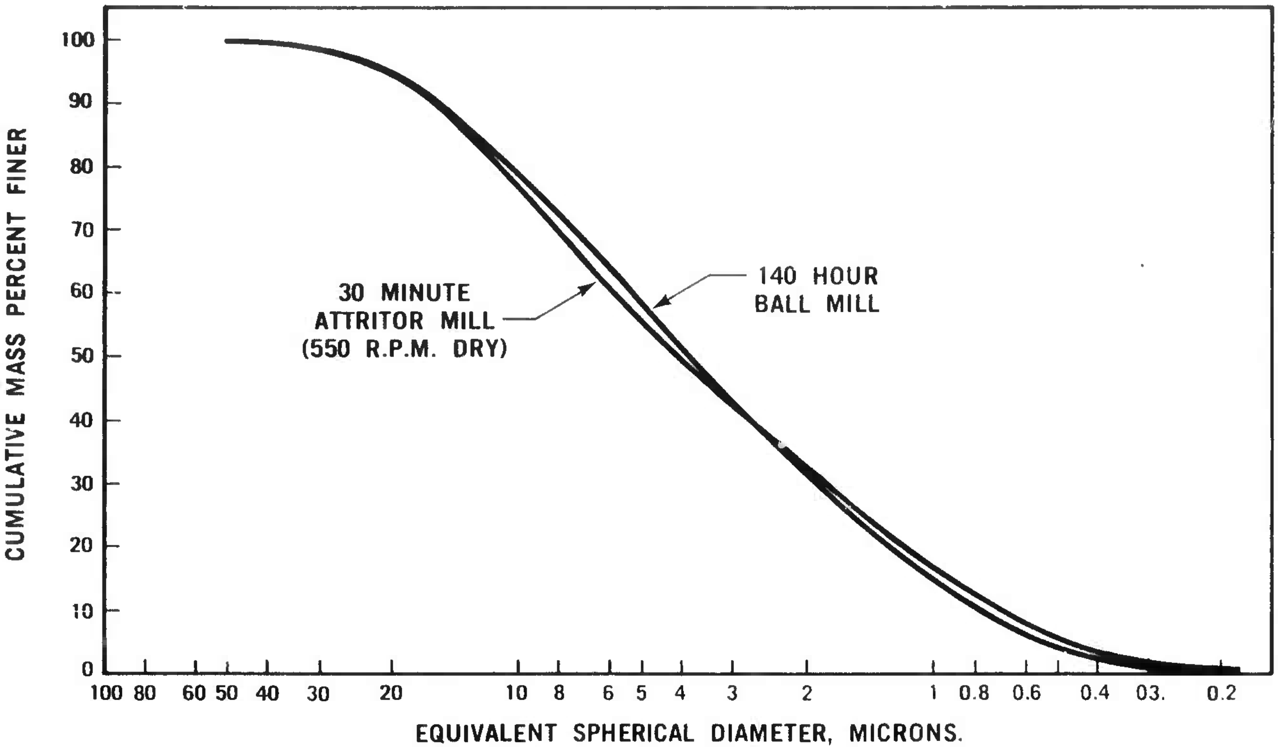

Figure 4.5 Attritor Mill vs Ball Mill Particle Size Distribution

During this reporting period, work was initiated to evaluate an Attritor mill as a means of producing the equivalent of 140 hour ball milled silicon in a relative short time. The Attritor mill used was a 2-1/2 gallon unit manufactured by Union Process of Akron, Ohio. This is a bench top unit with a water cooled stainless steel jacket. Grinding media used was 3/16 inch diameter steel balls. Grinding is accomplished by a circular movement of the agitator arm through the mixture of balls and silicon material.

Results

The wet grinding versus dry grinding characteristics of the Attritor mill are shown in Figure 4.6. These curves show that the dry ground material has a very broad particle size distribution very similar to 140 hour ball milled silicon. In contrast, the wet ground material has a narrowed distribution of particles.

The effect of agitator speed on particle size distribution of dry ground silicon can be seen in Figure 4.7. All of these runs produced particle size shapes with the broad distribution typical of dry mill grinding. Of the three speeds studied, 550 rpm produced the closest simulation to 140 hour grind in the ball mill.

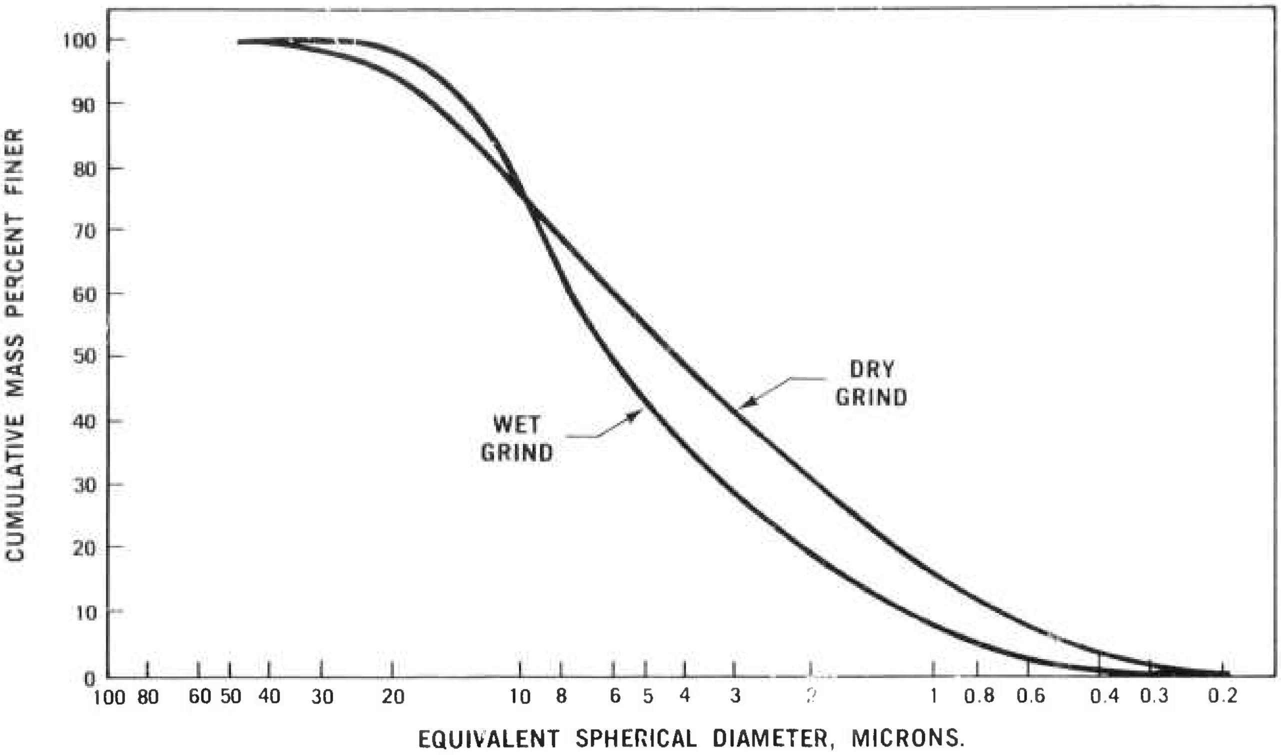

Figure 4.6 Effect of Wet Grind vs Dry Grind on Silicon From Attritor Mill (550 rpm)

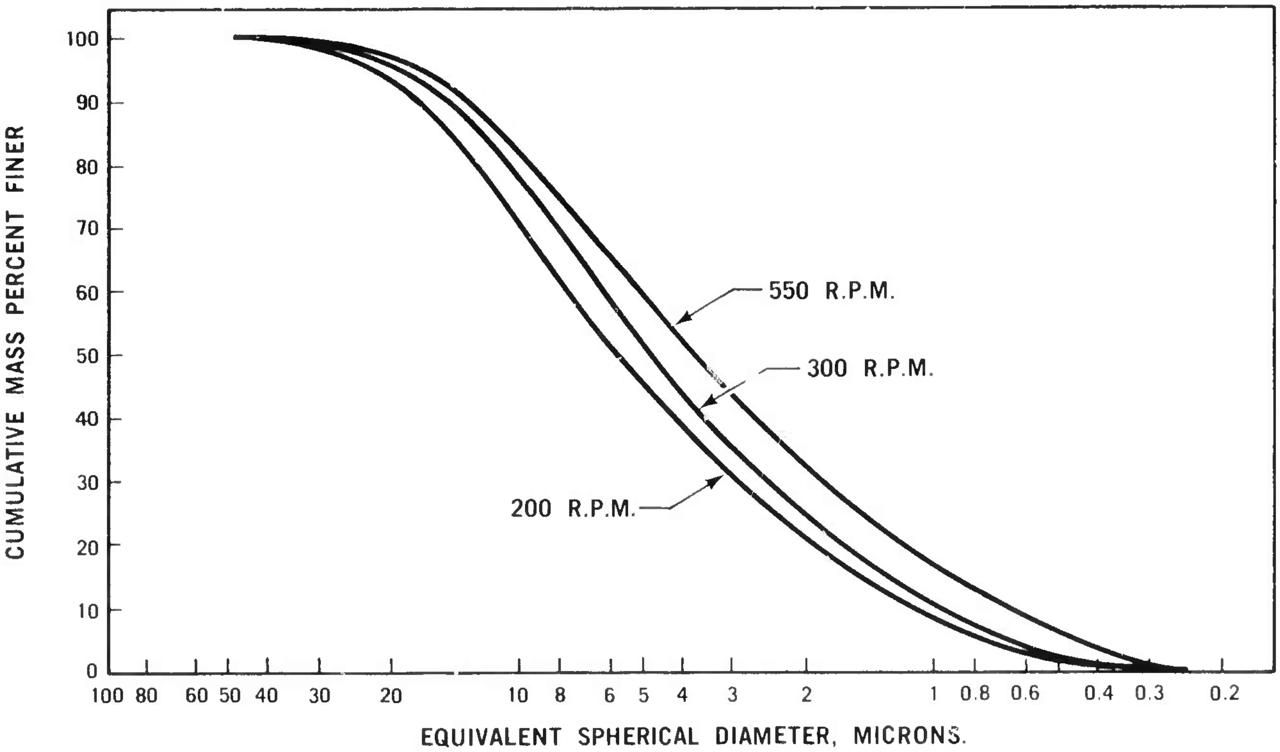

Figure 4.7 Effect of Attritor Mill Speed on Particle Size of Silicon (30 Minute Dry Grind)

Figure 4.8 illustrates the effect of milling time on particle size and distribution. Again the shapes of these distributions are similar. However, overall degree of grinding differed between the 15 minute and 60 minute grinding time as would be expected.

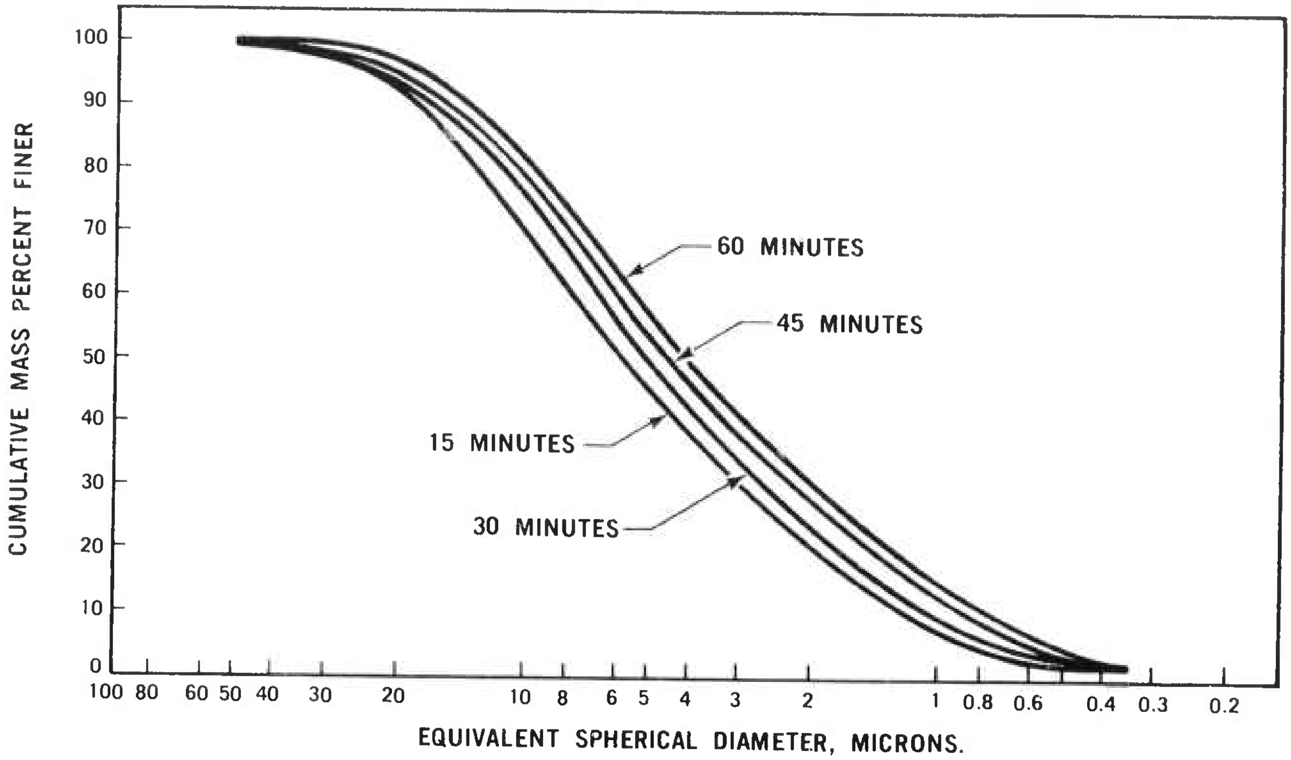

Figure 4.8 Effect of Attritor Milling Time on Particle Size of Silicon (300 rpm Dry)

The best results were achieved using a grinding time of 30 minutes and an agitator speed of 550 rpm. The particle size distribution of this material is shown in Figure 4.5 along with the 140 hour ball milled material. Several additional runs were made with reproducibility within ± 1 percent.

All of the above milling was done using the normal discharge rate of the Attritor, which amounts to approximately 10 minutes for a 2500 gram batch of silicon. One batch of silicon was milled 30 minutes at 550 rpm and the material was removed by hand without discharging. This procedure produced a coarser particle size with a somewhat narrower distribution as shown in Figure 4.9. These results support the belief that the increased retention time during material removal is important to achieving the equivalent of 140 hour milled silicon in the Attritor mill.

The effect of Attritor milling on oxygen pickup and iron contamination has been studied. The results are shown in Table 4.10. There is no significant difference in oxygen content between Attritor milled and 140 hour ball milled silicon. The iron content on the other hand increased from 0.72 to 1.1 percent for the 30 minute Attritor grind. This difference is not considered significant, and could be compensated for by reducing the amount of iron oxide nitriding aid, added later, by a like amount.

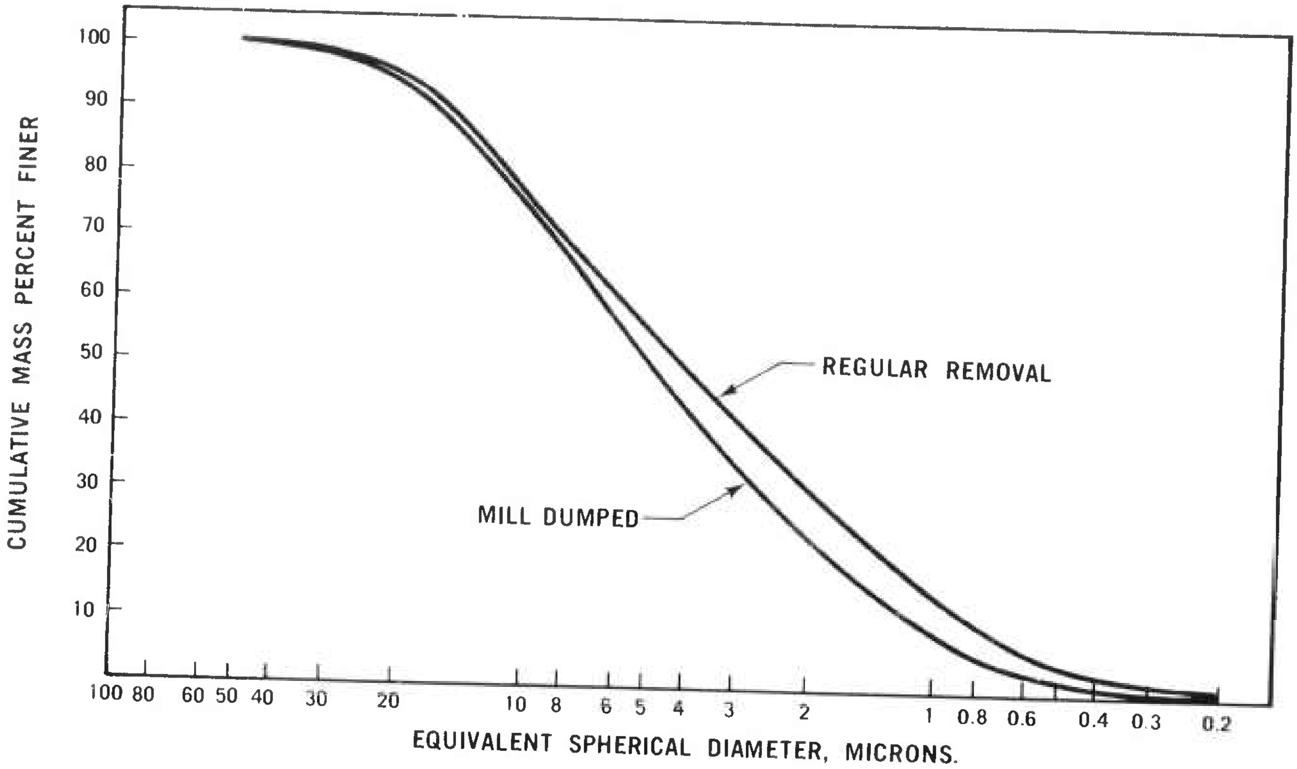

Figure 4.9 Effect of Fast Silicon Removal From Attritor Mill vs Regular Removal (550 rpm Dry)

TABLE 4.10

OXYGEN AND IRON ANALYSIS OF ATTRITOR MILLED SILICON

Dry Mill Time (Minute	Iron (%)	Oxygen (%)
30	1.1	1.31
60	1.4	N.M.
90	1.6	N.M.

*Feed material 0.72% iron and 0.6% oxygen. 140 hour ball milled silicon 0.72% iron and 1.17% oxygen after milling.

An injection molding batch was formulated using Attritor milled material and compared to an equivalent batch using 140 hour ground silicon. The spiral flow results are identical as shown in Table 4.11, illustrating that the flow properties are dependent only on the particle distribution, not how that distribution is achieved.

TABLE 4.11

SPIRAL FLOW TEST ON ATTRITOR MILLED AND
140 HOUR GRIND INJECTION MOLDING COMPOSITIONS

Test Method	140 Hour Grind	Attritor Mill
ASTM D3123-72		
Test Conditions		
T Material = 200°F	10"	10"
T Die = 80°F		
P Injection = 2000 psi		

4.5 TESTING OF CERAMIC MATERIALS EXPOSED TO EXHAUST GASES OF GASOLINE CONTAINING LEAD

Introduction

Gas turbine engines have multi-fuel operating capability, however, the most widely distributed and used fuel is gasoline. There is no benefit to be gained by adding lead to gas turbine fuels, therefore the most likely fuel would be gasoline as free from impurities as economically possible. However, the use of gasoline does risk the chance that leaded fuel could be burned, either accidently or by contamination from storage and handling facilities. Since the effects of lead-containing exhaust products on turbine ceramics were not known, a series of short term tests were performed to determine if any catastrophic problems exist.

Initial Testing Procedure

Initial testing employed lead-sterile research gasoline with 0.05 grams per gallon of tetraethyl lead (TEL) added. This was the maximum allowable TEL content of unleaded gasoline under current regulations.

The ceramics chosen for the initial tests were lithium-aluminum-silicate (LAS) materials typically used in gas turbine regenerators. These materials are very rich in silica (SiO_2), and therefore a reaction with leaded exhaust gases would form undesirable low-melting lead silicates. The two selected compositions of LAS, were Corning Glass Works Code 9458 and Owens-Illinois C-140.

Samples were prepared for testing in the Westinghouse pressurized test passage (1,2,3,4,6,8). The test bars of the C-140 material were 1/4 inch in diameter by 2 inches long while the 9458 bars were 1/4 inch square by 2 inches long. The bars were exposed for 25 hours at a sample temperature of 1780°F (representative of regenerator operating temperatures), 3 atmospheres pressure, and 500 feet per second gas velocity.

Test Results

Both materials developed a reddish-orange stain, which penetrated up to a depth of 50μ. No additional deposits were noted, length and weight determinations, before and after exposure, revealed no measurable changes. Optical microscopy, SEM, and electron microprobe were employed to examine the samples.

The stain contained iron, probably from both the fuel and the upstream ferrous components of the test rig. No differences in structure were observable by microscopy, and no lead was detected by microprobe either on the surface or within the interior of either sample. Figure 4.10, at 210x, shows a portion of a fractured section of the Corning 9458 material after this test. The stained surface is a thin light-colored coating; the arrows indicate the approximate depth of stain penetration.

Second Test Procedure

Since nothing catastrophic occurred in the inital tests a second set of tests were performed at a higher lead level. Gasoline was blended to obtain a TEL content of 0.50 grams per gallon, (the maximum amount of TEL permitted in low-lead gasoline). Other materials, including Norton NC-203 hot pressed SiC, Norton HS-130 hot pressed Si_3N_4, and Ford injection molded Si_3N_4 (2.2 gm/cm^3 density) were added to the two LAS materials previously evaluated.

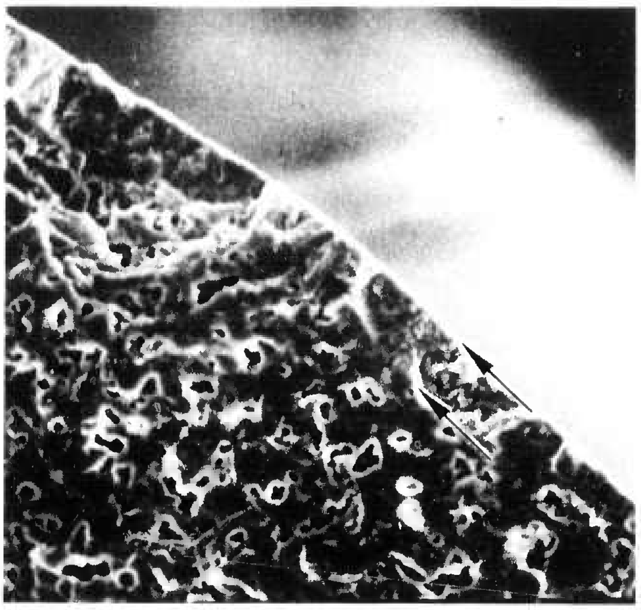

Figure 4.10 Scanning Electron Micrograph of Fracture Surface of Corning 9458 LAS After Exposure to Lead-Containing Exhaust Gases (210x)

Fresh samples of both Corning and Owens-Illinois materials were prepared to the dimensions mentioned previously. Samples of both hot-pressed materials, 1/4 inch by 1/4 inch by 2 inches long, were cut from large billets. The reaction-sintered Si_3N_4 was molded and nitrided in the form of round bars, 1/4 inch in diameter by 2 inches long. The samples were then exposed to 45 hours in the Westinghouse pressurized test passage to the exhaust from the combustion of 0.50 grams per gallon TEL gasoline. The temperature was 2000°F, at the test samples with a gas velocity of 500 feet/second at 3 atmospheres pressure.

Second Test Results

Weight changes for the various samples tested are given in Table 4.12. Very slight weight gains were observed in the case of both hot pressed materials. Higher weight gains were noted for the very porous reaction sintered Si_3N_4, as expected. While 2000°F is a higher temperature than would normally be used when operating LAS materials in a gas turbine regenerator system, the Corning 9458 material appeared only slightly affected. However, the O-I C-140 material was considerably deformed and chipping occurred at one end of each sample rendering the weight change data meaningless.

Photographs of the various samples after this exposure are shown in Figures 4.11 through 4.19. All samples exhibited some degree of surface discoloration. Deposit build-up was more noticeable on the reaction sintered Si_3N_4 and the C-140 LAS material. These nine ceramic bars were submitted for analysis. The study was made to determine the effect of lead on the samples and in particular whether low-melting lead silicates were formed. X-ray diffraction, X-ray fluorescence and scanning electron microscopy with energy dispersive X-ray analysis were performed on exterior surfaces and longitudinal and cross section surfaces.

In the test passage, the bars were supported at the ends and exposed to the exhaust stream over most of their length. The square bars were oriented such that one corner pointed upstream. Two adjacent sides on each bar were thus exposed at a 45° angle to the exhaust flow. All of the bars had fine-grained reddish-brown coatings and colorations of various shades on their upstream sides and, in general, some reddish-brown discoloration on their downstream surfaces. C-140 LAS bars No. 6 and No. 7 were warped.

TABLE 4.12

WEIGHT GAIN DATA ON SECOND SET OF TEST BARS

Specimen	Original Weight gm	Final Weight gm	Change in Weight gm
1. Norton NC 203 SiC	6·79410	6·79714	+ 0·00304
2. Norton HS 130 Si_3N_4	6·55480	6·56077	+ 0·00597
3. Norton HS 130 Si_3N_4	6·56375	6·56973	+ 0·00598
4. Ford Reaction Sintered Si_3N_4	3·46510	3·66340	+ 0·19830
5. Ford Reaction Sintered Si_3N_4	3·45564	3·67054	+ 0·21490
6. Owens-Illinois C-140	4·57889	4·53492	- 0·04397*
7. Owens-Illinois C-140	4·73907	4·38746	- 0·35161*
8. Corning 9458	4·43722	4·43957	+ 0·00235
9. Corning 9458	4·44455	4·43914	- 0·00541

* Specimen softened and chipped at one end.

The sequence of analyses performed was as follows:

1. Exterior surfaces (upstream and downstream) of all samples were first individually examined (as-is) for phase content by X-ray diffractometry. Qualitative X-ray fluorescence analysis was performed on all the upstream surfaces. For all the paired specimens, the two identical bars were mounted and analyzed together. Downstream surfaces were not examined by X-ray fluorescence.

2. Some of the samples were fractured into several pieces. Portions of these were ground down for X-ray diffraction and fluorescence examination of the interior (longitudinal section) surfaces.

3. Untouched exterior surfaces were examined by scanning electron microscopy.

4. Portions of the bars were cross-sectioned, polished, and examined by electron microprobe and scanning electron microscopy.

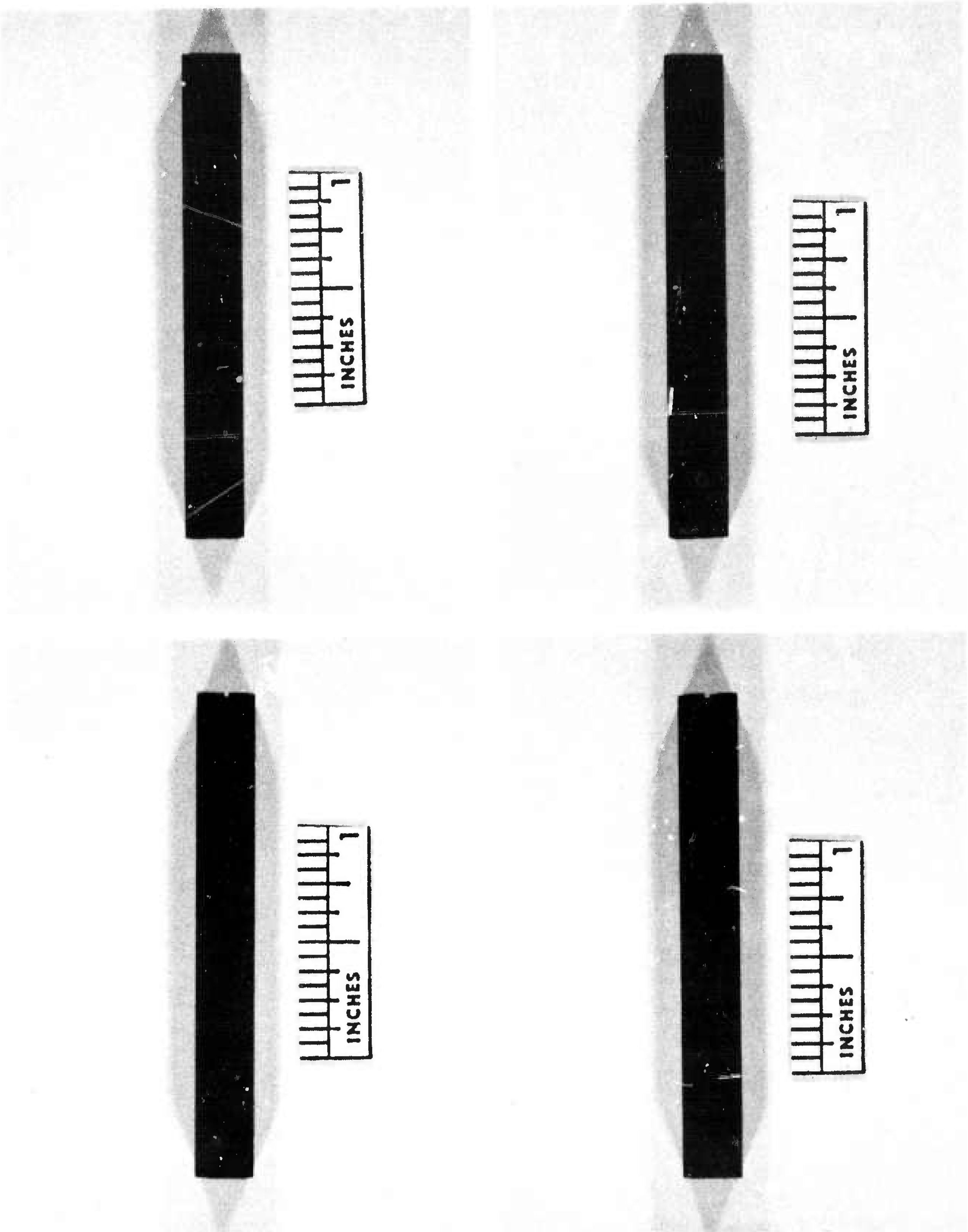
1
INCHES
1
INCHES
1
INCHES
1
INCHES

Figure 4.11 Surface Appearance of Four Sides of Norton NC-203 Hot-Pressed SiC, Specimen 1

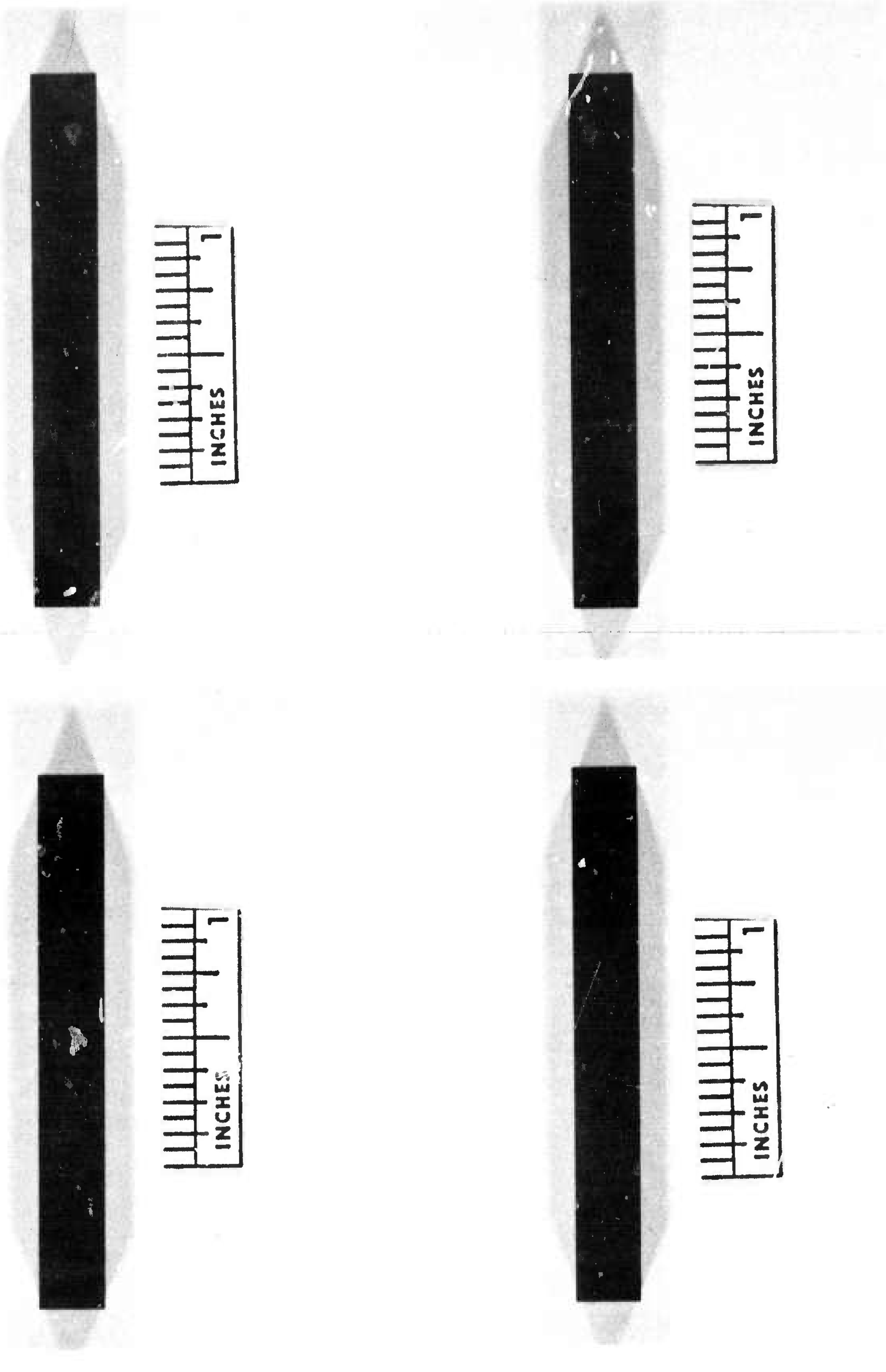
1
INCHES
1
INCHES
1
INCHES
1
INCHES

Figure 4.12 Surface Appearance of Four Sides of Norton HS-130 Hot-Pressed Si_3N_4, Specimen 2

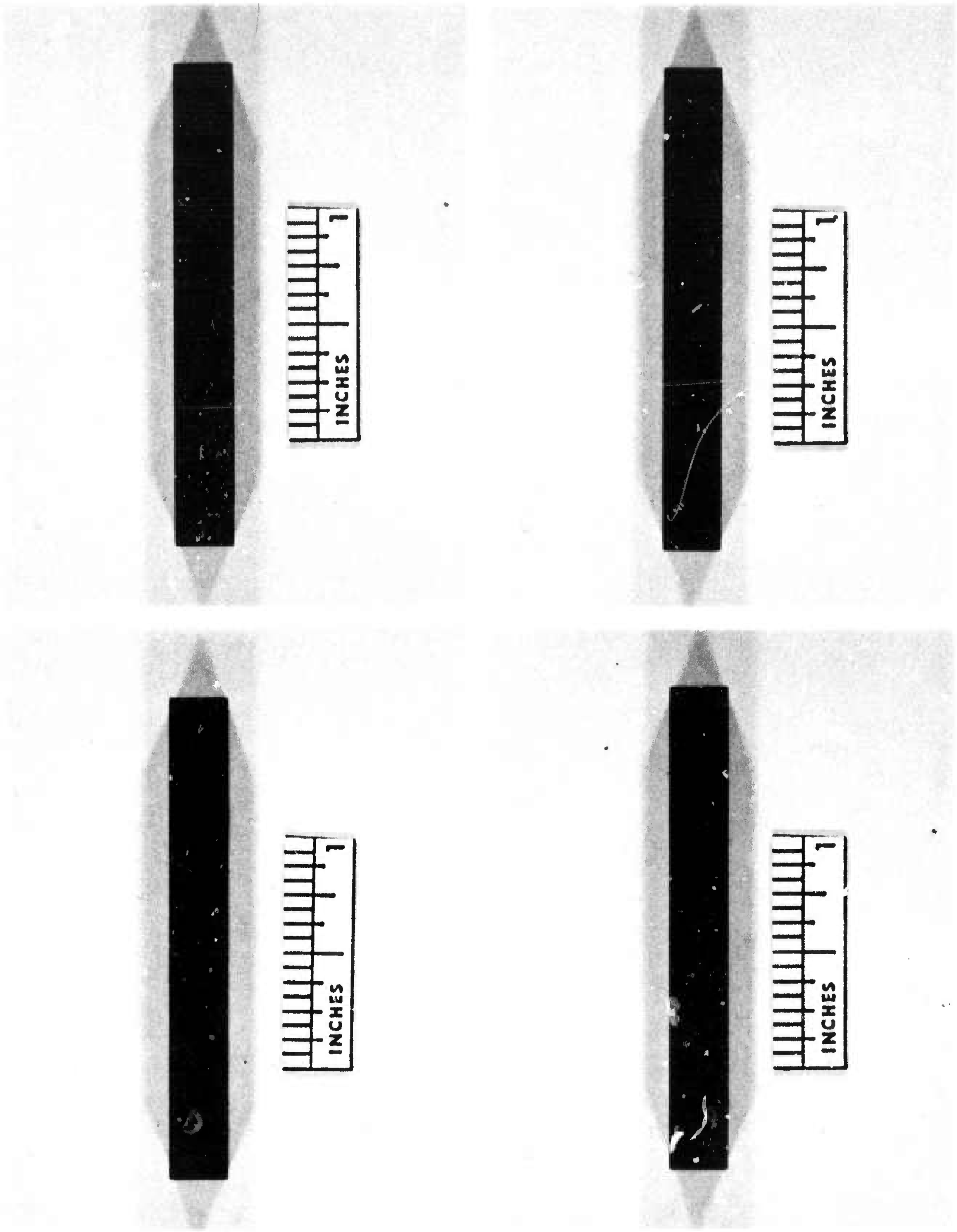
1
INCHES
1
INCHES
1
INCHES
1
INCHES

Figure 4.13 Surface Appearance of Four Sides of Norton NC-132 Hot-Pressed Si_3N_4, Specimen 3

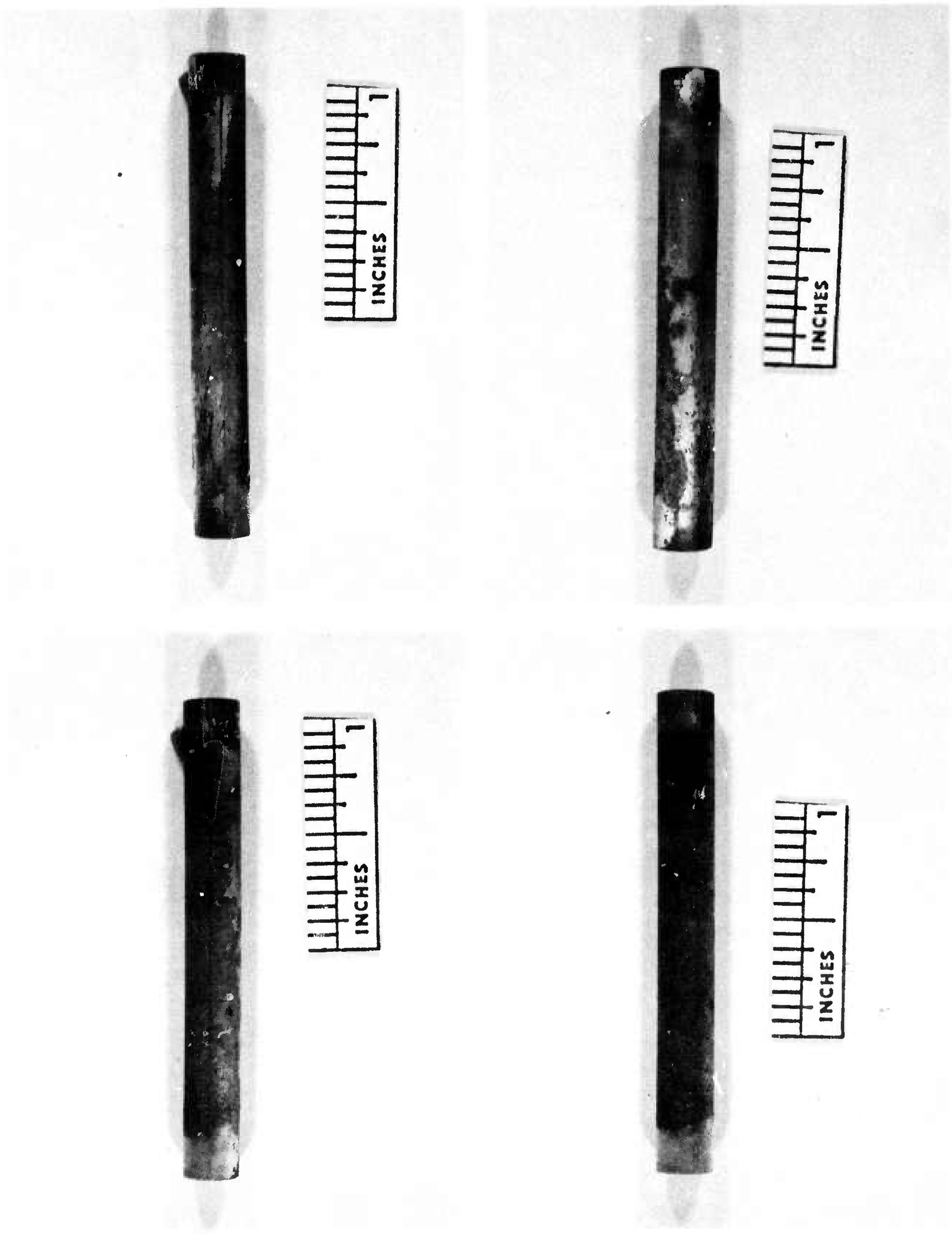
1
INCHES
1
INCHES
1
INCHES
1
INCHES

Figure 4.14 Four Views of Ford Reaction Sintered Si_3N_4, Specimen 4

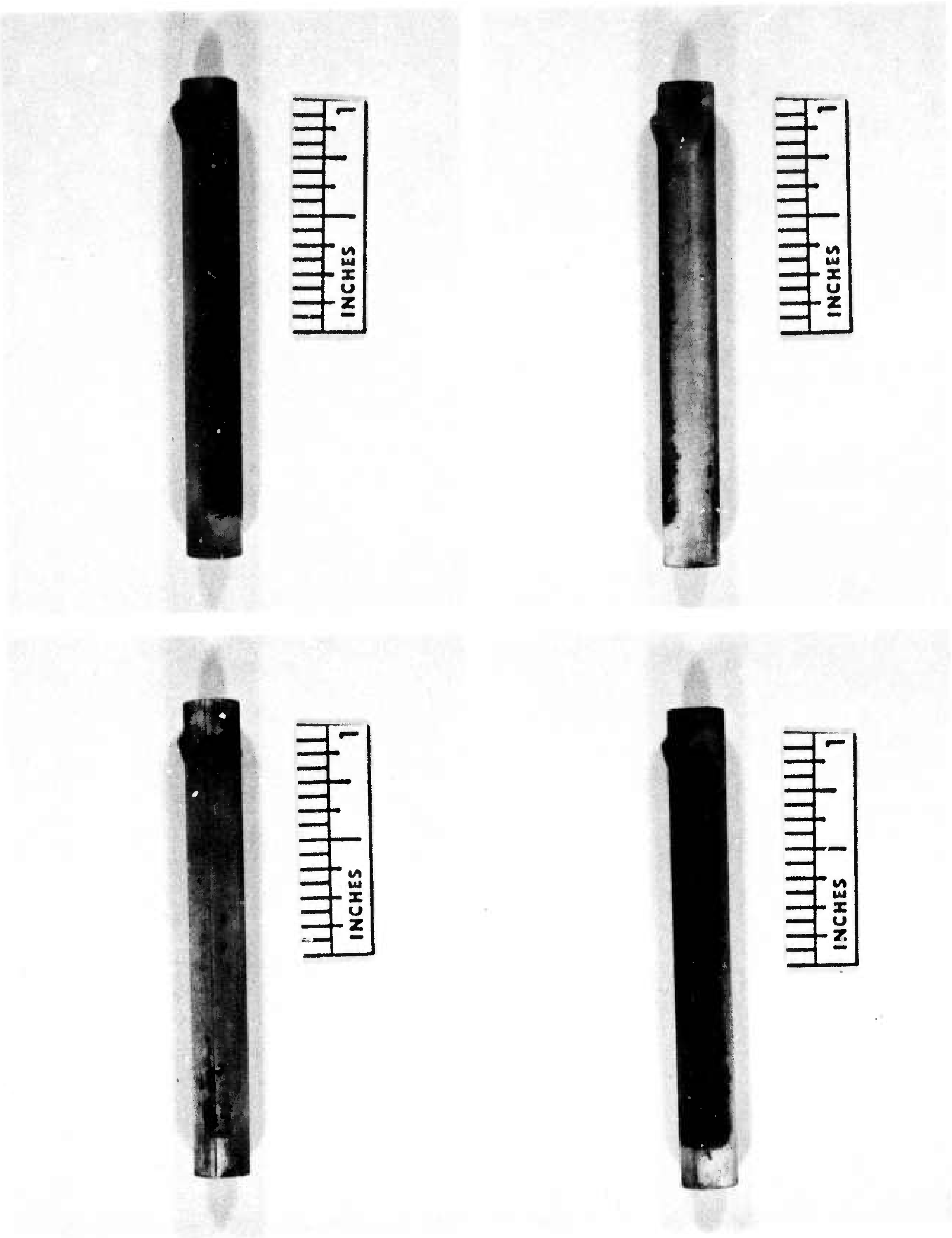
1
INCHES
1
INCHES
1
INCHES
1
INCHES

Figure 4.15 Four Views of Ford Reaction Sintered Si_3N_4, Specimen 5

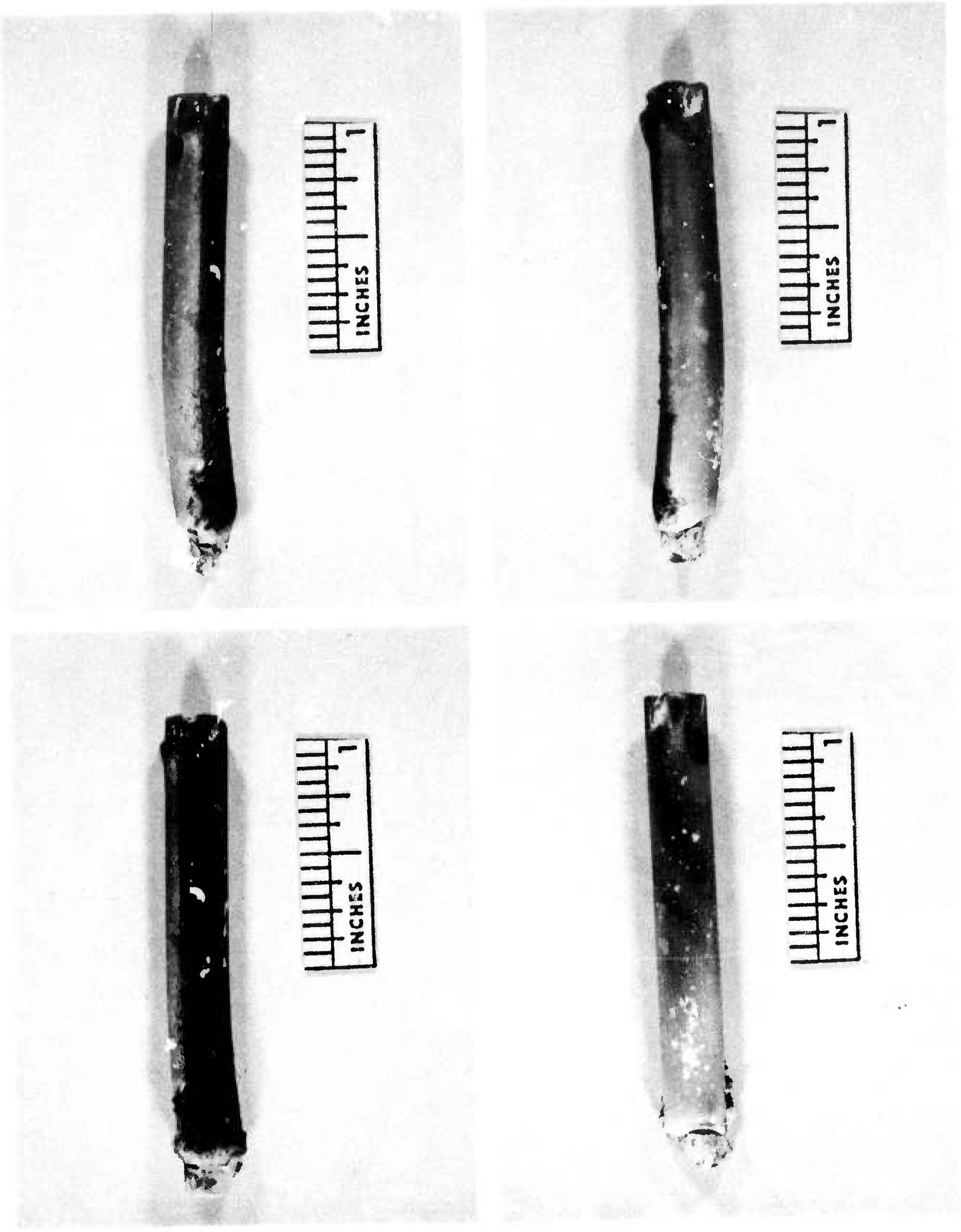
1
INCHES
1
INCHES
1
INCHES
1
INCHES

Figure 4.16 Four Views of Owens-Illinois C-140 LAS, Specimen 6

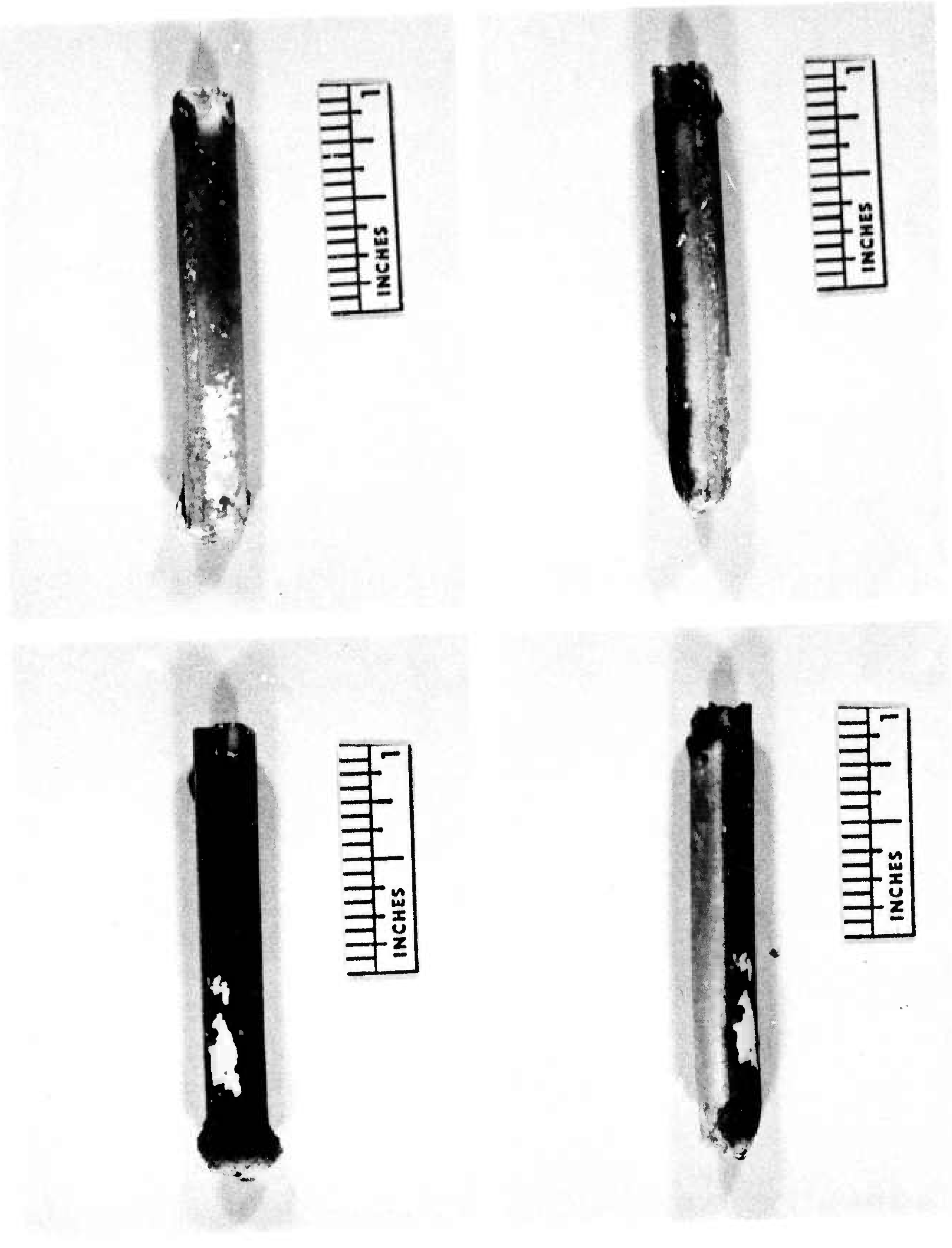
1
INCHES
1
INCHES
1
INCHES
1
INCHES

Figure 4.17 Four Views of Owens-Illinois C-140 LAS, Specimen 7

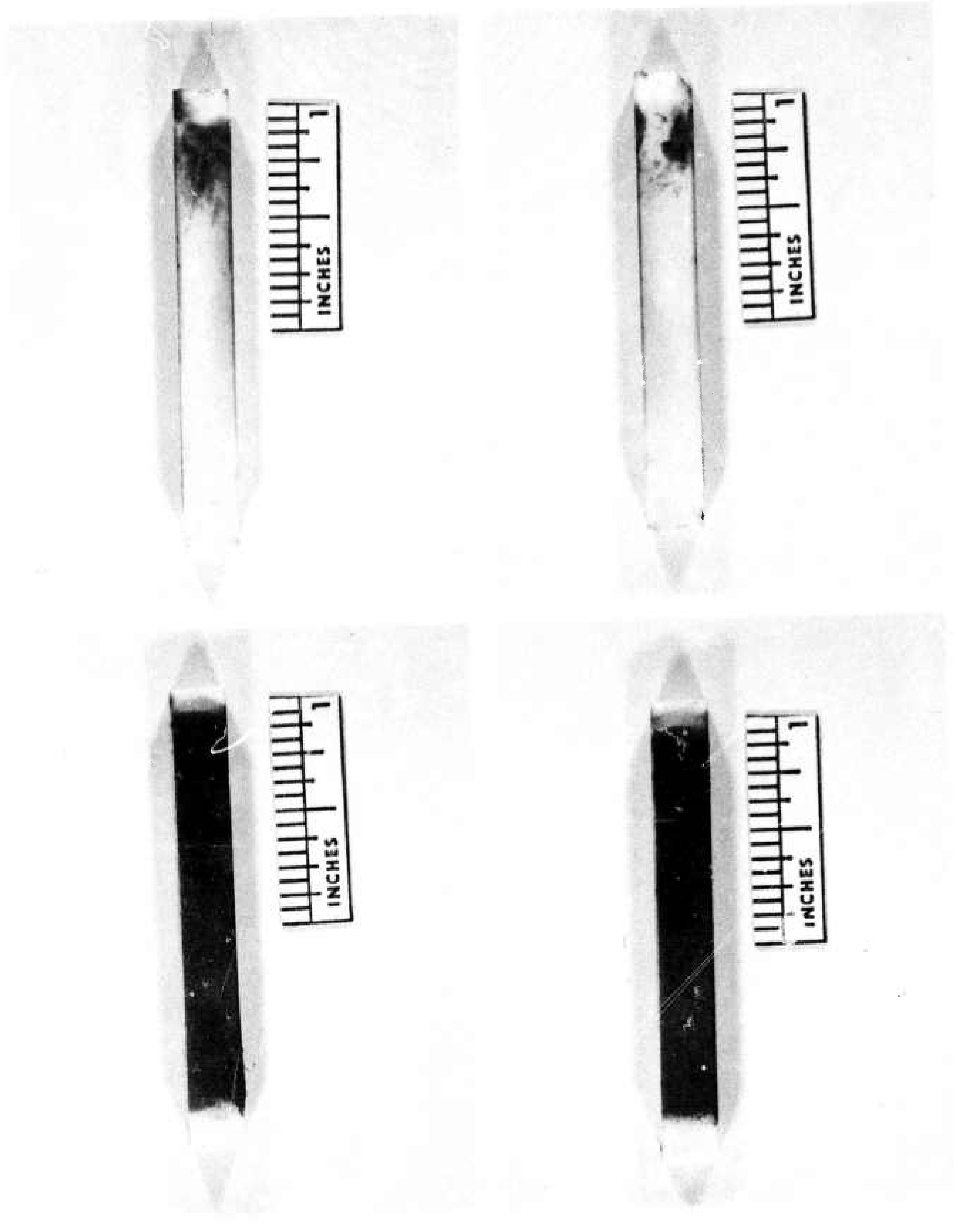
1
INCHES
1
INCHES
1
INCHES
1
INCHES

Figure 4.18 Surface Appearance of Four Sides of Corning 9458 LAS, Specimen 8

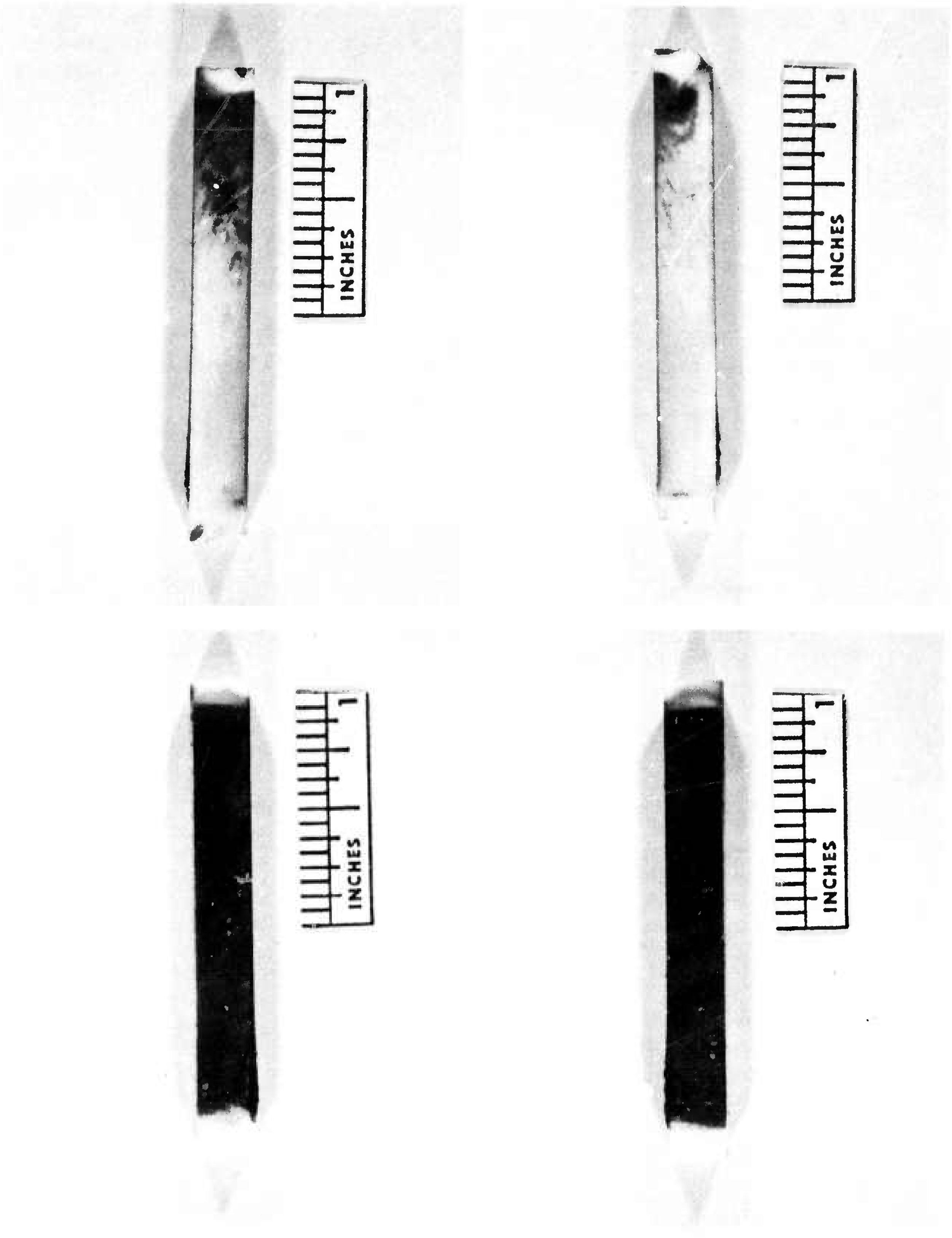
1
INCHES
1
INCHES
1
INCHES
1
INCHES

Figure 4.19 Surface Appearance of Four Sides of Corning 9458 LAS, Specimen 9

The X-ray analytical results may be summarized as follows:

1. While small amounts of lead were detected by fluorescence on the upstream surfaces of the bars, no lead-bearing phases were identified by diffraction. Some unidentified minor phases were found which could have included one or more lead silicates (among other possibilities) but no lead silicates could be positively identified.

2. Iron oxides appear to be the major contaminants deposited on the upstream surfaces. The ratio of Fe_3O_4 to Fe_2O_3 appeared generally higher on the SiC and Si_3N_4 specimens than on the LAS. Aluminum was also a major contaminant element on all upstream surfaces, although no aluminum-bearing contaminant phases were identified by diffraction.

3. The upstream and downstream sides of all specimens contained various amounts of alpha-cristobalite (SiO_2). The reaction-bonded Si_3N_4 contained large amounts of cristobalite on all exterior surfaces, more than the hot pressed Si_3N_4. Both types of LAS also contained significant amounts of cristobalite on all exterior surfaces. Examination of ground surfaces on No. 1 SiC, No. 6 LAS, and No. 8 LAS showed that cristobalite did not persist in depth in any significant amounts.

4. Tungsten and cobalt were detected by fluorescence on the upstream surfaces of No. 1 SiC and Nos. 2 and 3 Si_3N_4. X-ray diffraction examination of a ground downstream surface (0.04" removed) showed that No. 1 contained WC, probably as cobalt-bonded WC, and possibly alpha-Al_2O_3. Examination of a ground downstream surface on No. 2 Si_3N_4 showed no WC. The WC was apparently only on the surface.

5. In cross section, Corning 9458 sample No. 8 showed a thin (approximately 0.025") white outer zone around a gray central region. Ne unique phases or elemental constituents were found in either zone.

The scanning electron microscopy results are listed as follows:

1. The surface morphology of the bars was examined. Figures 4.20-4.24 are micrographs of the contamination on the upstream surfaces. The contamination on sample No. 1, hot pressed SiC, took the form of rod shaped particles while that on all other samples was a uniform agglomeration of equiaxed particles.

2. Polished cross sections of samples Nos. 8, 6, 4, and 1 were examined. The microprobe mode of the scanning electron microscope was used to determine the elemental contamination on sample Nos. 8 and 1. X-ray maps of LAS sample No. 8 (Figure 4.25) show that a barium containing phase has filled the surface pores and an iron-rich phase is present on the surface. No localized concentration of lead-bearing phases was found as can be seen in the lead X-ray maps. X-ray maps of the hot pressed SiC sample No. 1 (Figure 4.26) show barium and iron-rich phases on the surface. These barium-rich phases were not detected on sample Nos. 6 or 4.

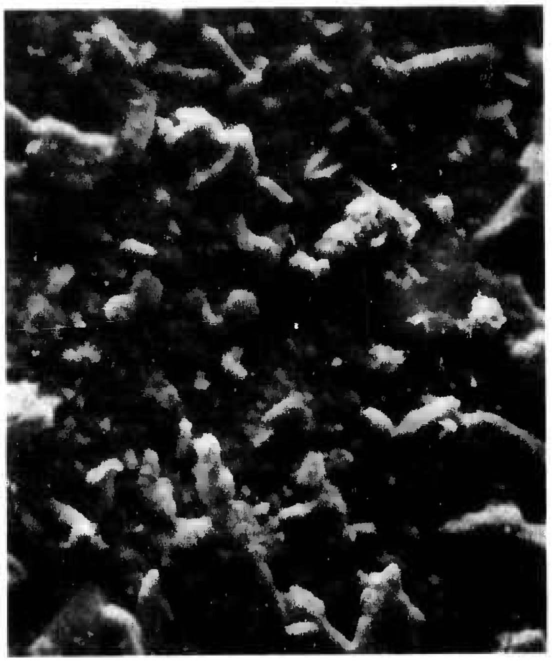

Figure 4.20 SEM of Upstream Surface of Sample 1 Norton NC 203 SiC (1000x)

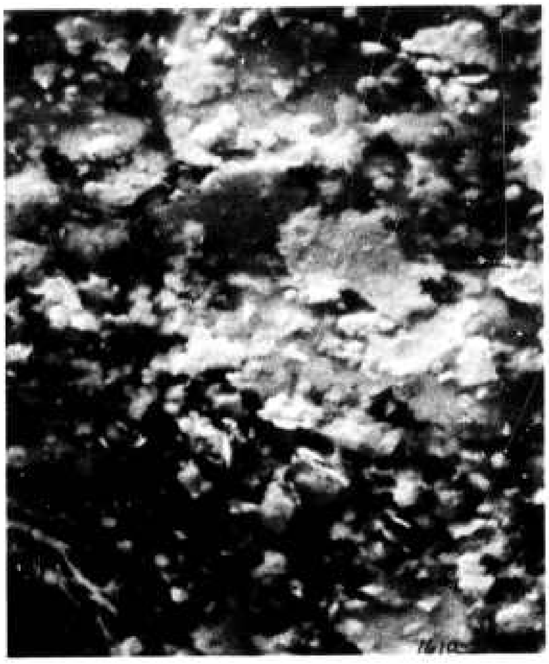

Figure 4.21 SEM of Upstream Surface of Sample 2 Norton HS 130 Si N (1000x)

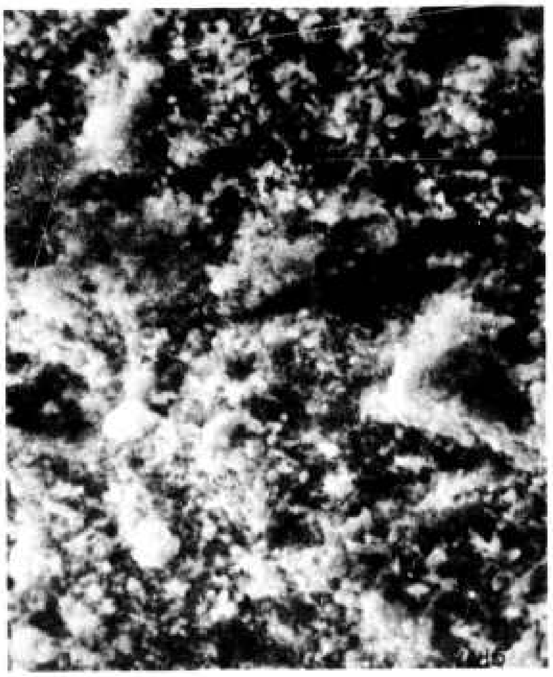

Figure 4.22 SEM of Upstream Surface of Sample 5 Ford Reaction Sintered Si_3N_4 (1000x)

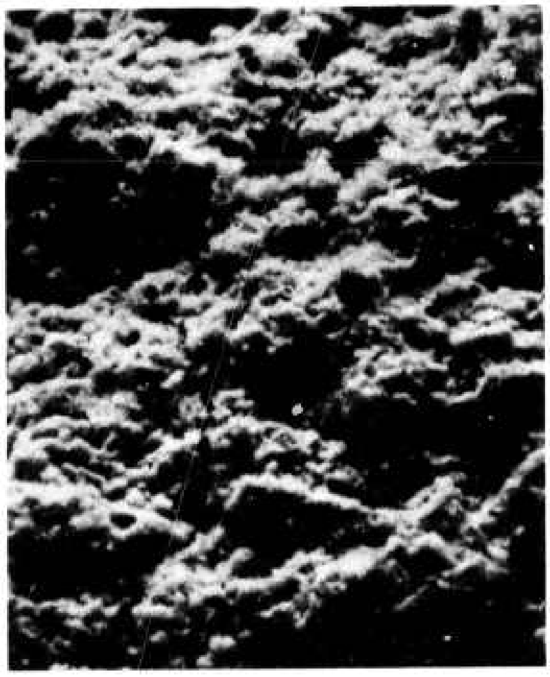

Figure 4.23 SEM of Upstream Surface of Sample 6 O-I C-140 LAS (1000x)

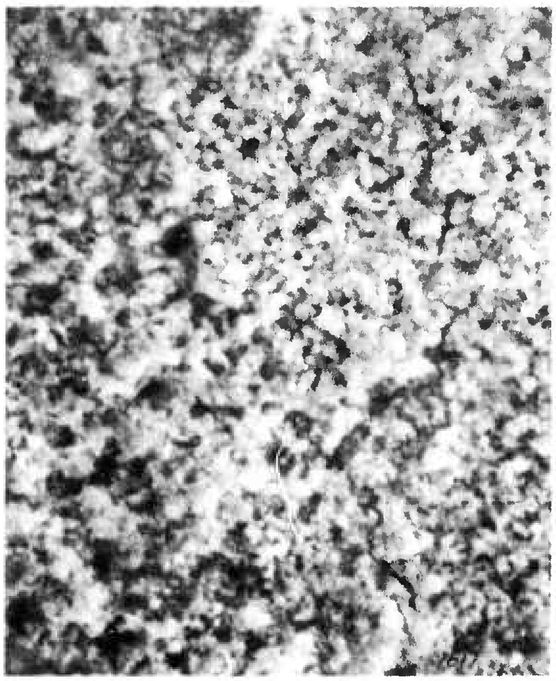

Figure 4.24 SEM of Upstream Surface of Sample 8 Corning 9458 LAS (1000x)

Conclusions

No evidence was found to suggest that the lead in the fuel had any deleterious effects on any of the bars tested. Minor amounts of lead were detected on the exposed, upstream surfaces of all the samples, however, no surfacial lead bearing phases were identified by electron microprobe or X-ray diffraction. The major surface contaminants appear to be iron oxides.

On the basis of both tests, it was felt that enough preliminary evidence had been gathered to conclude that lead additions in fuel was not a major detriment to current gas turbine ceramic materials. However, long time exposure of many test samples to lead-containing turbine exhaust gases, coupled with detailed mechanical property determination, would be required to firmly establish what effect lead would have.

On the basis of these tests, it was decided to switch fuels used in the Ford ceramic turbine engines and test rigs to a research grade gasoline containing 0.012-0.015 gm/gallon TEL, considerably less than the 0.50 gm/gallon TEL used in the second test. No deleterious effects on the ceramic components have been noted in several months of operation using this fuel.

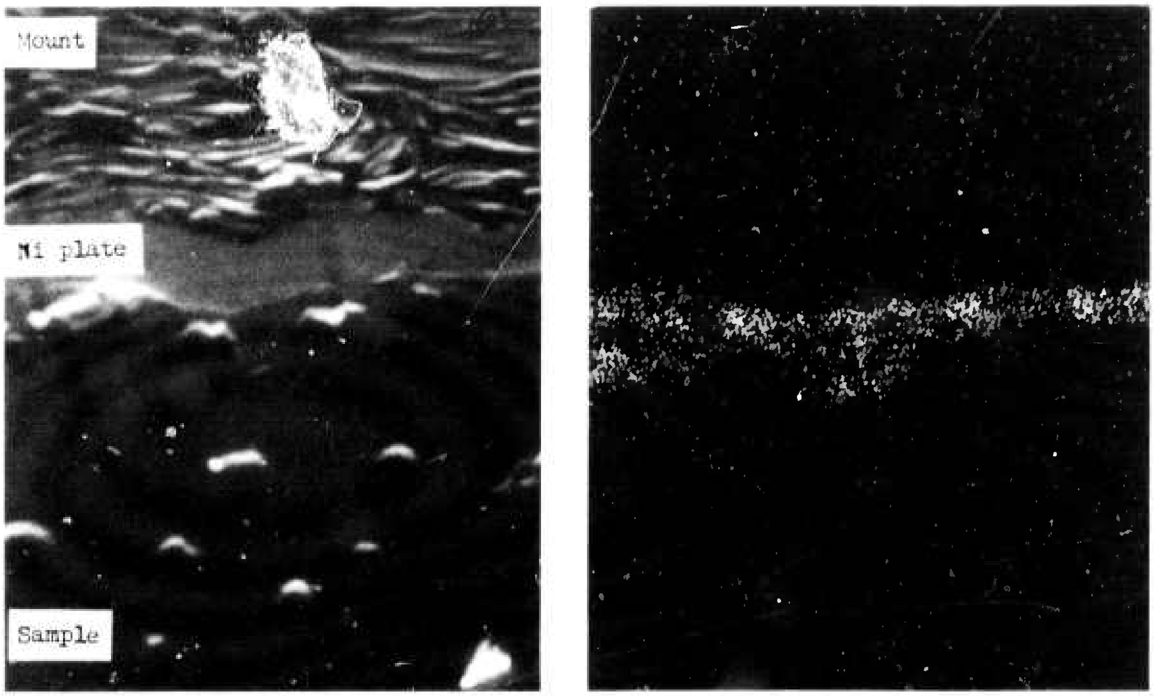
Mount
Ni plate
Sample

Backscattered Electrons

Barium

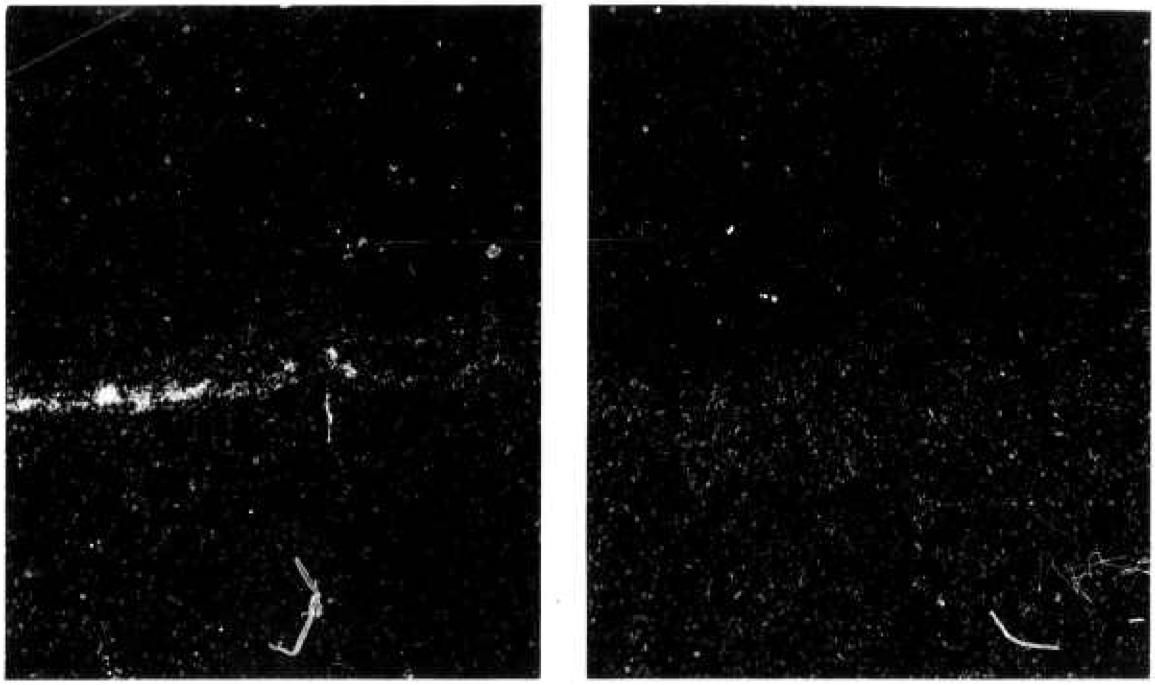

Iron

lead

Figure 4.25 X-Ray Diffraction Map of Polished Cross-Section of Sample 8, Corning 9458 LAS. SEM 1000x

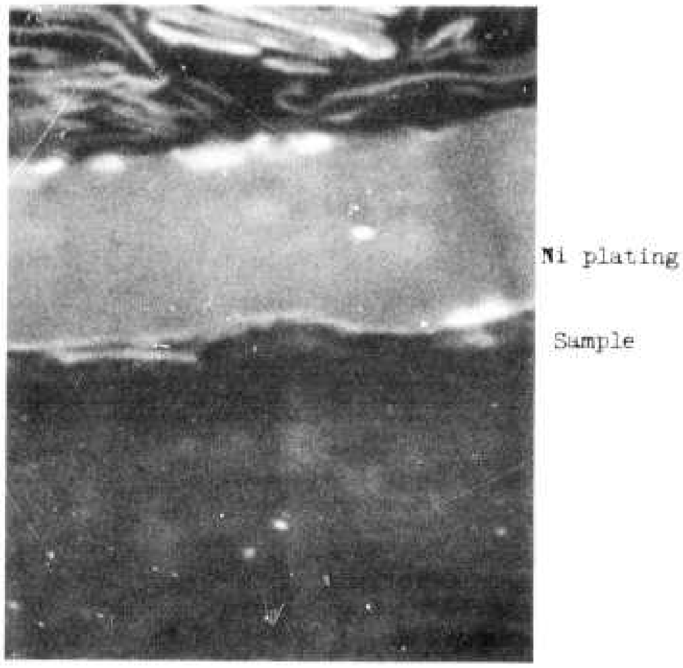
Ni plating
Sample

Backscattered Electrons

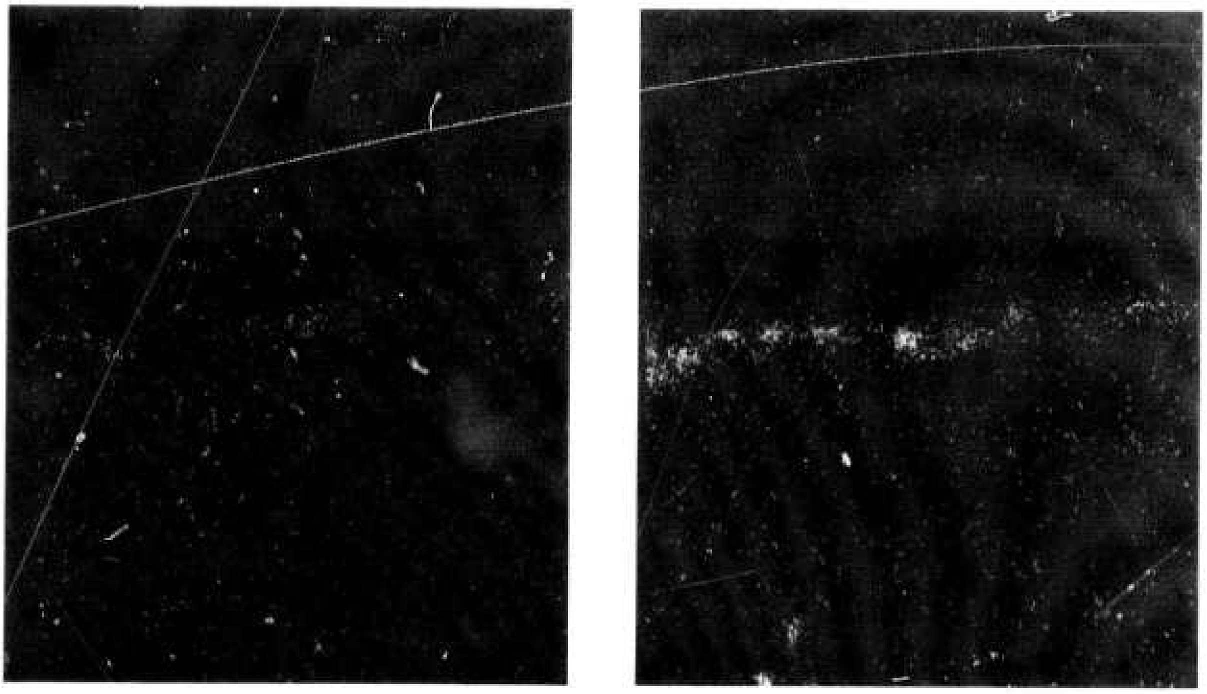

Barium

Iron

Figure 4.26 X-Ray Diffraction Map of Polished Cross-Section of Sample 1 Norton NC 203 SiC. SEM 1000x

4.6 HIGH TEMPERATURE FRACTURE BEHAVIOR OF CERAMIC MATERIALS

Introduction

The high temperature fracture characteristics of ceramic turbine materials continued to be evaluated. The conventional four-point loading flexural test, as described earlier (3), is the principal mode employed with special attention given to the recognition of subcritical crack growth or other time (rate) dependent fracture phenomenon (7) that showed up in these comparatively high loading rate fracture tests (conventional Instron testing machine crosshead rates). A key procedure in testing and fractography was to employ preplaced fracture initiating flaws of controlled size (7). During this report period, the principal activity was fracture examination of reaction sintered Si_3N_4, Sialon, and Refel SiC which is being utilized for combustor tubes.

Reaction Sintered Silicon Nitride

Fracture behavior from room temperature to 1400°C was evaluated routinely during process development of injection molded reaction sintered Si_3N_4. Expectedly, the fracture stresses experienced a rather wide variation during material development. While the injection molded reaction sintered silicon nitride contains some strength-limiting porosity, the precracking technique (6) was found to be usable and was employed routinely. The single most significant observation to date is that no fractographic evidence of subcritical crack growth was observed up to 1400°C. This is consistent with observations on other reaction sintered silicon nitrides but is different from those of hot pressed silicon nitride. The key feature seems to be an absence of densifying additives typical of hot pressed material. To confirm the findings of these fast-fracture observations, more sensitive techniues are required to evaluate time-dependent failure. Fracture mechanics techniques for measuring crack velocity and stress-rupture/creep tests will therefore be investigated.

REFEL Silicon Carbide

A commercially available composite material of alpha silicon carbide and silicon designated REFEL by the producer, UKAEA, is being evaluated. Findings to date are consistent with similar published observations of other investigators (16) so far as the relative importance of the silicon phase to the fracture behavior is concerned.

The as-processed surface of REFEL SiC is silicon rich, (Figure 4.27), containing occasional relatively large pockets (grains) of silicon. These large grains can, and apparently do, tend to function as fracture initiating flaws (17), lowering the strength of the as-processed material below that typically achieved by removing the silicon rich layer. The temperature dependence of the flexural strength of the material in the latter state (1μ polish) appears in a form common for brittle materials (Figure 4.28 (7)). The increase in fracture resistance, at approximately 900°C, corresponds to the onset of significant plasticity in the silicon phase. Subcritical crack extension occurring at temperatures in excess of approximately 1250°C at fast loading rates, presents a failure mode that bears further investigation at lower temperatures and lower strain rates (7). Figure 4.29a is a scanning electron micrograph (SEM) at low magnification of a crack that has extended about an indentation under load at 1300°C. Figures 4.29b and 4.29c are progressively higher magnifications illustrating the path of fracture to be principally, though not always, between silicon carbide grains and through the silicon phase. The path through the silicon occasionally appears (in Figure 4.29c) to be accomodated plasticly.

Evidence of the complexities of plastic accomodation in silicon (P) as well as transgranular fracture of silicon carbide grains (TG) are marked in Figure 4.29. The subcritical crack growth in composite silicon/silcion carbide appears to be influenced principally by the mechanical properties of the silicon phase.

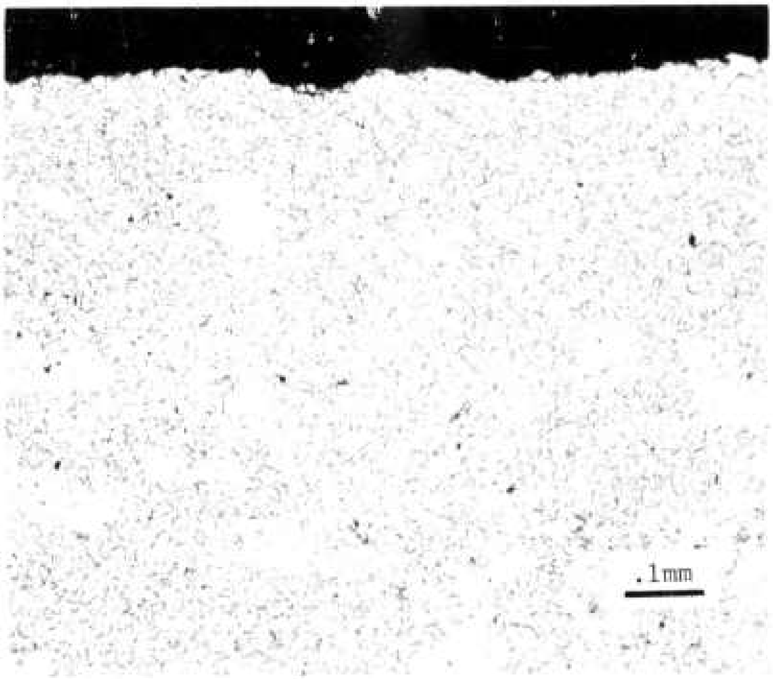

Figure 4.27 Optical Micrograph of a Section Through the As-Pressed Surface of REFEL SiC, Illustrating the Disposition of the Silicon Phase in Proximity to the Surface

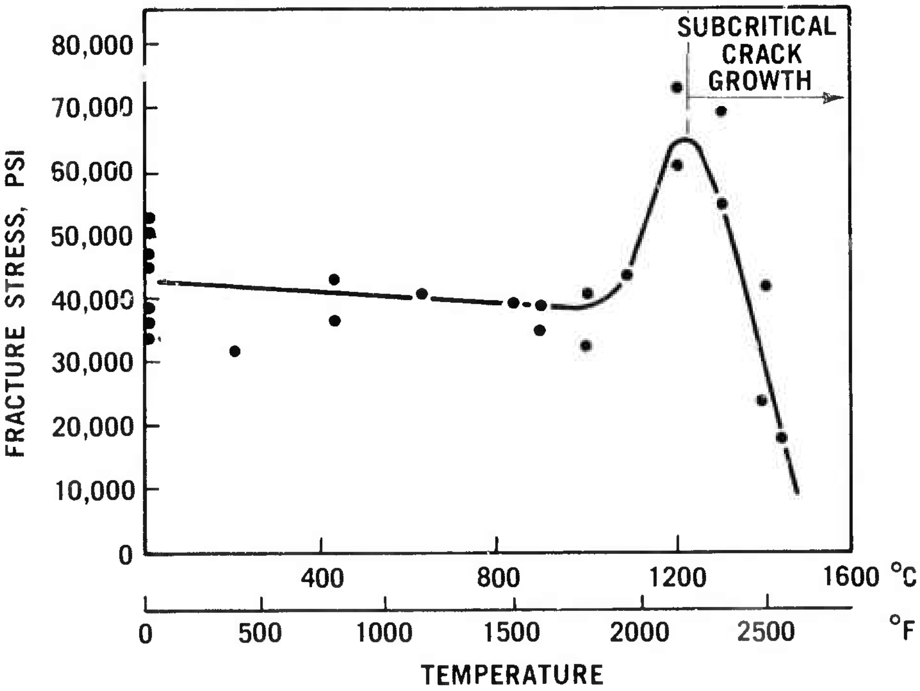

Figure 4.28 Temperature Dependence of Flexural Strength of REFEL SiC. Range Over Which Subcritical Crack Growth Was Observed is Indicated

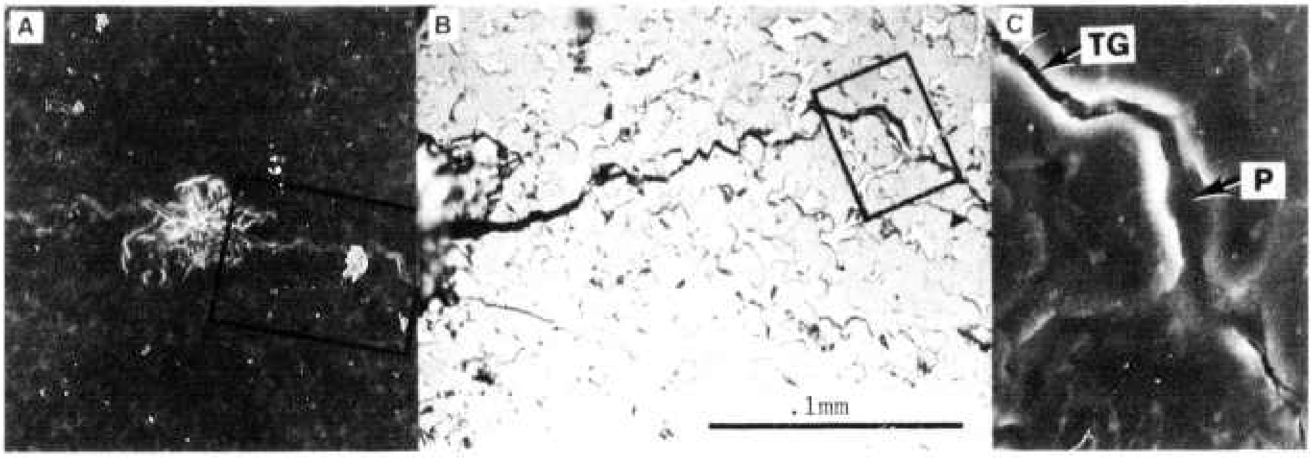

Figure 4.29 (a) SEM Micrograph of Crack Extension Around an Indented Surface Under Load at 1300°C. (b) Optical Micrograph of Area Indicated in (a) Illustrating the Disposition of the Silicon Phase and the Fracture Path. (c) SEM Micrograph of Area Marked in (b)

Sialon Materials

As an integral part of the development of Sialon type materials, the high temperature fracture resistance was evaluated in several Y_2O_3 bearing materials (Figure 4.30). The temperature dependent fracture behavior observed is portrayed in Figure 4.30, where each line at temperature is based on an average of the measured strength. While the data scatter, particularly at room temperature, was significant and could be reduced through greater care in processing and materials preparation, some of the results at temperature appears to be typical of brittle material behavior, i.e. a slight "improvement" in fast fracture strength at high temperature. Such behavior is usually a precursor to dominant time-dependent fracture phenomena. The Sialons seem to behave this way, though the degree is strongly influenced by composition and process history (i.e. disposition of phases, both crystalline and glassy). Subcritical crack growth is a common phenomenon at temperatures as low as 1000°C in some of the materials listed in Figure 4.30.

The extent of subcritical crack growth as a function of temperature in precracked specimens is displayed fractographically in Figure 4.31. At the optical microscopy magnifications employed, the general fracture photography appears like that of hot pressed silicon nitride (7). As is evident from the higher magnification pictures, the fracture mode at temperature in the slow crack growth regime radiates outward from the initiating emplaced flaw, whereas at room temperature the fracture originating crack is less well defined.

In another Sialon, the time-dependent processes leading to failure at first worked to blunt the initial flaw, causing it to widen prior to lengthening via a myriad of small branching cracks (Figure 4.32). The entire stressed tensile face became covered with slow growing cracks prior to catastrophic failure, a unique fracture chronology for a brittle material. Thus, while the gross temperature dependent behavior is similar among the Sialons observed, the details of failure process are complex and are almost certain to be altered by control of the microstructural disposition of phases.

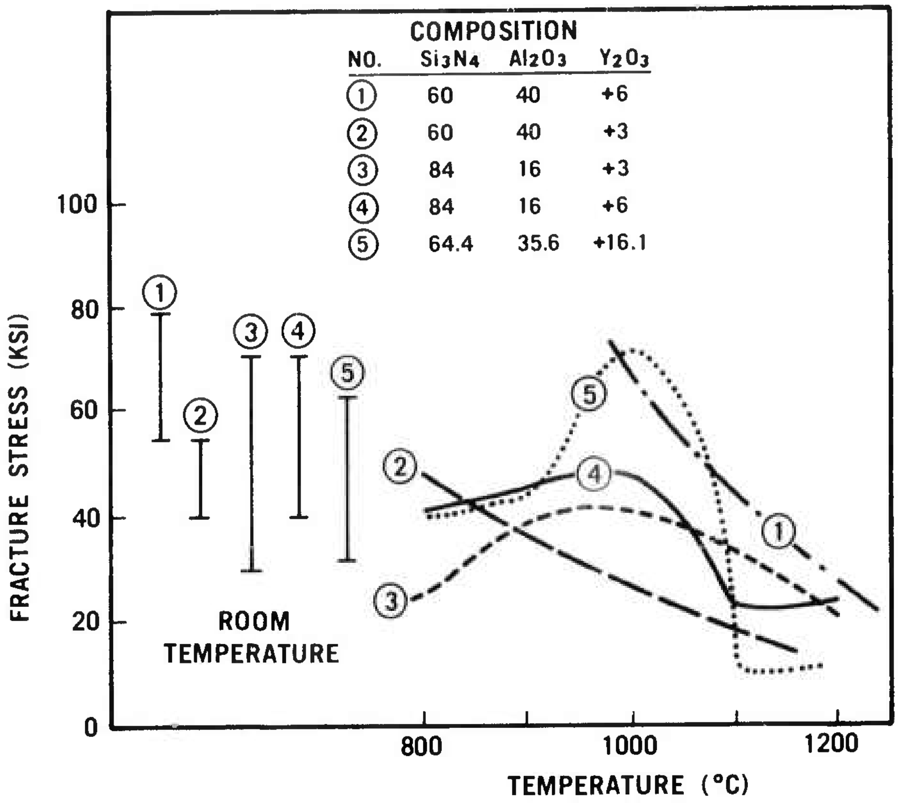

Figure 4.30 Temperature Dependence of Fracture Strength in Selected Yttria Containing Sialon Type of Materials

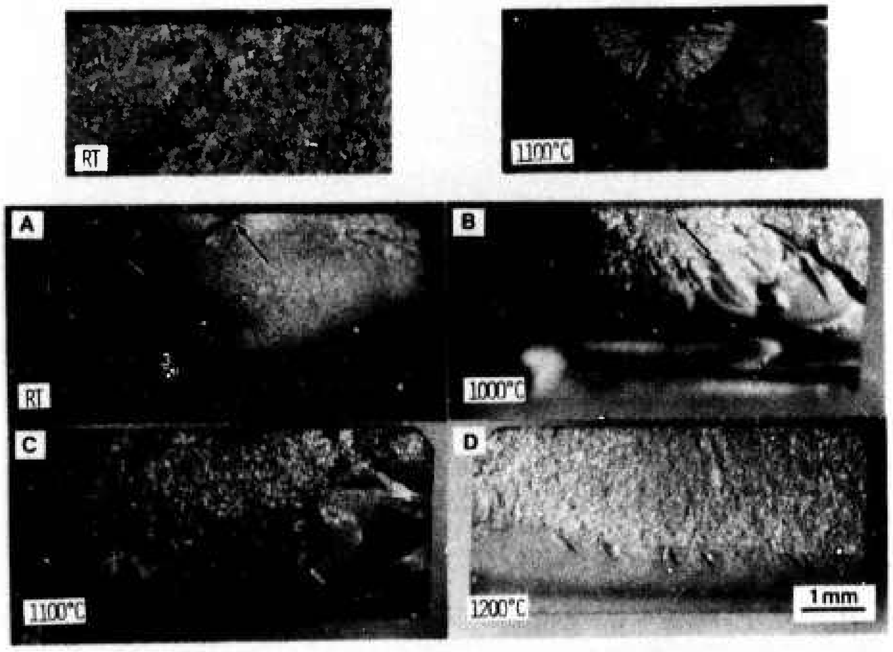

SIALON

60% Si_3N_4 40% AL_2O_3 + 6% Y_2O_3

Figure 4.31 Temperature Dependence of the Extent of Subcritical Crack Growth in a 60% Si_3N_4 - 40% Al_2O_3 + 6% Y_2O_3 Sialon Material. Top Insets Are High Magnification Micrographs of the Fracture Utilizing Flaws Indicated by Arrow

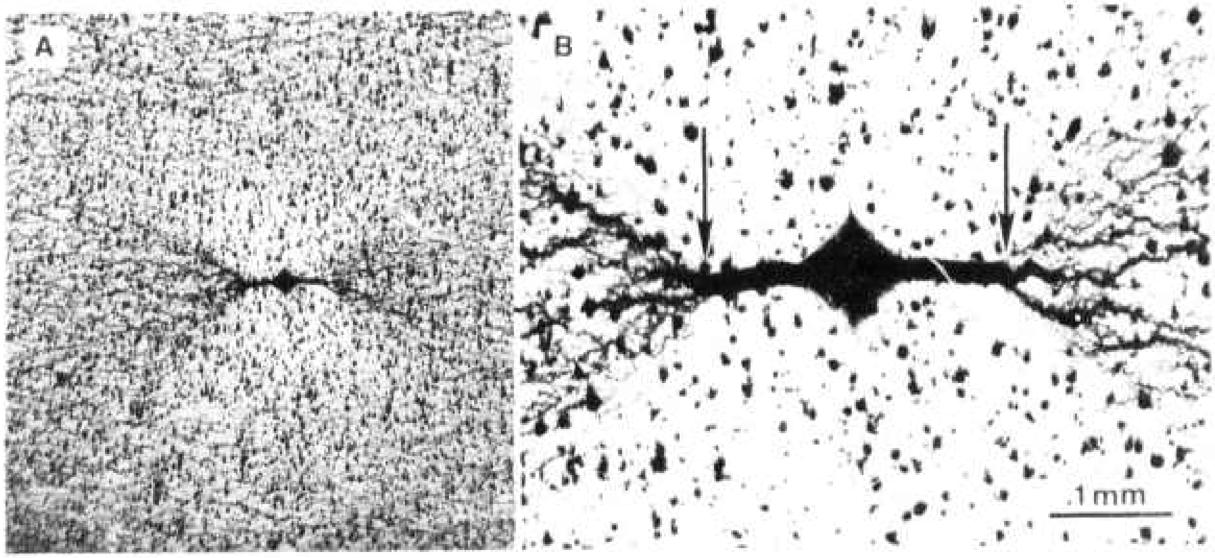

Figure 4.32 Crack Blunting Through Microcrack Formation in a $64.4\%\ Si_3N_4 - 35.6\%\ Al_2O_3 + 16.1\%\ Y_2O_3$ Sialon

4.7 NONDESTRUCTIVE EVALUATION OF CERAMIC COMPONENTS

Introduction

Nondestructive evaluation (NDE) methods have been used to monitor fabrication developments toward producing improved quality engine test hardware. Many problems associated with specific fabrication steps have been identified and solutions verified using NDE methods. Radiography, dye penetrant and visual (20-30x) inspections as well as sonic velocity measurements are routinely employed to define the effectiveness of material and process changes.

Sonic Velocities of Silicon Nitride

The relationship between sonic velocity and the density of silicon nitride has been previously discussed (7). A linear relationship was observed between sonic velocity and final density when nitriding parameters were held constant. Recently, variations in material velocity have been observed when the nitriding parameters such as time, temperature, and gaseous atmosphere were changed.

Two lots of rotor tip shrouds, each machined from the same slip cast, sintered silicon preform, were nitrided using the same time-temperature schedule but different gaseous atmospheres. Previously, a good correlation between nitrided density and sonic velocity was always observed (7). However, varying the nitriding atmosphere resulted in a final product which no longer exhibited this relationship. The material velocities, elastic moduli and densities are shown in Table 4.13 for the two lots of rotor shrouds.

TABLE 4.13

PROPERTIES OF NITRIDED ROTOR SHROUDS

Series Identification	Nitriding Atmosphere	Average Sonic Velocities (10^5cm/sec) V_L	V_T	MOE (10^6 psi)	Density (gm/cm^3)
11	4%H - 96% N_2	8.4	5.05	21.0	2.50
12	100% N_2	7.4	4.5	16.0	2.49

In order to further verify these apparent differences, test bars (1/8 x 1/4 x 1-1/4 inches) were machined from shrouds representing each nitrided lot. The flexural strengths were then determined on an Instron testing machine using a 3/8 x 3/4 inch, 4-point bending fixture. The average strength of one series was 25.4 ksi compared to 21.0 ksi for the other series; again indicating an increase in the mechanical properties achieved in the 4% H_2 -96%N_2 firing.

Further discussion concerning nitriding cycles appears in Section 4.2 and 4.3 of this report.

The current relationship between silicon nitride density and sonic velocity obtained using a furnace atmosphere of 4% H_2 - 96% N_2 is shown in Figure 4.33. Sonic velocities increased for both longitudinal and transverse modes over the density range 2.5 - 2.9 gm/cm^3. This increase is also presented in Figure 4.34 where the acoustic impedance versus modulus of elasticity curves are shown for recent and previous nitridings.

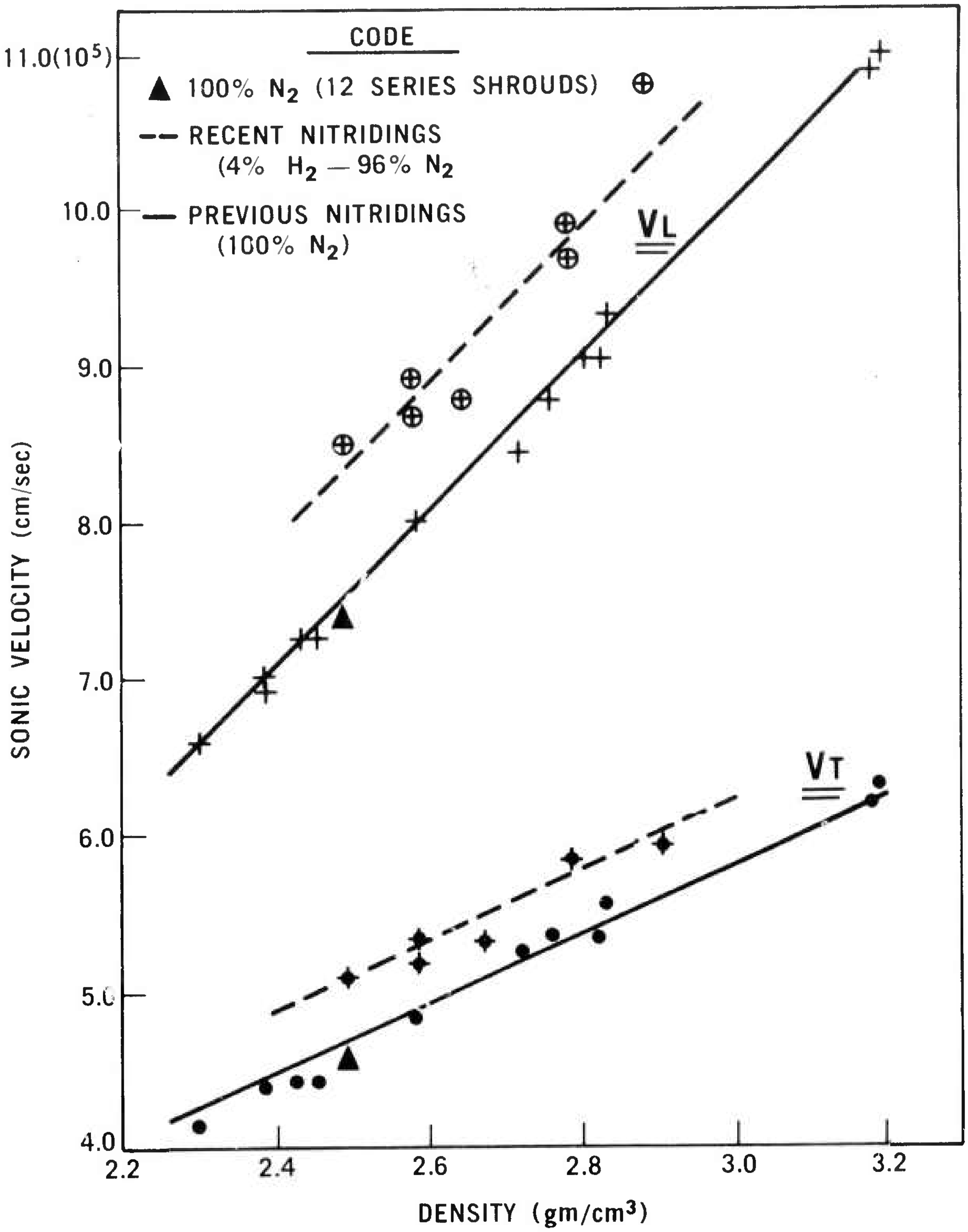

Figure 4.33 Longitudinal (V_l) and Transverse (V_t) Sonic Velocity vs Density of Silicon Nitride

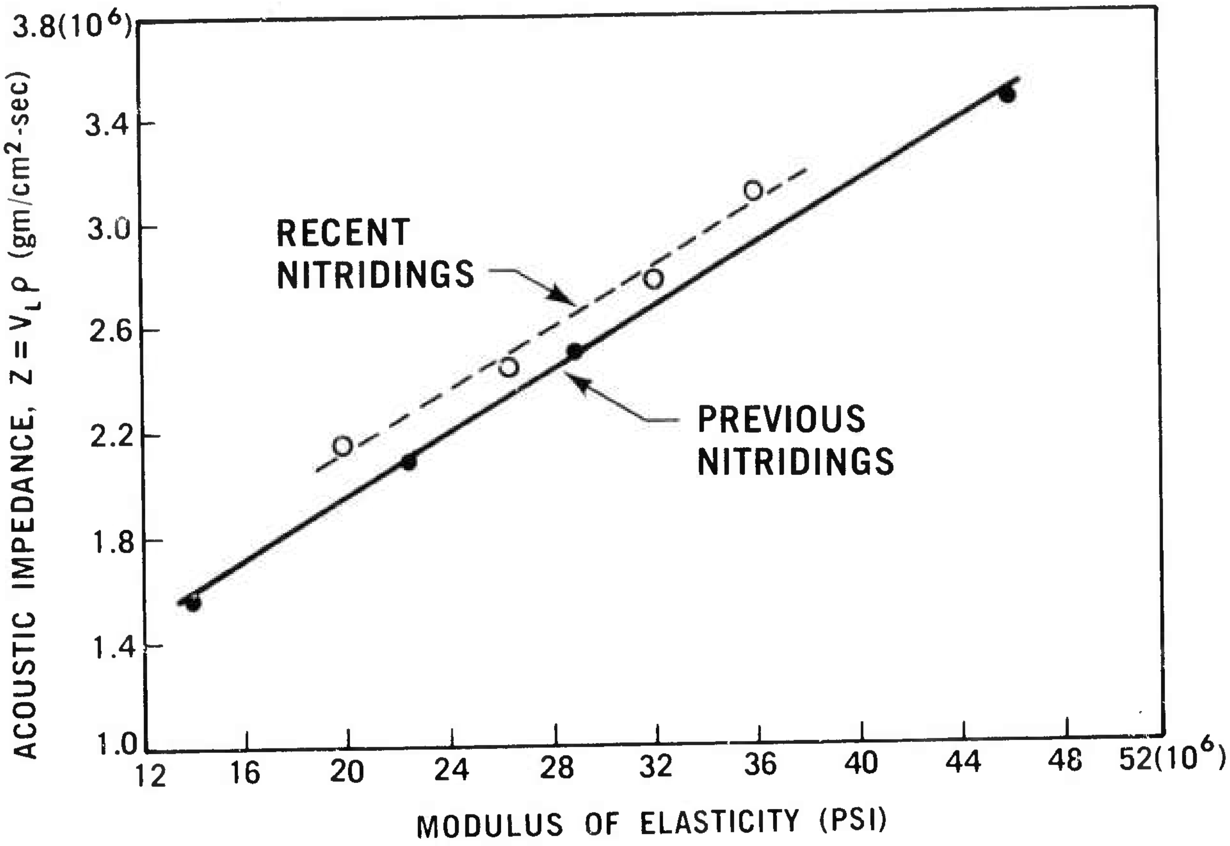

Figure 4.34 Acoustic Impedance vs Modulus of Elasticity of Silicon Nitride

The implications of this data are that sonic velocity measurements can be used to effectively and nondestructively detect improvements in the inherent properties of silicon nitride ceramics. While many tests would be required to establish the direct relationship between material strength and sonic velocity, a relative evaluation can be made with respect to fabrication changes. Similar data can also be obtained on engine tested components to evaluate the effectiveness of fabrication changes and their response to an engine environment.

NDE-General Technology

Radiographic and visual inspections at 20x-30x of as-molded rotor blade rings, stator assemblies and nose cones and dye penetrant inspection of these components after nitriding continue to be the primary NDE methods used to obtain the best quality hardware. Further discussion concerning the specific use of these methods can be found in Sections 3.1.2 and 3.2.2 of this report.

5. PROGRESS ON THE STATIONARY TURBINE PROJECT

Introduction and Summary

The principal objective of the Stationary Gas Turbine Project is to demonstrate the use of uncooled ceramic first stage stator vanes operating at a peak inlet temperature of 2500°F. The demonstration as now planned is to be accomplished in a static rig under controlled transient conditions which closely simulate stationary gas turbine operation rather than in an actual test turbine of 30 MW frame size. Successful completion of the test program should establish ceramics (i.e. hot-pressed silicon nitride) as viable engineering materials for use in demanding high temperature structural applications. While working toward the ceramic stator vane demonstration, very significant developments have been made in the areas of brittle material design technology, materials science and technology, materials fabrication, and component testing. The baseline technology developed on the ARPA program thus becomes the keystone to further component and engine development that will provide high performance gas turbines with potential benefit for both the military and domestic sectors of our nation.

Gas turbine power generation represents a proven technology which today has the lowest capital cost per kW of installed capacity of any fossil fuel system. Currently, the stationary gas turbine generator is used primarily to meet peaking power requirements. Available in sizes which range nominally from 19 to 70 megawatts, these units are applicable to DOD installations that require on-site power generation. They are also suitable for mounting on barges to supply remote locations accessible only by way of natural waterways. As a prime mover in ship propulsion, the heavy-duty gas turbine is attracting considerable attention because of its potential for improved performance and reliability at lower cost.

There is renewed interest in the combined cycle for electrical power generation as a result of the fuel crisis and energy conservation. When gas turbines and steam turbines are used together in a combined cycle system, significant increases in efficiency accrue in the conversion of fuel to electrical energy. For example, present-day turbo-generating machinery (inlet temperature 1900-2000°F) operating in series with steam turbines via waste heat boilers attain total system thermal efficiencies of 38-42% making combined cycle plants competitive for intermediate load power generation. At 2500°F, turbine inlet temperature, 50% efficiency is achievable making combined cycle installations competitive for base load service. It is here that the importance of ceramics is emphasized because refractory ceramics provide the only direct materials approach to reaching 2500°F turbine inlet temperatures. In addition, the hot corrosion-erosion resistance of ceramics such as silicon nitride and silicon carbide is expected to provide extended long-term reliability when using a wide variety of fuels including coal derivatives.

5.1 STATIONARY TURBINE PROJECT PLAN

The Stationary Turbine Project was organized to design a turbine with ceramic stator vanes in the first stage of the power section. This, then, represents the initial step in the development of a high temperature ceramic turbine using a philosophy of successive stage replacement whereby ceramic blade development for the first stage rotor follows logically with subsequent stage development downstream emphasizing design modification and scale up problems. The Westinghouse 251, 30 MW stationary power turbine was selected for the ceramic vane demonstration. A recent change in the program plan, however, indicates that ceramic stator vane performance be demonstrated in a pressurized static rig at a peak inlet temperature of 2500°F only. The rig is illustrated in Figure 5.1.

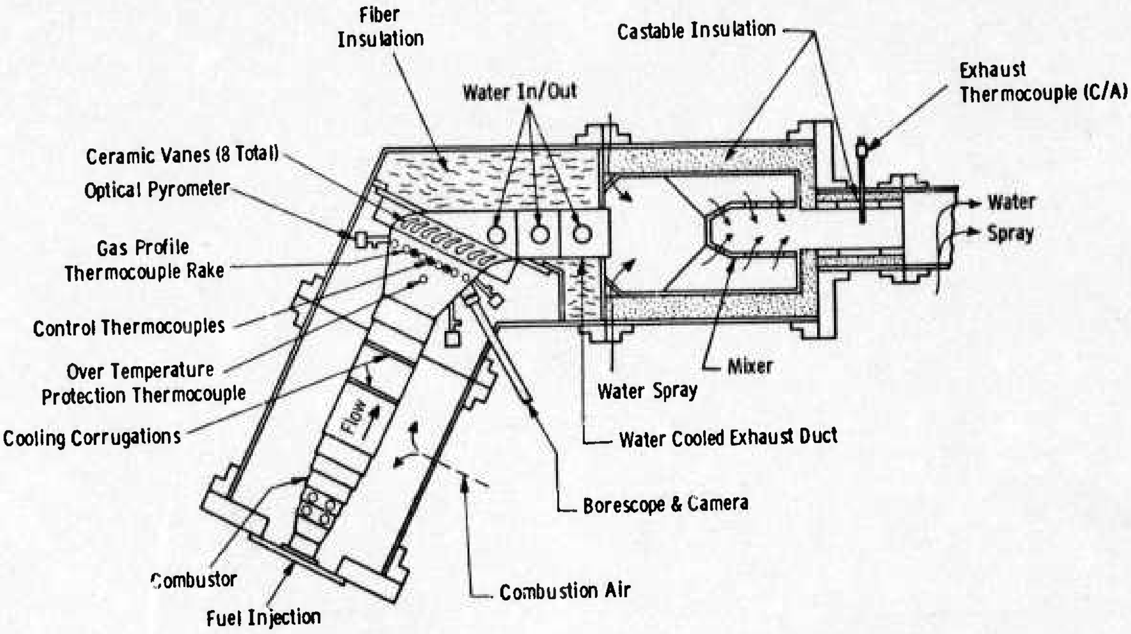
Fiber Insulation
Castable Insulation
Exhaust Thermocouple (C/A)
Water In/Out
Ceramic Vanes (8 Total)
Optical Pyrometer
Water
Spray
Gas Profile Thermocouple Rake
Control Thermocouples
Over Temperature Protection Thermocouple
Cooling Corrugations
Flow
Mixer
Water Spray
Water Cooled Exhaust Duct
Borescope & Camera
Combustor
Fuel Injection
Combustion Air

Figure 5.1 Plan View of 2500°F Static Test Rig

Preheated air at 8 atmospheres pressure is supplied to the rig from an external steam driven compressor. Air mixes with fuel and is ignited in the primary zone of a Haynes 188 combustor which is equivalent in size to combustors used in the commercial 251, 30 MW power turbine but modified for short-term, high temperature service (peak 2500°F at the vane inlet position). Hot gas passes downstream through the combustion section mixing with secondary air. Flow continues through a partially constricted, conventionally designed transition zone (also Haynes 188 for high temperature service) to enter and be diverted in direction by the eight ceramic vane cascade. Exhaust is accomplished through a jacketed, water cooled metal duct which is followed downstream by a water spray cooled mixer, a pressure valve and finally, an exhaust manifold which is vented to the atmosphere via a stack.

This is a test of actual size component hardware under realistic turbine conditions at 0.8 simulation. Plant facilities limit the pressure ratio within the laboratory to 8:1, whereas production machinery is designed for 10.5:1.

The first stage stator vane was selected for development and demonstration on the ARPA program because it represents the highest temperature material application ultimately affecting power and efficiency. Solving the design problems associated with the inlet stator vane and developing the analytical capability for design evaluation should establish definite feasibility for the design of other turbine components, i.e., first stage turbine blades.

Once feasibility and a performance base is achieved in the static rig, full scale testing in an actual test turbine becomes possible. Production and adaptability to larger production turbines may then be logical.

5.2 STATUS SUMMARY -- STATIONARY TURBINE PROJECT

As originally conceived, the ARPA Stationary Turbine Project had a two-fold objective: 1) the design, development, evaluation and demonstration of ceramic stator vanes in a gas turbine operating at a peak temperature of 2500°F for 100 cycles simulating peaking service conditions and 2) ceramic rotor blade design with performance simulation by computer. This scope of work has proven too formidable for a five-year program at the funding level proposed considering the current state-of-the-art in materials technology. Therefore, the revised goals include ceramic vane evaluation and a design demonstration only in a static rig at 2500°F peak temperature under controlled transient conditions of cyclic service. One hundred cycles simulating peaking service are proposed. Work continues within two major task areas subdivided as follows:

I. Component Development
   (a) Design
   (b) Fabrication
   (c) Testing

II. Material Technology
   (a) Material Engineering Data
   (b) Material Science
   (c) Non-Destructive Evaluation

Current status is summarized according to Task in Sections 5.2.1 and 5.2.2 of this report.

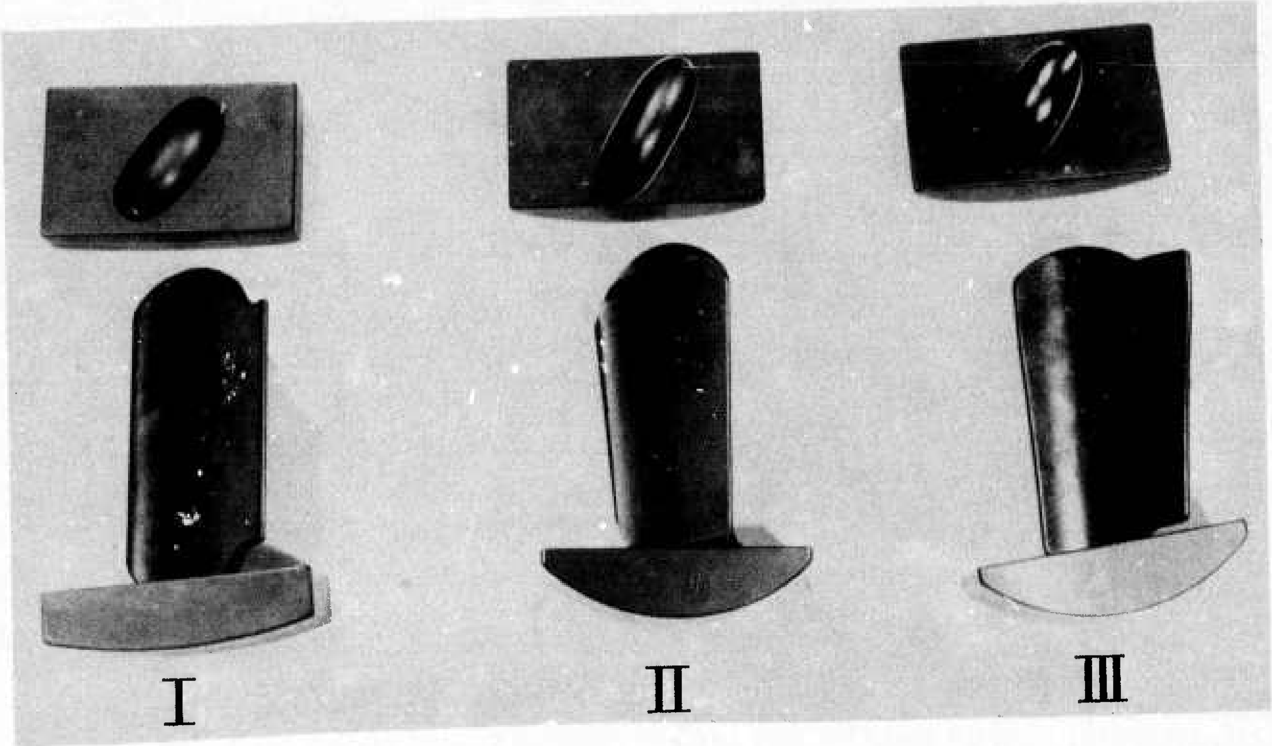

Figure 5.2 Stator Vane Design Iterations
I. Parallel Sided Airfoil
II. Tapered-Twisted Airfoil with Full Cavity Filling Tenons
III. Tapered-Twisted Airfoil

5.2.1 COMPONENT DEVELOPMENT

Component Development deals with the design and analysis of the first stage stator vane, fabrication of first stage stator vane design iterations, and the testing of first stage stator vanes in the static rig at 2200° and 2500°F.

Design

A novel, power-generation size ceramic stator vane has evolved from a unique sandwich type multiple component concept. The concept utilizes a three-piece vane that is insulated, cushioned and supported in such a manner as to minimize critical steady state and transient thermal stresses which would otherwise preclude the use of brittle materials in an industrial turbine. The configuration to be tested in the static rig at 2500°F represents the third design iteration featuring a tapered-twisted airfoil with modified end cap construction. Component evolution is illustrated in Figure 5.2.

Since the problem of stress concentration is foremost in the design and use of brittle materials for engineering applications, stress distribution in critical elements of a component design must be defined. Two-dimensional finite element arrays are adequate for the definition and analysis of most stress distributions in the three-piece stator vane assembly but interfacial contact stresses and the stress developed in rotor blades require a more sophisticated volume element (3-dimensional) program for resolution. ARPA partially supported the development of this valuable tool as part of the Stationary Gas Turbine Project.

Status

- A novel 3-piece, uncooled, simply-supported ceramic stator vane assembly was selected and designed.(1,2,3,4)

- To minimize stress, the ceramic vane was reduced to 1/2 size and cross-section from that of the metal vane counterpart.(2)

- Critical stresses of the 3-piece ceramic vane assembly have been evaluated for both transient and steady state conditions expected during turbine operation at 2500°F.(2,3,4,5)

- A full scale kinematic model was built to show that the stator vane assembly as designed was functional even when subjected to differential motions well in excess of design limits.(3)

- The detailed design of stator vane assembly, including compressive spring loading and the ceramic/metal insulation and support system was completed.(2,3)

- 3-D finite element code (WISEC) has been completed except for creep and contact stress analysis.(2,3,4,5,6)

- Preliminary analysis of a ceramic rotor blade using the 3-D finite element code has been completed.(4,5,6)

- A first stage air-cooled metal blade has been designed for the advanced test turbine. Design modifications for the air-cooled, metal second stage vanes and rotor blades were also completed before the program revision was made not to perform the actual turbine test.(7)

Fabrication

Fabrication is equally as important an aspect as design in the successful application of ceramics for gas turbines. Only fully dense, high-strength Si_3N_4 and SiC were selected for component development in the Stationary Turbine Project. The ARPA program has provided the first full-scale, power generation size, ceramic stator vanes fabricated from hot-pressed Si_3N_4 and SiC. These were made to Westinghouse specifications by the Norton Company of Worcester, Massachusetts and their vendors from hot-pressed billets. Diamond tools and tracer grinding techniques were employed to produce the stator vane geometry.

Status

- Over 40 prototype vane sets for testing have been successfully fabricated by hot-pressing and machining from both Si_3N_4 and SiC.(3,4,5,6)

- 28 tapered-twisted airfoils and 24 end caps machined to the 3 in. radius and 3/8 nominal cavity depth specified for the 3rd generation (advanced turbine) design were received for the 2500°F static rig test.

- Experimental silicon nitride billets hot-pressed with yttria have been received for evaluation as an improved stator vane material.(9)

Testing

The verification of design and materials by test of full scale parts under realistic conditions represents a very important step in the ARPA program to develop ceramic vanes. The plan is to test in an extensively instrumented static rig first at 2200°F and then 2500°F under conditions very similar to those encountered in an actual gas turbine.

Status

- Design and construction of the instrumented static rig was completed after considerable delays due to procurement and installation difficulties.(3,4)

- 2200°F static rig testing was successfully completed using parallel sided Si_3N_4 vane assemblies (Figure 5.3).(5)

- Silicon nitride stator vane assemblies were shown to be tougher, more thermal shock resistant, and generally more compatible with a transient turbine environment than silicon carbide stator vanes of the same design after 5 cycles of static rig testing at 2500°F (Figure 5.4).(8)

- The static rig for the continuation of 2500°F testing has been rebuilt a second time to include a more extensively air-cooled combustor, a water-cooled exhaust duct and water spray cooled mixer.(8)

- Static rig testing at 2500°F was resumed in October. Steady-state runs were made to define gas temperature profiles and establish operating parameters for cyclic testing.

- After 25 cycles of transient temperature testing, shifts in outer end cap locations caused an edge loading condition at inner airfoil end cap positions. Chips were observed in four of eight airfoils under test.

- An additional 35 cycles were run after damaged components were replaced. Cracks developed in the airfoil section of vane 5 after 22 cycles. The test was terminated after the 35th cycle when cracks developed in airfoil #6; one of the airfoils that had been preoxidized.

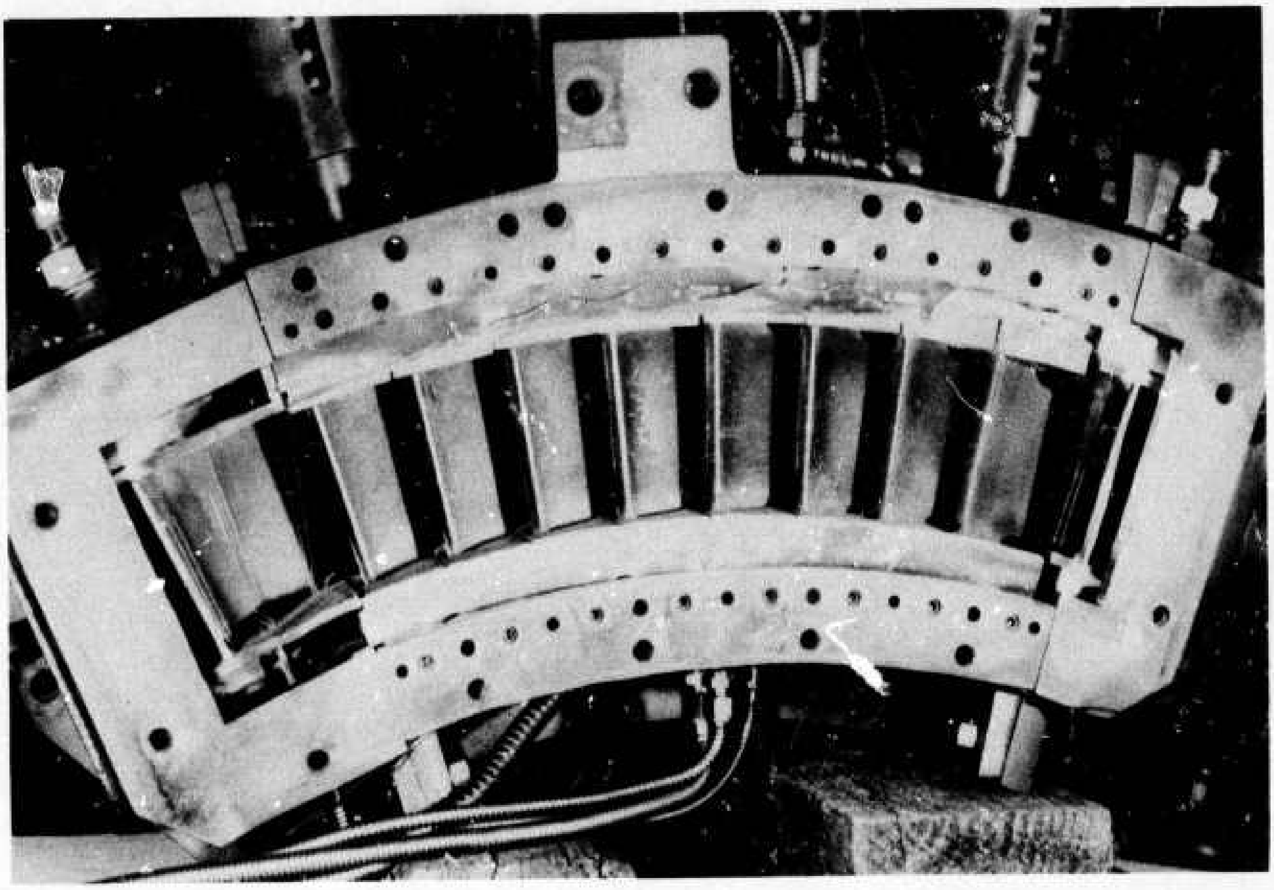

Figure 5.3 Stator Vane Test Assembly with Si_3N_4-3 Piece Stator Vanes and LAS Insulator at the Completion of 2200°F Static Rig Tests (105 cycles)

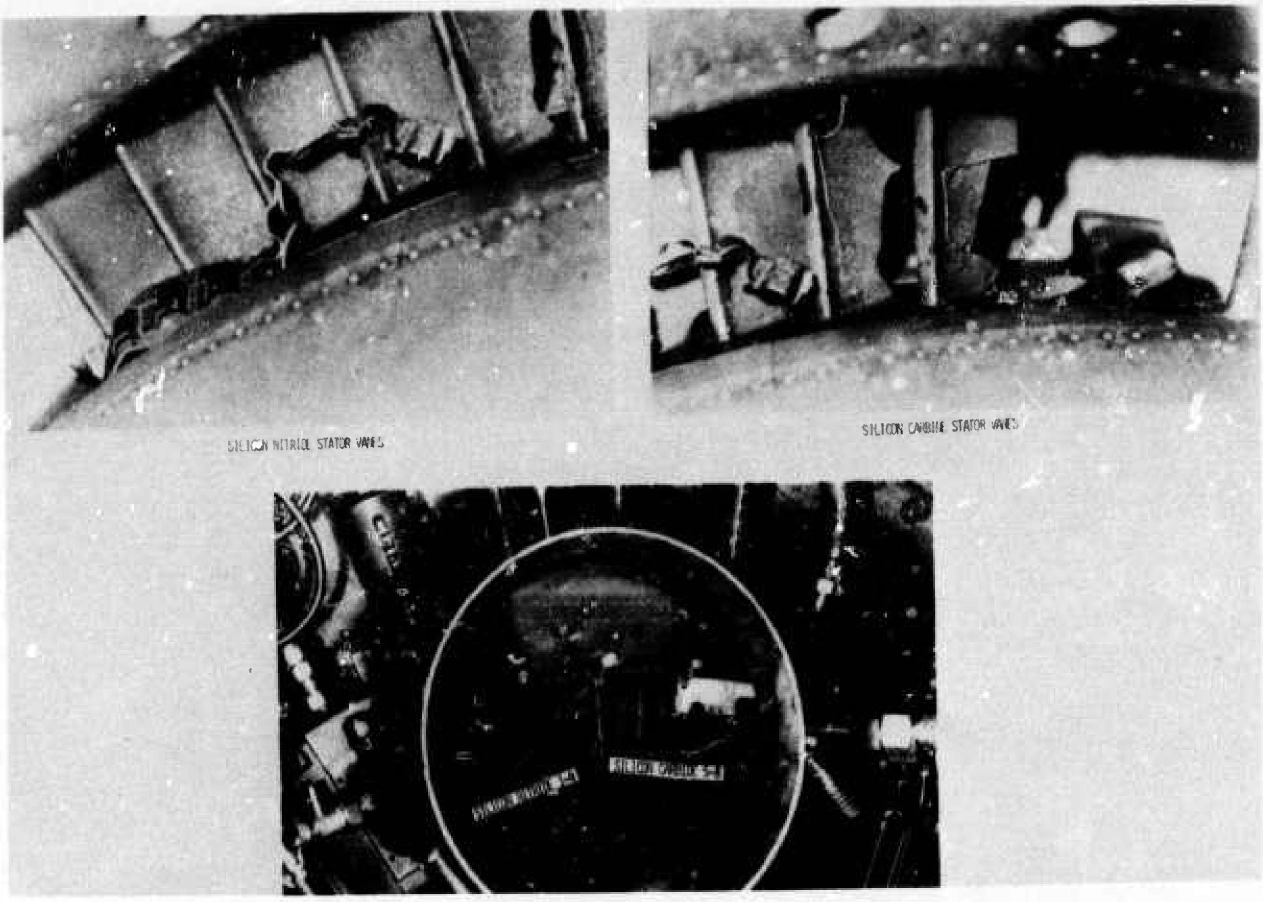
SILICON NITRIDE STATOR VANES
SILICON CARBIDE STATOR VANES

Figure 5.4 Results of Initial 2500°F Static Rig Test - Abortive Combustion Failure After 5 Cycles

5.2.2 MATERIALS TECHNOLOGY

Materials technology is considered a basic building block for design, fabrication and testing. The sub-tasks consist of Materials Engineering Data, Materials Science, and Non-Destructive Evaluation of Materials. The plan has been to continue this phase throughout the program in order to properly evaluate material improvements and design changes that evolve naturally in a focused engineering program.

Material Engineering Data

Design technology is highly dependent upon the thermal, physical and mechanical properties of the materials being used. A substantial effort has been expended to collect engineering property data for commercial hot-pressed Si_3N_4 and SiC to make the design code more comprehensive. The interaction between properties and design is shown in Figure 5.5. Since the present design code uses an elastic-to-fracture criterion for stator vane ceramics and since the transient stresses are much larger than those of the steady-state, thermal properties have been measured extensively. Both established and new testing procedures have been utilized to evaluate the physical and mechanical properties of gas turbine ceramics at temperatures up to 2500°F.

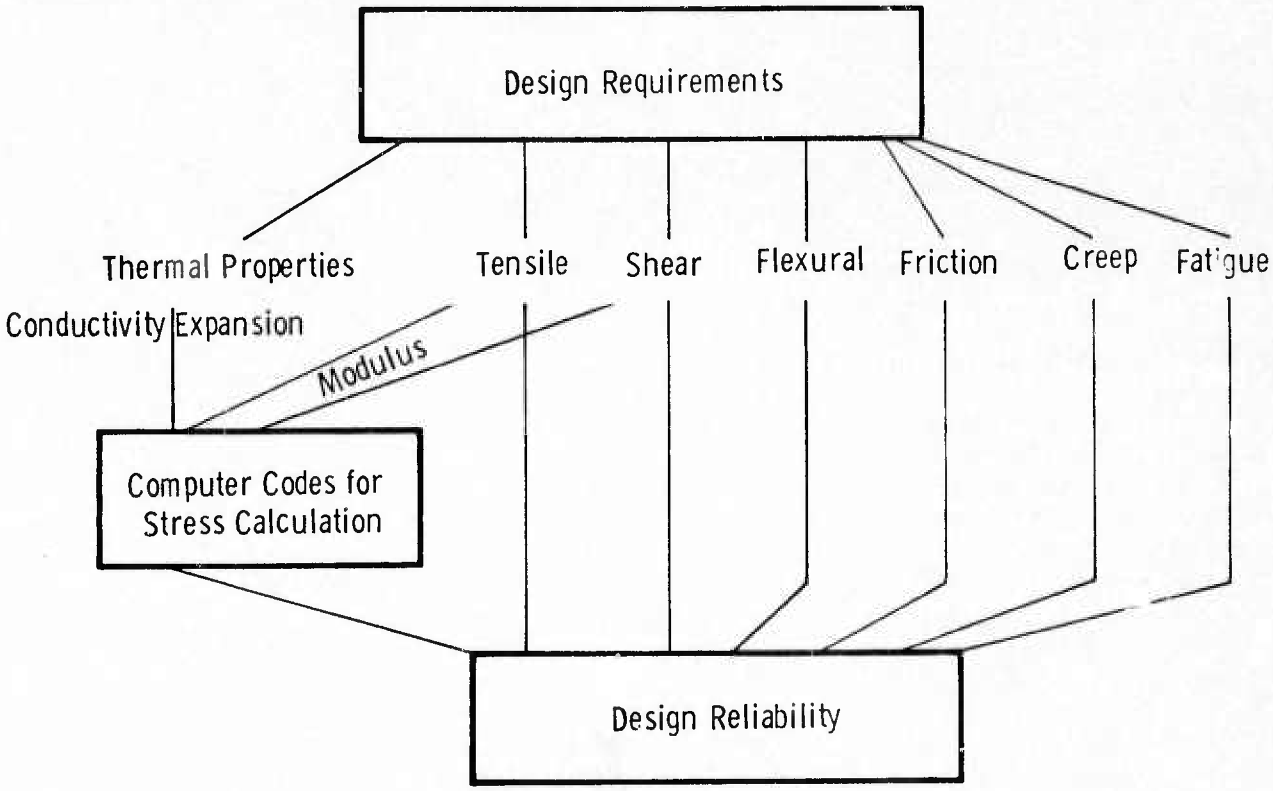
Design Requirements
Thermal Properties
Tensile
Shear
Flexural
Friction
Creep
Fatigue
Conductivity
Expansion
Modulus
Computer Codes for Stress Calculation
Design Reliability

Figure 5.5 The Interactions between Material Properties and Design

Status

- Thermal properties (expansion, conductivity and specific heat) have been characterized from RT to 2500°F for hot-pressed Si_3N_4 (Norton HS-130) and hot-pressed SiC (Norton NC-203).(3,4)

- Flexural strength, tensile strength, shear strength, friction behavior, high cycle fatigue and elastic properties have been characterized from RT to 2500°F for both HS-130 Si_3N_4 and NC-203 SiC.(2-6)

- Creep, stress rupture, low cycle fatigue, and corrosion-erosion behavior have been evaluated because these properties relate to reliability.(3-7)

- Statistical treatment of engineering property data continues. Additional information is continually added to the data base.(2-4)

- Stress-strain data in the tensile mode indicate that Norton HS-130 (NC-132) silicon nitride is essentially elastic to failure up to 2200°F at loading rates in the range of 0.001 in/in/minute. Plastic deformation is apparent at temperatures of 2300°F and above.(7)

- 4000 hour static oxidation tests of silicon nitride and silicon carbide indicate significant flexural strength degradation after 100 hours due to surface reaction between the oxide film and substrate material.(8)

- An evaluation of hot-pressed silicon nitride hot-pressed with yttria shows improvements in high temperature strength and creep resistance. The material is subject to a low temperature instability (at 1800°F) which causes decrepitation and subsequent loss of strength(8).

- Ten thousand hours stress rupture life is reported for Norton NC-132 silicon nitride at 2100°F under 10,000 psi stress.

- The physical properties of the boron nitride insulation materials have been determined to verify vendor data. Flexural strength, elastic modulus, shear modulus and thermal expansion are reported for prominent directions of the material.

Materials Science

Detailed investigations into materials science develop an understanding of material behavior which will hopefully lead to property improvements. This is particularly important since the ceramic materials being utilized in turbine engines are relatively new and appear capable of considerable improvement. The material science investigation has been defined by the engineering requirements of the system and thereby relates mainly to the commercial materials being used. They contribute to better control of the fabrication process, better properties, and tend to extend the useful life of the ceramic materials through property improvement.

The value of the material science work has already been demonstrated by the property improvements that have been made since the onset of the ARPA program. By discovering that certain impurities and foreign inclusions were detrimental to the strength of hot-pressed Si_3N_4 above 1800°F and learning how to process starting powders to achieve a desired microstructure, strength at 2550°F has been improved. The task of material development and improvement remains far from being completed. Westinghouse has recently added Si_3N_4 powder preparation and an experimental hot-pressing study to the Material Sciences work scope because materials remain a critical aspect of high temperature turbine technology.

Status

- Identification of microstructural details of commercial hot-pressed Si_3N_4 (Norton HS-110 and 130) and hot-pressed SiC (Norton NC-203) are complete.(1,2,3,4)

- Correlations between properties, microstructure and fabrication processing for HS-130 Si_3N_4 and NC-203 SiC are complete.(3,4,5,6)

- Chemical analyses of Norton HS-130 Si_3N_4 and NC-203 SiC are complete.(6)

- Analyses of thermodynamic data for Si_3N_4 and SiC are complete.(1,2)

- Static oxidation kinetics of HS-130 Si_3N_4 and NC-203 SiC are complete.(3,4,5)

- The loss of strength in hot-pressed silicon nitride after prolonged oxidation at 2500°F is attributed to a surface reaction between the oxide film developed (MgO · SiO_2 · CaO · etc.) and the substrate which appears soluble in it.(8)

- The poor low temperature phase instability of yttria hot-pressed silicon nitride appears to be associated with a $Si_3N_4 \cdot Y_2O_3$ phase in the microstructure.(8)

- Furnace modifications now permit the production of high purity alpha silicon nitride powder of low oxygen content at the rate of 8-9 kg/month.

- Static oxidation tests of NC-132 silicon nitride in an alumina lined muffle furnace indicate strength degradation at 2000° and 2200°F as well as 2500°F.

Non-Destructive Evaluation

Microstructural uniformity is necessary for reliable structural ceramics for gas turbine engine applications. The objectives of NDE are to identify and classify microstructural and macrostructural defects and relate these to the component fabrication process. The ultimate goal is to define meaningful inspection methods that can be used to accept/reject components prior to installation in the engine. Procedures utilizing ultrasonics, x-ray radiography, dye penetrants, and acoustic emission are currently being applied to ceramic systems for evaluation purposes.

Status

- Suitability of dye penetrants for detecting surface connected porosity and surface cracks has been established for ceramic gas turbine components.(5)

- Sensitivity of commercial techniques in ultrasonic A&C scanning to low density inclusions and segregated voids in hot-pressed Si_3N_4 and SiC has been established.(5,6)

- Detection limits and sensitivity by ultrasonic inspection has been established for hot-pressed ceramic turbine components.(5,6)

- Feasibility of applying acoustic emission to proof testing of ceramic components has been established.(4)

- Detection limits and sensitivity by x-ray radiographic inspection has been established for hot-pressed ceramic turbine components.(5,6)

- NDE of ceramic turbine components is continuing. The 28 Si_3N_4 vane sets for static rig testing at 2500°F have been qualified.(8)

- All components from the 2500°F static rig testing were re-examined after 25 and an additional 35 cycles, respectively, as part of the failure analysis. Dye penetrant techniques were used to define the full extent of component cracking.

5.3 FUTURE PLANS

The scope of work for the last six months of the current contract have been revised to be consistent with the overall program objectives as discussed in previous sections of this report. Work will continue under categories of Component Development, Material Technology and Material Fabrication. The total program will be summarized in final report form.

Ceramic Stator Vane Development

- Assemble the static rig and complete the thermal cyclic testing of Si_3N_4 stator vane assemblies and boron nitride insulators at 2500°F.
- Complete performance evaluation of static rig test and perform stress analysis of Si_3N_4 vanes using temperature profiles compiled from 2500°F test.

Material Technology

- Optimize improved Si_3N_4 compositions for hot-pressing.
- Conduct oxidation and hot corrosion experiments on improved candidate materials to determine environmental effects on mechanical properties.
- Accelerate process development of the high purity Si_3N_4 powder required to fabricate improved Si_3N_4.
- Evaluate the high temperature properties of improved Si_3N_4 materials.
- Evaluate the oxidation resistance of CVD coated, hot-pressed Si_3N_4.
- Complete the determination of the pertinent thermal and mechanical properties of boron nitride.
- Complete microstructure, NDE and failure analysis of stator vane assemblies and associated hardware from 2500°F static rig tests.

Material Fabrication

- Develop hot-pressing schedules and produce fully dense billets of improved materials.
- Purchase billets of improved materials from qualified vendors for evaluation of properties.

Program Management

- Complete final report.

6. PROGRESS ON CERAMIC COMPONENT DEVELOPMENT - STATIONARY TURBINE PROJECT

6.1 STATOR VANE DEVELOPMENT

Summary

The static rig testing of silicon nitride stator vanes and boron nitride insulators at 2500°F was resumed in October. After steady state temperature runs at 1400, 2000 and 2300°F to establish gas temperature profiles, a cyclic mode of testing was imposed in compliance with the test requirements. Twenty-five cycles from 2500°F to 1200°F under controlled transient conditions were completed in the first series. The rig was opened after the second and fifth cycles primarily to check the condition of the newly designed Haynes 188 combustor. Combustor cooling was more than adequate and the vane assemblies appeared to be functioning normally.

When the test was interrupted after cycle 25 for visual inspection of vanes and insulators, a shift at the outer end cap positions was observed. This condition caused contact between the airfoils and inner end caps at the tenon-trailing edge blend radius of the respective airfoils. No damage was apparent on the pressure side of the airfoils, however. Chips were identified on the suction sides of airfoils 5, 6, 7 and 8. An eighth-inch crack was located in the trailing edge of airfoil 3, a preoxidized airfoil. Outer end cap #1 was cracked and the outer insulator over vane positions 1 and 2 was damaged.

The rig was reassembled using new components to replace those damaged during the first 25 cycles. Thirty-five additional transients were run. A crack appeared in the leading edge of vane 5 during the 22nd cycle. The crack was observed to propagate diagonally upward toward the trailing edge as a result of 8 to 10 subsequent cycles. This test series was terminated at the end of the 35th cycle (test cycle #60) when a crack developed in the trailing edge of airfoil 6. A piece had been lost from the trailing edge of vane 6. Vane 5 was extensively cracked. Failure analysis confirmed the cause of damage as thermal stress in origin but failed to disclose any additional defects in the remaining vane assemblies or insulators.

Fourteen additional Si_3N_4 airfoils were received from Norton during the report period. NDT was used to qualify these as static rig test component spares pending the results of dimensional inspection. Billet certification test data from Norton are also reported.

PRECEDING PAGE BLANK NOT FILMED

6.1.1 STATIC RIG TESTING

Introduction

The 2500°F static rig testing of silicon nitride stator vanes and boron nitride insulators was resumed in October using the modified and rebuilt version of the water cooled rig illustrated in Figure 5.1. Since the combustor had been redesigned to provide more cooling in the secondary zone, it was necessary to rerun the preliminary test schedule under steady state conditions to establish gas temperature profiles and confirm that the programmed start up and shut down transients had been achieved. Sixty of a proposed 100 cycles of testing to simulate the operation of a stationary power turbine in peaking service were completed. A peak temperature of 2500°F was achieved at 0.8 simulation (8 atmospheres pressure). The total time at temperature (2500°F) approached three hours.

The Test Configuration

The spring loaded test assembly with metal support structure is essentially the same as that used earlier in the 2200°F(5) and aborted 2500°F static rig(7) tests. The upstream air baffle (Figure 6.1) was changed from 0.032 in. Hastelloy X to 0.125 inch Haynes 188 to withstand local hot spots. It was also possible to reduce the amount of shoe cooling air because Carborundum Type M boron nitride (the current insulator material) has a higher temperature capability than the lithium alumina silicate (LAS) used previously. By reducing this cooling air to permit a higher insulator temperature, the steady state thermal gradients in the end caps can be reduced proportionately.

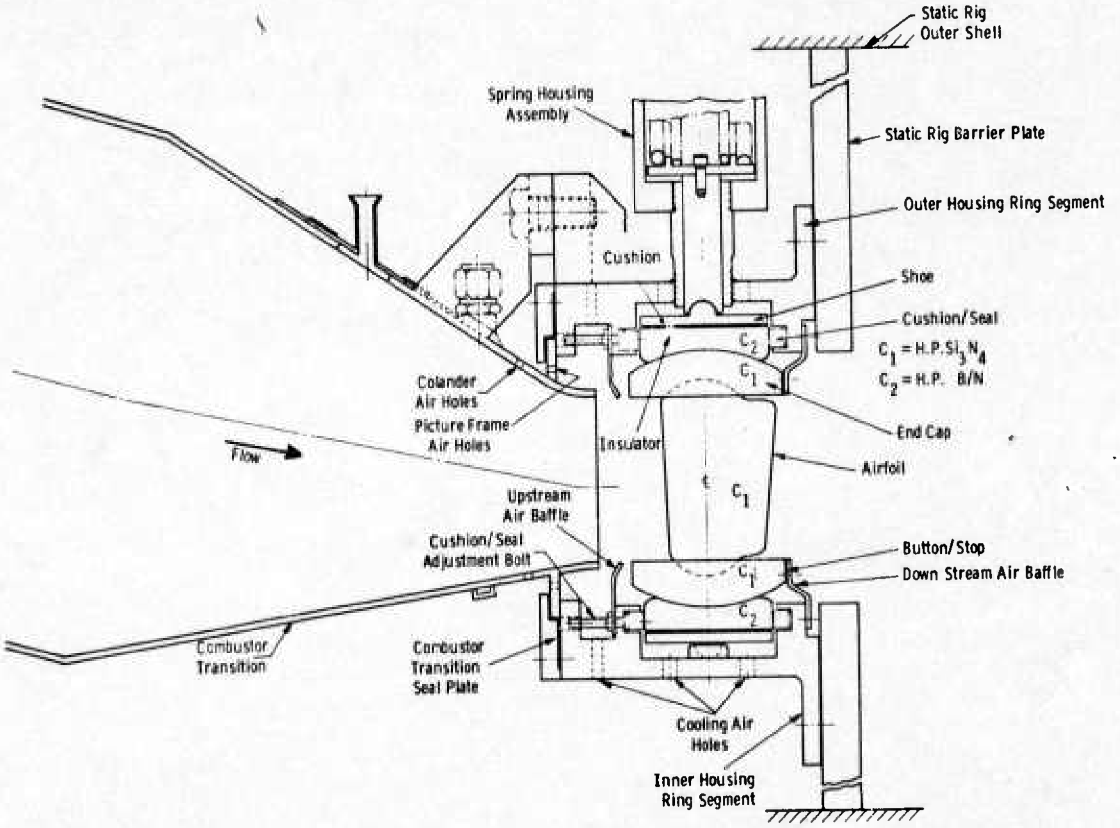
Static Rig Outer Shell
Spring Housing Assembly
Static Rig Barrier Plate
Outer Housing Ring Segment
Cushion
Shoe
Cushion/Seal
C_1 = H.P. Si_3N_4
C_2 = H.P. B/N
C_2
C_1
Colander Air Holes
Picture Frame Air Holes
Flow
Insulator
End Cap
Airfoil
C_1
Upstream Air Baffle
Cushion/Seal Adjustment Bolt
Button/Stop
Down Stream Air Baffle
C_1
C_2
Combustor Transition
Combustor Transition Seal Plate
Cooling Air Holes
Inner Housing Ring Segment

Figure 6.1 Longitudinal View of the Ceramic Vane 2500°F Static Rig Test Article

As stated above, the insulators for the 2500°F test were made from hot-pressed boron nitride. The thick insulator design(3) was used in osition 1 and 3 (left to right, Figure 6.2). All of these components were ew except for inner insulator 4 (the small one) which was salvaged from the first attempt to test at 2500°F.(7)

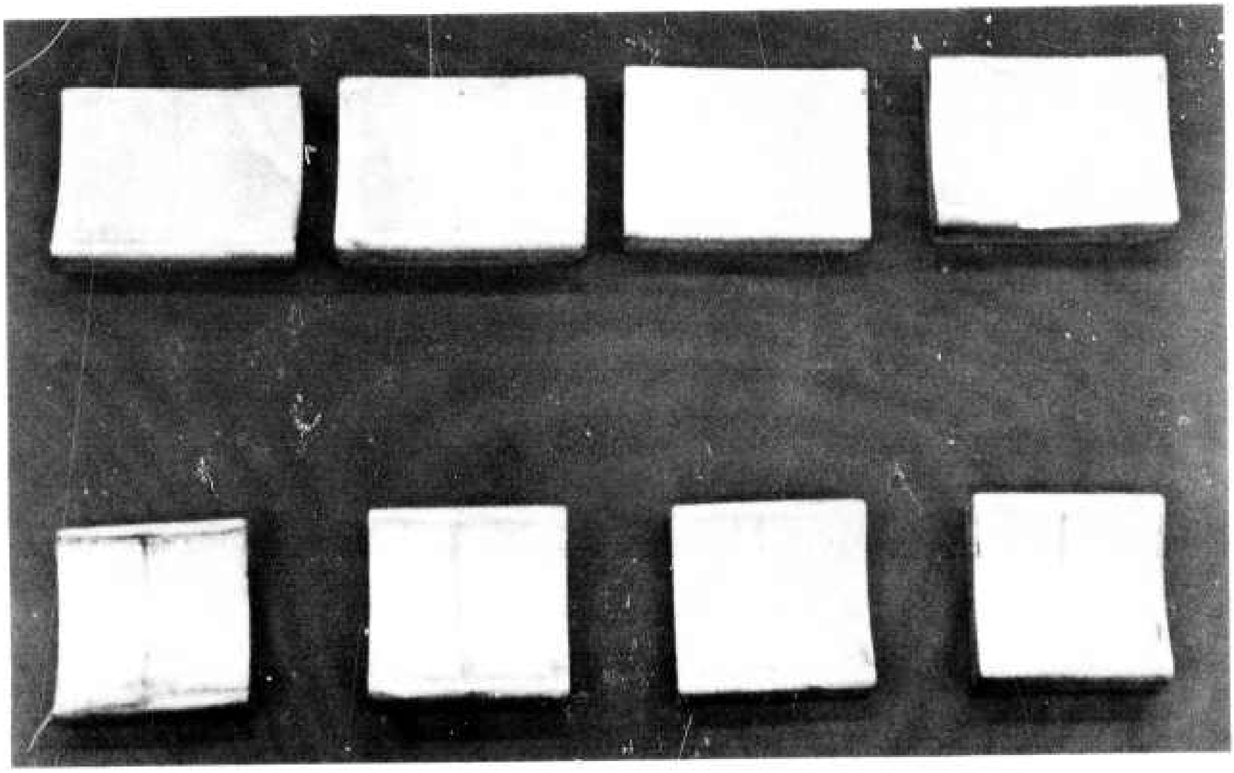

Figure 6.2 Inner and Outer Boron Nitride Insulators from 2500°F Static Rig

The initial eight test vane components are shown in Figure 6.3. Norton NC 132 silicon nitride is used exclusively. The airfoils are of the tapered twisted configuration to be used with the 3 in. outer radius end caps designated the third generation design.(8) Position 3 and 6 airfoils were pre-oxidized in an alumina lined muffle furnace at 2500°F for 103 hours to determine the effect of thermal transients on silicon nitride material degraded by oxidation.(8) The stator vanes, as they were assembled in the static rig prior to the start of testing, appear in Figure 6.4.

Steady State Profile Tests

Following 24 hours of mixer section castable insulation bake out at an average gas temperature of 1500°F, the static rig was run under various steady state conditions to check rig performance, to determine gas temperature profiles, to correlate rig control parameters and to calibrate optical pyrometer measurements.

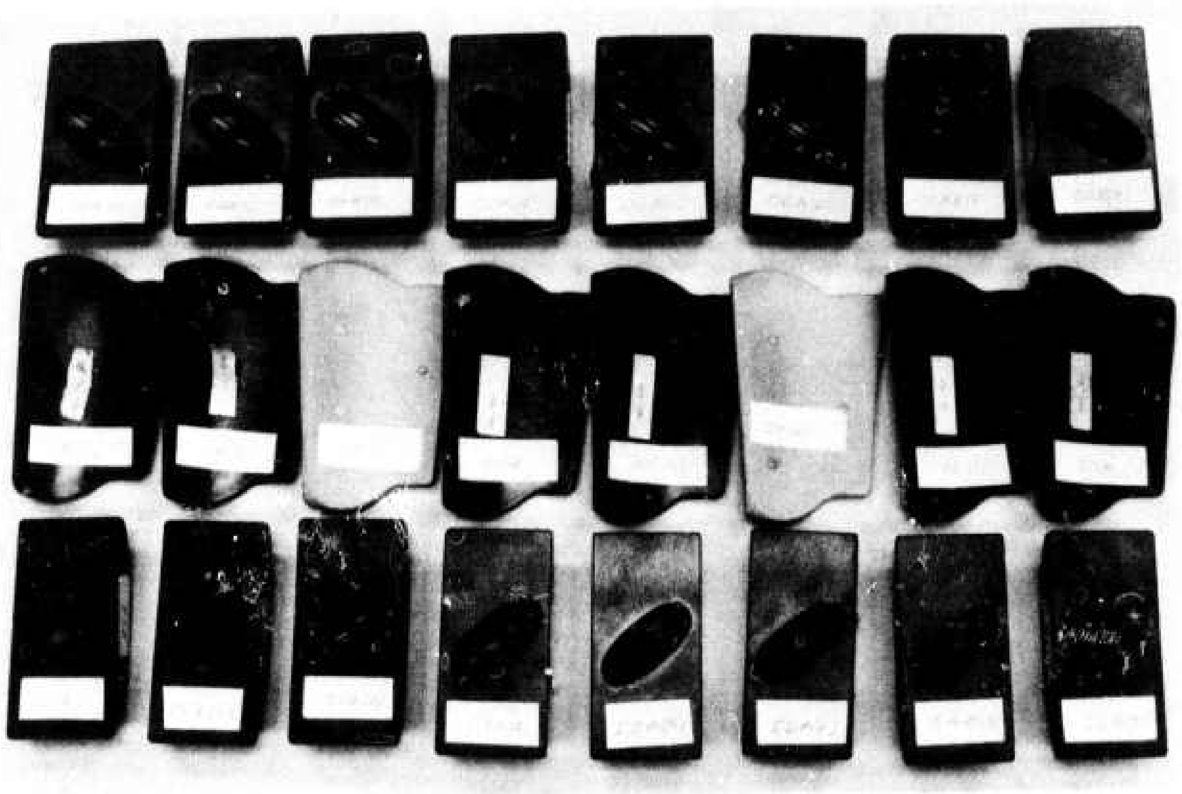

Figure 6.3 Hot Pressed Silicon Nitride Stator Vanes (Norton NC 132) for 2500°F Static Rig Testing - Airfoils 3 and 6 (from left) Were Preoxided 103 hours in an Alumina Lined Muffle Furnace at 2500°F (Static Air)

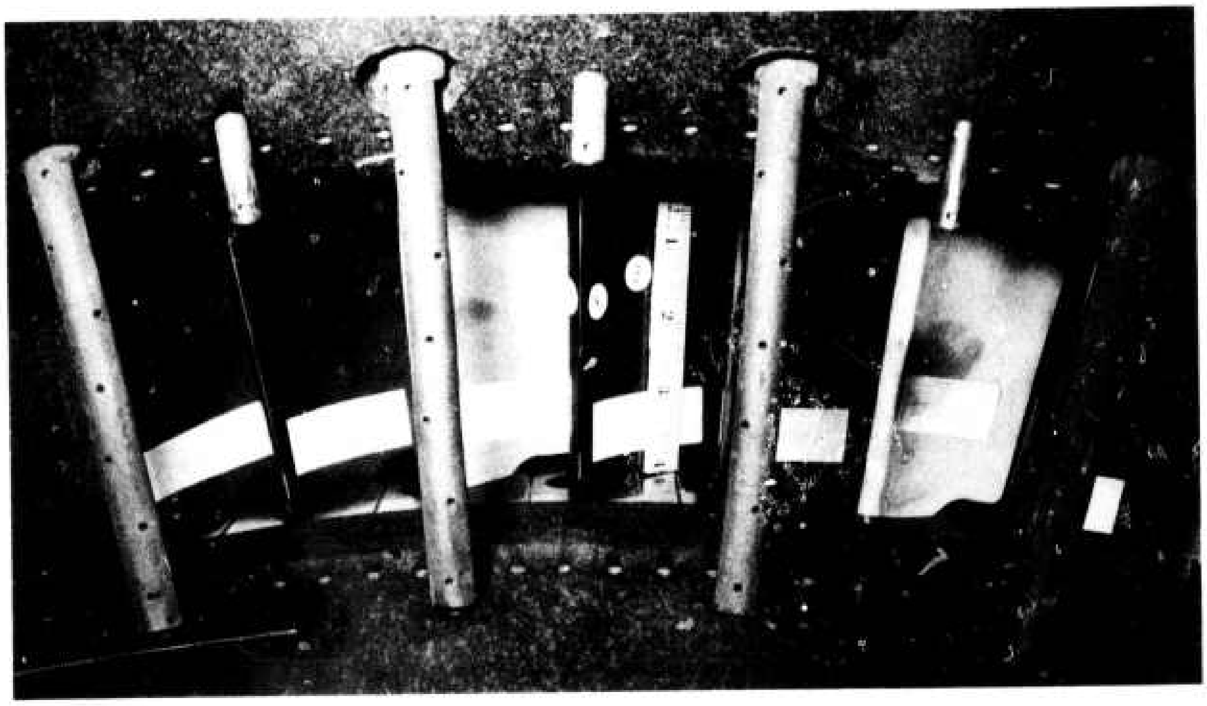

Figure 6.4 2500°F Static Rig Test Assembly in Place Showing Aspirating Thermocouple Rakes

Operating conditions applicable to the static rig at peak load are listed as follows:

Fuel/Air Ratio	0.0194
Airflow	30.88 lb/sec
Air Preheat Temperature	600°F
Fuel Flow	0.598 lb/sec
Fuel Temperature	70°F
Shell Pressure	100 psig
Exit Temperature	1750°F
Combustor Simulation	0.80

Six aspirating thermocouple rakes containing 7 thermocouples per rake (Figure 6.4) were used to determine gas stream temperatures at the idle temperature, 1400°F, at mid-load, 2000°F, and at the thermocouple limit, 2300°F. The gas temperature profiles derived from these data appear in Figure 6.5 (1400°F), 6.6 (2000°F) and 6.7 (2300°F). The temperature profile at peak load (2500°F) shown in Figure 6.8 was extrapolated from the established profiles using airfoil temperatures as monitored on the leading and trailing edges of airfoil 4 by the optical pyrometers and three surveillance thermocouples protruding a short distance from the transition wall into the gas path.

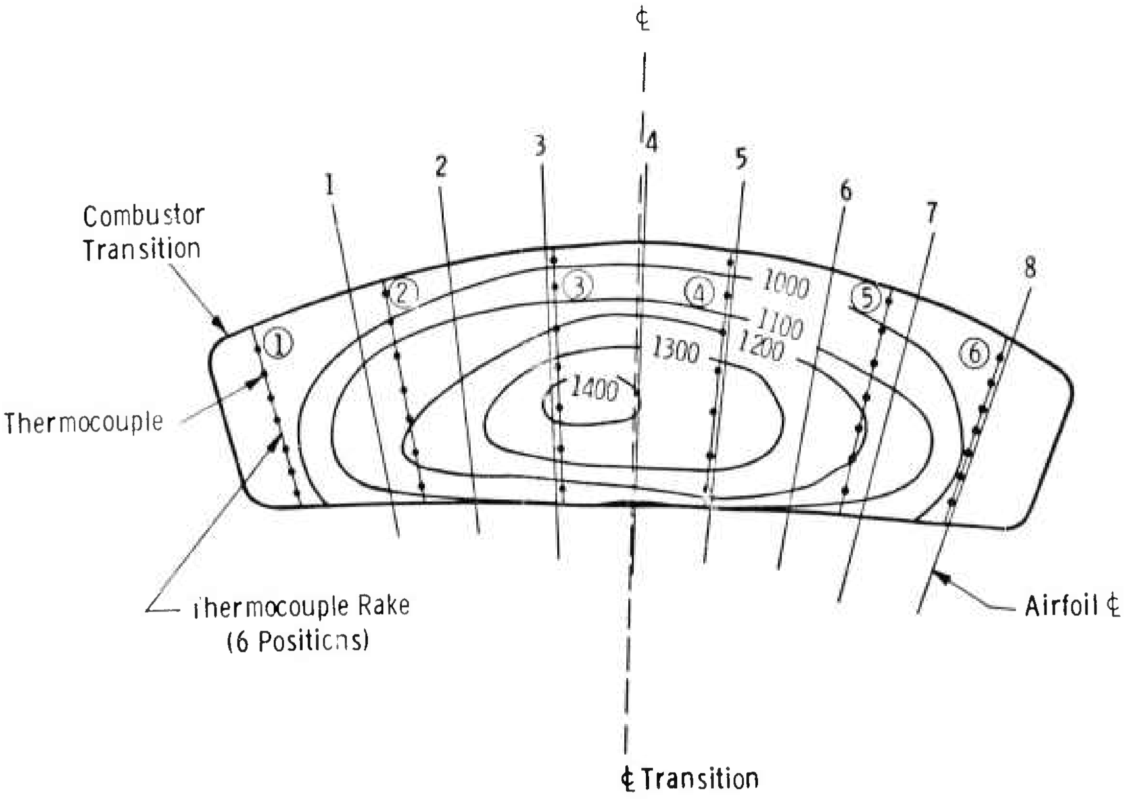
℄
1
2
3
4
5
6
7
8
Combustor Transition
①
②
③
④
⑤
⑥
1000
1100
1200
1300
1400
Thermocouple
Thermocouple Rake (6 Positions)
Airfoil ℄
℄ Transition

Figure 6.5 Gas Temperature Profile Under Steady State Conditions at 1400°F (Idle Temperature)

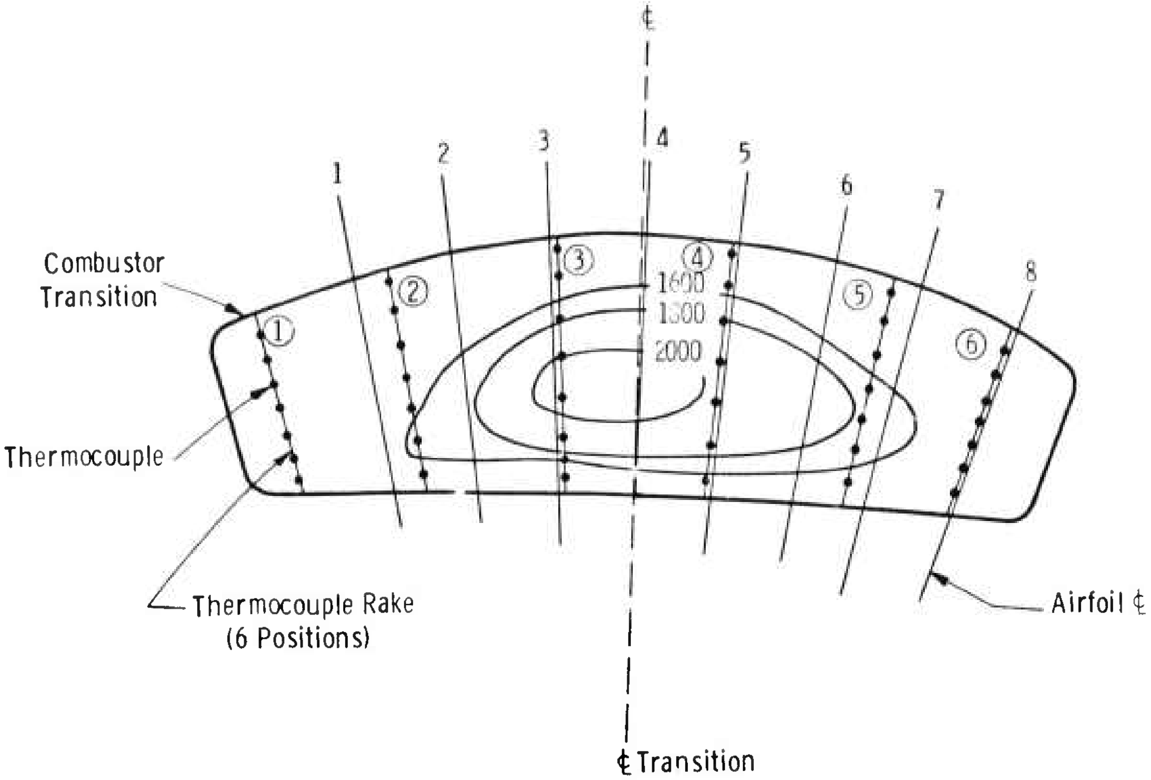
℄
1
2
3
4
5
6
7
8
①
②
③
④
⑤
⑥
1600
1800
2000
Combustor Transition
Thermocouple
Thermocouple Rake (6 Positions)
Airfoil ℄
℄ Transition

Figure 6.6 Gas Temperature Profile Under Steady State Conditions at 2000°F (Mid Load Temperature)

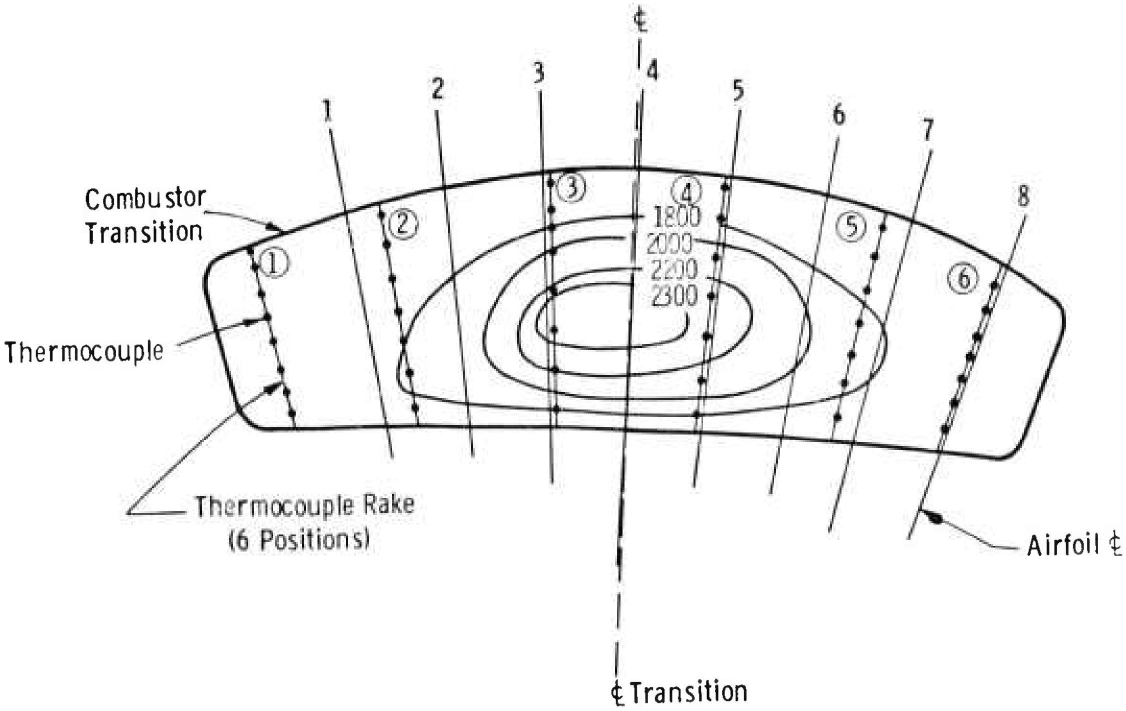
℄
1
2
3
4
5
6
7
8
①
②
③
④
⑤
⑥
1800
2000
2200
2300
Combustor Transition
Thermocouple
Thermocouple Rake (6 Positions)
Airfoil ℄
℄ Transition

Figure 6.7 Gas Temperature Profile Under Steady State Conditions at 2300°F (Thermocouple Rake Temperature Limitations)

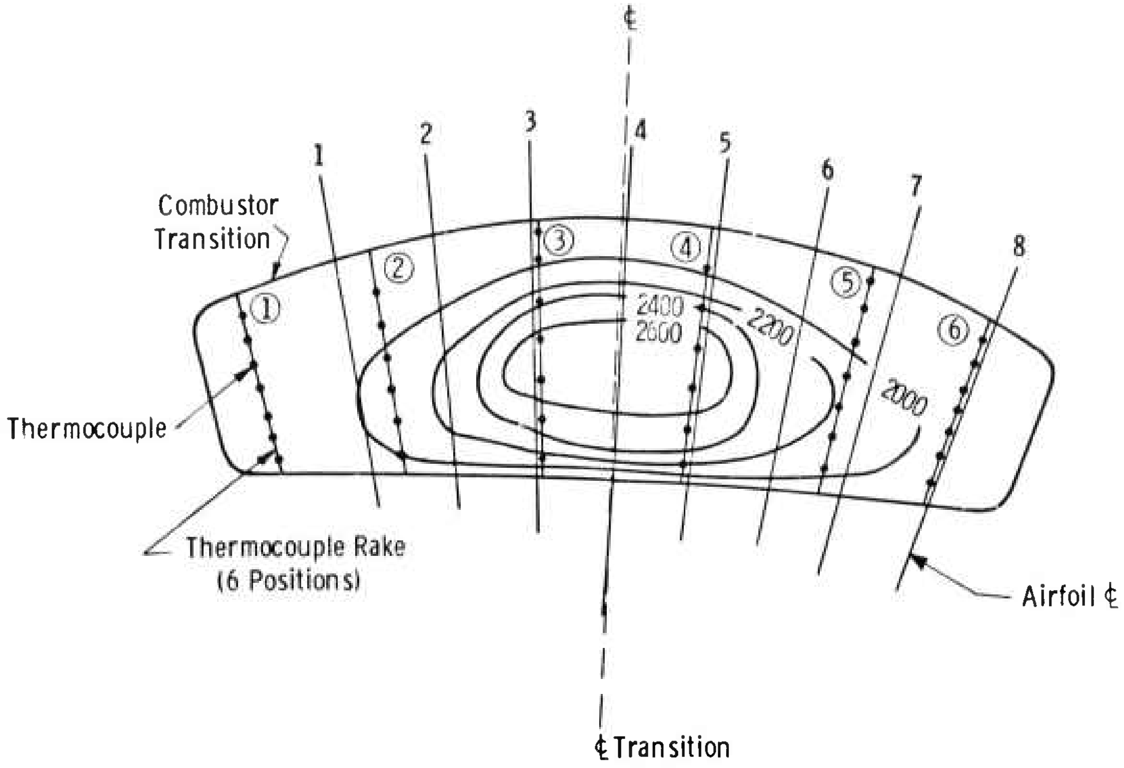

Figure 6.8 Extrapolated Gas Temperature Profile Under Steady State Conditions at 2500°F (Peak Load Temperature)

The profiles thus established reflect a peak to average temperature variation much larger than those of the previous tests.(5,7) This is to be expected because of the change in combustor design(8). An attempt was made to reduce the peak to average temperature in the temperature profile by replacing a fuel nozzle of 53° included angle (227 GPH) with one of 85° included angle (199 GPH), but the effect was negligible.

Rake temperature is plotted as a function of height at the rake transition plane location (∿5 in. upstream of the vane inlet) in Figure 6.9. Clearly, the inner region of the airfoil is hotter than the outer region. The peak temperature of rake 3 occurs at 40% height and the peak temperature of rakes 2, 4 and 5 occurs at 60% height (rake 6 was removed to permit viewing through the boroscope). However, the supercooled nature of the combustor, as evidenced by the metal temperature distributions of Figure 6.10 (peak temperature = 1420°F) as well as the angular manner in which cooling air enters the outer area of the vanes leads to the initial conclusion that the peak temperature location on the airfoil is closer to 40% height than it is to mid-height as assumed initially.

Vanes 3, 4, and 5 operate in the hottest (2500°F+) zone, while vanes 2 and 6 operate in the 2200°F+ region. Vanes 1 and 8 probably experience temperatures below 2200°F.

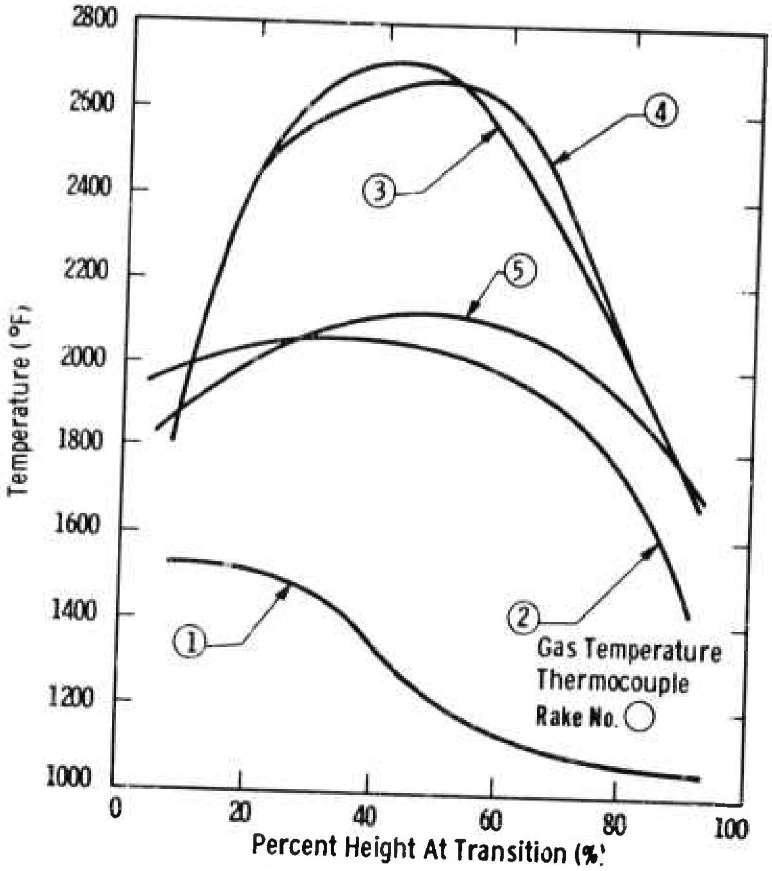

Figure 6.9 Gas Temperature vs Percent Airfoil Height (Leading Edge) for Extrapolation of Peak Load Gas Temperature Profile

The static rig functioned without difficulty in the steady state operation. All of the metal temperatures remained well below critical levels. For example, the water cooled hot gas exhaust duct temperatures at peak load never exceeded:

Cooled sections = 275°F peak

"Uncooled" entrance lip = 553°F peak

"Uncooled" exit lip = 1626°F (peak at top)
= 1599°F (peak at bottom)
= 1422°F (peak at side)

Transient Thermal Cycles 1-25

The transient thermal cycle described by Figure 6.11 was established for 100 cycles of static rig testing at 2500°F peak vane temperature to preclude transient thermal stresses above 20,000 psi in the airfoil. The cycle is defined further as follows:

1. Idle (1100°F) to peak of 2500°F at 10°F/sec.
2. Hold at peak for 3 to 5 minutes.
3. Instant fuel cut back to mid-load condition of 2000°F.
4. Hold at mid-load for 45 seconds.
5. Controlled shutdown from mid-load to idle at 25°F/sec.

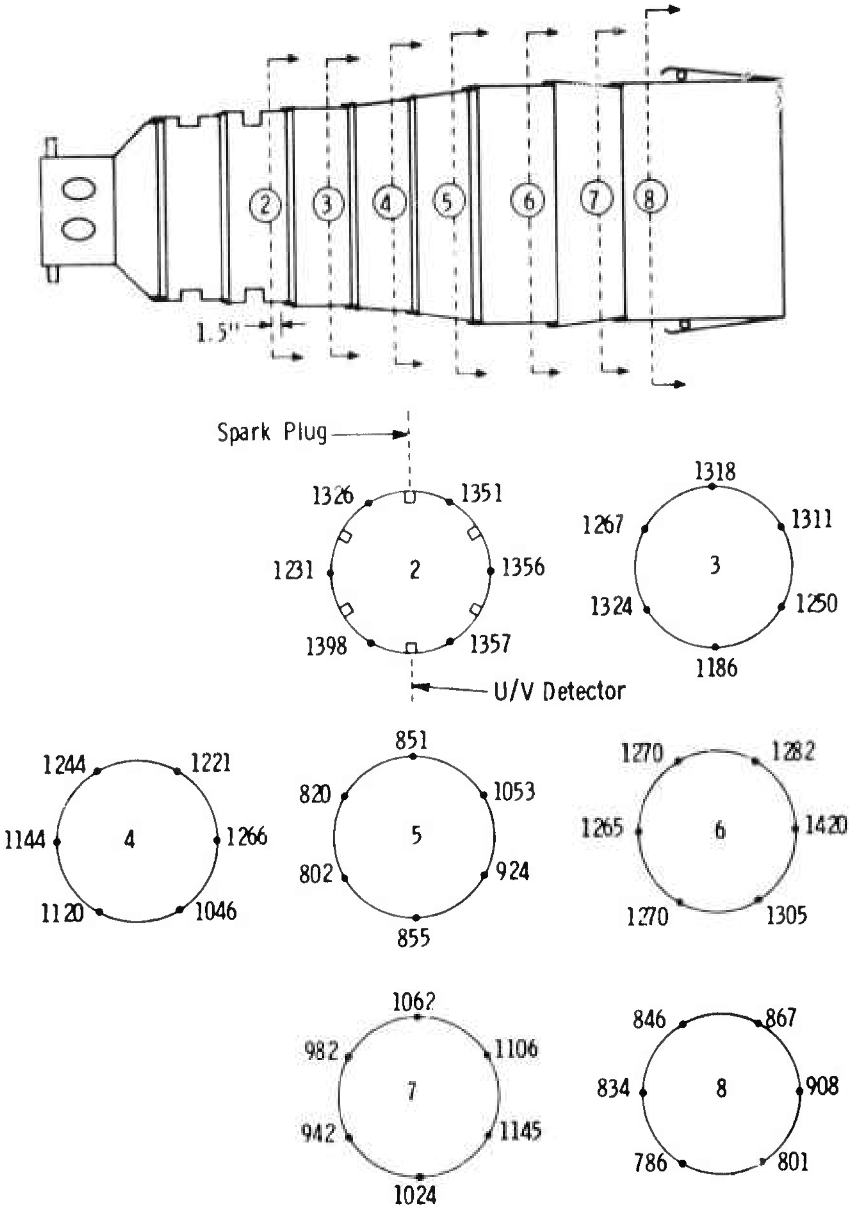
2
3
4
5
6
7
8
1.5"
Spark Plug
U/V Detector
1326
1351
1231
2
1356
1398
1357
1318
1267
1311
3
1324
1250
1186
851
1244
1221
1144
4
1266
1120
1046
820
1053
5
802
924
855
1270
1282
1265
6
1420
1270
1305
1062
982
1106
7
942
1145
1024
846
867
834
8
908
786
801

Figure 6.10 Combustor Wall Temperature Under Peak Load Conditions at 2500°F

Cyclic testing resumed in October. The cyclic response actually achieved is indicated by the dashed lines in Figure 6.12. The up ramp was about 8°F/sec. The 45 second hold during controlled shut down occurred at 2360°F rather than at 2000°F as planned. The temperature decay from hold to idle (1350°F actual) never exceeded 8°F/sec as recorded on the suction side of vane 4 by the "Z" pyrometer which was used for control.

The static rig was shut down for visual vane inspection through the transition after cycles 2, 5 and 25. Heavy reddish brown deposits were observed after two cycles. It was difficult to differentiate the pre-oxidized airfoil in positions 3 and 6 from the other airfoils. There was no evidence of damage or malfunction. After the fifth cycle of testing, no changes were detected in the appearance of the vanes, although only the pressure side surfaces were accessible.

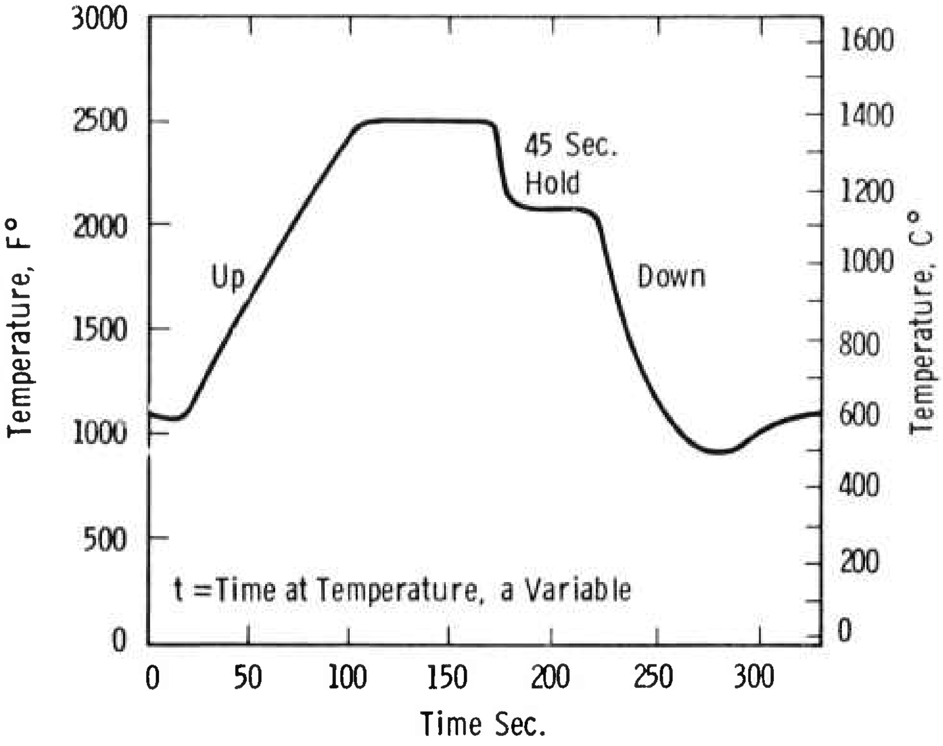

Figure 6.11 Planned Stator Vane Transient Thermal Cycle for 2500°F Tests

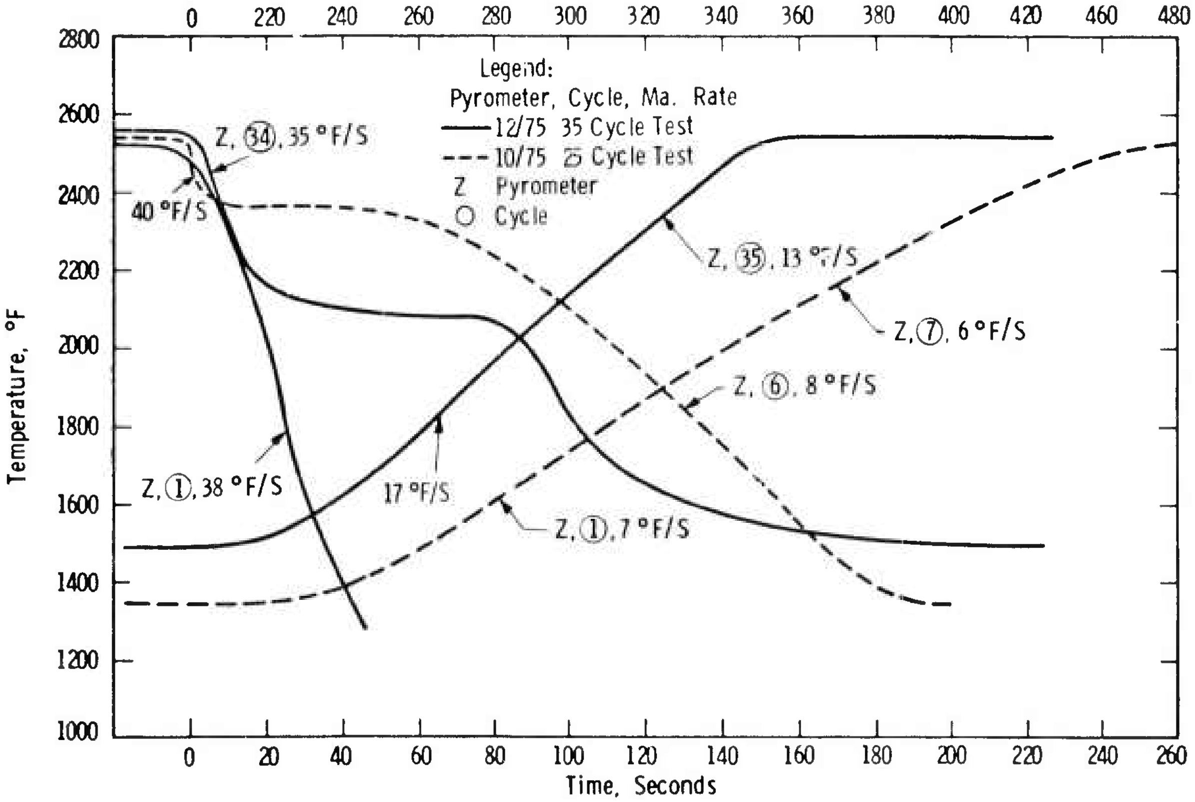

Figure 6.12 Typical Transient Thermal Cycles as Recorded from Static Rig Testing at 2500°F (Cycles 1-25 and 26-60) respectively.

At the 25 cycle point, the rig was again opened for routine inspection. The outer end caps were found to be misaligned. These end caps had apparently translated and rotated downstream with respect to the outer insulators, as indicated in Figure 6.13. The inner end cap alignment remained relatively good but a shift in airfoil position caused edge loading as illustrated in Figure 6.14. Chips were found at this location on the suction side of airfoils 5, 6, 7 and 8.

Outer insulator 1 was damaged (Figure 6.15) apparently by a combination of downstream edge contour radius loading by Outer End Cap 2 as well as a downstream circumferential wedging type load caused by Outer End Cap 3.

The vane assembly components as they appeared after being removed from the test assembly are shown in Figure 6.16.

The end cap movement which caused the damage would normally have been prevented by the downstream outer air baffle. A review of the test assembly following its removal from the static rig revealed that the outer housing ring segment had been misaligned with respect to the inner housing ring segment in such a manner so as to cause the downstream outer baffle to be out of position and therefore ineffective. The misalignment may also have prevented the full translation of spring restraining forces to the ceramic stator vane assemblies.

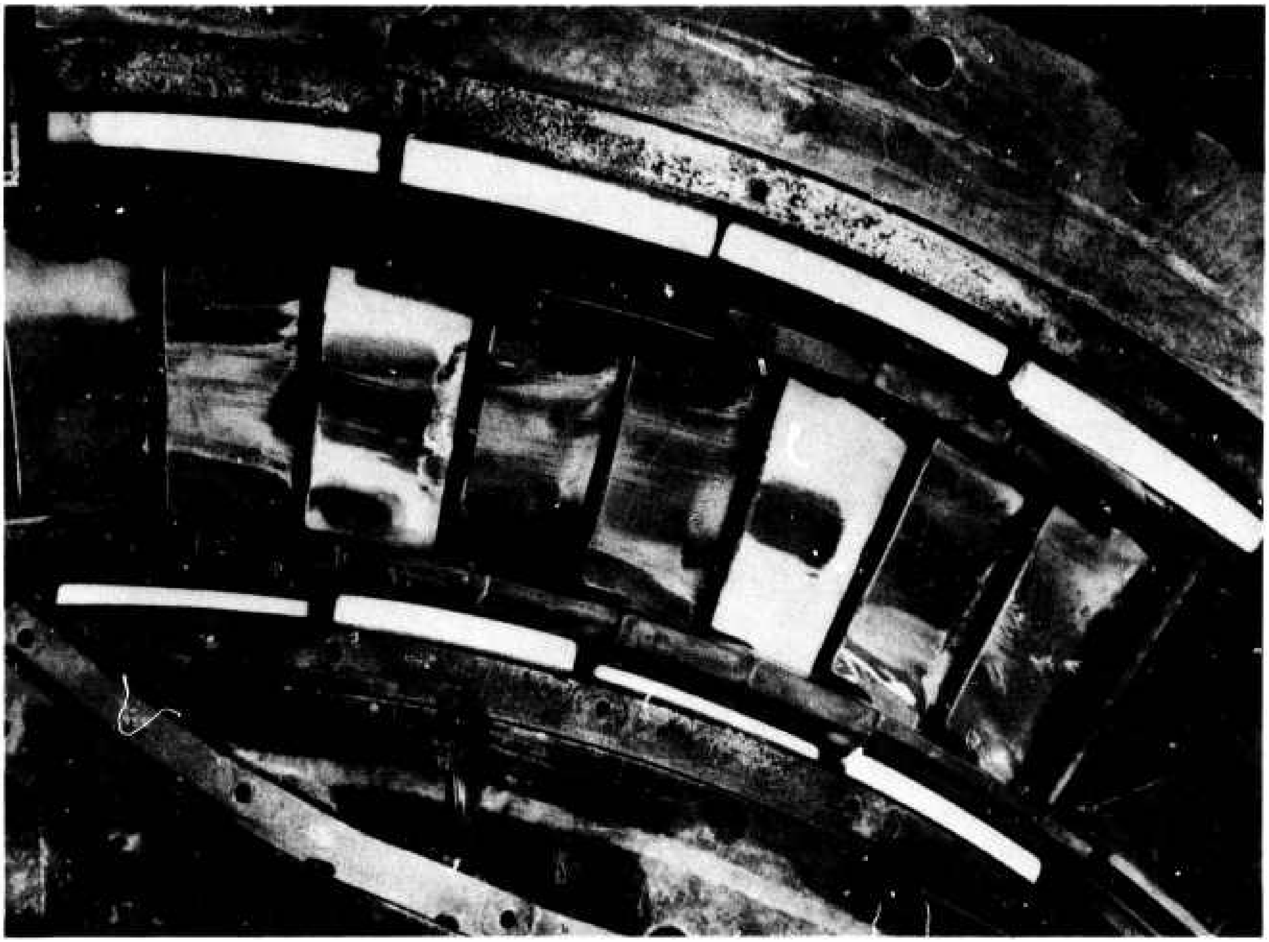

Figure 6.13 Stator Vane Test Assembly as It Appeared in the Static Rig After 25 Cycles of Testing to 2500°F

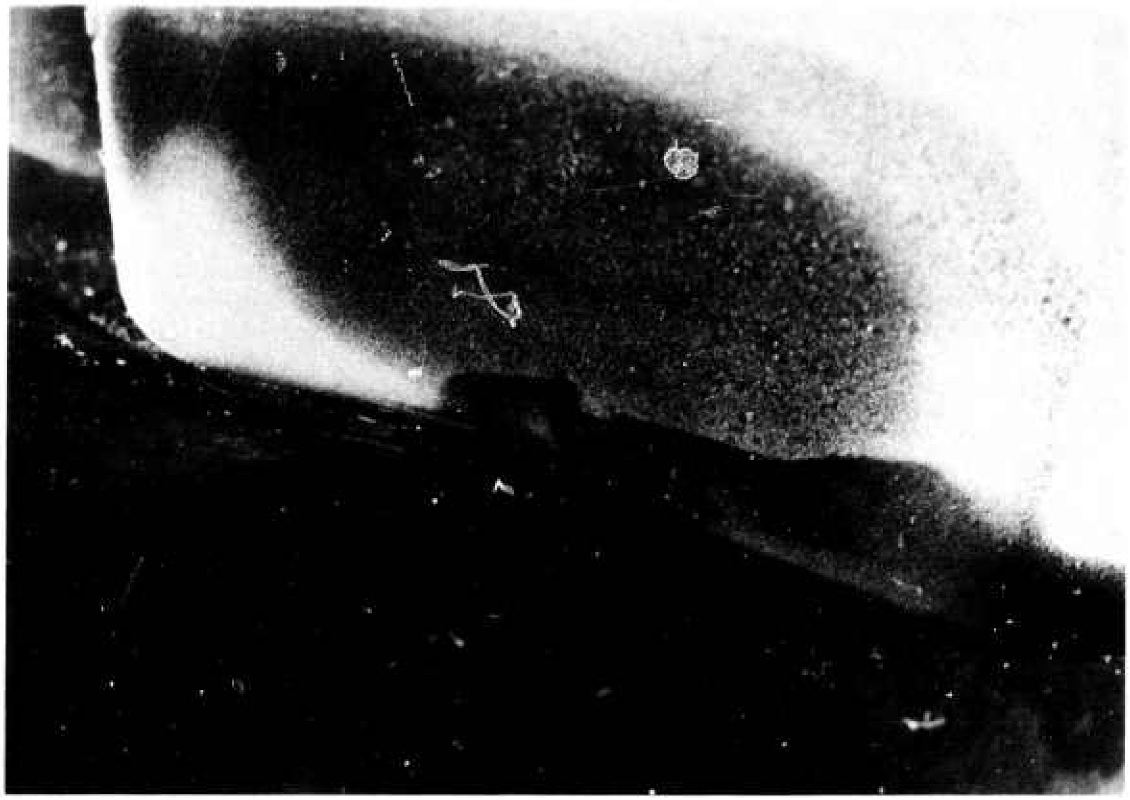

Figure 6.14 Typical Example of Airfoil-End Cap Edge Loading Resulting from the Shift in Outer End Cap Position (Cycles 1-25:2500°F Static Rig Test)

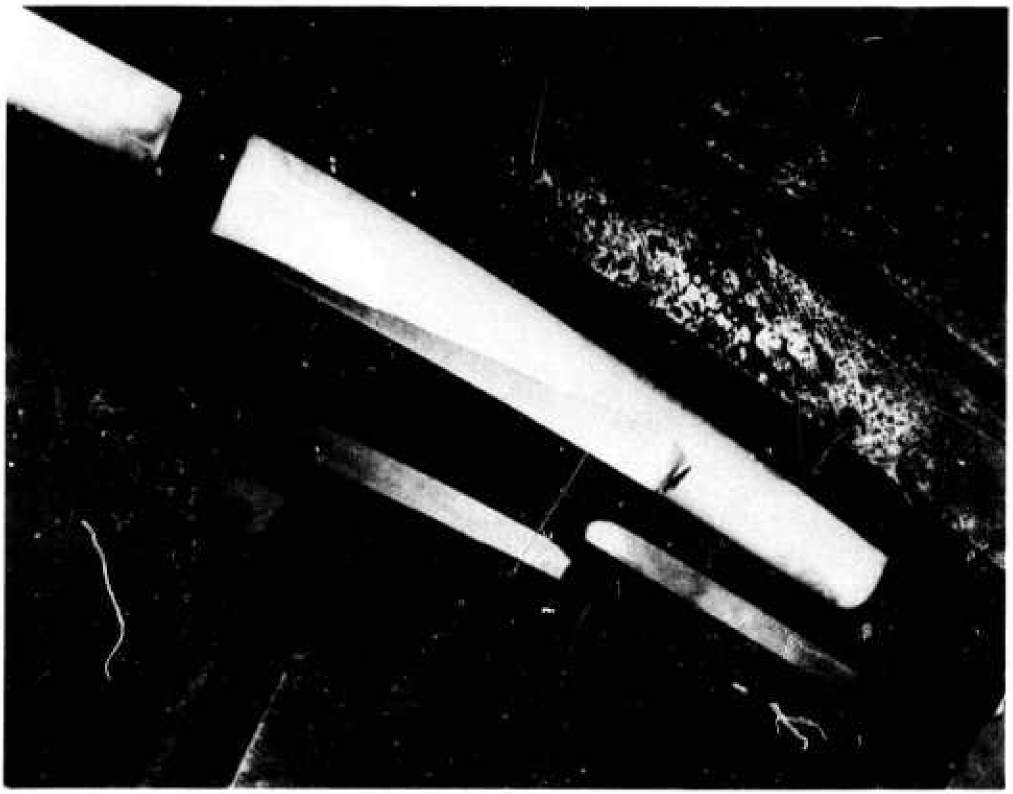

Figure 6.15 Illustration of Outer End Cap Position Shift During Static Rig Tests at 2500°F (Cycles 1-25)

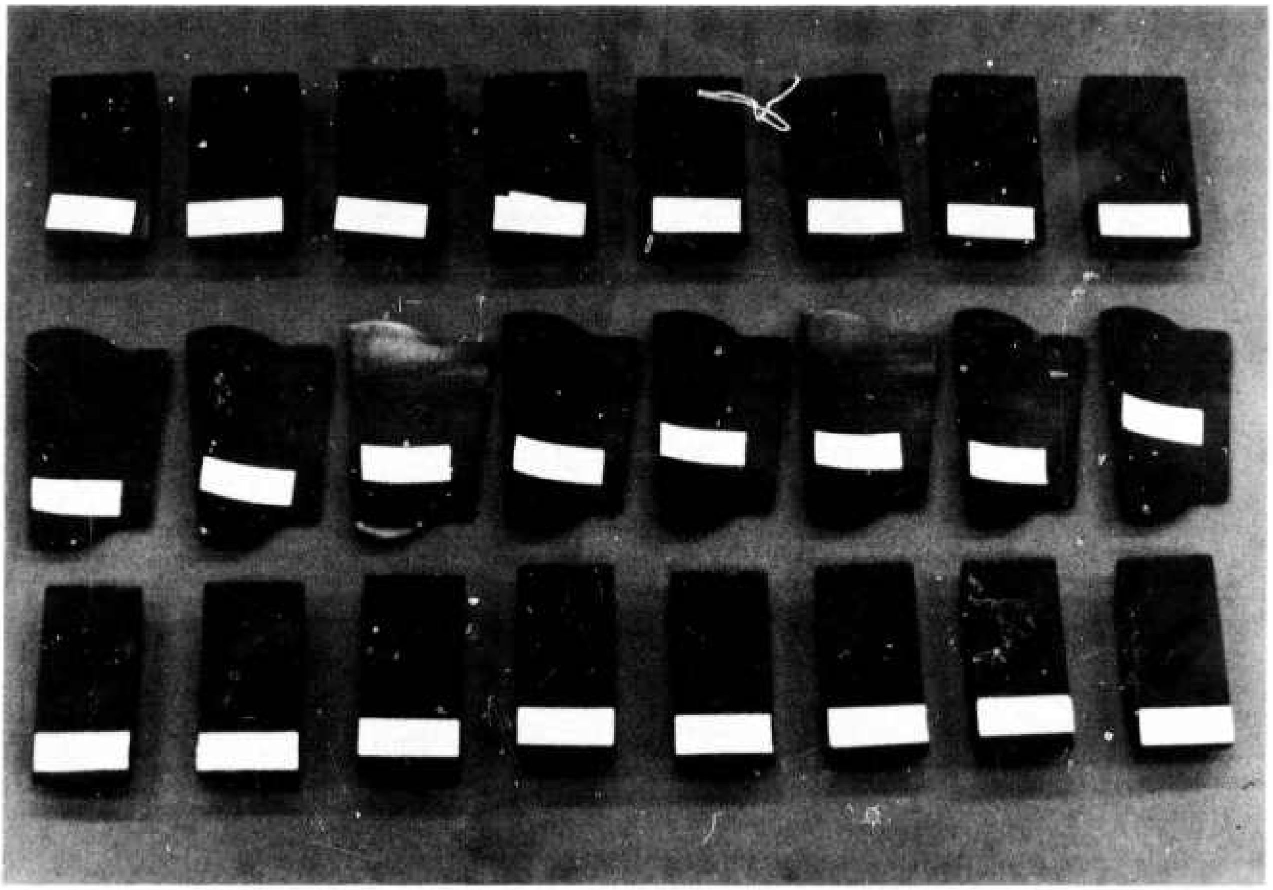

Figure 6.16 Silicon Nitride Stator Vane Components as they Appeared After 25 Cycles of Testing in the Static Rig at 2500°F

Failure Analysis - First 25 Cycles

An in situ examination of the vane end cap assembly after the first 25 cycles of testing at 2500°F showed that several outer end caps had dislocated during testing. A close examination of the Si_3N_4 components showed that the dislocated end caps had caused several vanes to shift and contact at the periphery of the toroidal cavity in the inner end caps. The undesirable rubbing contact between the vanes and the inner end caps resulted in the chipping of the vanes as shown in Figure 6.17.

The vanes and end caps were removed from the static rig test section assembly for further inspection.

After visually inspecting each vane and end cap with a binocular microscope, each component was lightly sandblasted to remove the deposits produced by the test to facilitate inspection for cracks and other surface irregularities. A phosphorescent dye penetrant was used.

Chips and/or small circular cracks which would lead to a chip were observed on vanes 5, 6, 7 and 8. The chips were located in the same position as shown in Figure 6.17 for vane 5. Observations revealed that several small cracks, shown in Figure 6.18 for vane 6, were located beneath the chipped off piece of material. Such chips and the associated small cracks are caused by highly localized, edge-loading conditions.

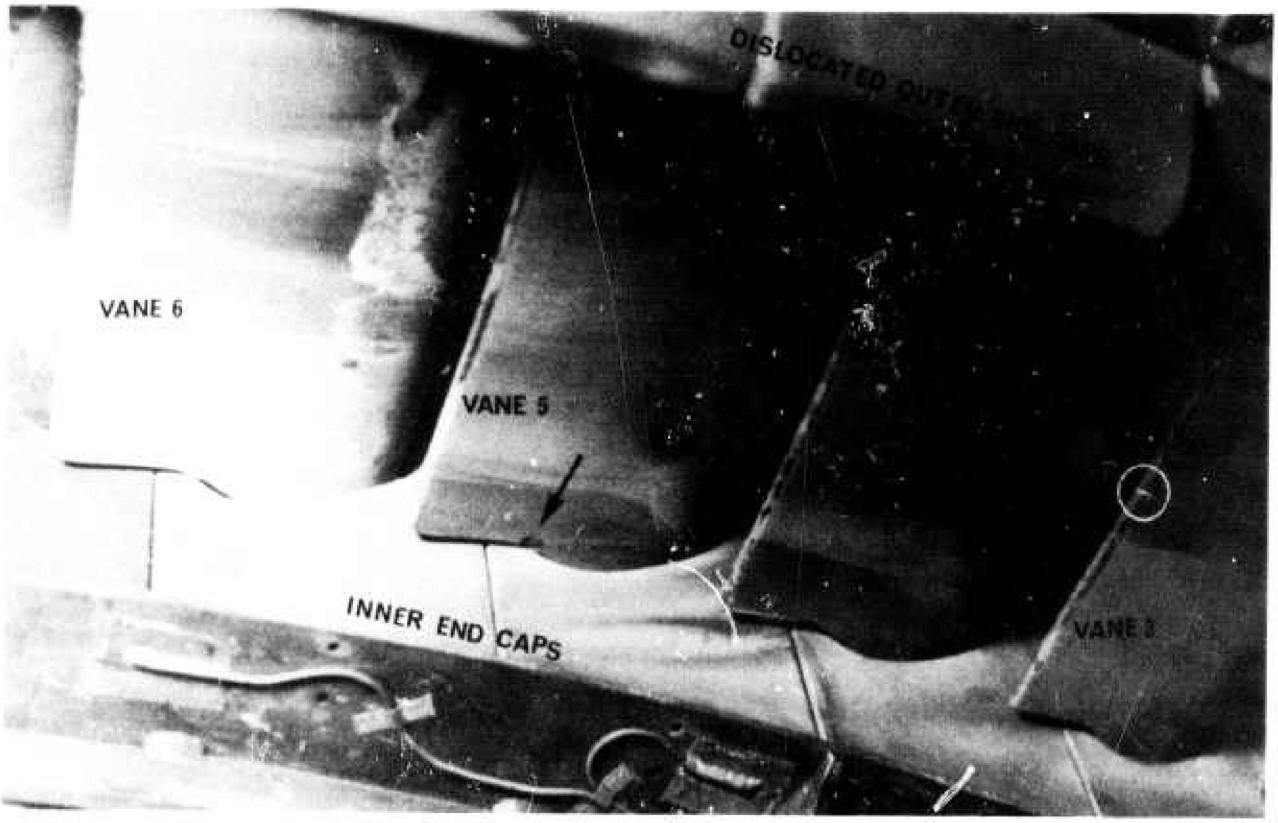
DISLOCATED OUT
VANE 6
VANE 5
INNER END CAPS
VANE 3

Figure 6.17 Failure Indications in Silicon Nitride Stator Vane Components After 25 Cycles of Transient Testing in the Static Rig at 2500°F

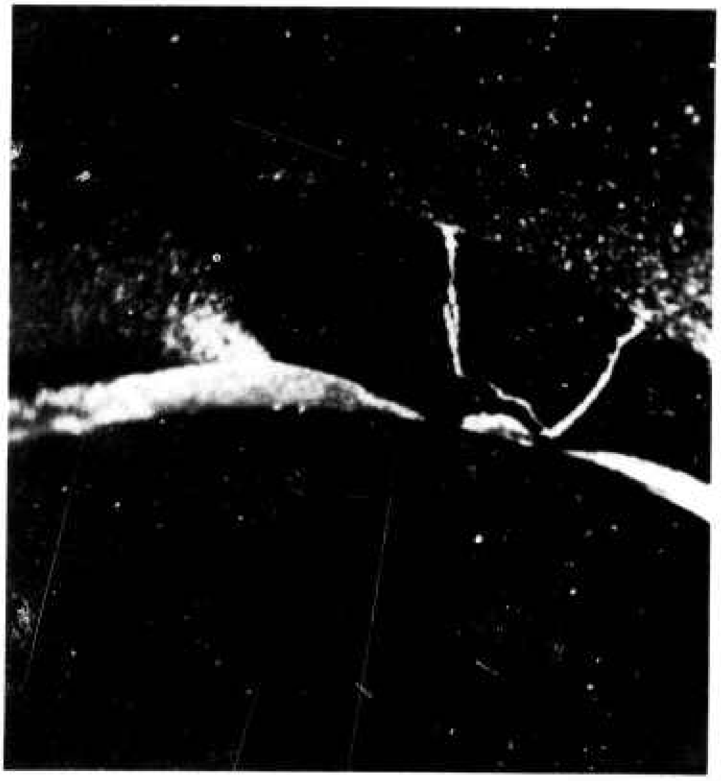

Figure 6.18 Typical Example of Chipping at the Inner End Cap-Airfoil Tenon Interface (Cycles 1-25 Static Rig Test at 2500°F)

Phosphorescent penetration revealed a small, straight crack (0.2 inches long) located in the trailing edge of vane 3. The approximate location and size of this crack is shown within the circled area of Figure 6.17. Vane 3 was one of the two pre-oxidized vanes in this test. The analysis could not indicate whether the small trailing edge crack was caused by either thermal stresses arising from the test or rough handling after the vane had been nondestructively inspected prior to oxidation and rig testing.

Inner end cap number 1 was observed to have a small indentation which proved to be the origin of a large crack. Both the indentation and the approximate path of the large crack are shown in Figure 6.19. Since this end cap was positioned adjacent to a protruding metal component in the test assembly, it is strongly suspected that both the indentation and the large crack were caused by an impact condition with the adjacent metal component during assembly.

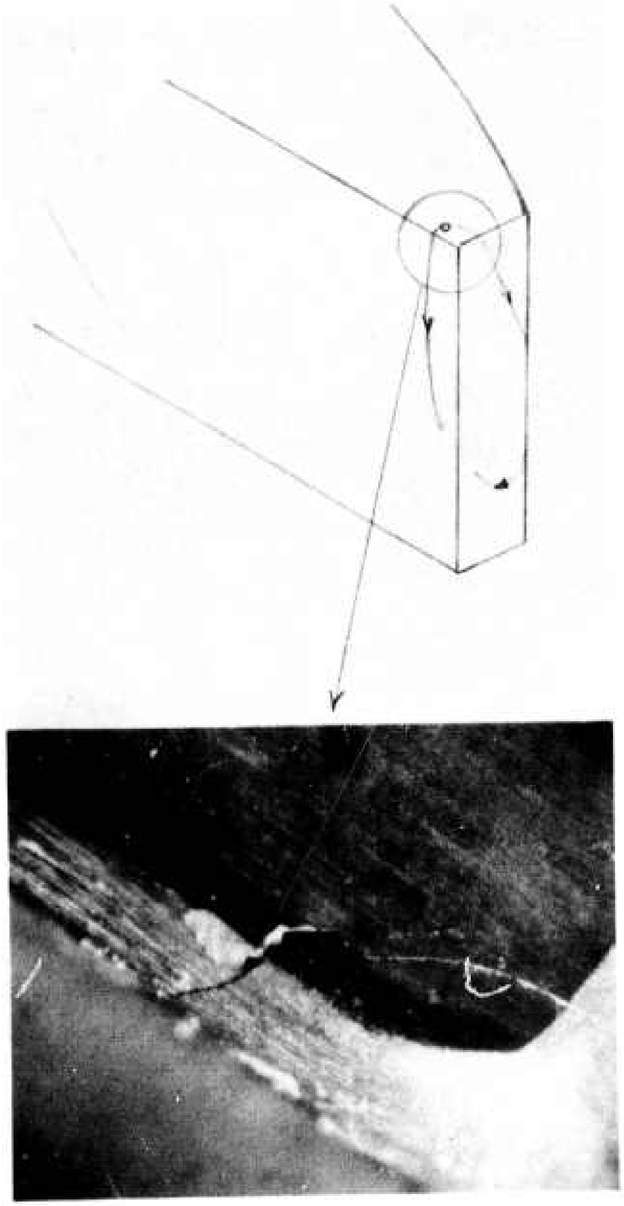

Figure 6.19 End Cap Failure (Outer 1) from 2500°F Static Rig Test (Cycles 1-25)

Transient Thermal Cycles 26-60

All damaged components from the first 25 cycles of testing at 2500°F were replaced when static rig testing was resumed in December. These test vanes are shown in Figure 6.20. Airfoils 3 and 6 are new parts which were again pre-oxidized for 100 hours at 2500°F. Airfoils 5, 6, 7 and 8 and Outer End Cap 1 are also new. The replacement for Outer Insulator 1 was made from hot-pressed Si_3N_4. It had been used previously in the original five cycles of testing at 2500°F.(7)

The problem of inner and outer housing ring segment alignment was corrected. The assembly was modified to add dowel pins which guarantee proper location. The test section with vanes installed ready for test is shown in Figure 6.21.

This next series of cycles ran very smoothly after control was established in cycle 3. Again, none of the metal rig components even approached critical temperature status. As with the first 25 cycle series, the leading edge suction side pyrometer was used to control the desired vane response. The typical response, attained with cycle 3, also appears in Figure 6.12 as cycle 35 up and cycle 34 down. The typical peak load condition reached 2560°F, the mid-load condition was 2080°F, up ramp was 17°F/sec, initial step down was 35°F/sec and final ramp down after hold was 18°F/sec. On cycle 1, an overtemperature condition created a fuel trip. The cause was a supervisory thermocouple being located in a local hot spot position, which resulted in a continuous down ramp at 38°F/sec. Cycle 2 was partially unstable oscillating ± 25°F during the ≈2000°F mid-load hold. Thirty-five additional cycles were run in all.

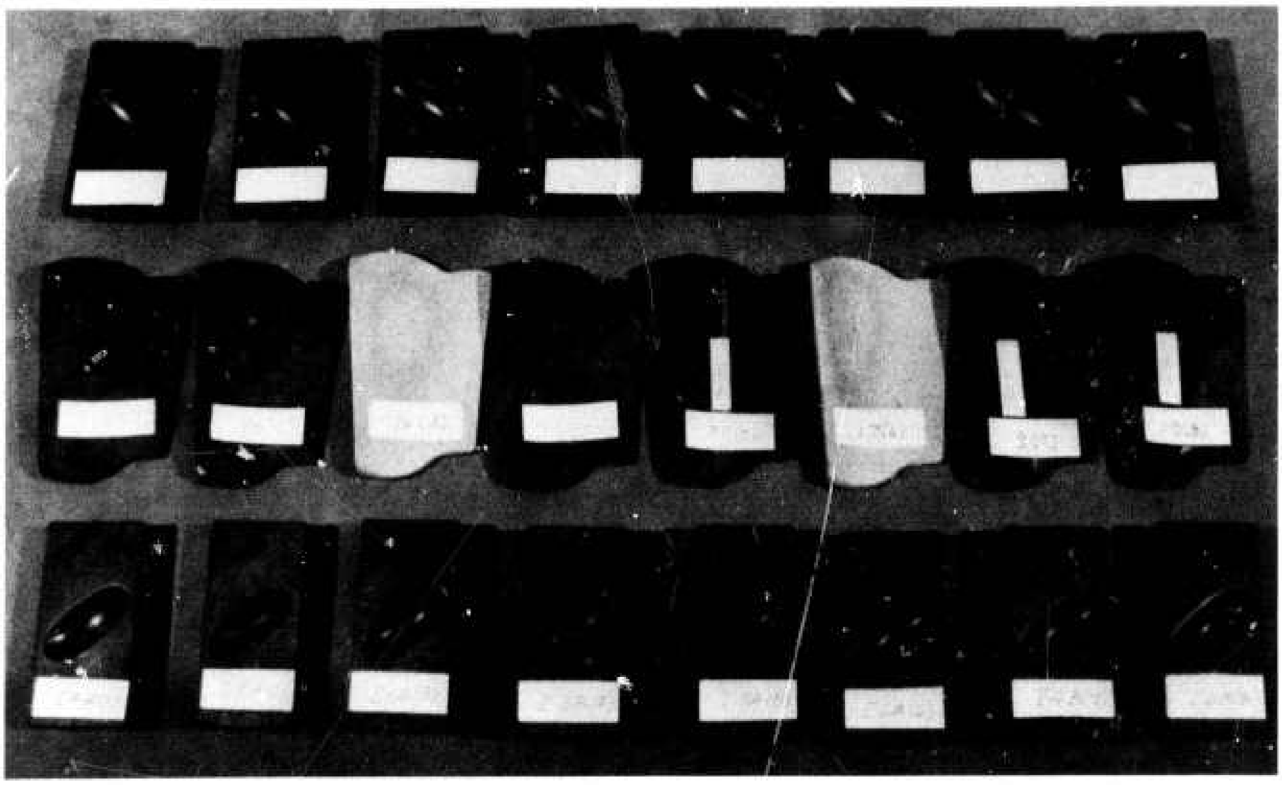

Figure 6.20 Silicon Nitride Stator Vane Components for Static-Rig Testing at 2500°F (Outer End Cap 1 Together With Airfoils 3, 5-8 Represent Replacement Hardware)

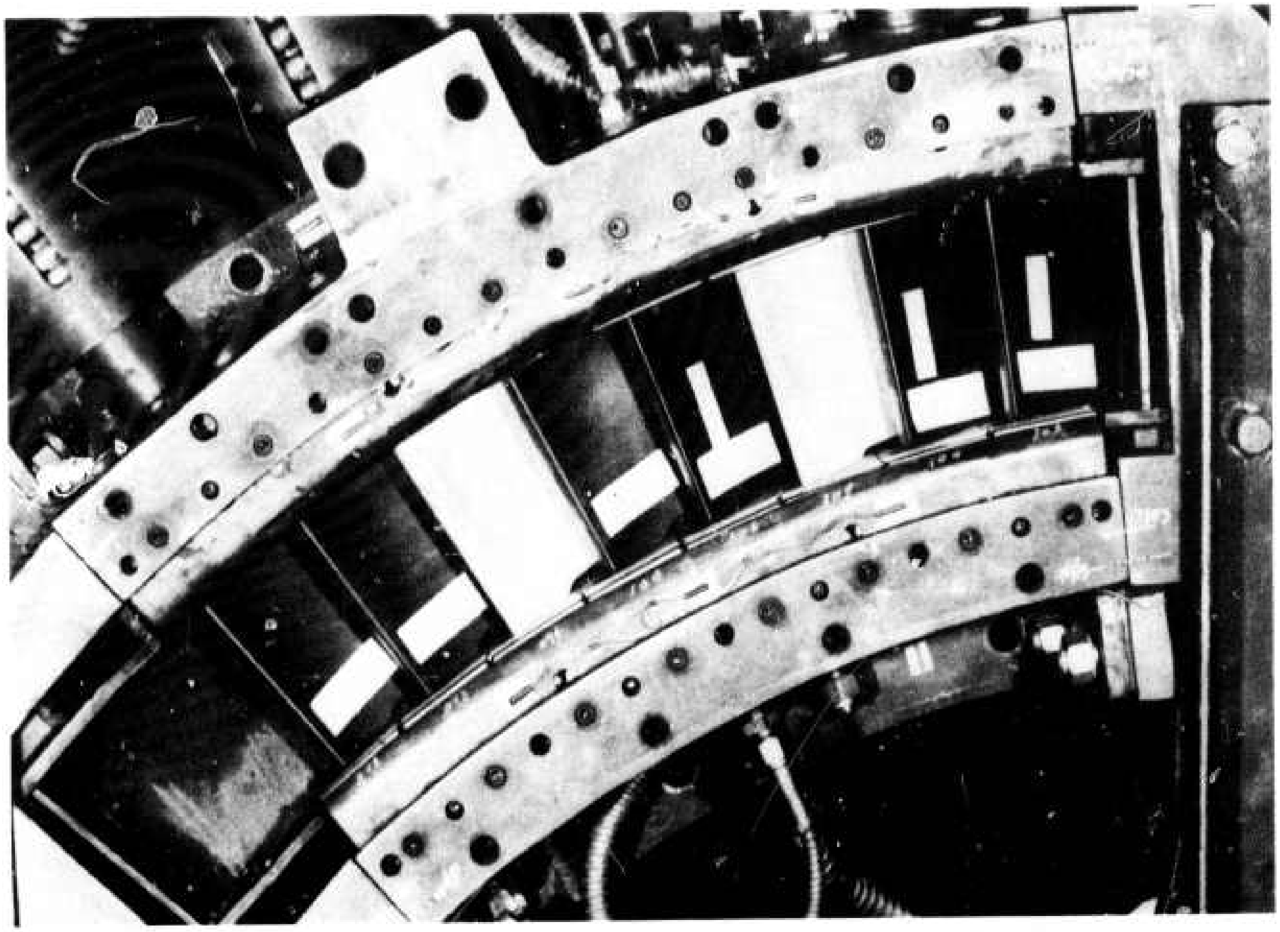

Figure 6.21 Silicon Nitride Stator Vanes Installed in Static Rig for Contamination of 2500°F Tests - Airfoils 3 and 6 were Preoxided. For 100 hours in an Alumina Lined Muffle Furnace at 2500°F.

Following cycle 22, a crack appeared in airfoil 5 starting at ≈40% height on the leading edge of the pressure side and propagated toward the outer trailing edge area. This crack was clearly visible; it was glowing at a different color than that of the airfoil proper. The crack pattern did not change appreciably after cycle 29 until cycle 34 when a chip appeared at the trailing edge.

A crack was observed at the trailing edge of airfoil 6 during the 35th cycle. This crack apparently started near mid-height and propagated toward the outer tenon-trailing edge blend radius. These failures are illustrated in Figures 6.22 and 6.23 as they appeared when the rig was opened following the termination of testing after the 35th cycle (total 60 cycles). A section was missing from the trailing edge of vane 6. Cracks were clearly evident on the suction sides as well as the pressure sides of vanes 5 and 6. No other damage was noted, however. Excellent alignment of the test components had been maintained Figure 6.23. All of the vane assemblies and insulators are shown after test in Figure 6.24. Airfoil 5 was broken into two pieces. None of the end caps or insulators appeared to be damaged.

It is interesting to note that the airfoil tenon area contact with the end cap cavity occurred along the lines of machine chatter marks as previously identified.(8) The condition is illustrated in Figure 6.25.

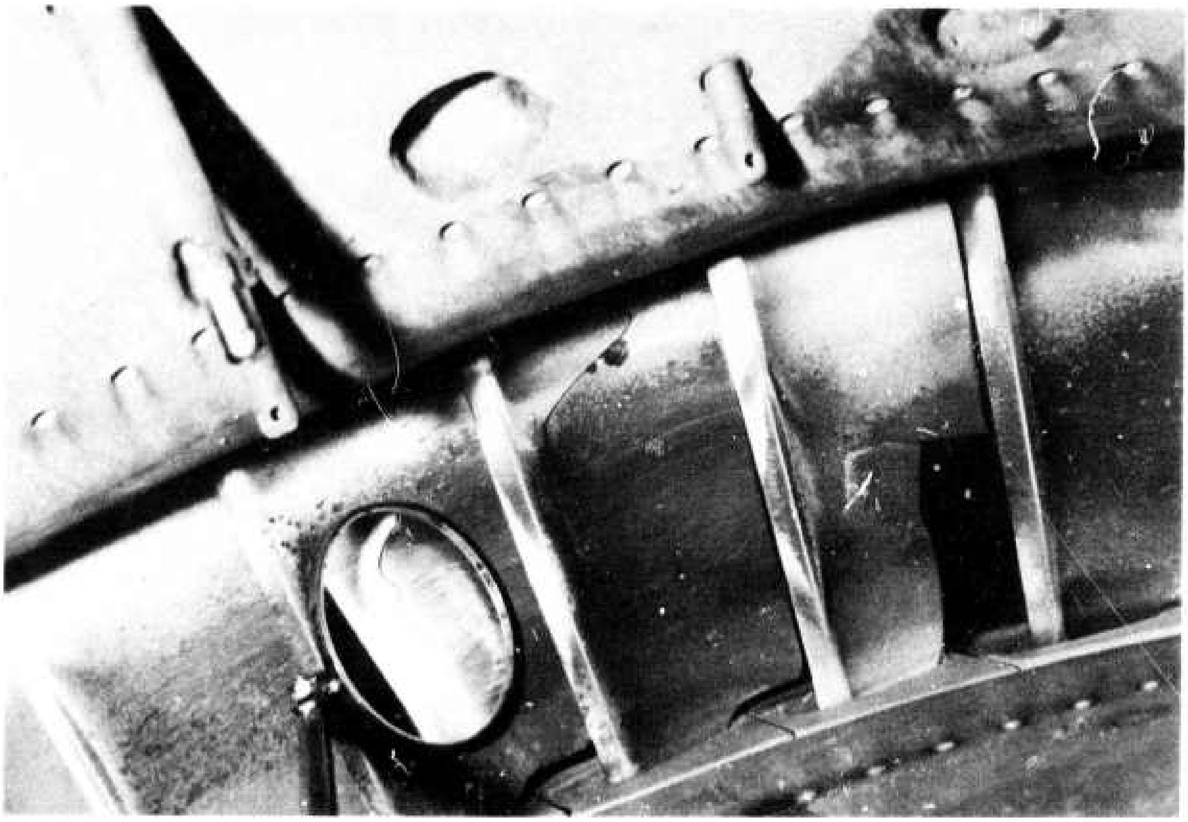

Figure 6.22 Failure Indications in Silicon Nitride Stator Vane Airfoils (Cycles 26-60 Static Rig Testing at 2500°F)

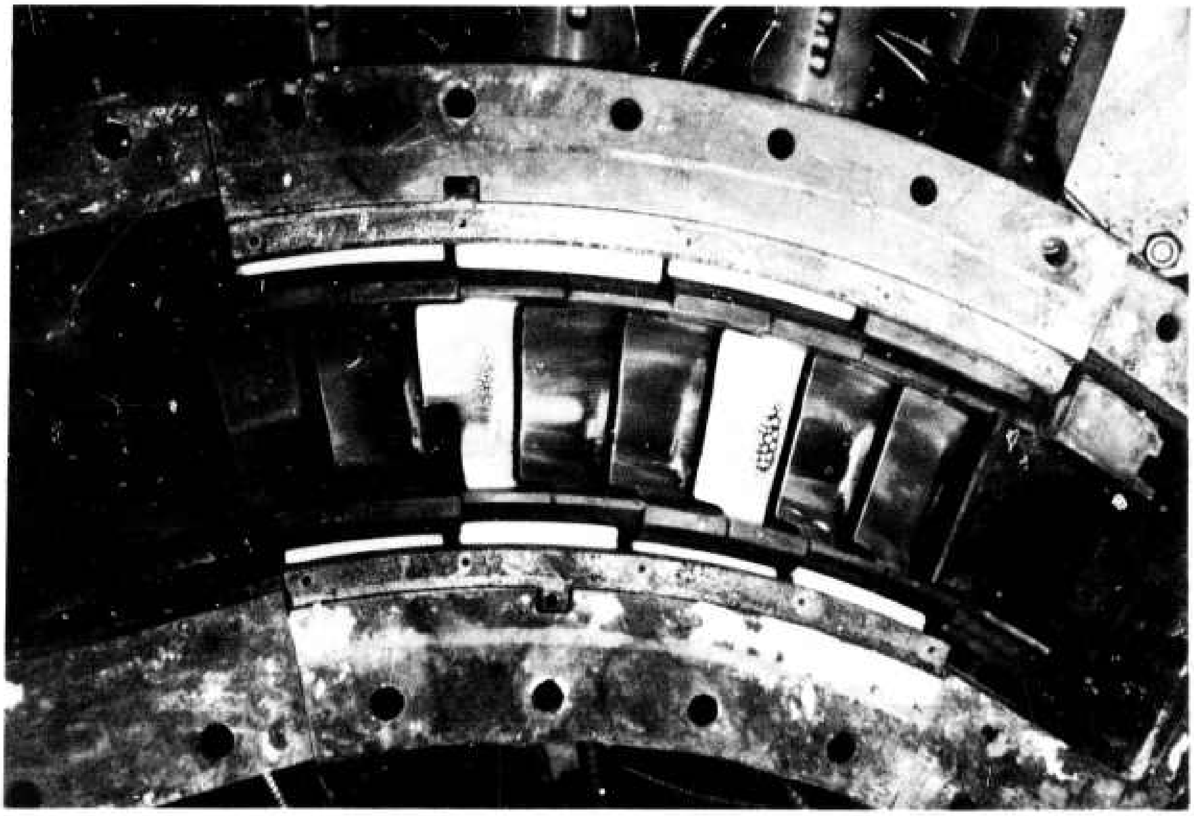

Figure 6.23 Trailing Edge View of Si_3N_4 Components After 2500°F Static Rig Test (Cycles 26-60) Note End Cap Alignment

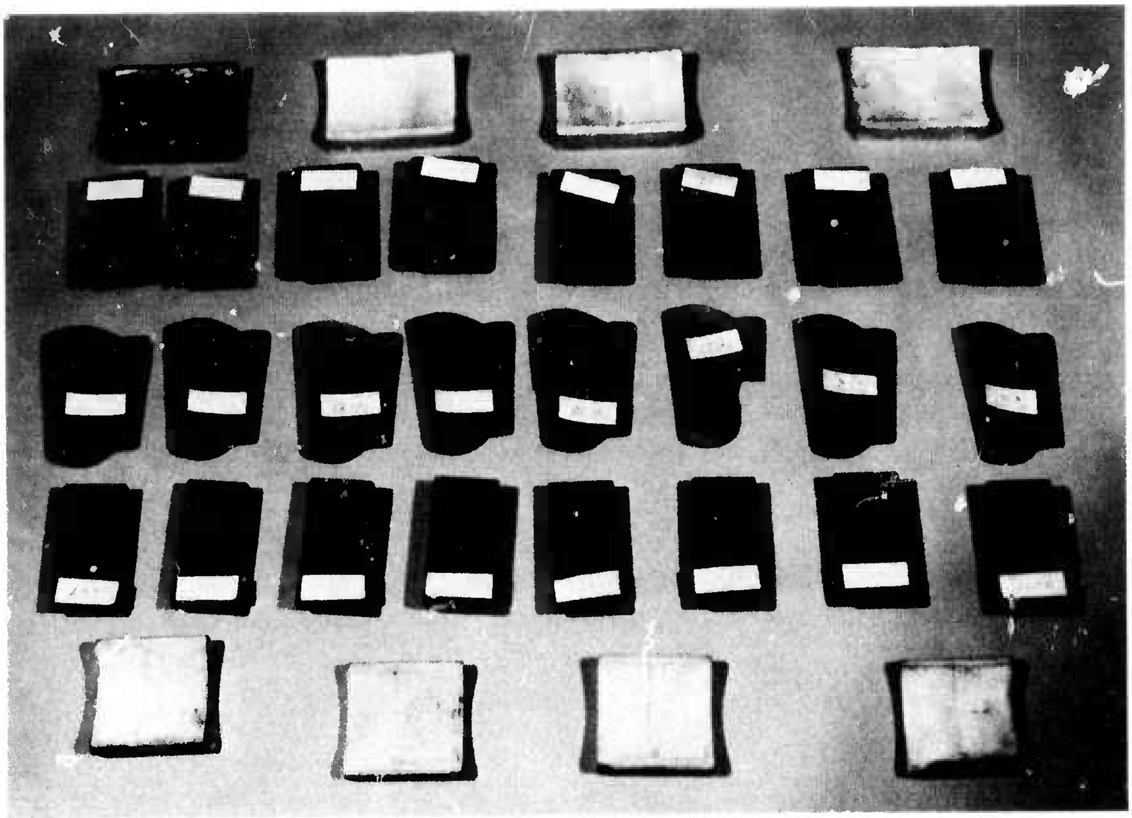

Figure 6.24 Stator Vane Components and Insulators from Static Rig Testing at 2500°F (Cycles 26-60).

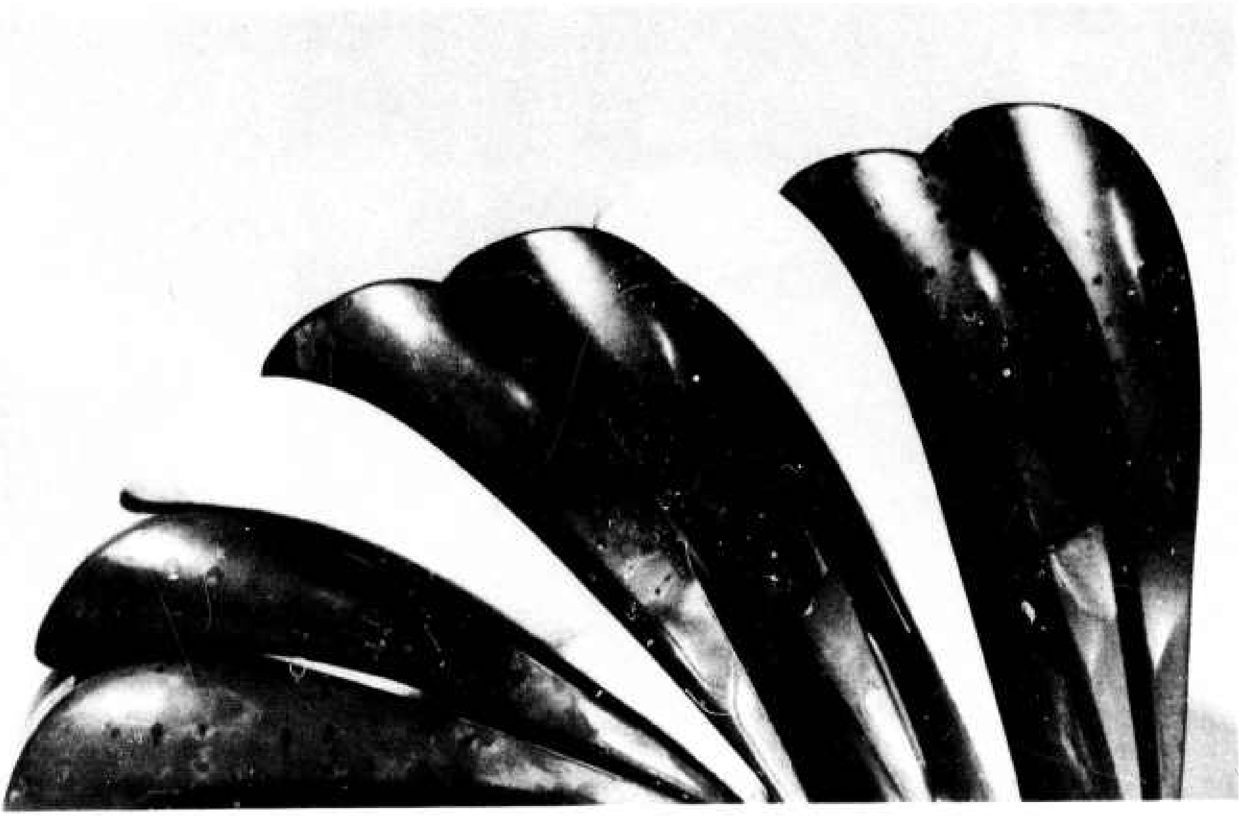

Figure 6.25 Contact Areas on Outer Airfoil Tenons Defined Along Machine Chatter Marks

Failure Analysis Cycles 26-60

All airfoils and end caps were inspected for cracks in the same manner as that described under Failure Analysis Cycles 1-25. No cracks or surface irregularities were observed on any components except those previously identified on airfoils 5 and 6.

An analysis of the crack pattern (Figures 6.26 and 6.27) and the markings on the fractured surfaces showed that the cracks in vane 5 initiated at the leading edge, those in vane 6 initiated at the trailing edge. The vane areas close to the end cap were closely scrutinized for possible contact stress crack origins. Although several cracks propagated toward these areas, no crack origins were observed. This fracture analysis strongly suggests that the cracks observed in vanes 5 and 6 during the second 35 cycles at 2500°F were caused by thermal stresses.

No definite conclusions will be drawn until testing and subsequent stress analysis are completed.

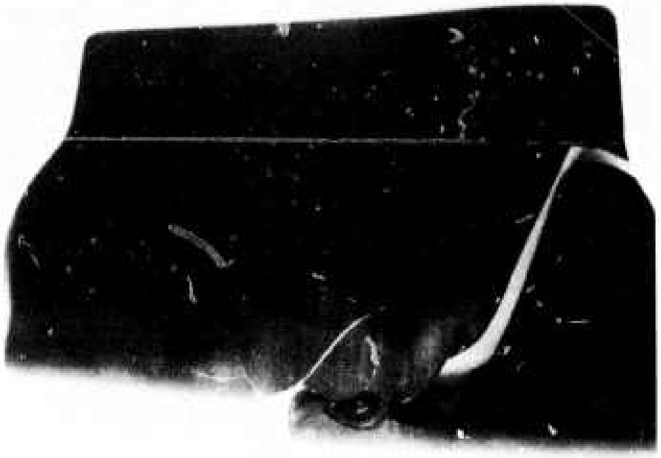

a. vacuum side

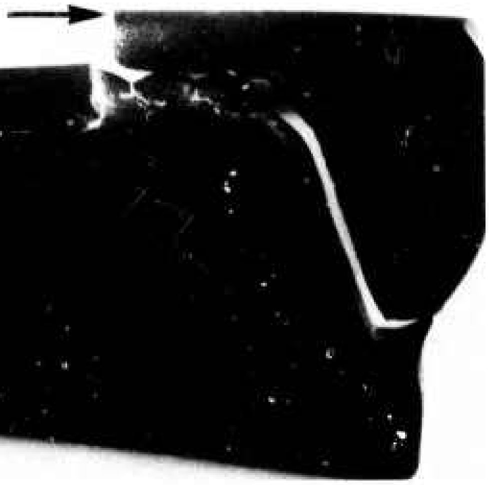

b. pressure side

Figure 6.26 Ultraviolet Macrographs of Vane 5 Showing Cracks as Revealed by Dye Penetrant

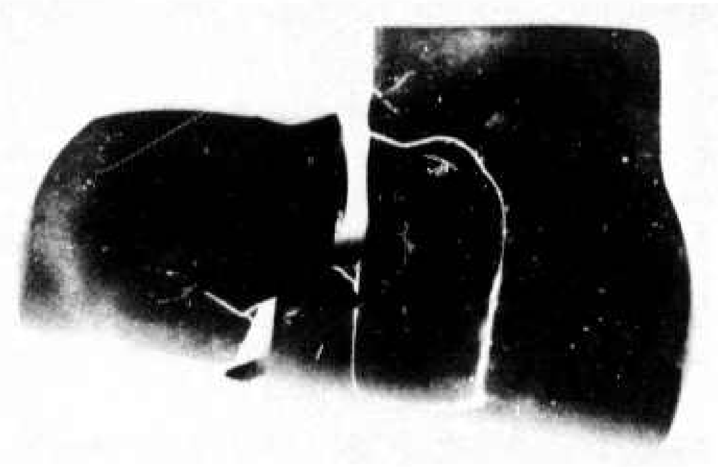

a. vacuum side

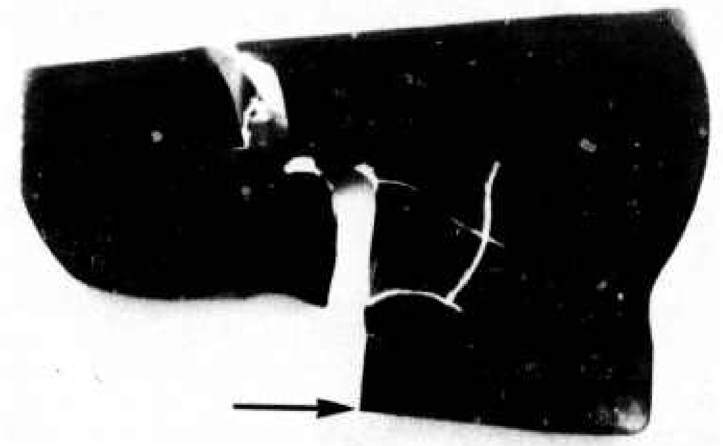

b. pressure side

Figure 6.27 Ultraviolet Macrographs of Vane 6 (Preoxided) Showing Cracks as Revealed by Dye Penetrant

6.1.2 VANE FABRICATION

Introduction

The Norton Company continues as the sole source of hot-pressed materials for the fabrication of stator vane assemblies. Rework of the fourteen tapered-twisted airfoil sections for the 2500°F static rig test was completed satisfactorily early in the report period. An additional fourteen airfoil sections were also delivered. Twenty end caps are scheduled for delivery in early March to complete all the requirements for hardware under the present scope of the project. Billet certification data are reported.

Static Rig Test Hardware

Fourteen additional airfoil sections manufactured from Norton NC 132 silicon nitride billets were delivered in December. These will be used as needed to replace airfoil sections which are damaged in subsequent cycles of static rig testing at 2500°F to complete the 100 cycle program objective.

Routine inspection of these airfoil parts by dye penetrant technique, x-ray radiography, and ultrasonic scanning failed to disclose any defect or abnormality worthy of mention. All components were found to be of high quality when inspected to the NDT specifications. Dimensional inspection is in progress.

The 10 end cap sets required to complete the total hardware order are still being manufactured by Norton. Norton promises final delivery in early March. As it now stands, 28 airfoil sections and 24 end caps have been delivered as part of the original order for 100 vane sets. The 100 vane set order was canceled after the initial 10 sets of stator vane hardware were received with a partial order requirement for the 10 additional sets. Norton is currently conducting an inventory of billets and partially completed parts in compliance with government requirements.

Vane Certification Data

Airfoils and end caps are manufactured from billet material by precision diamond grinding. All billet material used in the manufacturing process must meet a mean strength minus 2 standard deviation specification of 80,000 psi in 4 pt flexural loading at room temperature. The density must exceed 3.18 gm/cc at a calcium concentration not to exceed 1000 ppm.

The room temperature strength and density certification data as supplied by Norton in compliance with the airfoil specification are summarized in Table 6.1 for all completed airfoils and airfoil blanks. It is obvious that wide scatter exists in both strength and density from billet to billet. These data are currently being correlated with airfoil performance in the static rig to see if failures can be explained by differences in material properties within the scatter band. When this analysis is complete, the probability of failure will be reported for Norton NC 132 silicon nitride in the stator vane configuration under conditions of static rig testing. The results should be applicable to full turbine operation.

Norton has not supplied certification data for the billets used in end cap manufacture. These data will be discussed as part of the final report.

TABLE 6.1

AIRFOIL CERTIFICATION DATA

Vane No.	Mean Strength* (psi)	Mean-2 Std Deviation	Density (g/cc)
3	127,400	86,000	3.27
4	132,300	110,100	3.27
6	132,300	90,300	3.27
8	117,600	97,400	3.24
9	130,300	98,100	3.27
11	119,400	106,000	3.25
12	119,159	80,400	3.24
13	131,600	112,400	3.21
14	134,600	99,200	3.25
15	125,600	80,800	3.26
16	138,700	113,100	3.26
17	129,500	98,100	3.27
18	119,200	81,800	3.26
19	133,400	104,400	3.25
20	132,000	98,200	3.27
21	118,700	92,300	3.21
22	125,000	90,400	3.22
23	124,200	90,400	3.21
24	130,000	100,200	3.21
25	132,400	115,000	3.22
26	126,300	96,700	3.24
27	133,300	111,300	3.22
28	131,100	108,900	3.22
29	128,500	97,900	3.22
30	129,800	104,400	3.22
64	120,205	84,800	3.22
65	132,600	120,000	3.22
66	141,054	131,300	3.22
67	130,300	103,100	3.21
68	122,000	96,400	3.22
69	124,100	105,300	3.22
70	117,300	92,100	3.22
73	123,900	101,100	3.27
76	117,200	82,400	3.26
79	123,300	80,700	3.21
80	125,000	102,200	3.21
81	124,200	91,600	3.21
82	123,100	87,500	3.22
83	114,397	82,600	3.21
84	119,700	80,500	3.22
86	121,300	91,900	3.21
87	117,126	102,500	3.20
89	115,203	93,800	3.20
90	113,870	87,900	3.21
92	112,541	92,300	3.20
31	124,700	92,700	3.22
32	120,200	94,400	3.22
33	111,100	88,700	3.21
35	125,000	103,600	3.22
37	131,200	118,200	3.23
38	122,000	90,800	3.23
39	132,200	100,000	3.22
40	134,700	113,700	3.22
41	124,470	92,768	
42	113,600	86,000	3.21
43	128,700	101,700	3.22
44	124,000	106,200	3.22
45	125,200	95,600	3.23
46	131,100	114,900	3.23
47	123,800	106,200	3.22
48	127,600	102,000	3.22
49	125,800	96,800	3.22
50	117,115	85,100	3.23
57	122,400	101,200	3.24
58	128,100	91,900	3.24
59	122,228	90,952	
60	116,700	100,100	3.23
61	115,300	95,100	3.24
62	121,100	82,100	3.24
63	119,200	82,600	3.20
94	113,878	87,300	3.21
95	124,200	89,200	3.21
96	127,900	90,100	3.20
97	123,800	90,000	3.20
98	123,800	96,600	3.21
99	121,100	87,100	3.21
100	115,300	83,500	3.21
101	122,500	90,100	3.20
102	124,500	91,700	3.21
103	125,500	105,300	3.21
104	116,800	95,200	3.21
105	114,800	86,400	3.24
107	114,556	80,000	3.24
108	118,300	83,700	3.24
109	120,000	85,800	3.21
110	116,500	86,900	3.22
113	118,900	95,300	3.24
114	123,800	93,100	3.22
115	127,300	104,500	3.22
122	122,000	81,200	3.20

*Norton Data at Room Temperature, Quarter Point Loading - 1-1/2" Outer Span; Specimen 1/8" x 1/8" x 6" Multiple Breaks from Contoured Billets Used in Airfoil Fabrication

7. PROGRESS ON MATERIAL TECHNOLOGY - STATIONARY TURBINE PROJECT

7.1 MATERIAL ENGINEERING DATA

Summary

In the stationary turbine project, commercially produced hot-pressed silicon nitride and silicon carbide have been subjected to intensive investigation to provide design engineers and stress analysts with physical, mechanical and thermal property data as required. This work is expected to continue throughout the program in order to update properties as material improvements evolve and to verify billet properties to assure reliability of test components fabricated from the hot-pressed billets. This section reports the acquisition of additional property information.

The properties of boron nitride insulator material have been determined to verify vendor data. Results to date include flexural strength, elastic modulus, shear modulus, Poisson's ratio and thermal expansion. Thermal conductivity measurements are in progress, but data are incomplete at this time.

The tensile creep life of Norton NC 132 silicon nitride exceeds 10,000 hours at 2100°F, 10,000 psi stress.

PRECEDING PAGE BLANK-NOT FILMED

7.1.1 PROPERTIES OF BORON NITRIDE INSULATOR MATERIAL

Introduction

The material properties of a hot-pressed boron nitride[*] insulator material were characterized to verify the vendor data used in design calculations. Specimens were prepared from five pieces of hot-pressed boron nitride cut from billets used to manufacture insulators for static rig tests at 2500°F. The list of properties measured includes: density, flexure strength vs. temperature, compression strength, Poisson's ratio, elastic modulus, sonic velocity, flexure creep, thermal expansion and thermal conductivity.

Density

The density of each of the five pieces was measured by water immersion. Results are tabulated below:

Piece No.	1	2	3	4	5
Density g/cc	2.11	2.13	2.14	2.12	2.13
Water Absorption 100 hours in 50% humidity	.007%	.004%	.005%	.004%	.006%

Flexure Strength vs. Temperature

Flexural strength was determined up to 2000°F in four point loading. The load span was 0.50 inch over an outer support span of 1 inch. Nominal specimen dimensions were 0.125 inch thick, 0.250 inch wide and 1.25 inch long. In the "B" direction, the specimens were finished with the tool marks in the longitudinal direction and in the "A" direction the tool marks were perpendicular to the longitudinal direction (Figure 7.1). Final grinding was done with Al 320 grit diamond wheel. Drawings of the flexure specimens are shown in Figures 7.2 and 7.3. Three specimens from each direction were tested at each temperature condition. Flexure strength is reported in Tables 7.1 and 7.2. The results are plotted as a function of temperature in Figure 7.4.

Other flexure tests were conducted on .125 inch thick, .250 inch wide and 2 inches long specimens (Figure 7.5) at test temperatures of 75°F, 1800°F and 2000°F using a three rod deflectometer to obtain stress-strain curves. All of these specimens were cut from the "B" direction orientation. These test results appear in Table 7.3. Typical stress-strain curves at 2000°F is shown in Figure 7.6.

---

[*] Carborundum Combat "M" Boron Nitride

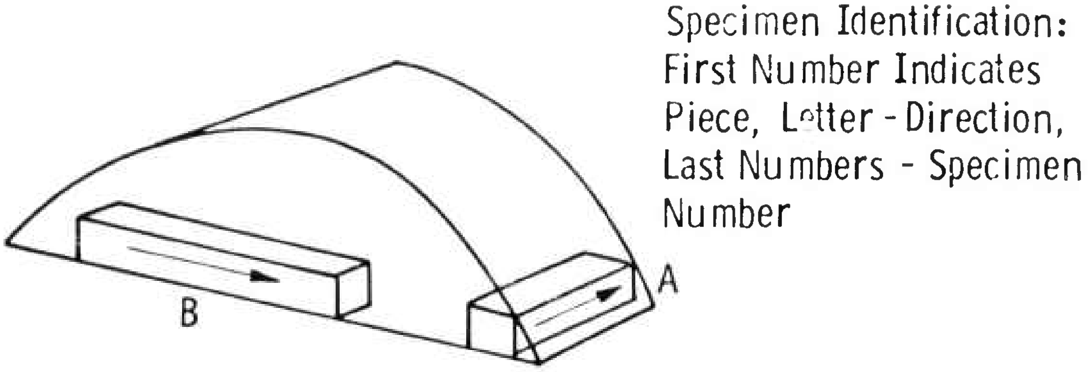
Specimen Identification:
First Number Indicates
Piece, Letter - Direction,
Last Numbers - Specimen
Number
A
B

Figure 7.1 Specimen Orientation in Boron Nitride Insulator Materials

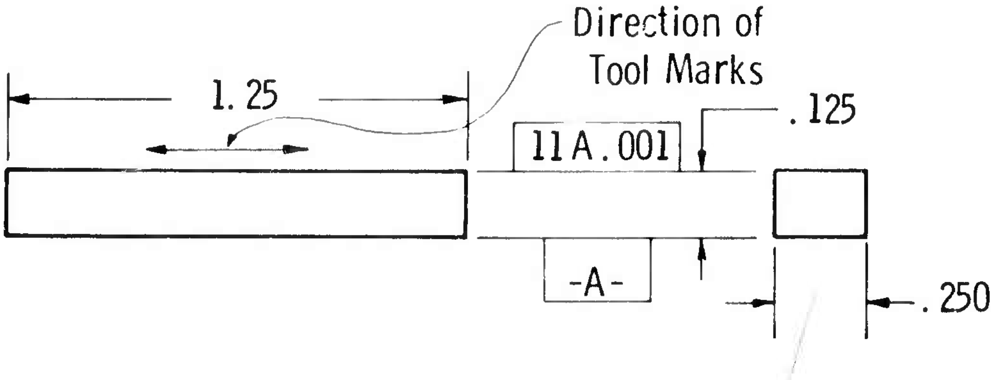
Direction of
Tool Marks
1.25
.125
11A.001
-A-
.250

Figure 7.2 Flexural Specimen "B" Direction

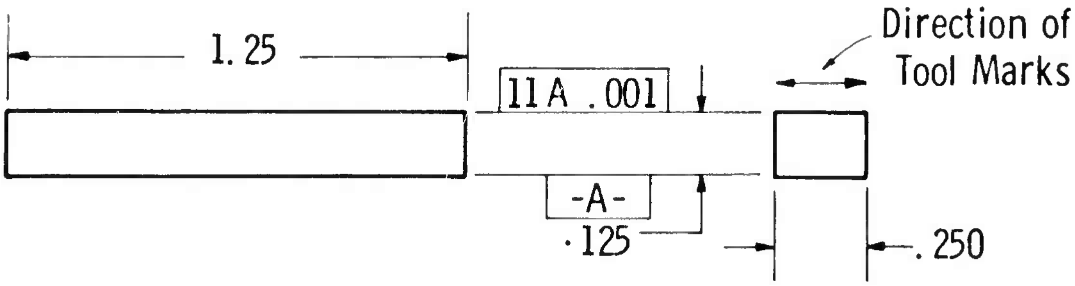
Direction of
Tool Marks
1.25
11A .001
-A-
·125
.250

Figure 7.3 Flexural Specimen "A" Direction

TABLE 7.1
FLEXURE STRENGTH OF HOT-PRESSED BORON NITRIDE "A" DIRECTION

Spec. No.	Test Temp.	Spec. Size (in)		Ultimate Flex. Strength	
		(WD)	(TK)	(LB)	(PSI)
2A1	RT	.2500	.1224	20.2	4090
2A2	RT	.2520	.1234	20.2	3990
2A3	RT	.2491	.1229	19.6	3950
2A4	1200°F	.2526	.1230	20.4	4040
2A5	1200°F	.2530	.1232	20.8	4100
2A6	1200°F	.2538	.1225	21.4	4260
2A7	1500°F	.2509	.1230	24.6	4910
2A8	1500°F	.2509	.1232	25.7	5110
2A9	1500°F	.2471	.1234	22.6	4550
2A10	1800°F	.2506	.1234	24.8	4920
2A11	1800°F	.2508	.1234	20.4	4050
2A12	1800°F	.2493	.1224	22.0	4460
2A13	2000°F	.2441	.1234	22.8	4650
2A14	2000°F	.2499	.1229	22.4	4490
2A15	2000°F	.2530	.1231	23.1	4560

TABLE 7.2
FLEXURE STRENGTH OF HOT-PRESSED BORON NITRIDE "B" DIRECTION

Spec. No.	Test Temp.	Spec. Size (in)		Ultimate Flex. Strength	
		(WD)	(TK)	(LB)	(PSI)
2B1	RT	.2509	.1292	58.4	10650
2B2	RT	.2515	.1274	60.5	11350
2B3	RT	.2516	.1278	63.4	11800
2B4	1200°F	.2512	.1244	60.2	11850
2B5	1200°F	.2494	.1280	58.4	10950
2B6		.2510	.1285		
2B7	1500°F	.2524	.1287	57.7	10450
2B8	1500°F	.2530	.1243	48.9	9480
2B9	1500°F	.2521	.1281	68.3	12500
2B10	1800°F	.2528	.1280	75.1	13750
2B11	1800°F	.2519	.1289	63.0	11400
2B13	1800°F	.2540	.1280	56.0	10200
2B14	2000°F	.2506	.1284	66.4	12150
2B15	2000°F	.2488	.1277	86.1	16100
2B21	2000°F	.2504	.1267	69.0	13000

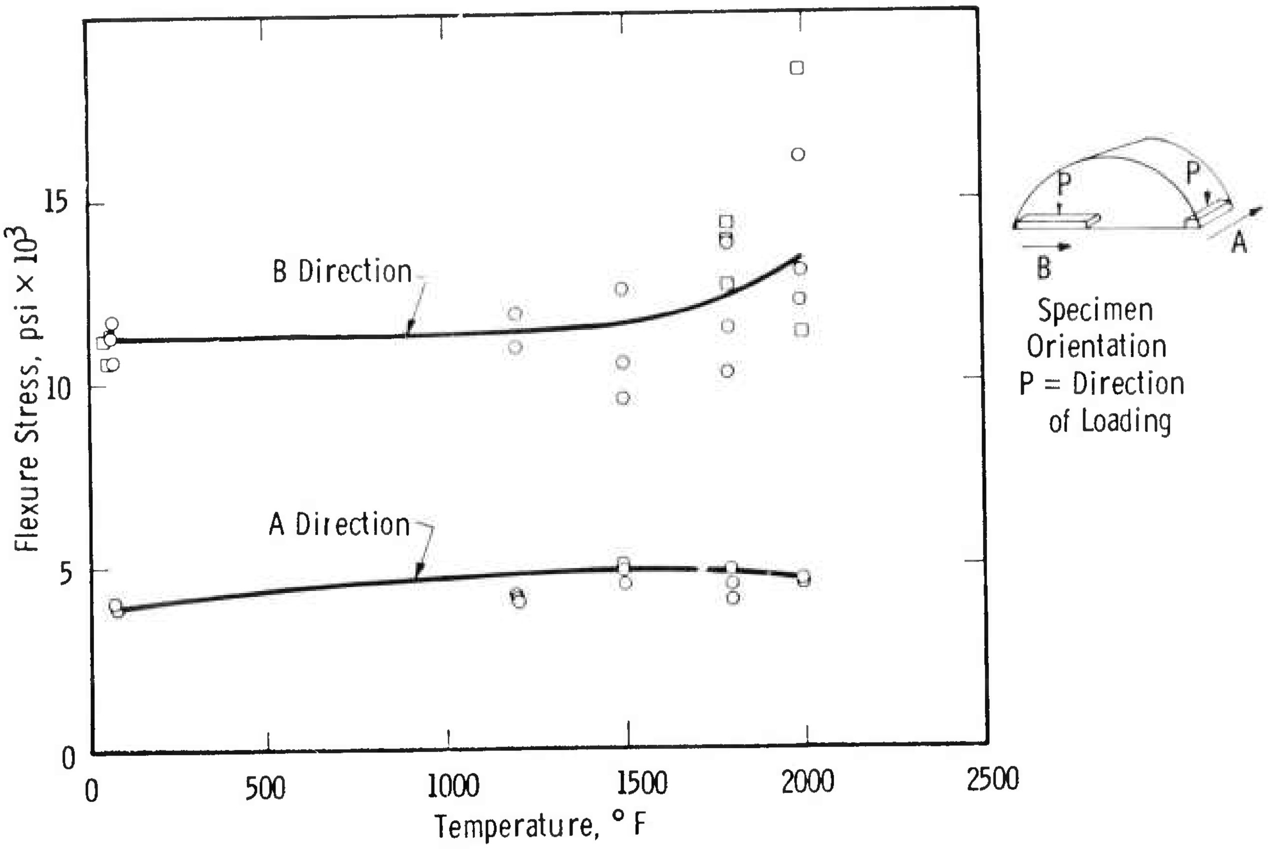

Figure 7.4 The Effect of Temperature on the Flexured Strength of Boron Nitride Insulator Material.

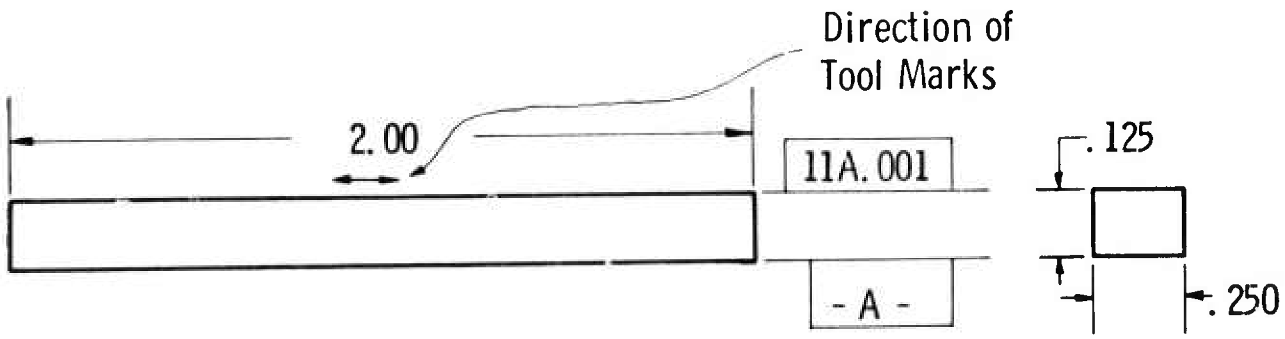
Direction of
Tool Marks
2.00
11A.001
-A-
.125
.250

Figure 7.5 Flexural Specimen for Stress-Strain Determinations

TABLE 7.3

ELASTIC MODULUS MEASUREMENTS FROM FLEXURE TESTS

Specimen No.	Test Temperature	Ultimate Strength, psi	Elastic Modulus x 10^6 psi
3B1	75°F	11,300	12.43
1B3	75°F	11,450	11.38
1B4	75°F	10,550	7.22
3B2	1800°F	15,400	7.33
3B3	1800°F	14,400	8.44
1B5	1800°F	14,200	9.71
1B6	2000°F	18,600	8.58
3B4	2000°F	11,250	6.91

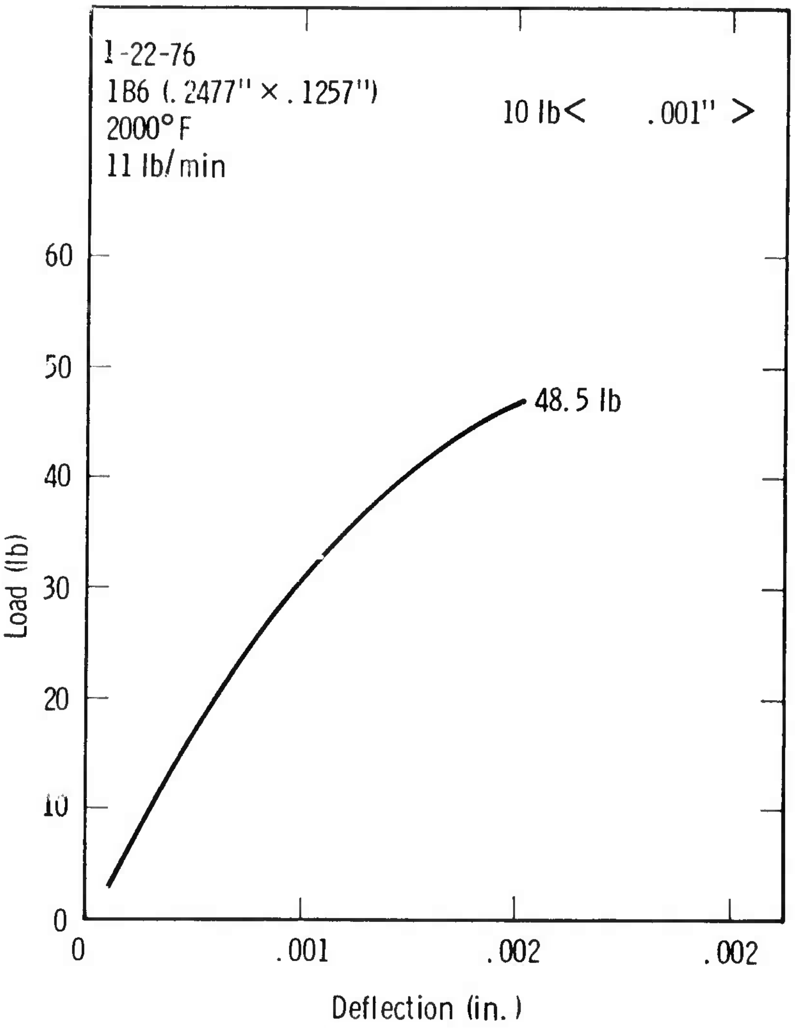

Figure 7.6 Typical Load Deflection Curve for Boron Nitride Insulator Material

Compression Tests

Compression tests were conducted at 75°F, 1500°F, 1800°F and 2000°F, using specimens illustrated in Figure 7.7. At 75°F, specimens from both directions were strain gaged to provide elastic modulus and Poisson's ratio data for comparison with sonic velocity test results. Compression results are shown in Table 7.4. The material acts isotropically in compression tests.

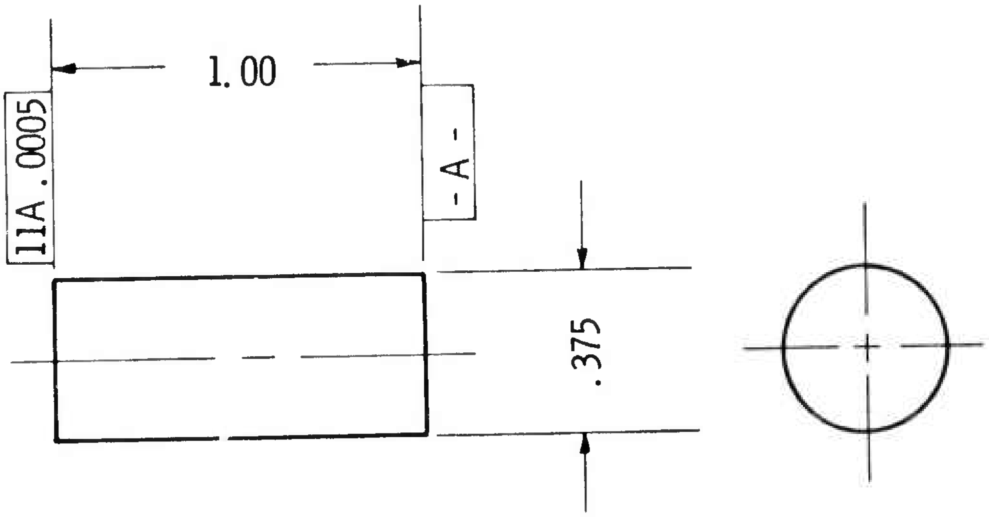

Figure 7.7 Compression Specimen

TABLE 7.4

COMPRESSION RESULTS FOR HOT-PRESSED BORON NITRIDE

Specimen No.	Test Temp. °F	Ultimate Strength, psi	Elastic Modulus x 10^6 psi	Poisson's Ratio
4A1	75	25,350	1.24	.053
4B9	75	27,250	8.91	.114
4A4	1500	23,500	No Data	No Data
4A2	1800	36,150	No Data	No Data
4B10	1800	37,400	No Data	No Data
4A3	2000	36,700	No Data	No Data

Flexure Creep Tests

A flexure creep test was conducted at 1800°F and 5000 psi on a "B" direction specimen and at 1800°F and 2500 psi on "A" direction specimens. The same loading spans and specimen configuration that was used in the flexure strength tests were used. A flexure creep curve is shown in Figure 7.8.

Sonic Velocity

Elastic and shear moduli were computed from the extensional and torsional wave velocities through the material. Poisson's ratio was calculated, the E and G values obtained. Cylindrical specimens were used (Figure 7.9).

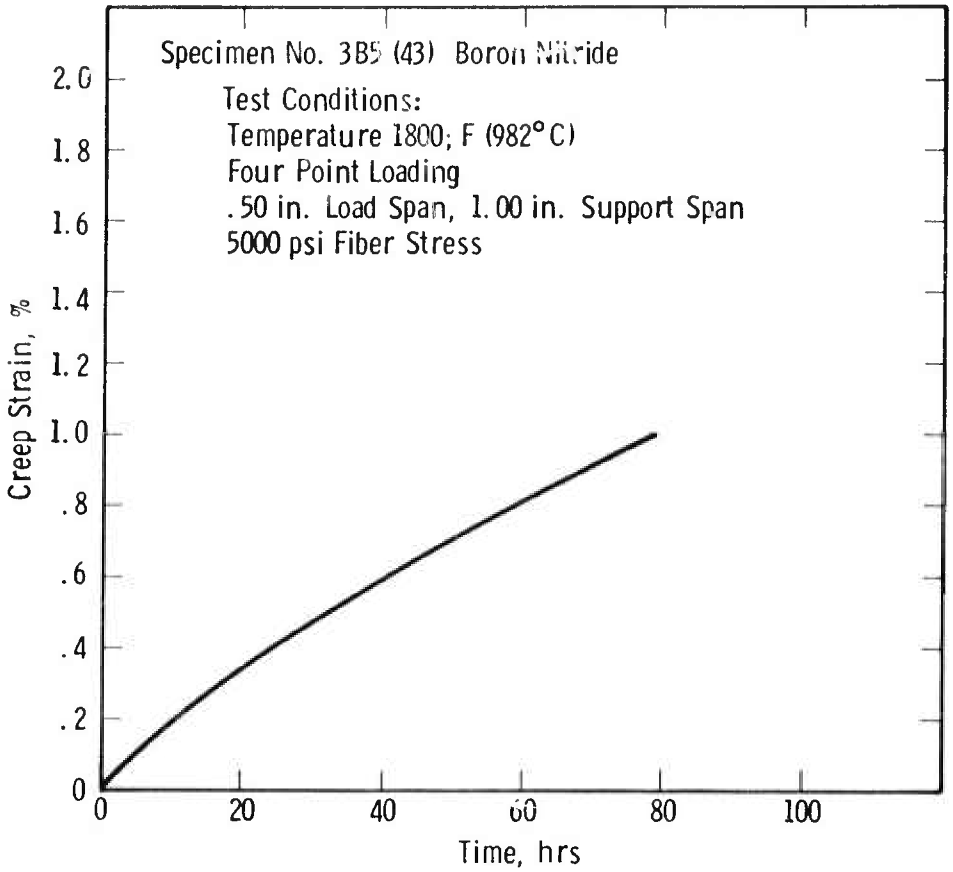

Figure 7.8 Flexural Creep in Boron Nitride Insulator Material

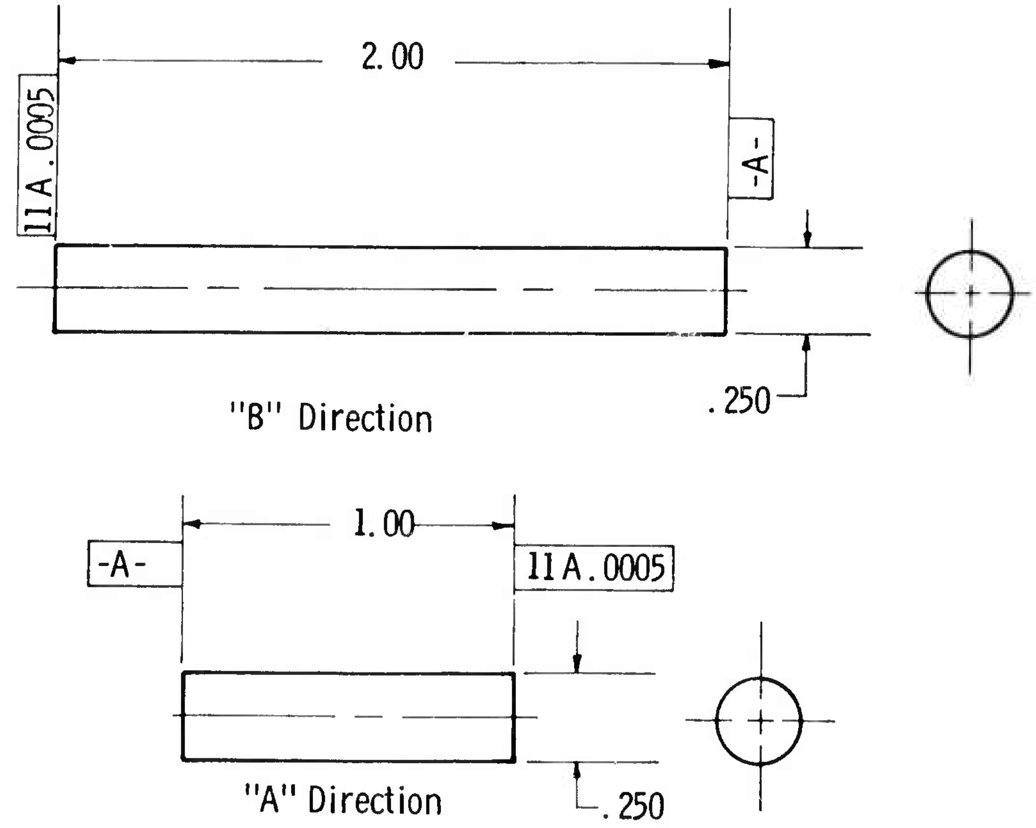
2.00
11 A .0005
-A-
.250
"B" Direction
1.00
-A-
11 A .0005
"A" Direction
.250

Figure 7.9 Thermal Expansion and Sonic Velocity Test Specimens

Thermal Expansion

Thermal expansion to 1800°F was measured with a quartz tube dilatometer using specimens 0.25 dia. x 2 inches long (Figure 7.9). In the "A" direction two 1 inch long pieces were stacked. Two specimens from the "B" direction were tested because of the low thermal expansion elongation obtained. Thermal expansion curves are shown in Figures 7.10, 7.11 and 7.12.

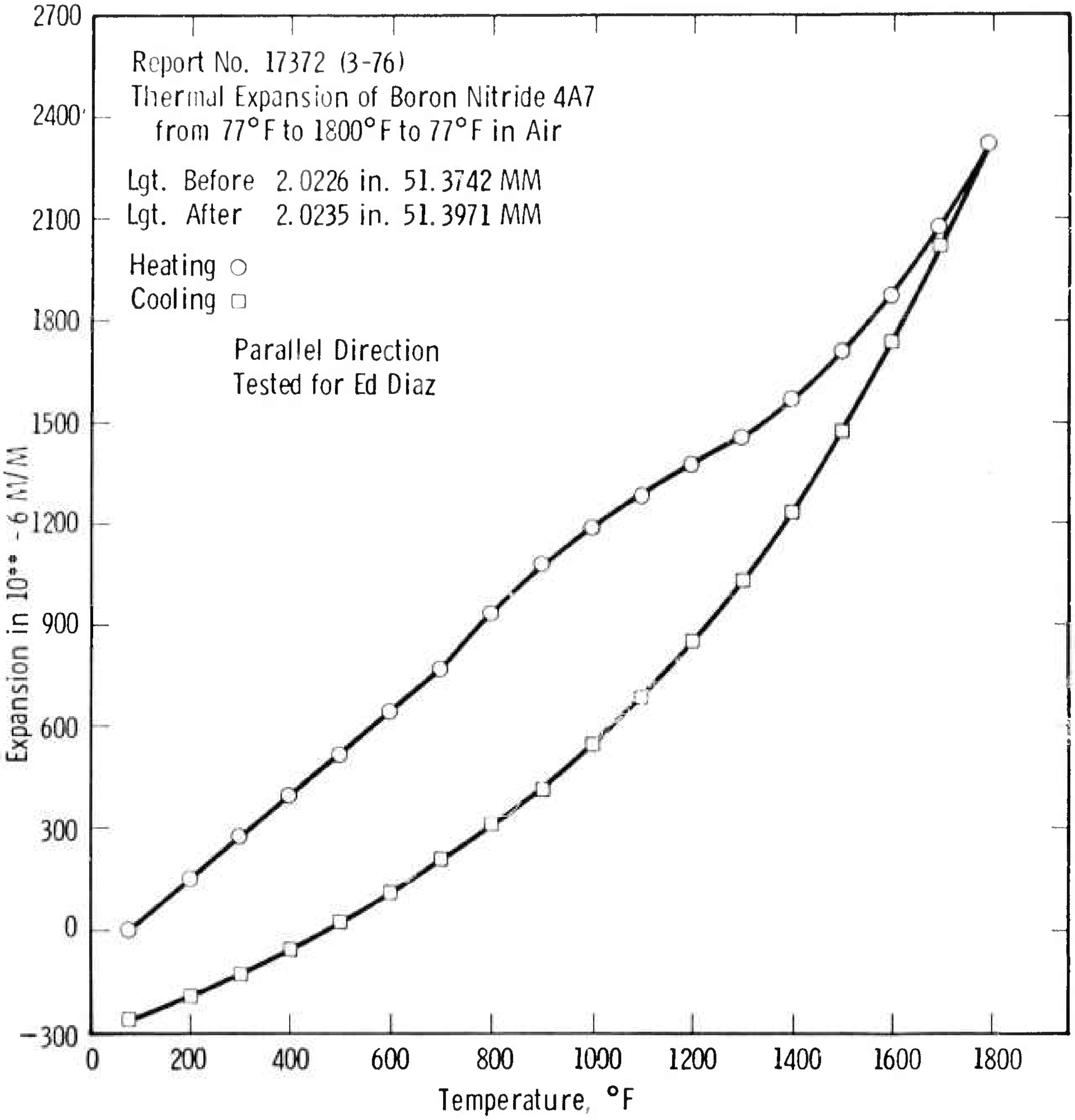

Figure 7.10 Thermal Expansion of Boron Nitride Insulator Material Parallel to the Hot Press Direction "A" (Across Insulator)

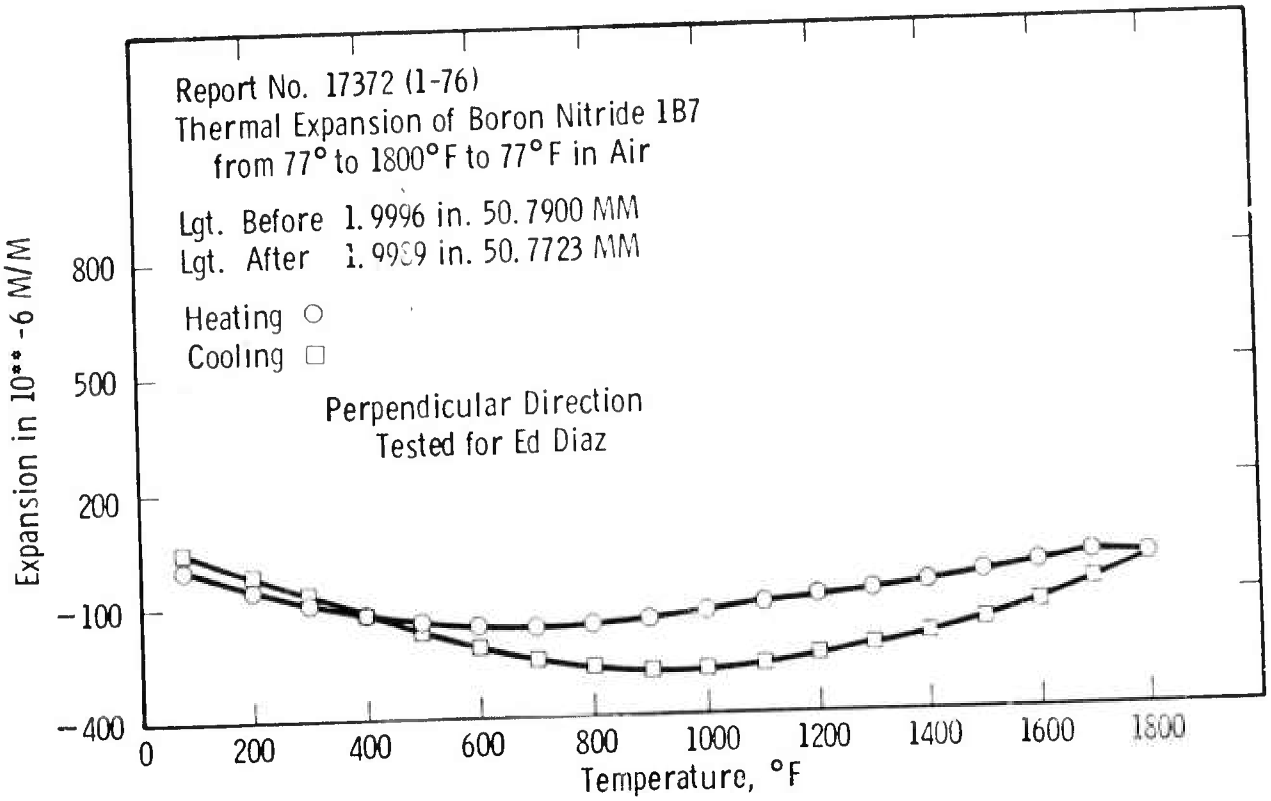

Figure 7.11 Thermal Expansion of Boron Nitride Insulator Material Perpendicular to the Hot Press Direction "B" (Through the Insulator)

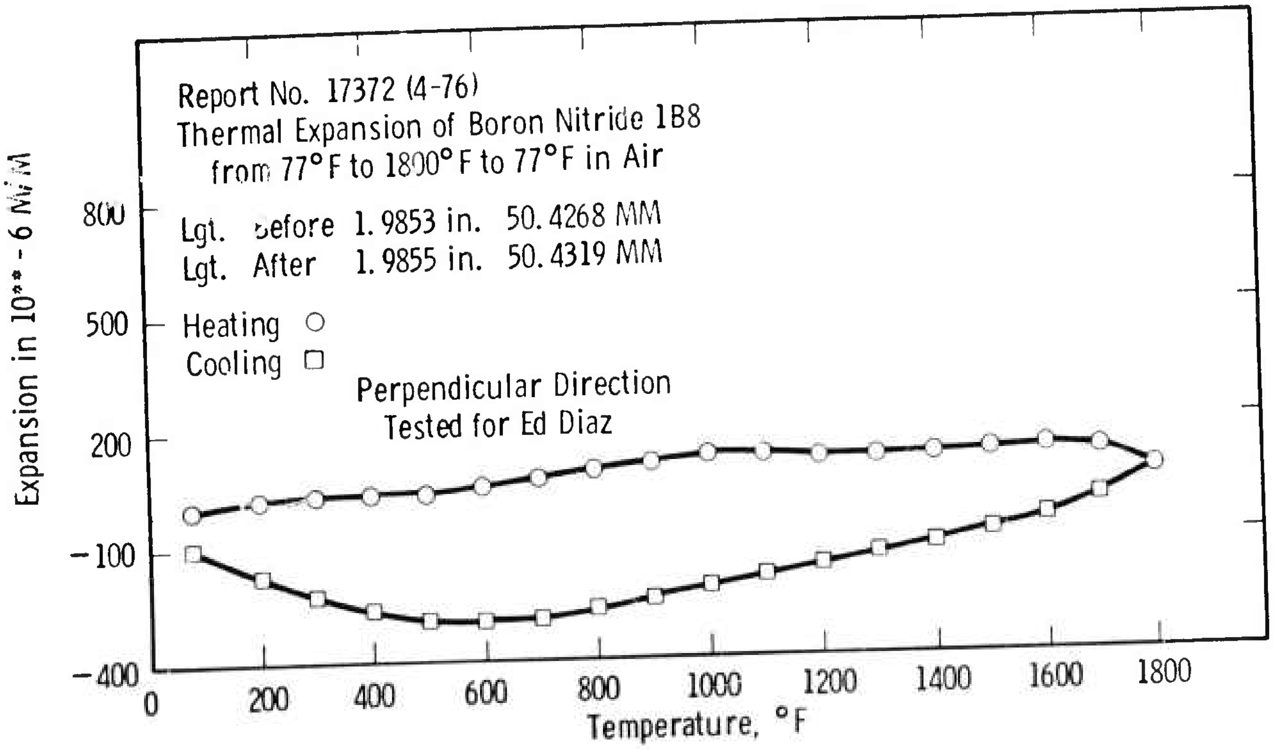

Figure 7.12 Thermal Expansion of Boron Nitride Insulator Material Perpendicular to the Hot Press Direction "B" (Repeat Determination)

Thermal Conductivity

The thermal conductivity is being determined in both the "A" and "B" directions by a comparative bar technique. Both specimens could not be made to the same dimensions because of the bulk dimensions of the piece from which they were to be obtained. The thermal conductivity specimens are shown in Figure 7.13. Test results are not complete and, therefore, are not presented here.

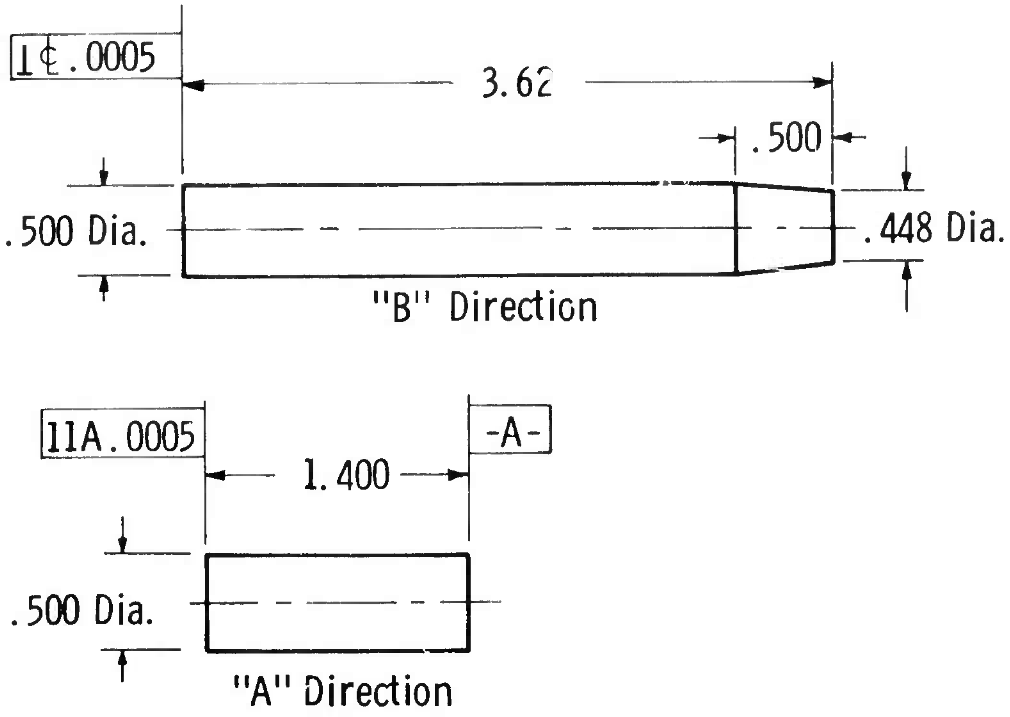
⊥ ¢ .0005
3.62
.500
.500 Dia.
.448 Dia.
"B" Direction
∥A .0005
1.400
-A-
.500 Dia.
"A" Direction

Figure 7.13 Thermal Conductivity Specimen

7.1.2 LONG TERM TENSILE CREEP PROPERTIES OF HOT-PRESSED Si_3N_4

Introduction

A tensile creep test matrix was developed to describe the tensile creep behavior of hot-pressed silicon nitride in a regime compatible with stator vane applications. The conditions of temperature and stress were selected to yield meaningful data within a reasonable time frame (1000 hrs if failure did not occur first) for the most part. In some instances, tests extended beyond 2000 hours, but estimates of creep life were made by extrapolation. These results were reported previously.(3-7) A 10,000 hour creep test was performed to confirm the life estimate calculations. At 2100°F, 10,000 psi stress, the specimen did not fail after 10,020 hours.

Stress Rupture Testing

A standard tensile creep specimen(3) was set up in a lever arm creep machine and loaded to 10,000 psi at 2100°F using TD Nickel Chromium grips as part of the established procedures. The test was finally terminated after 10,000 hours when the final set of windings in the furnace burned out. Results are plotted in Figure 7.14. The test confirms a stress rupture life for Norton NC 132 silicon nitride in excess of 10,000 hours at 2100°F, 10,000 psi stress.

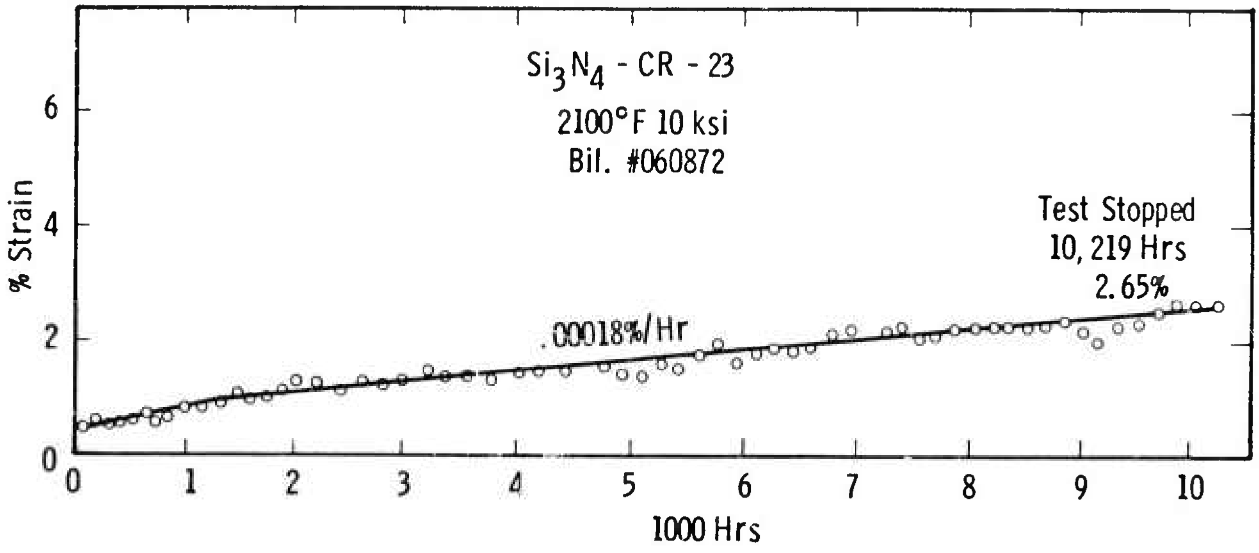

Figure 7.14 Creep Life of Si_3N_4 (NC 132) at 2100°F

7.2 IMPROVED SILICON NITRIDE MATERIALS

Introduction

With the exception of a small experimental program with Energy Research(1,2) in 1972 to develop CVD silicon carbide vanes for initial evaluation, Westinghouse has relied solely on the Norton Company for silicon nitride and silicon carbide hot-pressed billets and components manufactured therefrom. Norton demonstrated the great potential of silicon nitride as a structural ceramic in high temperature applications with the continued improvement of their hot-pressed material from the HS-110 series through HS-130 to NC -132 which must be considered the highest quality hot-pressed silicon nitride commercially available today. Norton's development of NC 203 hot-pressed silicon carbide was also achieved in support of the ARPA turbine project. While the improvements in material properties have been impressive, test results to date indicate that further refinement is necessary to reach the standard of reliability required for turbo machinery. To accomplish this, a material improvement task has been added to the Stationary Turbine Project to support ongoing other DOD activities in this area. Silicon nitride powder preparation, hot-press studies of the Si_3N_4-$Si_3N_4 \cdot SiO_2$ - $Y_2O_3 \cdot 2SiO_2$ system and fabrication processing are reviewed in Sections 7.2.1, 7.2.2 and 7.2.3, respectively.

7.2.1 Si_3N_4 POWDER

A task was initiated to accelerate the production of laboratory quantities of a high purity Si_3N_4 powder that has been developed at Westinghouse. The purpose is to make available a sufficient quantity of the powder for use in the fabrication and characterization of improved hot-pressed Si_3N_4. This report provides information on the characteristics of the starting Si and the resultant Si_3N_4 powders.

Silicon Metal Powder Characteristics

A spectrochemical analysis and oxygen content of the silicon metal powder are shown in Table 7.5. Oxygen analysis is obtained by an inert gas fusion technique. The particle size distribution of screened silicon powder as determined with a Micromeritics Model 5000 Particle Size Analyzer is given in Figure 7.15. Studies have shown that silicon powder finer than -200 mesh is necessary to minimize the amount of unreacted silicon in the nitride powder. Present processing produces powder with < 1% unreacted silicon. As described elsewhere(18), the oxygen content of the final nitrided powder is important to optimizing the properties of the final hot-pressed material. Oxygen content can be varied by either the addition or deletion of SiO_2 in the silicon powder.

TABLE 7.5

SPECTROCHEMICAL ANALYSIS
(wt%)

	Silicon Powder	Silicon Nitride Powder
Al	.064	.062
Ag	< .001	< .001
B	.003	< .003
Bi	< .003	< .01
Ca	.019	.012
Co	< .001	.002
Cr	.12	.01
Cu	< .01	< .01
Fe	>.1	>.1
Mg	< .003	< .003
Mo	< .003	< .003
Ni	.008	.012
Pb	< .01	< .01
Ti	.028	.011
V	.011	.021

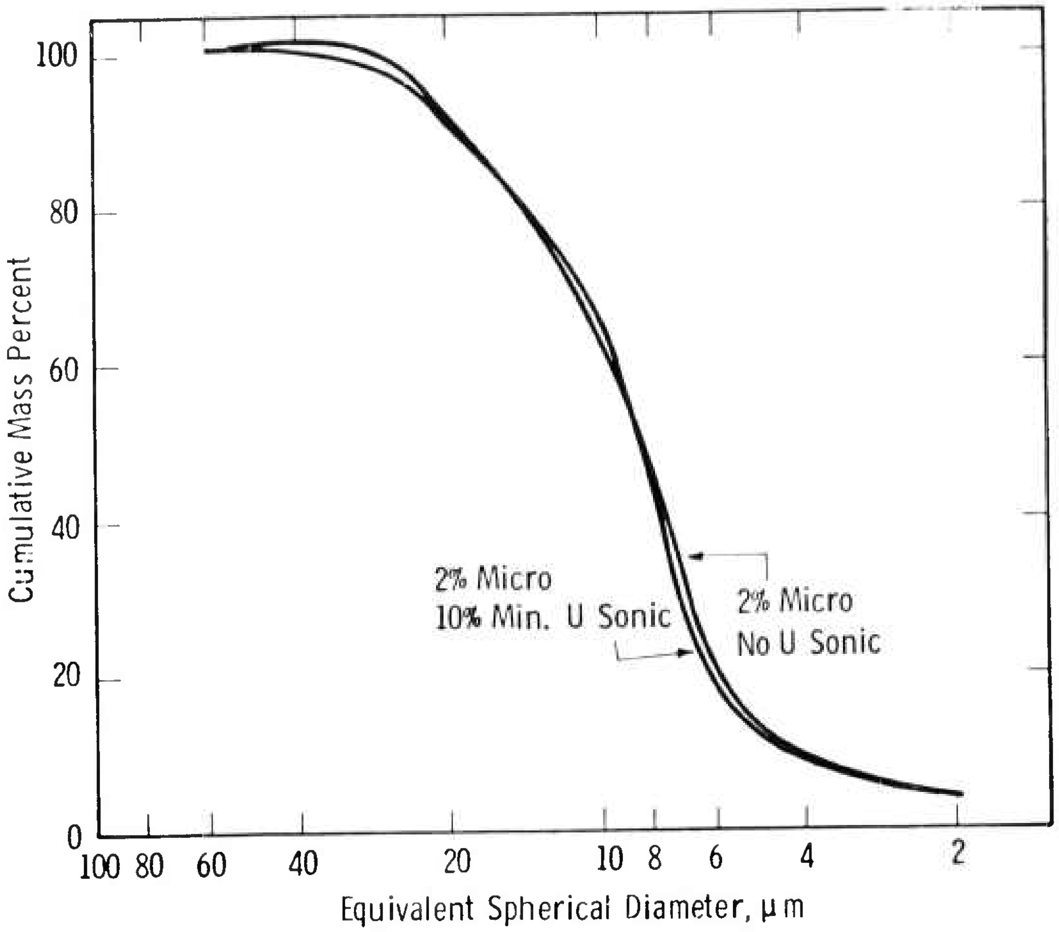

Figure 7.15 Particle Size Distribution In Screened Silicon Metal Powder

Scale-Up of Si_3N_4 Powder

High purity silicon nitride powder has been scaled up to produce laboratory quantities of ~8-9 Kg/month. The type of furnace used in the powder nitriding process was modified in order to prevent excessive oxygen pickup. A common source of oxygen is water vapor contained in the refractory linings of large furnaces. This problem as well as excessive deterioration of heating elements has been prevented by the use of closed-end mullite tubes fitted with leak-tight gaskets and end caps. The modified furnace arrangement has been used about three months with no maintenance problems.

Characterization of Nitrided Powder

Spectrochemical analysis for metallic impurities and oxygen analysis were performed to describe the nitride powders produced. Phase content, i.e., α-Si_3N_4, β-Si_3N_4, Si, etc. was determined by x-ray diffraction. The Si_3N_4 powder had to be jet milled and dry screened with all particles of size > 100 mesh (150 micron) separated out to prevent clogging of the Micromeritics Particle Size Analyzer. These particles may also be harmful to strength specimens when hot pressed. Average particle size was approximately 12 microns. The current powder being produced has an α/β ratio of approximately 90/10 (just about all > 85/15), an unreacted silicon content of $\leq$ 1%, and an oxygen content in the 0.5-0.8 wt% range.

7.2.2 THE Si_3N_4-$Si_3N_4 \cdot SiO_2$ - $Y_2O_3 \cdot 2SiO_2$ SYSTEM

Investigations of the ternary system Si_3N_4 - Y_2O_3 - SiO_2 have disclosed that materials whose compositions lie within the compatibility triangle Si_3N_4 - $Si_3N_4 \cdot SiO_2$ - $Y_2O_3 \cdot 2SiO_2$ display extraordinary resistance to oxidation. In addition, strengths at certain compositions were comparable to those of the Si_3N_4 - MgO system. Further investigation of the compatibility triangle was undertaken to optimize the properties.

Two inch diameter by 1/4 inch discs were hot-pressed from the compositions near the high Si_3N_4 corner of the phase triangle (listed in Table 7.6). Compositions containing greater than 89 m/o Si_3N_4 could not be pressed to full density, nor could those containing less than 3 m/o Y_2O_3. Compositions near the Si_3N_4 - $Y_2O_3 \cdot 2SiO_2$ tie line were most easily pressed as were those containing less than 80 m/o Si_3N_4. This inability to densify is attributed to insufficient liquid eutectic at the higher Si_3N_4 and lower Y_2O_3 contents.

Flexural strength specimens were machined from the dense discs for tests at room temperature and at 2550°F. The results, appearing in Table 7.6, indicate that room temperature strengths were greater for higher Si_3N_4 contents. Elevated temperature strengths appeared to improve at higher SiO_2/Y_2O_3 ratios, i.e., away from the SiO_2/Y_2O_3 = 2 tie line.

TABLE 7.6

CHARACTERISTICS OF EXPERIMENTAL HOT-PRESSED DISCS

	Composition, mole percent				Avg Flexure Str, ksi	
No.	Si_3N_4	Y_2O_3	SiO_2	Fully Dense	R.T.	1400°C
1	93.2	1.5	5.3	No	--	--
2	90.0	2.0	8.0	No	--	--
3	89.0	3.0	8.0	No	--	--
4	89.0	3.5	7.5	*	86	48
5	89.5	0	10.5	No	--	--
6	86.5	3.0	10.5	*	78	63
7	87.0	4.3	8.7	Yes	74	45
8	85.5	4.0	10.5	*	83	62
9	84.5	5.0	10.5	Yes	**	**
10	84.0	3.0	13.0	*	71	59
11	79.8	6.2	14.0	Yes	73	46
12	76.3	6.2	17.5	Yes	65	59
13	70.4	10.1	19.5	Yes	55	46

---

* Discs thermally cracked

** Inconsistant: some pressings were fully dense and others not.

A good compromise between fabricability, room temperature strength, and elevated temperature strength seems to occur in the region of the ternary diagram between 85.5 to 86.5 m/o Si_3N_4, 3 to 4 m/o Y_2O_3 and 10 to 11 m/o SiO_2. Therefore, large pressings (5-1/2" x 3-1/2" x 1") were made in this region: a) 86.5 m/o Si_3N_4 - 3 m/o Y_2O_3 - 10.5 m/o SiO_2, and b) 85.5 m/o Si_3N_4 - 4 m/o Y_2O_3 - 10.5 m/o SiO_2. Neither composition densified fully, although the block containing 4 m/o Y_2O_3 had core regions that reached high density. The inability to fully compact seems to be associated with the dissociation and subsequent loss of material from the periphery of the block. X-ray results indicate a loss of SiO_2 which alters the composition toward higher Si_3N_4, thus making it more difficult to press.

A large block containing 84.5 m/o Si_3N_4 - 5 m/o Y_2O_3 and 10.5 m/o SiO_2 was successfully compacted. Unfortunately, thermally induced cracking was observed in the piece even though a slow cool down cycle (150°C/hr) had been employed. A 2" diameter disc of similar composition also contained cracks. As a result, strengths of both were low. Examination by SEM of the fracture surface of specimens of the composition close to the Si_3N_4 - $Y_2O_3 \cdot 2SiO_2$ tie line showed the structure to be more glassy than compositions further from the tie line. There appears to be more low melting eutectic which is less tough than the Si_3N_4 matrix. Work on both large and small blocks will continue in an effort to solve these problems.

Several different compositions within the compatibility triangle were subjected to static oxidation at both 1800°F and 2500°F. Although previous Si_3N_4 materials containing Y_2O_3 have displayed catastrophic phase instability at 1800°F in an oxidizing atmosphere, these materials are extremely resistant. Within the errors of measurement, no weight gain was observed up to 100 hrs. Oxidation resistance at 2500°F is also excellent.

Fabrication and Processing

In order to achieve a more homogeneous, higher grade hot-pressed product, improvements are being made in processing procedures. After nitriding and crushing, all powder is now jet milled and dry screened through at least 220 mesh. An additional wet screening step has been added after ball milling to further eliminate any contaminants such as WC chips from the grinding media.

The effect of Si_3N_4 particle size on strength is being investigated to determine if particle classification should be used. Two vendors of air classifiers have each separated a powder of known size distribution into six size groupings. These are presently being hot-pressed. The discs will be tested for strength and the microstructure will be evaluated to determine the effect of the starting powder particle size on the resultant product.

The thermally induced cracking which sometimes occurs during the cool down from hot-pressing temperatures in the more deformation resistant materials has been largely eliminated by slower controlled cooling rates. However, some cracking still occurs in large billets of certain compositions and residual thermal stresses are suspect in the rest. In addition to the lower cooling rates, the effect of an annealing step should be evaluated.

Density variations between the billet interior and exterior continue to plague the hot-pressing of Si_3N_4 - Y_2O_3 - SiO_2 material. As mentioned above, this seems to be caused by the loss of some of the material from the periphery, with an accompanying shift in the constituent balance. The difference between large and small billet pressing is not clearly understood. Thermal gradient differences between the dies may be significant. Decomposition might be a function of the total surface area of the billets. Attempts will be made to overcome these problems. Initially, the thermal insulation of the die will be improved. Also, the inner walls of the die will be coated with a high SiO_2, high Y_2O_3 powder mixture to reduce the driving force for decomposition below the surface.

7.3.1 OXIDATION BEHAVIOR OF EXPERIMENTAL Si_3N_4 HOT-PRESSED WITH Y_2O_3 AND SiO_2

The oxidation behavior of experimental Si_3N_4 materials hot-pressed with Y_2O_3 and SiO_2 was studied in order to obtain a comparison with commercial hot-pressed Si_3N_4. However, due to the limited availability of these materials, only a few oxidation experiments were carried out. These results are considered to be preliminary.

Experimental

The Si_3N_4 used was prepared by hot-pressing the powder with controlled amounts of Y_2O_3 and SiO_2 to avoid the formation of various deleterious Y-Si-O-N phases. These phases and materials containing these phases have been shown to oxidize catastrophically at temperatures ~1800°F.[8] In order to confirm the absence of these deleterious phases, the Si_3N_4 material was exposed to air at 1800°F for extended periods of time. Under these conditions, the oxidation of the material was insignificant, and it was not prone to catastrophic failure.

The oxidation experiments were performed by exposing test samples, in the form of 1/8" x 1/4" x 1-1/8" rectangular bars, to an environment of static air in a globar-resistance furnace. The change in the weight of the sample was determined by weighing the sample both before and after oxidation. The weight gain data at 2500°F for specimens from three different billets (all same composition) are summarized in Table 7.7:

TABLE 7.7

Billet Identification	Number of Specimens	Oxidation Time, hr	Weight Gain mg/cm^2	Parabolic Rate Constant† $mg^2cm^{-4}hr^{-1}$
R7-18-75*	1	235	0.15	9.57×10^{-5}
CP-30**	2	288	0.29	2.92×10^{-4}
CP-51*	5	303	0.21	1.45×10^{-4}

*Small billet (2" diameter x 1/4" thick)

**Large billet (5-1/2" x 3-1/2" x 1")

†Assuming oxidation to be perfectly parabolic

The oxidation rates of these materials are much smaller than those for Norton's HS-130 Si_3N_4 as reported previously. Moreover, these oxidation rates are comparable to that of chemically-vapor-deposited Si_3N_4.

The surface oxide formed on these materials after oxidation at 2500°F consisted predominantly of $Y_2O_3 \cdot 2SiO_2$ and cristobalite.

The flexural strength of the hot-pressed Si_3N_4 material with Y_2O_3 addition (CP-51) was also determined both before and after oxidation at 2500°F. These strength measurements were carried out at 2500°F under conditions of 4-point loading with a cross-head speed of 0.00025 in/min.

The 2500°F strength before any oxidation was measured to be 75,800 (± 2,600) psi. After 303 hours of oxidation at 2500°F, this strength decreased to 63,800 (± 5,800) psi. Thus, approximately 16% reduction in strength occurred in 303 hours of oxidation at 2500°F. This reduction in strength is much smaller than that observed for Norton's HS-130 Si_3N_4 under similar oxidation conditions.

When the material in the Si_3N_4-Y_2O_3-SiO_2 system becomes available in sufficient quantity, a detailed investigation of its oxidation behavior, and effect of oxidation on strength will be carried out.

7.3.2 EFFECT OF LONG-TERM OXIDATION ON THE STRENGTH OF COMMERCIAL HOT-PRESSED Si_3N_4

The flexural strengths of Norton's HS-130 Si_3N_4 after long-term oxidation at 2500°F were reported in the previous report.(8) Similar measurements have now been carried out for oxidation temperatures of 2000 and 2200°F. Briefly, the flexural strength of 1/8" x 1/4" x 1-1/8" specimens, oxidized for different periods of time were measured under conditions of 4-point loading using a strain rate of 0.002 per minute.

Results

Figure 7.16 shows the 2000°F flexural strength of the materials after different periods of oxidation at 2000°F using an alumina lined muffle furnace and Si_3N_4 supports in a static air environment. The flexure strength decreases from ~100 ksi for the unoxidized material to 65 ksi after about 400 hours of oxidation at 2000°F. With further oxidation, the strength appears to remain constant. Similarly, the 2200°F strength after different periods of oxidation at 2200°F is shown in Figure 7.17. Here again, a sharp decrease in strength in the first few hundred hours of oxidation is observed, after which the strength apparently becomes stable at ~60 ksi. As reported previously, the 2300°F strength after long-term oxidation at 2500°F apparently stabilizes at ~40 ksi. Thus, the reduction in strength becomes greater with increasing temperature of oxidation.

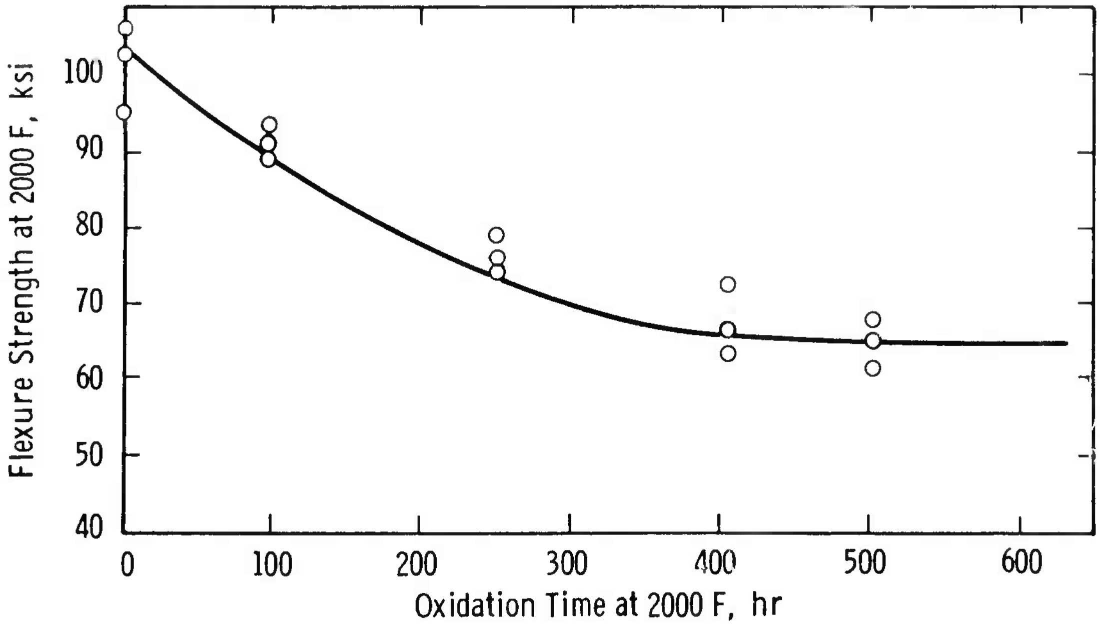

Figure 7.16 Effect of Oxidation On the Strength of Hot-Pressed Si_3N_4 - 2000°F

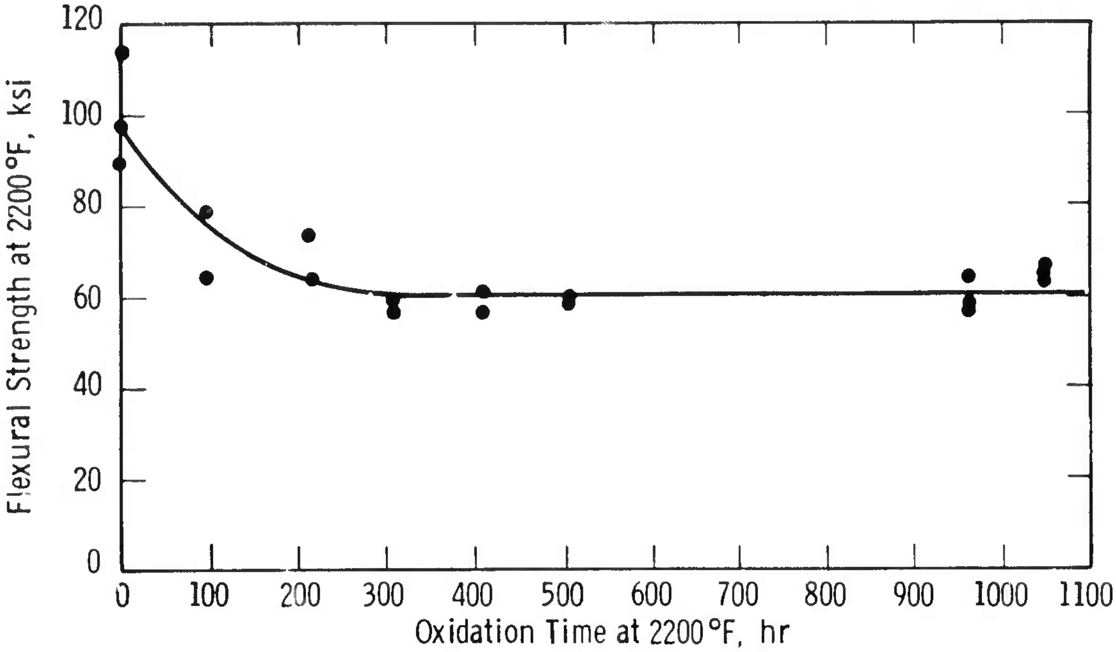

Figure 7.17 Effect of Static Oxidation On the Strength of Hot-Pressed Si_3N_4 - 2200°F

The reduction in strength is apparently caused by surface degradation which occurs during oxidation at high temperatures. The predominant oxidation product on hot-pressed Si_3N_4 after long-term oxidation at temperatures in the range 2000-2500°F is $MgSiO_3$. This $MgSiO_3$ can react with the Si_3N_4 substrate causing formation of microcavities on the surface. As oxidation progresses, sharp microcavities are formed on the surface causing sharp reduction in strength of the material. However, with further oxidation, at some stage the microcavities on the surface become only shallower and wider, and the further effect on strength is not as great as from the formation of initial sharp cavities. This is illustrated schematically in Figure 7.18. Thus, after the first few hundred hours of oxidation, the strength becomes practically constant.

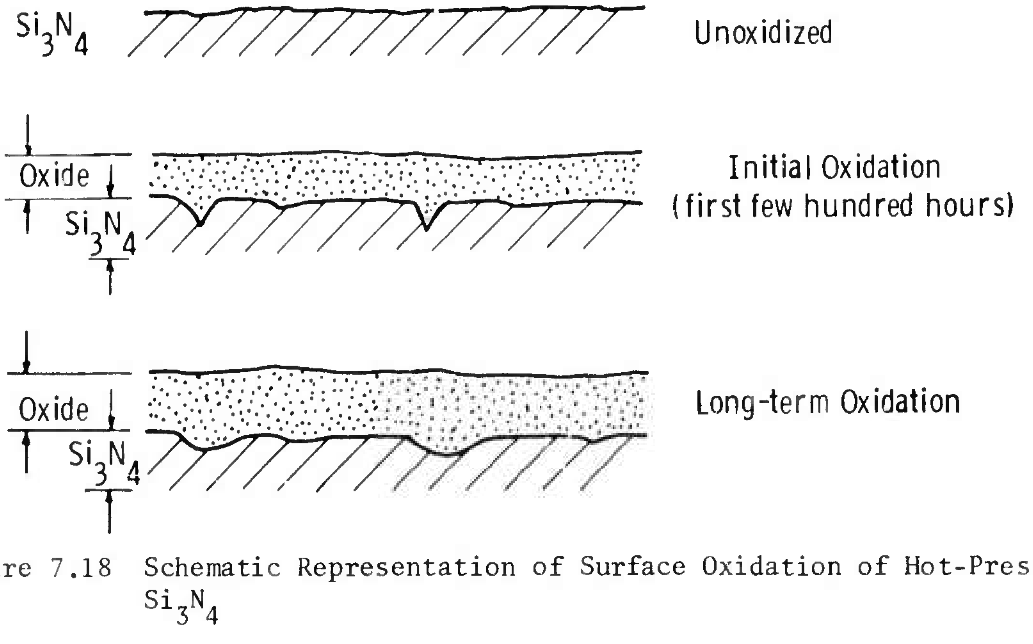

Figure 7.18 Schematic Representation of Surface Oxidation of Hot-Pressed Si_3N_4

7.3.3 EVALUATION OF CHEMICALLY-VAPOR-DEPOSITED Si_3N_4 COATINGS ON HOT-PRESSED SILICON NITRIDE

It has been shown previously by extensive oxidation studies that MgO, which is used as a densification aid for hot-pressing Si_3N_4, diffuses outwards during oxidation and forms $MgSiO_3$ on the surface. In addition, other mixed silicates of various impurities present in the hot-pressed material (e.g. (Ca, Mg) SiO_3) are also observed in the surface oxide layer on hot-pressed Si_3N_4. These silicates react with substrate Si_3N_4 and adversely affect the strength of the material. In an attempt to eliminate or reduce this oxidative degradation in strength, a surface coating program was initiated to provide much greater oxidation-resistance than monolithic hot-pressed Si_3N_4 normally exhibits.

Experimental

The following coatings were deposited on Norton's NC-132 Si_3N_4 for purposes of preliminary screening:

(a) Al_2O_3
(b) HfO_2
(c) SiC
(d) SiC/Si_3N_4
(e) Si_3N_4

These coatings were formed by chemical vapor deposition process by Materials Technology Corporation, Dallas. The thickness of the coatings varied from about 1 to 10 mils. These were the first attempts by the Materials Technology Corporation to deposit coatings on hot-pressed Si_3N_4. For this reason, the coatings were not very uniform in thickness, and contained many imperfections such as microcracks, porosity, etc.

The Si_3N_4 samples with above coatings were oxidized in air at 2500°F for up to 100 hours. All specimens, except those coated with CVD-Si_3N_4, showed severe cracking and spalling on the surface which could be seen with the unaided eye. These coatings, thus, did not provide the hot-pressed Si_3N_4 material with any protection against oxidation. The cracking and spalling was not completely unexpected because of the significant differences in the thermal expansion coefficients between the coatings and the hot-pressed Si_3N_4. For this reason, it is believed that, under cyclic thermal conditions, CVD-Si_3N_4 has the best potential for providing protection to hot-pressed Si_3N_4 since (i) the thermal expansion coefficients of CVD-Si_3N_4 and hot-pressed Si_3N_4 are nearly identical, and (ii) pure CVD-Si_3N_4 possesses extremely high oxidation resistance due to the formation of pure SiO_2 on the surface. Further efforts, therefore, have been concentrated on the deposition and evaluation of pure CVD-Si_3N_4 coatings.

Initial Si_3N_4 coatings were deposited on Norton's NC-132 by the Materials Technology Corporation by chemical vapor deposition. The thickness of these coatings was $\sim$2.5 mil. Figure 7.19 shows the coating in cross-section before any oxidation. It is evident from this micrograph that the coating contained numerous microcracks and porosity. The coated specimens were oxidized in air at 2500°F for periods ranging from 20 to 300 hours. The coated specimens exhibited oxidation rates similar to that of uncoated hot-pressed Si_3N_4. The predominant oxidation product was $MgSiO_3$. This shows that the diffusion of magnesium through the coating was extremely rapid and that this might be due to the presence of porosity and microcracks in the coating. The flexural strength of the coated Si_3N_4 specimens was reduced to ~34,800 psi after 300 hours of oxidation at 2500°F. Thus, the CVD-Si_3N_4 coating deposited by Materials Technology Corporation did not provide any protection against oxidative strength reduction in hot-pressed Si_3N_4.

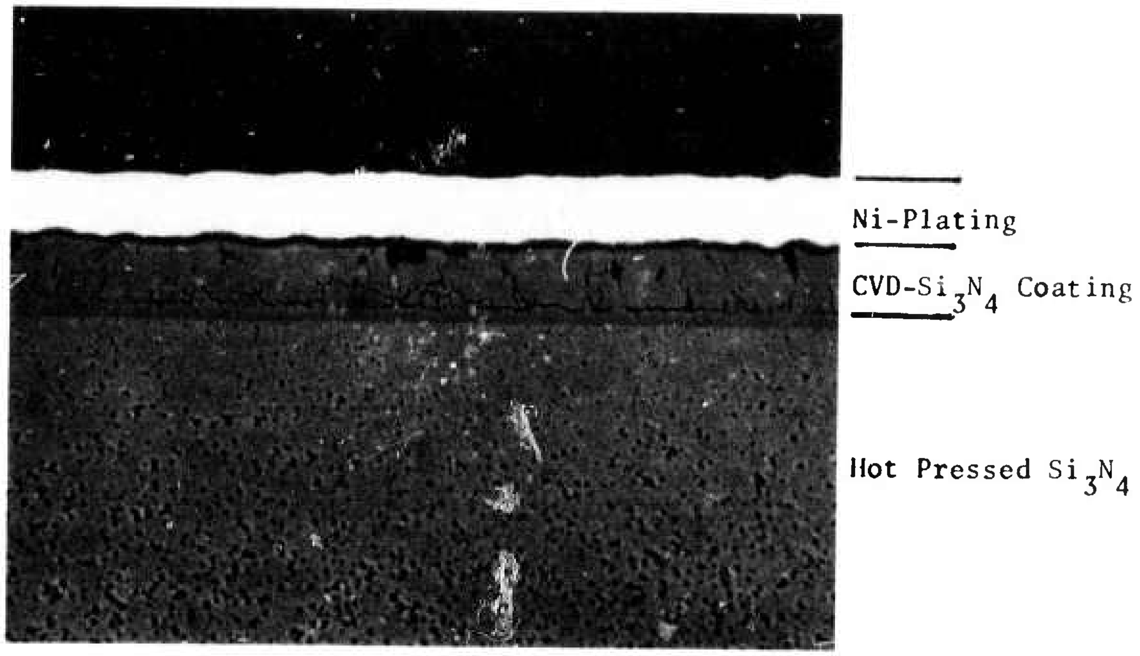

Figure 7.19 CVD Si_3N_4 Coating On Hot-Pressed Si_3N_4 (Deposited by Materials Technology Corp.) 200X

The vendor subsequently made several changes in the chemical vapor deposition process for Si_3N_4 by varying gas flow rates, substrate temperature and the surface cleaning method for hot-pressed Si_3N_4 before coating. Unfortunately, all coatings received from Materials Technology continued to be non-uniform in thickness and to contain numerous microcracks. These coatings did not provide any protection against oxidation to the hot-pressed Si_3N_4. An in-house investigation was initiated to optimize the chemical vapor deposition process in an effort to obtain dense crack-free Si_3N_4 coatings on hot-pressed Si_3N_4.

The deposition of silicon nitride coatings at Westinghouse was carried out in a horizontal quartz reaction chamber through which a gaseous mixture of silane (SiH_4), N_2, NH_3 and H_2 was continuously passed. The hot-pressed Si_3N_4 specimens, in the form of 1/8" x 1/4" x 1-1/8" rectangular bars, were thoroughly cleaned and placed inside the reaction chamber on a graphite susceptor, which was precoated with CVD-Si_3N_4. The susceptor was heated by a RF induction heater. During this process, silane reacts with ammonia and nitrogen to form Si_3N_4 coating on the heated hot-pressed Si_3N_4 specimens according to the following reactions:

$$3SiH_4 + 4NH_3 \longrightarrow Si_3N_4 + 12H_2$$

$$3SiH_4 + 2N_2 \longrightarrow Si_3N_4 + 6H_2$$

An excess of hydrogen in the gas mixture is used to suppress the premature decomposition of silane.

In initial experiments, the deposition rates were extremely small, of the order of 0.1 mil/hr. Moreover, the Si_3N_4 coating tended to spall upon heating to 2500°F. This spalling was apparently due to the thin film of SiO_2 which always exists on hot-pressed Si_3N_4 specimens. In order to prevent this problem and to increase the deposition rates, numerous experimental runs were made to assess the effect of: 1) the surface cleaning methods for hot-pressed Si_3N_4 before coating, 2) the ratio of different constituents in the gas mixture, 3) the total gas flow rate, and 4) the substrate temperature. The best coatings were obtained under the following conditions:

(a) In-situ cleaning of the surfaces of the hot-pressed Si_3N_4 specimens by exposing them to a gas mixture of H_2-1% HCl at 2100°F for about two minutes.

(b) Using a gas mixture containing approximately 0.3% SiH_4, 9.3% H_2, 22% NH_3 and 68.4% N_2.

(c) Using total gas flow rate of about 45 liters/min, and

(d) Keeping the hot-pressed Si_3N_4 substrate at ∿1600°F.

Under these conditions, very dense and uniform Si_3N_4 coatings were formed at a deposition rate of 0.8 mil/hr. A micrographic cross-section of the Si_3N_4 coating, thus produced, is shown in Figure 7.20. It is evident from this micrograph that the coating is free of any porosity or microcracks. Si_3N_4 coatings have now been deposited on about 20 samples for detailed evaluation.

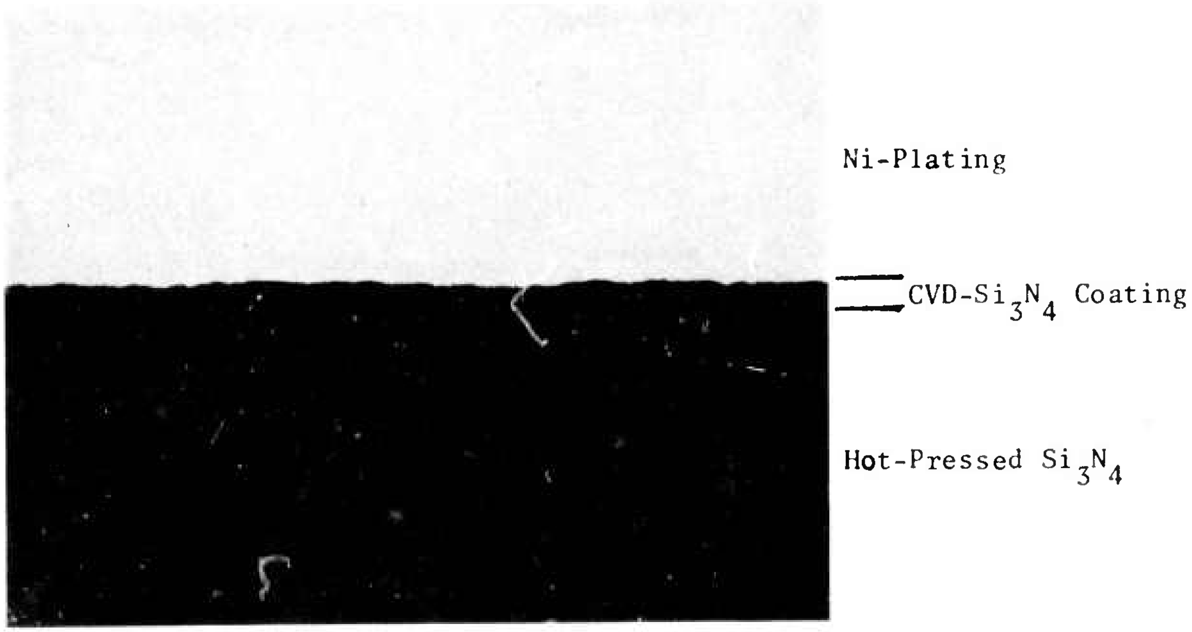

Figure 7.20 CVD Si_3N_4 Coating On Hot-Pressed Si_3N_4 (Deposited by Westinghouse Research Laboratories) 500X

Preliminary oxidation experiments on the coated specimens indicate that the diffusion of magnesium through the coating is extremely rapid. The coated samples are presently being oxidized at 2500°F for different periods of time. In these oxidized specimens, the magnesium concentration profile will be determined through the coating and the oxide layer to obtain an estimate of the magnesium diffusion rates. This will aid in the estimation of a minimum coating thickness for prevention of magnesium diffusion to the outer surface, and thus reduce oxidative losses in strength of hot-pressed Si_3N_4.

8. REFERENCES

1. McLean, A. F., Fisher, E. A., Harrison, D. E., "Brittle Materials Design, High Temperature Gas Turbine". AMMRC-CTR-72-3, Interim Report, March, 1972.

2. McLean, A. F., Fisher, E. A., Bratton, R. J., "Brittle Materials Design, High Temperature Gas Turbine". AMMRC-CTR-72-19, Interim Report, September, 1972.

3. McLean, A. F., Fisher, E. A., Bratton, R. J., "Brittle Material Design, High Temperature Gas Turbine". AMMRC-CTR-73-9, Interim Report, March, 1973.

4. McLean, A. F., Fisher, E. A., Bratton, R. J., "Brittle Materials Design, High Temperature Gas Turbine". AMMRC-CTR-73-32, Interim Report, September, 1973.

5. McLean, A. F., Fisher, E. A., Bratton, R. J., "Brittle Materials Design, High Temperature Gas Turbine". AMMRC-CTR-74-26, Interim Report, April, 1974.

6. McLean, A. F., Fisher, E. A., Bratton, R. J., "Brittle Materials Design, High Temperature Gas Turbine". AMMRC-CTR-74-59, Interim Report, September, 1974.

7. McLean, A. F., Fisher, E. A., Bratton, R. J. Miller, D. G., "Brittle Materials Design, High Temperature Gas Turbine". AMMRC-CTR-75-8, Interim Report, April, 1975.

8. McLean, A. F., Fisher, E. A., Bratton, R. J. Miller, D. G., "Brittle Materials Design, High Temperature Gas Turbine". AMMRC-CTR-75-28, Interim Report, September, 1975.

9. McLean, A. F., Baker, R. R., Bratton, R. J., Miller, D. G., "Brittle Materials Design, High Temperature Gas Turbine". AMMRC-CTR-76-12, Interim Report, April, 1976.

10. Ainley, D. C. and Mathieson, G. C. R., "A Method of Performance Estimation for Axial-Flow Turbines", Reports and Memoranda No. 2974, December, 1951, Her Majesty's Stationary Office.

11. Dunham, J. and Came, P. M., "Improvements to the Ainley-Mathieson Method of Turbine Performance Prediction", ASME Paper 70-GT-2, 1970.

12. Norris, D. M. and Grantham, P. V., "Thermal Stress Analysis of a Ceramic Gas Turbine Stator Blade", Lawrence Livermore Laboratory, Report UCRL-51923, October 3, 1975.

13. Proposed Military Standard, "Test Methods for Structural Ceramics", Army Materials and Mechanics Research Center, October 15, 1973.

14. Thoman, D. R., Bain, L. J., and Antle, C. E. 1969. "Inferences on the Parameters of the Weibull Distribution", Technometrics, 11, 445-460.

15. Andersson, C. A., Lange, F. F., and Iskoe, J. L. "Effect of the MgO/SiO_2 Ratio on the Strength of Hot-Pressed Si_3N_4", USGRDR 7526, Technical Reports 3, 4 and 5.

16. Edington, J. W., Rowcliffe, D. J. and Henshall, J. L., "The Mechanical Properties of Silicon Nitride and Silicon Carbide", Powder Metallurgy International, Volume 7, Number 2, 1975.

17. Rice, R. W., Symposium on the Fracture Mechanics of Ceramics, Plenum Press, N.Y., pp 323 (1974).

18. Andersson, C. A., Lange, F. F., and Iskoe, J. L., "Effect of the MgO/SiO_2 Ratio on the Strength of Hot-Pressed Si_3N_4," ONR Technical Report #3, ARPA Contract N00014-74-C-0284, October 15, 1975.

ARMY MATERIALS AND MECHANICS RESEARCH CENTER
WATERTOWN, MASSACHUSETTS 02172

TECHNICAL REPORT DISTRIBUTION

No. of Copies	To
1	Office of the Director, Defense Research and Engineering, The Pentagon, Washington, D.C. 20301
12	Commander, Defense Documentation Center, Cameron Station, Building 5, 5010 Duke Street, Alexandria, Virginia 22314
1	Metals & Ceramics Information Center, Battelle Memorial Institute, 505 King Avenue, Columbus, Ohio 43201
2	Dr. James 1. Bryant, Office of the Chief of Research, Development and Acquisition, ATTN: DAMA-CSS, The Pentagon, Washington, D.C. 20310
1	Commanding Officer, Army Research Office (Durham), Bx CM, Duke Station Durham, North Carolina 27706 ATTN: Dr. H. M. Davis
2	Commanding General, U.S. Army Material Command, Washington D.C. 20315 AMCRD-TC (Dr. El-Bisi) ANCDL (Dr. Dillaway)
1	Commanding General, U.S. Army Missile Command, Redstone Arsenal, Alabama 35809 ATTN: Technical Library
4	Commanding General, U.S. Army Tank-Automotive Command, Warren, Michigan 48090, ATTN: AMSTA-BSL, Research Library Br, ATTN: AMSTA-RKM (Mr. C. Green), ATTN: AMSTA-RGR (Mr. Engel), ATTN: AMSTA (Dr. Banks)
1	Commanding General, U.S. Army Weapons Command, Research and Development Directorate, Rock Island, Illinois 61201, ATTN: AMSWE-RDR
1	Commanding Officer, Aberdeen Proving Ground, Maryland 21005, ATTN: Technical Library, Building 313
1	Commanding Officer, U.S. Army Aviation Material Laboratories, Fort Eustis, Virginia 23604
1	Librarian, U.S. Army Aviation School Library, Fort Rucker, Alabama 36360 ATTN: Bldg. 5907
1	Commanding Officer, USACDC Ordnance Agency, Aberdeen Proving Ground, Maryland 21005 ATTN: Library, Building 350

ARMY MATERIALS AND MECHANICS RESEARCH CENTER
WATERTOWN, MASSACHUSETTS 02172

TECHNICAL REPORT DISTRIBUTION

No. of Copies	To
1	U.S. Army Air Mobility Research and Development Laboratory ATTN: J. White, Assistant Technical Director, Eustis Directorate, Ft. Eustis, Virginia 23604
1	U.S. Army Air Mobility Research and Development Laboratory ATTN: R. Berrisford, Chief, Structures Division, Eustis Directorate, Ft. Eustis, Virginia 23604
1	U.S. Army Air Mobility Research and Development Laboratory ATTN: T. Coleman, Director, Langley Directorate, Langley Research Center, Langley Field, VA 23365
2	U.S. Army Air Mobility Research and Development Laboratory ATTN: J. Accurio, Director, Lewis Directorate, NASA, Lewis Research Center, 21000 Brookpark Road, Cleveland, Ohio 44135
1	Commanding General, U.S. Army Aviation Systems Command, ATTN: R. Long, Deputy Director RD&E, P.O. Box 209, St. Louis, MO 63166
1	Office Chief Research & Development, Department of Army, ATTN: Col. J. Barnett, Physical & Engineering Sciences Division, Washington, D.C. 20315
1	Commanding General, Army Missile Command, ATTN: AMCDL, Webb Taylor, 5001 Eisenhower Avenue, Alexandria, VA 22304
1	Commanding General, Army Missile Command, ATTN: AMCRD-F, J. Beebe, Washington, D.C. 20315
1	Office, Chief Research & Development, Department of the Army, ATTN: R. Ballard, Physical & Engineering Sciences Division, Washington, D.C. 20315
1	Commander, USA Foreign Science & Technology Center, ATTN: AMXST-SD3, Mr. C. Petschke, 220 7th Street NE, Charlottesville, VA 22901
1	Mr. Irving Machlin, High Temperature Materials Div., Materials and Processes Branch, (NAIR-52031D), Naval Air Systems Command, Department of the Navy, Washington, D.C. 20360

ARMY MATERIALS AND MECHANICS RESEARCH CENTER
WATERTOWN, MASSACHUSETTS 02172

TECHNICAL REPORT DISTRIBUTION

No. of Copies	To
1	Commanding Officer, U.S. Army Engineer Waterways Experiment Station, Vicksburg, Mississippi 39180 ATTN: Research Center Library
4	Commanding Officer, U.S. Army MERDEC, Fort Belvoir, Virginia 22060 ATTN: STSFB-EP (Mr. Frank Jordan) STSFB-EP (Mr. W. McGovern) AMCPM-FM (Mr. Allen Elkins) AMXFB-EM (Mr. George F. Sams
	Director, Army Materials and Mechanics Research Center, Watertown, Massachusetts 02172
2	ATTN: AMXMR-PL
1	AMXMR-PR
1	AMXMR-CT
1	AMXMR-AP
1	AMXMR-X (Dr. Wright)
1	AMXMR-EO (Dr. Katz)
2	AMXMR-TM (Dr. Lenoe)
2	AMXMR-D (Dr. Priest)
1	AMXMR-EO (Dr. Messier)
2	AMXMR-P (Dr. Burke)
1	AMXMR-MS (Mr. MacDonald)
1	AMXMR-E (Dr. Larson)
1	Lt. Col. E. E. Chick
	Advanced Research Projects Agency, 1400 Wilson Blvd., Arlington, Virginia 22209
2	ATTN: Director
1	Dep Director
1	Director of Materials Sciences - Dr. Bement
1	Dep. Director Materials Sciences - Dr. van Reuth
1	Tech Information Office - Mr. F. A. Koether
1	Mr. R. M. Standahar, Office of the Director of Defense, Research and Engineering, Room 3D1085, Pentagon, Washington, D.C. 20301
1	Mr. Charles F. Bersch, Department of the Navy, Naval Air Systems Command, Washington, D.C. 20360
1	Dr. A. M. Diness, Metallurgy Branch, Code 471, Office of Naval Research, 800 N. Quincy Street, Arlington, Virginia 22217
2	U.S. Army Air Mobility Research and Development Laboratory, Advanced Systems Research Office, Ames Research Center, Moffett Field, California 94035 ATTN: F. Immen, J. Wheatly

ARMY MATERIALS AND MECHANICS RESEARCH CENTER
WATERTOWN, MASSACHUSETTS 02172

TECHNICAL REPORT DISTRIBUTION

No. of Copies	To
1	Mr. Keith Ellingsworth, Office of Naval Research, Power Program, Arlington, VA 22217
1	Mr. John Fairbanks, Naval Ships Engineering, Prince George Center, Hyattsville, Maryland 20782
1	Capt. D. Zabierek, Air Force Aeropropulsion Lab, Wright-Patterson Air Force Base, Ohio 45433
1	Capt. Smyth, Air Force Materials Laboratory, Wright-Patterson Air Force Base, Ohio 45433
1	Mr. S. Lyons, Wright-Patterson Air Force Base, Ohio 45433
4	Aerospace Research Laboratory, ATTN: ARL-LL, Wright-Patterson Air Force Base, Ohio 45433 ATTN: Dr. Henry Graham Dr. James Wimmer Maj. L. Jacobson Mr. Larry Hjelm
4	NASA Lewis Research Center, 21000 Brookpark Road, Cleveland, Ohio 44135 ATTN: Mr. W. Sanders Dr. Hubert Probst Dr. Robert C. Bill Mr. Donald Guentert
1	Dr. G. C. Deutsch, Ass't Director of Research (Materials), Code RR-1 NASA, Washington, D.C. 20546
1	Mr. George Staber, Office of Coal Research, U.S. Department of the Interior, Washington, D.C. 20240
1	Dr. S. Wiederhorn, Physical Properties Section, Institute for Materials Research, National Bureau of Standards, Washington, D.C. 20234
1	Mr. R. Reynik, Director, Div. of Materials Research, National Science Foundation, 1800 G. Street, N.W., Washington, D.C. 20550
1	Dr. Robb Thomson, Senior Research Scientist, Rm B109, Bld. 225, National Bureau of Standards, Washington, D.C. 20234
1	Mr. H. Morrow, Eustis Directorate, AMRDL, Fort Eustis, VA 23604
1	Dr. R. Warren, Contact Officer, Defense Research & Development Staff, British Embassy, 3100 Massachusetts Avenue N.W., Washington, D.C. 20008

ARMY MATERIALS AND MECHANICS RESEARCH CENTER
WATERTOWN, MASSACHUSETTS 02172

TECHNICAL REPORT DISTRIBUTION

No. of Copies	To
3	Div. of Transportation & Energy Conservation Energy Research and Development Administration, 20 Massachusetts Avenue, NW Washington, D.C. 20545 ATTN: Mr. George Thur Mr. Robert Schulz Mr. Thomas Sebestyen
1	Dean Daniel C. Drucker, Engineering College, University of Illinois, Urbana, Illinois 61801
1	Professor Merton Flemings, Massachusetts Institute of Technology, Cambridge, Massachusetts 02139
1	Professor Edward E. Hucke, Materials and Metallurgical Engineering, The University of Michigan, Ann Arbor, MI 48104
1	Professor Frank A. McClintock, Department of Mechanical Engineering, Massachusetts Institute of Technology, Cambridge, Massachusetts 02139
1	Dr. R. M. Spriggs, Assistant to the President, Lehigh University, Bethlehem, Pennsylvania 18015
1	Mr. J. D. Walton, Jr., EES, Georgia Tech., Atlanta, Georgia 30332
1	Mr. Y. Baskin, Manager Inorganic Chemical Research, Technical Center, Ferro Corporation, 7500 East Pleasant Valley Road, Independence, Ohio 44131
3	Mr. Robert Beck, Dept. Head, Development Materials, Teledyne CAE, 1330 Laskey Road, Toledo, Ohio 43601 Dr. Eli Benstien, Director of Engineering Mrs. Marlene S. Dowdell, Librarian
1	Dr. J. E. Burke, General Electric Company, Corporate Research & Development, P.O. Box 8, Schenectady, New York 12301
1	Dr. C. A. Bruch, Manager, Advanced Studies, General Electric Company, Aircraft Engine Group, Cincinnati, Ohio 45215
1	Mr. A. R. Canady, Caterpillar Tractor Company, Technical Center Building F, Peoria, Illinois 61602
1	Mr. Seymour Bortz, IIT Research Institute, 10 West 35th Street, Chicago, Illinois 43601

ARMY MATERIALS AND MECHANICS RESEARCH CENTER
WATERTOWN, MASSACHUSETTS 02172

TECHNICAL REPORT DISTRIBUTION

No. of Copies	To
1	Mr. L. M. Donley, Owens Illinois Glass, 1900 North Westwood Avenue, Toledo, Ohio 43601
1	Mr. E. J. Dulis, President, Colt Industries, Materials Research Center, Box 88, Pittsburgh, PA 15230
1	Mr. O. Prachar, Passenger Car Turbine Department, Engineering Staff, General Motors Technical Center, Warren, MI 48090
1	Mr. Winston Duckworth and Mr. Lewis E. Hulbert, Battelle Columbus Laboratories, 505 King Avenue, Columbus, Ohio 43201
1	Energy Research Corporation, Bethel, Connecticut 06801
1	Dr. Peter L. Fleischner, National Beryllia Corp., Haskell, New Jersey 07420
1	Mr. O. I. Ford, Technical Manager, Combustor Systems, Aerojet Liquid Rocket Company, P.O. Box 18222, Sacramento, Calf. 95813
1	Mr. Chester T. Sims, Manager, Advanced Materials General, Electric Company, Gas Turbine Products Div., Schenectady, N.Y. 12301
1	Mr. E. W. Hauck, Market Manager, Engine Components, Norton Company, 1 New Bond Street, Worcester, Massachusetts 01606
1	Mr. M. Herman, Detroit Diesel Allison Division, General Motors Corporation, Indianapolis Operations, P.O. Box 894, Indianapolis, Indiana 46206
1	Mr. J. B. Mann, Director of Research, Chrysler Corporation, P.O. Box 1118, Detroit, MI 48231
1	Mr. James F. Holloway, Materials Project Engineer, Pratt & Whitney Corporation, 400 Main Street, E. Hartford, Connecticut 06108
1	Dr. Paul Jorgensen, Associate Director, Materials Laboratory, Stanford Research Institute, Menlo Park, California 94025
1	Dr. A. V. Illyn, Technical Director, Refractories Division, Babcock & Wilcox, Old Savannah Road, Augusta, Georgia 30903
1	Mr. Paul F. Jahn, Vice President, Fiber Materials, Inc., Broadway and Main Streets, Graniteville, Massachusetts 01829

ARMY MATERIALS AND MECHANICS RESEARCH CENTER
WATERTOWN, MASSACHUSETTS 02172

TECHNICAL REPORT DISTRIBUTION

No. of Copies	To
1	Dr. Robert F. Kirby, Materials Engineering Dept. 93-393M, AiResearch Manufacturing Company, Div. of the Garrett Corporation, Sky Harbor Airport, 402 South 36th Street, Phoenix, Arizona 85034
1	Mr. John G. Lanning, Corning Glass Works, Corning, NY 14830
1	Mr. William D. Long, Manager, Product Development, K-Ramics, Kaman Sciences Corporation, Garden of the Gods Road, Colorado Springs, Colorado 80907
1	Mr. James Lynch, Metals & Ceramics Information Center, Battelle Columbus Laboratories, 505 King Avenue, Columbus Ohio 43201
1	Mr. C. H. McMurtry, Project Manager, Research and Development Div., The Carborundum Company, Niagara Falls, New York 14302
1	Mr. Deo Mattoon, Sing Sing Road, Horseheads, New York 14845
1	Mr. G. Kookootsedes, Market Development, Resins and Chemicals, Dow Corning, Midland, Michigan 48640
1	Professor Burton Paul, Dept. of Mechanical Engineering, University of Pennsylvania, Philadelphia, Pennsylvania 19104
1	Mr. Y. K. Pei, Owens Illinois Glass, 1020 North Westwood Avenue, Toledo, Ohio 43607
1	Dr. Jerry D. Plunkett, President, Materials Consultants, Inc., 2150 South Josephine Street, Denver, Colorado 80210
1	Mr. J. A. Rubin, President, Ceradyne Incorporated, 8948 Fullbright Avenue, Chatsworth, California 91311
1	Mr. Jack W. Sawyer, Gas Turbine International, 4519 Eighteen Street North, Arlington, VA 22207
1	Mr. D. W. McLaughlin, Research & Development Div., Mechanical Technology, Inc., 968 Albany-Shaker Road, Latham, New York 12110
1	Dr. C. Martin Stickley, U. S. Energy Research and Development Administration, Division of Laser Fusion, Mail Station A-364, Washington, D. C. 20545.

ARMY MATERIALS AND MECHANICS RESEARCH CENTER
WATERTOWN, MASSACHUSETTS 02172

TECHNICAL REPORT DISTRIBUTION

No. of Copies	To
1	Mr. A. R. Stetson, Chief, Process Research Laboratories, Mail Zone R-1, Solar Div. of Int. Harvester Company, 2200 Pacific Highway, San Diego, California 92112
1	Dr. M. L. Torti, Norton Company, 1 New Bond Street, Worcester Massachusetts 01606
1	Dr. T. Vasilos, Applied Technology Division, Avco Corp., Lowell Industrial Park, Lowell, Massachusetss 01851
1	Mr. Francis L. VerSnyder, Manager, Materials Engineering and Research Lab, Pratt & Whitney Corporation, 400 Main Street, E. Hartford, Connecticut 06108
1	Mr. McCoy, Materials Engineering, Garrett-AiResearch Dept. 93-393M, 412 South 36th Street, Phoenix, Arizona 85034
1	Mr. Donald E. Weyer, Dow Corning Corporation, Midland, MI 48640
1	Dr. Michael Guinan, B. Div./L-24, P.O. Box 808, Lawrence Livermore Laboratory, Livermore, California 94550
1	Dr. Mark Wilkins, B Div./L-24, P.O. Box 808, Lawrence Livermore Laboratory, Livermore, California 94550
1	Dr. Charles J. McMahon, Jr., Assoc. Prof. Materials Science, School of Metallurgy & Materials Science, University of Pennsylvania, 3231 Walnut Street, Philadelphia, Pennsylvania
1	Mr. Gaylord D. Smith, The International Nickel Co., Inc., 1 New York Plaza, New York, New York 10004
1	Mr. H. R. Schelp, Garrett Corporation, 9851 Sepulveda Blvd., Los Angeles, California 90009
1	Dr. Robert Widmer, President, Industrial Materials Technology 19 Wheeling Avenue, Woburn, Massachusetts
1	Prof. R. P. Kroon, University of Pennsylvania, Philadelphia, Pennsylvania
1	Dr. Paul G. Shewmon, D212, Argonne National Laboratory, 9700 South Cass Avenue, Argonne, Illinois 60439
1	Dr. S. M. Wolf, U. S. Energy Research and Development Administration, Division of Physical Research, Mail Station J-309, Washington, D. C. 20545.

ARMY MATERIALS AND MECHANICS RESEARCH CENTER
WATERTOWN, MASSACHUSETTS 02172

TECHNICAL REPORT DISTRIBUTION

No. of Copies	To
1	Dr. Thomas D. McGee, Professor of Ceramic Engineering, Iowa State University, Ames, Iowa 50010
1	Mr. Joe Glotz, Department of the Navy, Naval Air Propulsion Test Center, Trenton, New Jersey 08628
1	Mr. John Miguel, Naval Underwater System Center, Newport, Rhode Island
1	Mr. Robert Benham, AEP-22, U.S. Naval Air Propulsion Test Center (AE), Philadelphia, PA 19112
1	Mr. R. Barry Strachan, Williams Research Corp., Walled Lake, Michigan 48088
1	Mr. S. Walosin, Curtis-Wright Corp. One Passaic Street, Woodridge, N.J. 07075
1	Prof. Marc Richman, Engineering Division, Brown University, Providence, Rhode Island 02912
1	Mr. R. Rice, Naval Research Laboratory, Washington, D.C. 20390
1	Mr. George A. Wacker, Head Metal Physics Br., Naval Ships Research & Development Center, Annapolis, Md. 21402, ATTN: Code 2812
1	Dr. R. Charles, Manager Ceramics Branch, General Electric Co., Corporate R & D Center, P.O. Box 8, Schenectady, New York 12301
1	Mr. C. F. Cline, Manager, Strength Physics Department, Allied Chemical Corporation, P.O. Box 1021R, Morristown, New Jersey 07960
1	Dr. J. T. Bailey, American Lava Corp., Chattanoga, Tennessee 37405
1	Mr. S. T. Wlodek, Cabot Corp. Stellite Div., 1020 West Park Avenue, Kokomo, Indiana 46901
2	Cummins Engine Company, Inc., Columbus, Indiana 47201 Mr. R. Kano, Mr. K. J. Mather
1	Mr. J. D. Mote, EF Industries, Inc., 1301 Courtesy Rd. Louisville, Colorado 80027
1	Mr. William E. Gurwell, Eaton Corporation, Research Center 26201 Northwestern Highway, Southfield, MI 48076

ARMY MATERIALS AND MECHANICS RESEARCH CENTER
WATERTOWN, MASSACHUSETTS 02172

TECHNICAL REPORT DISTRIBUTION

No. of Copies	To
1	Mr. Robert W. Gibson, Jr., Head, Library Dept. General Motors Corporation GM Technical Center, Warren, MI 48090
1	Mr. R. L. Lormand, Lawrence Radiation Lab, P.O. Box 808, Livermore, California 94550
2	Ms. Bolick, National Aeronautics and Space Adminstration Goddard Space Flight Center, Greenbelt, Maryland 20771
1	Mr. Neil T. Saunders, Ch. Mat'ls Appl'n Branch, National Aeronautics and Space Administration, Lewis Research Center, Cleveland, Ohio 44135
1	Ms. Rayna Lee Caplan, Librarian, Northern Research and Engineering Corp., 219 Vassar Street, Cambridge, Mass. 02139
1	Mrs. Jame Bookmyer, Info. Services Div., PPG Industries, Inc., P.O. Box 11472, Pittsburgh, Pennsylvania 15238
1	Mr. P. W. Parsons, Manager, Commercial Research Dept., Stackpole Carbon Company, St. Marys, Pennsylvania 15857
1	Ms. Lucille Steelman, Order Librarian, Stanford Research Institute ATTN: G-037 Library, Menlo Park, Calif. 94025
1	Technical Library, TRW Equipment, TRW Inc., 23555 Euclid Avenue, Cleveland, Ohio 44117
1	Dr. E. P. Flint, U.S. Department of Interior, Bureau of Mines, Room 4513, Interior Bldg., Washington, D.C. 20240
1	Mr. W. Wheatfall, Naval Ship R & D Lab, Code 2812, Annapolis, Maryland 21402
1	Dr. Joseph E. Motherway, University of Bridgeport, Bridgeport, Connecticut 06602
1	Dr. Soloman Musikant, Manager, Metallurgy & Ceramics Lab, General Electric Valley Forge, Valley Forge, PA
1	Mr. Louis J. Fiedler, Mat'ls & Process Technology Lab., Avco Corporation, 550 S. Main Street, Stratford, Connecticut 06497
1	Mr. Donald Lapades, The Aerospace Corporation, P.O. Box 92957, Los Angeles, California 90009

ARMY MATERIALS AND MECHANCIS RESEARCH CENTER
WATERTOWN, MASSACHUSETTS 02172

TECHNICAL REPORT DISTRIBUTION

No. of Copies	To
1	Mr. Thomas J. Ahrens, Assoc. Prof. of Geophysics, California Institute of Technology, Seismological Laboratory, 295 San Rafael Avenue, P.O. Bin 2, Arroyo Annex, Pasadena, California 91109
1	Mr. Victor de Biasi, Editor, Gas Turbine World, P.O. Box 494, Southport, Connecticut 06490
1	SKF Industries, Inc., Engineering & Research Center, 1100 1st Avenue, King of Prussia, PA 19406, ATTN: Warren E. Jameson & Harish Dalal
1	Dr. Edward Reynolds, General Motors Technical Center, Passenger Car Turbine Division, Warren, MI 48090
1	Mr. Wm. R. Freeman, Jr., V.P. and Technical Director, Howmet Corporation, Superalloy Group, One Misco Drive, Whitehall, Michigan 47461
1	Mr. D. William Lee, Arthur D. Little, Inc. Acorn Park, Cambridge, Massachusetts 02140
1	Dr. L. Kaufman, Project Director, Manlabs, Inc., 21 Erie Street, Cambridge, Massachusetts 02139
1	Prof. Morris E. Fine, Northwestern University, The Technological Institute, Dept. of Materials Science, Evanston, Illinois
1	Raytheon Company, Research Division Library, Foundry Avenue, Waltham, Massachusetts 02154, ATTN: Ms. Madaleine Bennett, Librarian
1	Prof. T. L. Chu, Southern Methodist University, Institute of Technology, Electronic Sciences Center, Dallas, Texas 75222
1	Mr. H. Stuart Starrett, Head, Mechanics Section, Southern Research Institute, 2000 Ninth Avenue South, Birmingham, Alabama 35205
1	Dr. Robert A. Harmon, Program Development Consultant, 25 Schalren Drive, Latham, New York 12110
1	Dr. John A. Coppola, Project Manager, Research & Development Division The Carborundum Company, Niagara Falls, New York 14302

ARMY MATERIALS AND MECHANICS RESEARCH CENTER
WATERTOWN, MASSACHUSETTS 02172

TECHNICAL REPORT DISTRIBUTION

No. of Copies	To
1	Dr. O. Conrad Trulson, Union Carbide Corporation, Carbide Products Division, 270 Park Avenue, New York, New York 10017
1	Prof. Earl R. Parker, University of California, Department of Materials Science and Engineering, 286 Hearst Mining Building, Berkeley, California 94720
1	Mr. Willard H. Sutton Manager, Ceramics Projects, Special Metals Corporation, New Hartford, New York 13413
1	Dr. Maurice J. Sinnott, Department of Chemical & Metallurgical Engineering, The University of Michigan, Ann Arbor, MI 48104
1	Mrs. R. J. Benacquista, R.I.A.S., 9616 Labrador Lane, Cockeysville, MD 21030
1	Prof. M. C. Shaw, Head, Department of Mechanical Engineering, Cornegie-Mellon University, Pittsburgh, Pennsylvania 15213
1	Mr. Gail Eichelman, Manufacturing Processes Div., Air Force Mateials Laboratory, Wright-Patterson AFB, Ohio 45433
1	Dr. William A. Edminston, Jet Propulsion Laboratory - Bldg. 157, California Institute of Technology, 4800 Oak Grove Drive, Pasadena, California 91103
1	Massachusetts Institute of Technology, Cambridge, Massachusetts, 02139, ATTN: Prof. D. W. Kingery, Rm. 13-4090
1	Prof. Michael F. Ashby, Gordon McKay Professor of Metallurgy, Pierce Hall, Harvard University, Cambridge, Massachusetts 02138
1	Prof. I. B. Cutler, University of Utah, College of Engineering Division of Materials Science and Engineering, Salt Lake City, Utah 84112
1	Mr. J. A. Alexander, Manager, Materials Research Department, TRW 23555 Euclid Avenue, Cleveland, Ohio 44117
1	Airesearch Manufacturing Company, Sky Harbor Airport, 402 South 36th Street, Phoenix, Arizona 85034, Attn: Supervisor, Propulsion Engine Advanced Technology Dept., 93-12M
1	Mr. M. Blake, Norton Company, One New Bond Street, Worcester, Mass. 01606

ARMY MATERIALS AND MECHANICS RESEARCH CENTER
WATERTOWN, MASSACHUSETTS 02172

TECHNICAL REPORT DISTRIBUTION

No. of Copies	To
1	Dr. H. P. Kirchner, Ceramic Finishing Company, P.O. Box 498, State College, Pennsylvania 16801
1	Dr. Morris Berg, General Motors Corporation, AC Spark Plug Division Flint, Michigan 48556
1	Dr. Michael J. Noone, General Electric Company, Space Sciences Laboratory, Box 8555, Philadelphia, Pennsylvania 19101
1	Dr. Richard Kliener, GTE Sylvania, Tonawanda, Pennsylvania 18848
1	Mr. F. E. Krainess, Rockwell International Corporation, D/391-204 AB70 12214 Lakewood Boulevard, Downey, California 90241
1	Mr. David Cormier, Nuclear Planning Division, Stone & Webster Engineering Corporation, 87 Nash Memorial Road, Abington, Ma. 02351
1	Mr. V. A. Chase, Chief of Development Laboratory, Whittaker Corporation, Research and Development Division, 3540 Aero Court, San Diego, Cal. 92123
1	Dr. Stanley Waugh, Research Division, Raytheon Corporation, Research Division, 28 Seyon Street, Waltham, Massachusetts 02154
1	Coors Porcelain Company, Research Department, 17750 West 32nd Avenue, Golden, Colorado 80401
1	Professor Robert F. Davis, North Carolina State University, Department of Materials Science, Box 5427, Raleigh, North Carolina 27607
1	Dr. H. von E. Doering, Manager, Fuels/Corrosion Unit, General Electric Company, Gas Turbine Products Division, Building 53-311, Schenectedy, New York 12345
1	Dr. R. Ruh, AFML/LLS, Air Force Materials Laboratory, Wright-Patterson AFB, Ohio 45433
1	Mr. Michael E. Naylor, General Motors Technical Division, Passenger Car Turbine Division, Warren, Michigan 48090
1	Dr. John V. Milewski, ESSO Research and Engineering Company, Government Research Laboratory, P.O. Box 8, Linden, New Jersey 07036
1	Mr. M. J. Klein, Research Staff Specialist, Mail Zone R-1, Solar, 2200 Pacific Highway, P.O. Box 80966, San Diego, California 92138

ARMY MATERIALS AND MECHANICS RESEARCH CENTER
WATERTOWN, MASSACHUSETTS 02172

TECHNICAL REPORT DISTRIBUTION

No. of Copies	To
1	Dr. Frank Galasso, United Aircraft Research Laboratories, East Hartford Conn. 06108
8	Lt. Col. James Kennedy, Chief, Materials Branch, European Research Office U. S. Army R&D Group, (EUR), Box 15, FPO New York 09510
1	Dr. Joseph Griffo, U. S. Atomic Energy Commission Space Nuclear Systems Division, Century XXI Building, Mail Station F-309, Washington, D.C. 20545
1	Mr. Joseph Simpson, Rohr Industries, Inc., Technical Library P.O. Box 1516, Chula Vista, California 92012
1	Mr. Philip J. Willson, Chemical Research, Chrysler Corporation, Box 1118, CIMS 418-19-18, Detroit, Michigan 48231
1	Mr. William Combs, Battelle Memorial Institute, 2030 M Street N.W. Washington, D.C. 20036
1	Mr. M. A. Schwartz, U.S. Department of the Interior, Bureau of Mines Tuscaloosa Metallurgy Research Laboratory, P.O. Box 1, University, Alabama 35486
1	Turbo Power and Marine Systems, Inc., ATTN: Mr. Carl Merz, Farmington, Connecticut 06032
1	Mr. R. N. Singh, Argonne National Laboratory, Materials Science Division 9700 South Cass Avenue, Argonne, Illinois 60439
1	Mr. Richard E. Engdahl, Deposits & Composites, Inc., 1821 Michael Faraday Drive, Reston, Virginia 22090
1	Mr. Leonard Topper, Office of Energy Policy, National Science Foundation 1800 G Street N. W., Washington, D.C. 20550
1	Mr. Ron Lowrey, U.S. Bureau of Mines, P.O. Box 70, Albany, Oregon 97321
1	Materials Science Corporation, Technical Library, Blue Bell Office Campus, Merion Towle Building, Blue Bell, Pennsylvania 19422
1	Ms. Sharon Wright, Creare Inc., Technical Library, Hanover, New Hampshire 03755

ARMY MATERIALS AND MECHANICS RESEARCH CENTER
WATERTOWN, MASSACHUSETTS 02172

TECHNICAL REPORT DISTRIBUTION

No. of Copies	To
1	Dr. H. P. Kirchner, Ceramic Finishing Company, P.O. Box 498, State College, Pennsylvania 16801
1	Dr. Morris Berg, General Motors Corporation, AC Spark Plug Division Flint, Michigan 48556
1	Dr. Michael J. Noone, General Electric Company, Space Sciences Laboratory, Box 8555, Philadelphia, Pennsylvania 19101
1	Dr. Richard Kliener, GTE Sylvania, Tonawanda, Pennsylvania 18848
1	Mr. F. E. Krainess, Rockwell International Corporation, D/391-204 AB70 12214 Lakewood Boulevard, Downey, California 90241
1	Mr. David Cormier, Nuclear Planning Division, Stone & Webster Engineering Corporation, 87 Nash Memorial Road, Abington, Ma. 02351
1	Mr. V. A. Chase, Chief of Development Laboratory, Whittaker Corporation, Research and Development Division, 3540 Aero Court, San Diego, Cal. 92123
1	Dr. Stanley Waugh, Research Division, Raytheon Corporation, Research Division, 28 Seyon Street, Waltham, Massachusetts 02154
1	Coors Porcelain Company, Research Department, 17750 West 32nd Avenue, Golden, Colorado 80401
1	Professor Robert F. Davis, North Carolina State University, Department of Materials Science, Box 5427, Raleigh, North Carolina 27607
1	Dr. H. von E. Doering, Manager, Fuels/Corrosion Unit, General Electric Company, Gas Turbine Products Division, Building 53-311, Schenectedy, New York 12345
1	Dr. R. Ruh, AFML/LLS, Air Force Materials Laboratory, Wright-Patterson AFB, Ohio 45433
1	Mr. Michael E. Naylor, General Motors Technical Division, Passenger Car Turbine Division, Warren, Michigan 48090
1	Dr. John V. Milewski, ESSO Research and Engineering Company, Government Research Laboratory, P.O. Box 8, Linden, New Jersey 07036
1	Mr. M. J. Klein, Research Staff Specialist, Mail Zone R-1, Solar, 2200 Pacific Highway, P.O. Box 80966, San Diego, California 92138

ARMY MATERIALS AND MECHANICS RESEARCH CENTER
WATERTOWN, MASSACHUSETTS 02172

TECHNICAL REPORT DISTRIBUTION

No. of Copies	To
1	Mr. John Polyansky, Gas Turbine Design Engineering, Turbodyne Corporation, 626 Lincoln Avenue S E, St. Cloud, Minnesota 56301
1	Mr. Donald J. Legacy, Turbodyne Corporation, Wellsville, New York 14895
1	Mr. P. R. Miller, NASA Headquarters, Code RPD, 600 Independence Avenue S. W., Washington, D.C. 20546
1	Dr. Charles Berg, Chief Engineer, Federal Power Commission, Room 2100 825 North Capital Street, N.E., Washington, D.C. 20426
1	Mr. Michael Lauriente, Department of Transportation, 400 Seventh Street, S. W., Washington, D.C. 20590
1	Dr. Donald Vieth, National Bureau of Standards, Administration Bldg., Room A1002, Washington, D.C. 20234
1	Dr. Leonard Topper, National Science Foundation, Office of Energy R & D Policy, Room 537, 1800 G Street NW, Washington, D.C. 20550
2	Electric Power Research Institute, P.O. Box 10412, Palo Alto, California 94304 ATTN: Dr. Richard E. Balzhiser, Dr. Arthur Cohn
1	W. C. Christensen, Assistant for Resources, Directorate for Energy, OASD (I&L), Room 2B341 Pentagon, Washington, D.C. 20301
1	Mr. Tyler Port, Special Assistant, OASA (I&L), Room 3E620 Pentagon, Washington, D.C. 20301
1	Major Jose Baca, Hdqtrs., Air Force Systems Comman/DLFP, Propulsion and Power Branch, Andrews Air Force Base, Washington, D.C. 20034
1	Mrs. Patricia Mooney, Office of Management and Budget, Energy R&D Coordination Branch, Room 8001, New Executive Office Bldg., Washington, D.C. 20503
1	Dr. John S. Collman, Head, Power Systems Department, General Motors Corporation, Research Laboratories, Warren, Michigan 48090
1	Mr. Thomas Gross, Staff Member, Office of Energy Conservation, Federal Energy Office, Room 4234, Columbia Plaza Bldg., Washington, D.C. 20461

ARMY MATERIALS AND MECHANICS RESEARCH CENTER
WATERTOWN, MASSACHUSETTS 02172

TECHNICAL REPORT DISTRIBUTION

No. of Copies	To
1	Dr. John S. Foster, Jr., Vice President for Energy Research and Development, TRW Incorporated, One Space Park, Redondo Beach, California 90278
1	Dr. Raymond Bisplinghoff, Deputy Administrator, National Science Foundation, 1800 G. Street, N.W., Washington, D.C. 20550
1	Dr. Alan Womack, Assistant Director, Gas Cooled Reactors, Atomic Energy Commission, Washington, D.C. 20545
1	Dr. Donald Weidhuner, Chief, Power Division, Research Development & Engineering Directorate, Army Materials Command Headquarters, 5001 Eisenhower Avenue, Alexandria, Virginia 22304
1	Dr. A. Lovelace, Deputy Assistant Secretary (R&D), Office of Assistant Secretary of the Air Force (Research & Development), Room 4E973, Pentagon, Washington, D.C. 20330
1	Dr. Neal Richardson, TRW Incorporated, One Space Park, Redondo Beach, California 90278
1	Mr. Roy Peterson, Chief, Pollution Abatement & Gas Turbine Research, Ship Research & Technology Division, Naval Ship Systems Command Hqtrs., 2531 Jefferson Davis Highway, Arlington, Virginia 20362
1	Dr. Eugene C. Gritton, The Rand Corporation, Physical Sciences Department, 1700 Main Street, Santa Monica, California 90406
1	Mr. C. A. Vassilakis, Turbo Power & Marine Systems, New Britain Ave., Farmington, Conn. 06032
1	Mr. P. E. McConnell, Owens-Corning Fiberglas Corporation, Technical Center, Granville, Ohio 43023
1	Turbodyne Corporation, 711 Anderson Avenue North, St. Cloud, Minnesota 56301, ATTN: Diane Konsor
1	Mr. N. B. Elsner, General Atomics Corporation, Box 81608, San Diego, California 92037
1	Mr. Eldor R. Herrmann, Ceramic Systems, Inc., 11402 Schaefer Highway, Detroit, Michigan 48227
1	Dr. William H. Rhodes, GTE Laboratories, Waltham Research Center, 40 Sylvan Road, Waltham, Massachusetts 02154

ARMY MATERIALS AND MECHANICS RESEARCH CENTER
WATERTOWN, MASSACHUSETTS 02172

TECHNICAL REPORT DISTRIBUTION

No. of Copies	To
1	Mr. William Oldfield, Materials Research and Computer Simulation, 634 Berkeley Place, Westerville, Ohio 43081
1	Dr. Wilfred H. Dukes, Assistant Director Engineering for Development Bell Aerospace, P.O. Box 29307, New Orleans, Louisiana 70189
1	Dr. Keith E. McKee, Director of Research Engineering Mechanics Div., IIT Research Institute, 10 West 35th Street, Chicago, Illinois 60616
1	Dr. Donald R. Uhlmann, Associate Professor of Ceramics, Department of Metallurgy and Materials Science, Massachusetts Institute of Tech., Cambridge, Massachusetts 02139
1	Dr. John B. Wachtman, Jr., Division Chief, Inorganic Materials Div. National Bureau of Standards, Room A359, Materials Building, Washington, D.C. 20234
1	Mr. Donald G. Groves, Staff Engineer, National Materials Advisory Board, National Academy of Sciences, 2101 Constitution Ave., N.W., Washington, D.C. 20418
1	Major Roger Austin, Air Force Materials Laboratory, Wright-Patterson Air Force Base, Ohio 45433
1	Mr. James J. Gangler, Advanced Research & Technology Div., Code RRM, Room B556, National Aeronautics and Space Adminstration, Headquarters, Washington, D.C. 20546
1	Dr. W. Bunk, DFVLR - Institut fur Werkstoff-Forshung, 505 Porz-Wahn, Linder Hohe, Germany
1	Mr. Karl Koyama, General Atomic Company, Box 81608, San Diego, Ca 92138
1	Mr. M. Allen Magid, Materials Marketing Engineer, Florida R & D Center Pratt & Whitney Aircraft, P.O. Box 2691, West Palm Beach, Fla 33402
1	Mr. Nelson R. Roth, Bell Aerospace Company, P.O. Box #1, Dept. V70, Buffalo, NY 14240
1	Mr. F. G. Stroke, Asst. Mgr. Mrkt. Dev., PPG Industries, Inc., 1 Gateway Center, Pittsburgh, Pa 15222

ARMY MATERIALS AND MECHANICS RESEARCH CENTER
WATERTOWN, MASSACHUSETTS 02172

TECHNICAL REPORT DISTRIBUTION

No. of Copies	To
1	Dr. Mike Buckley, AFML - LLP, Wright Patterson AFB, Dayton, Ohio 45433
1	Dr. Don Thompson, Rockwell International Corporation, Science Center, 1049 Camino Dos Rios, Thousand Oaks, Ca 91360
1	Dr. W. Thielbaln, Code 4061, Naval Weapons Center, China Lake, Ca 93555
1	Dr. Arthur Cohn, EPRI, P.O. 10412, 3412 Hillview Avenue, Palo Alto, Ca 94304
1	Mr. A. E. Leach, Mgr., Process Development Engineering, Mail Zone C-33, Bell Aerospace Company, P.O. Box 1, Buffalo, NY 14240
1	Dr. Robert K. Thomas, FA4-4, Reactor Engineering, General Atomic Company, P.O. Box 81608, San Diego, Ca 92138
1	Mr. Arthur L. Ross, Valley Forge Space Center, General Electric Company, P.O. Box 8555, Philadelphia, Pennsylvania 19101
	Mr. Dennis W. Swain, Department 93-19 M, Airesearch Manufacturing Company, P.O. Box 5217, Pheonix, Arizona 85010
1	Mr. Wayne Everett, Wyman-Gordon Company, Research and Development, North Grafton, MA 01536
1	Mr. William A. Edmiston, Jet Propulsion Laboratory, California Institute of Technology, 4800 Oak Grove Drive, Pasadena, Ca 91103
2	Kawecki-Berylco Industries Inc., P.O. Box 1462, Reading, Pa 19603 ATTN: Mr. R. J. Longenecker, Mr. E. Laich

4 Authors

308 Total Copies Distributed

Army Materials and Mechanics Research Center
Watertown, Massachusetts 02172

AD ___________

BRITTLE MATERIALS DESIGN
HIGH TEMPERATURE GAS TURBINE

Arthur F. McLean, Robert R. Baker, Ford
Motor Company, Dearborn, Michigan 48121
Raymond J. Bratton, Donald G. Miller,
Westinghouse Electric Corporation, Pittsburgh,
Pennsylvania 15235

Technical Report AMMRC CTR 76-12, April, 1976
168 pages, 110 illus., 27 tables, 18 references.
Contract DAAG 46-71-C-0162, ARPA Order Number
1849 Ninth Interim Report, July 1, 1975 to
December 31, 1975.

Key Words

Gas Turbine Engine
Brittle Design
Ceramics
High Temperature Materials
Silicon Nitride
Silicon Carbide
Non-Destructive Tests
Mechanical Properties

ABSTRACT

The demonstration of uncooled brittle materials in structural applications at 2500°F is the objective of the "Brittle Materials Design, High Temperature Gas Turbine" program. Ford Motor Company, the contractor, will utilize a small vehicular gas turbine while Westinghouse, the subcontractor, will use a large stationary gas turbine. Both companies had in-house research programs in this area prior to this contract.

A significant achievement in the vehicular turbine project was the successful engine test, 175 hours at 1930°F, of a silicon nitride stator. Durability testing on a nose cone was extended to 256 hours, equalling the previously demonstrated durability of 255 hours on 1st and 2nd stage rotor tip shrouds. A "Refel" silicon carbide combustor previously demonstrated 171 hours durability, crack-free, including 20 hours at 2500°F. Two additional combustors of the same material were tested for 10 hours each. Eight hours of testing the stationary ceramic flowpath at 2500°F were accumulated; non-catastrophic cracks occurred in the nose cone and stator after surviving three hours crack-free. Two stator vanes survived 1000 cycles to 2500-2600°F plus 3720 cycles to 2900°F in the thermal shock rig. A poor quality partially bladed duo-density silicon nitride turbine rotor was tested for two hours with excursions to 1920°F and 33,600 rpm before failure. Two ceramic rotors with short blades were successfully proof spun to 65,000 rpm, cold, as part of a program to test ceramic rotors with phased increases in blade height. One of seven hot-pressed rotor hubs, spun to determine material strength, achieved 111,800 rpm before failure.

A concentrated effort on turbine rotor fabrication development was initiated. Improvements in the rotor fabrication processes have been made. Reduction of the MgO content increased the hot strength of the hot-pressed silicon nitride rotor hub material. Over 500 rotor blade rings were fabricated using the injection molding process and some high density rotor blade rings were also fabricated by slip-casting. The lower stressed Design 0' rotor blade ring injection molding tooling was received and checkout initiated. Improvements in the nitriding cycle and injection molding process produced 2.7 gm/cm³ test bars with a characteristic 4 point bend strength of 45.3 ksi with a Weibull slope of 6.8; this represents a considerable improvement over the 17,000 psi strength of 2.3 gm/cm³ silicon nitride developed earlier in the program. A stress rupture test on 2.7 gm/cm³ injection molded material was suspended without failure after 1159 hours at 2300-2500°F and stresses in 4 point bending of up to 35 ksi. This is a significant improvement over a previous creep test on 2.55 gm/cm³ material when failure occurred at 35 ksi at 2300°F.

The goal of the stationary turbine project is to demonstrate ceramic stator vanes operating at a maximum temperature of 2500°F for 100 cycles simulating peaking service conditions. The original goal to accomplish this in an advanced gas turbine engine was revised to complete the demonstration in a static test rig. Sixty cycles have been completed in the static test rig with the total time at temperature (2500°F) approaching three hours and three of the original eight vanes remain crack-free. Twenty-eight tapered-twisted silicon nitride airfoils and 24 end caps of the 3rd generation (advanced turbine) design were received for the 2500°F static rig test. Physical properties of the boron nitride insulators are reported. A tensile creep test of NC-132 silicon nitride was suspended without failure after 10,000 hours at 2100°F and 10,000 psi. The effect of static oxidation in the 2000-2500°F range on the high temperature strength of NC-132 was determined. Several CVD coatings were applied to NC-132 to reduce the strength degradation observed due to oxidation; preliminary results are presented. Experimental silicon nitride billets hot-pressed with yttria showed negligible weight gains at 1800 and 2500°F in an oxidizing atmosphere for periods up to 300 hours. High purity alpha silicon nitride powder of low oxygen content can now be produced at the rate of 8-9 kg/month.

Army Materials and Mechanics Research Center
Watertown, Massachusetts 02172

AD ___________

BRITTLE MATERIALS DESIGN
HIGH TEMPERATURE GAS TURBINE

Arthur F. McLean, Robert R. Baker, Ford
Motor Company, Dearborn, Michigan 48121
Raymond J. Bratton, Donald G. Miller,
Westinghouse Electric Corporation, Pittsburgh,
Pennsylvania 15235

Technical Report AMMRC CTR 76-12, April, 1976
168 pages, 110 illus., 27 tables, 18 references.
Contract DAAG 46-71-C-0162, ARPA Order Number
1849 Ninth Interim Report, July 1, 1975 to
December 31, 1975.

Key Words

Gas Turbine Engine
Brittle Design
Ceramics
High Temperature Materials
Silicon Nitride
Silicon Carbide
Non-Destructive Tests
Mechanical Properties

ABSTRACT

The demonstration of uncooled brittle materials in structural applications at 2500°F is the objective of the "Brittle Materials Design, High Temperature Gas Turbine" program. Ford Motor Company, the contractor, will utilize a small vehicular gas turbine while Westinghouse, the subcontractor, will use a large stationary gas turbine. Both companies had in-house research programs in this area prior to this contract.

A significant achievement in the vehicular turbine project was the successful engine test, 175 hours at 1930°F, of a silicon nitride stator. Durability testing on a nose cone was extended to 256 hours, equalling the previously demonstrated durability of 255 hours on 1st and 2nd stage rotor tip shrouds. A "Refel" silicon carbide combustor previously demonstrated 171 hours durability, crack-free, including 20 hours at 2500°F. Two additional combustors of the same material were tested for 10 hours each. Eight hours of testing the stationary ceramic flowpath at 2500°F were accumulated; non-catastrophic cracks occurred in the nose cone and stator after surviving three hours crack-free. Two stator vanes survived 1000 cycles to 2500-2600°F plus 3720 cycles to 2900°F in the thermal shock rig. A poor quality partially bladed duo-density silicon nitride turbine rotor was tested for two hours with excursions to 1920°F and 33,600 rpm before failure. Two ceramic rotors with short blades were successfully proof spun to 65,000 rpm, cold, as part of a program to test ceramic rotors with phased increases in blade height. One of seven hot-pressed rotor hubs, spun to determine material strength, achieved 111,800 rpm before failure.

A concentrated effort on turbine rotor fabrication development was initiated. Improvements in the rotor fabrication processes have been made. Reduction of the MgO content increased the hot strength of the hot-pressed silicon nitride rotor hub material. Over 500 rotor blade rings were fabricated using the injection molding process and some high density rotor blade rings were also fabricated by slip-casting. The lower stressed Design 0' rotor blade ring injection molding tooling was received and checkout initiated. Improvements in the nitriding cycle and injection molding process produced 2.7 gm/cm³ test bars with a characteristic 4 point bend strength of 45.3 ksi with a Weibull slope of 6.8; this represents a considerable improvement over the 17,000 psi strength of 2.3 gm/cm³ silicon nitride developed earlier in the program. A stress rupture test on 2.7 gm/cm³ injection molded material was suspended without failure after 1159 hours at 2300-2500°F and stresses in 4 point bending of up to 35 ksi. This is a significant improvement over a previous creep test on 2.55 gm/cm³ material when failure occurred at 35 ksi at 2300°F.

The goal of the stationary turbine project is to demonstrate ceramic stator vanes operating at a maximum temperature of 2500°F for 100 cycles simulating peaking service conditions. The original goal to accomplish this in an advanced gas turbine engine was revised to complete the demonstration in a static test rig. Sixty cycles have been completed in the static test rig with the total time at temperature (2500°F) approaching three hours and three of the original eight vanes remain crack-free. Twenty-eight tapered-twisted silicon nitride airfoils and 25 end caps of the 3rd generation (advanced turbine) design were received for the 2500°F static rig test. Physical properties of the boron nitride insulators are reported. A tensile creep test of NC-132 silicon nitride was suspended without failure after 10,000 hours at 2100°F and 10,000 psi. The effect of static oxidation in the 2000-2500°F range on the high temperature strength of NC-132 was determined. Several CVD coatings were applied to NC-132 to reduce the strength degradation observed due to oxidation; preliminary results are presented. Experimental silicon nitride billets hot-pressed with yttria showed negligible weight gains at 1800 and 2500°F in an oxidizing atmosphere for periods up to 300 hours. High purity alpha silicon nitride powder of low oxygen content can now be produced at the rate of 8-9 kg/month

Army Materials and Mechanics Research Center
Watertown, Massachusetts 02172

AD ___________

BRITTLE MATERIALS DESIGN
HIGH TEMPERATURE GAS TURBINE

Arthur F. McLean, Robert R. Baker, Ford
Motor Company, Dearborn, Michigan 48121
Raymond J. Bratton, Donald G. Miller,
Westinghouse Electric Corporation, Pittsburgh,
Pennsylvania 15235

Technical Report AMMRC CTR 76-12, April, 1976
168 pages, 110 illus., 27 tables, 18 references.
Contract DAAG 46-71-C-0162, ARPA Order Number
1849 Ninth Interim Report, July 1, 1975 to
December 31, 1975.

Key Words

Gas Turbine Engine
Brittle Design
Ceramics
High Temperature Materials
Silicon Nitride
Silicon Carbide
Non-Destructive Tests
Mechanical Properties

ABSTRACT

The demonstration of uncooled brittle materials in structural applications at 2500°F is the objective of the "Brittle Materials Design, High Temperature Gas Turbine" program. Ford Motor Company, the contractor, will utilize a small vehicular gas turbine while Westinghouse, the subcontractor, will use a large stationary gas turbine. Both companies had in-house research programs in this area prior to this contract.

A significant achievement in the vehicular turbine project was the successful engine test, 175 hours at 1930°F, of a silicon nitride stator. Durability testing on a nose cone was extended to 256 hours, equalling the previously demonstrated durability of 245 hours on 1st and 2nd stage rotor tip shrouds. A "Refel" silicon carbide combustor previously demonstrated 171 hours durability, crack-free, including 20 hours at 2500°F. Two additional combustors of the same material were tested for 10 hours each. Eight hours of testing the stationary ceramic flowpath at 2500°F were accumulated; non-catastrophic cracks occurred in the nose cone and stator after surviving three hours crack-free. Two stator vanes survived 1000 cycles to 2500-2600°F plus 3720 cycles to 2900°F in the thermal shock rig. A poor quality partially bladed duo-density silicon nitride turbine rotor was tested for two hours with excursions to 1920°F and 33,600 rpm before failure. Two ceramic rotors with short blades were successfully proof spun to 65,000 rpm, cold, as part of a program to test ceramic rotors with phased increases in blade height. One of seven hot-pressed rotor hubs, spun to determine material strength, achieved 111,800 rpm before failure.

A concentrated effort on turbine rotor fabrication development was initiated. Improvements in the rotor fabrication processes have been made. Reduction of the MgO content increased the hot strength of the hot-pressed silicon nitride rotor hub material. Over 500 rotor blade rings were fabricated using the injection molding process and some high density rotor blade rings were also fabricated by slip-casting. The lower stressed Design 0' rotor blade ring injection molding tooling was received and checkout initiated. Improvements in the nitriding cycle and injection molding process produced 2.7 gm/cm³ test bars with a characteristic 4 point bend strength of 45.3 ksi with a Weibull slope of 6.8; this represents a considerable improvement over the 17,000 psi strength of 2.3 gm/cm³ silicon nitride developed earlier in the program. A stress rupture test on 2.7 gm/cm³ injection molded material was suspended without failure after 1159 hours at 2300-2500°F and stresses in 4 point bending of up to 35 ksi. This is a significant improvement over a previous creep test on 2.55 gm/cm³ material when failure occurred at 35 ksi at 2300°F.

The goal of the stationary turbine project is to demonstrate ceramic stator vanes operating at a maximum temperature of 2500°F for 100 cycles simulating peaking service conditions. The original goal to accomplish this in an advanced gas turbine engine was revised to complete the demonstration in a static test rig. Sixty cycles have been completed in the static test rig with the total time at temperature (2500°F) approaching three hours and three of the original eight vanes remain crack-free. Twenty-eight tapered-twisted silicon nitride airfoils and 25 end caps of the 3rd generation (advanced turbine) design were received for the 2500°F static rig test. Physical properties of the boron nitride insulators are reported. A tensile creep test of NC-132 silicon nitride was suspended without failure after 10,000 hours at 2100°F and 10,000 psi. The effect of static oxidation in the 2000-2500°F range on the high temperature strength of NC-132 was determined. Several CVD coatings were applied to NC-132 to reduce the strength degradation observed due to oxidation; preliminary results are presented. Experimental silicon nitride billets hot-pressed with yttria showed negligible weight gains at 1800 and 2500°F in an oxidizing atmosphere for periods up to 300 hours. High purity alpha silicon nitride powder of low oxygen content can now be produced at the rate of 8-9 kg/month.

Army Materials and Mechanics Research Center
Watertown, Massachusetts 02172

AD ___________

BRITTLE MATERIALS DESIGN
HIGH TEMPERATURE GAS TURBINE

Arthur F. McLean, Robert R. Baker, Ford
Motor Company, Dearborn, Michigan 48121
Raymond J. Bratton, Donald G. Miller,
Westinghouse Electric Corporation, Pittsburgh,
Pennsylvania 15235

Technical Report AMMRC CTR 76-12, April, 1976
168 pages, 110 illus., 27 tables, 18 references
Contract DAAG 46-71-C-0162, ARPA Order Number
1849 Ninth Interim Report, July 1, 1975 to
December 31, 1975.

Key Words

Gas Turbine Engine
Brittle Design
Ceramics
High Temperature Materials
Silicon Nitride
Silicon Carbide
Non-Destructive Tests
Mechanical Properties

ABSTRACT

The demonstration of uncooled brittle materials in structural applications at 2500°F is the objective of the "Brittle Materials Design, High Temperature Gas Turbine" program. Ford Motor Company, the contractor, will utilize a small vehicular gas turbine while Westinghouse, the subcontractor, will use a large stationary gas turbine. Both companies had in-house research programs in this area prior to this contract.

A significant achievement in the vehicular turbine project was the successful engine test, 175 hours at 1930°F, of a silicon nitride stator. Durability testing on a nose cone was extended to 246 hours, equalling the previously demonstrated durability of 245 hours on 1st and 2nd stage rotor tip shrouds. A "Refel" silicon carbide combustor previously demonstrated 171 hours durability, crack-free, including 20 hours at 2500°F. Two additional combustors of the same material were tested for 10 hours each. Eight hours of testing the stationary ceramic flowpath at 2500°F were accumulated; non-catastrophic cracks occurred in the nose cone and stator after surviving three hours crack-free. Two stator vanes survived 1000 cycles to 2500-2600°F plus 3720 cycles to 2900°F in the thermal shock rig. A poor quality partially bladed duo-density silicon nitride turbine rotor was tested for two hours with excursions to 1920°F and 33,600 rpm before failure. Two ceramic rotors with short blades were successfully proof spun to 65,000 rpm, cold, as part of a program to test ceramic rotors with phased increases in blade height. One of seven hot-pressed rotor hubs, spun to determine material strength, achieved 111,800 rpm before failure.

A concentrated effort on turbine rotor fabrication development was initiated. Improvements in the rotor fabrication processes have been made. Reduction of the MgO content increased the hot strength of the hot-pressed silicon nitride rotor hub material. Over 500 rotor blade rings were fabricated using the injection molding process and some high density rotor blade rings were also fabricated by slip-casting. The lower stressed Design 0' rotor blade ring injection molding tooling was received and checkout initiated. Improvements in the nitriding cycle and injection molding process produced 2.7 gm/cm³ test bars with a characteristic 4 point bend strength of 45.3 ksi with a Weibull slope of 6.8; this represents a considerable improvement over the 17,000 psi strength of 2.3 gm/cm³ silicon nitride developed earlier in the program. A stress rupture test on 2.7 gm/cm³ injection molded material was suspended without failure after 1159 hours at 2300-2500°F and stresses in 4 point bending of up to 35 ksi. This is a significant improvement over a previous creep test on 2.55 gm/cm³ material when failure occurred at 35 ksi at 2300°F.

The goal of the stationary turbine project is to demonstrate ceramic stator vanes operating at a maximum temperature of 2500°F for 100 cycles simulating peaking service conditions. The original goal to accomplish this in an advanced gas turbine engine was revised to complete the demonstration in a static test rig. Sixty cycles have been completed in the static test rig with the total time at temperature (2500°F) approaching three hours and three of the original eight vanes remain crack-free. Twenty-eight tapered-twisted silicon nitride airfoils and 24 end caps of the 3rd generation (advanced turbine) design were received for the 2500°F static rig test. Physical properties of the boron nitride insulators are reported. A tensile creep test of NC-132 silicon nitride was suspended without failure after 10,000 hours at 2100°F and 10,000 psi. The effect of static oxidation in the 2000-2500°F range on the high temperature strength of NC-132 was determined. Several CVD coatings were applied to NC-132 to reduce the strength degradation observed due to oxidation; preliminary results are presented. Experimental silicon nitride billets hot-pressed with yttria showed negligible weight gains at 1800 and 2500°F in an oxidizing atmosphere for periods up to 300 hours. High purity alpha silicon nitride powder of low oxygen content can now be produced at the rate of 8-9 kg/month

Army Materials and Mechanics Research Center
Watertown, Massachusetts 02172

AD ____________

BRITTLE MATERIALS DESIGN
HIGH TEMPERATURE GAS TURBINE

Arthur F. McLean, Robert R. Baker, Ford
Motor Company, Dearborn, Michigan 48121
Raymond J. Bratton, Donald G. Miller,
Westinghouse Electric Corporation, Pittsburgh,
Pennsylvania 15235

Technical Report AMMRC CTR 76-12, April, 1976
168 pages, 110 illus., 27 tables, 18 references.
Contract DAAG 46-71-C-0162, ARPA Order Number
1849 Ninth Interim Report, July 1, 1975 to
December 31, 1975.

Key Words

Gas Turbine Engine
Brittle Design
Ceramics
High Temperature Materials
Silicon Nitride
Silicon Carbide
Non-Destructive Tests
Mechanical Properties

ABSTRACT

The demonstration of uncooled brittle materials in structural applications at 2500°F is the objective of the "Brittle Materials Design, High Temperature Gas Turbine" program. Ford Motor Company, the contractor, will utilize a small vehicular gas turbine while Westinghouse, the subcontractor, will use a large stationary gas turbine. Both companies had in-house research programs in this area prior to this contract.

A significant achievement in the vehicular turbine project was the successful engine test, 175 hours at 1930°F, of a silicon nitride stator. Durability testing on a nose cone was extended to 246 hours, equalling the previously demonstrated durability of 245 hours on 1st and 2nd stage rotor tip shrouds. A "Refel" silicon carbide combustor previously demonstrated 171 hours durability, crack-free, including 20 hours at 2500°F. Two additional combustors of the same material were tested for 10 hours each. Eight hours of testing the stationary ceramic flowpath at 2500°F were accumulated, non-catastrophic cracks occurred in the nose cone and stator after surviving three hours crack-free. Two stator vanes survived 1000 cycles to 2500-2600°F plus 3720 cycles to 2900°F in the thermal shock rig. A poor quality partially bladed duo-density silicon nitride turbine rotor was tested for two hours with excursions to 1920°F and 33,600 rpm before failure. Two ceramic rotors with short blades were successfully proof spun to 64,000 rpm, cold, as part of a program to test ceramic rotors with phased increases in blade height. One of seven hot-pressed rotor hubs, spun to determine material strength, achieved 111,800 rpm before failure.

A concentrated effort on turbine rotor fabrication development was initiated. Improvements in the rotor fabrication processes have been made. Reduction of the MgO content increased the hot strength of the hot-pressed silicon nitride rotor hub material. Over 500 rotor blade rings were fabricated using the injection molding process and some high density rotor blade rings were also fabricated by slip-casting. The lower stressed Design D' rotor blade ring injection molding tooling was received and checkout initiated. Improvements in the nitriding cycle and injection molding process produced 2.7 gm/cm^3 test bars with a characteristic 4 point bend strength of 44.3 ksi with a Weibull slope of 6.8, this represents a considerable improvement over the 17,000 psi strength of 2.3 gm/cm^3 silicon nitride developed earlier in the program. A stress rupture test on 2.7 gm/cm^3 injection molded material was suspended without failure after 1159 hours at 2300-2400°F and stresses in 4 point bending of up to 35 ksi. This is a significant improvement over a previous creep test on 2.55 gm/cm^3 material when failure occurred at 35 ksi at 2300°F.

The goal of the stationary turbine project is to demonstrate ceramic stator vanes operating at a maximum temperature of 2500°F for 100 cycles simulating peaking service conditions. The original goal to accomplish this in an advanced gas turbine engine was revised to complete the demonstration in a static test rig. Sixty cycles have been completed in the static test rig with the total time at temperature (2500°F) approaching three hours and three of the original eight vanes remain crack-free. Twenty-eight tapered-twisted silicon nitride airfoils and 24 end caps of the 3rd generation (advanced turbine) design were received for the 2500°F static rig test. Physical properties of the boron nitride insulators are reported. A tensile creep test of NC-132 silicon nitride was suspended without failure after 10,000 hours at 2100°F and 10,000 psi. The effect of static oxidation in the 2000-2500°F range on the high temperature strength of NC-132 was determined. Several CVD coatings were applied to NC-132 to reduce the strength degradation observed due to oxidation; preliminary results are presented. Experimental silicon nitride billets hot-pressed with yttria showed negligible weight gains at 1800 and 2500°F in an oxidizing atmosphere for periods up to 300 hours. High purity alpha silicon nitride powder of low oxygen content can now be produced at the rate of 8-9 kg/month.

Army Materials and Mechanics Research Center
Watertown, Massachusetts 02172

AD ____________

BRITTLE MATERIALS DESIGN
HIGH TEMPERATURE GAS TURBINE

Arthur F. McLean, Robert R. Baker, Ford
Motor Company, Dearborn, Michigan 48121
Raymond J. Bratton, Donald G. Miller,
Westinghouse Electric Corporation, Pittsburgh,
Pennsylvania 15235

Technical Report AMMRC CTR 76-12, April, 1976
168 pages, 110 illus., 27 tables, 18 references
Contract DAAG 46-71-C-0162, ARPA Order Number
1849 Ninth Interim Report, July 1, 1975 to
December 31, 1975.

Key Words

Gas Turbine Engine
Brittle Design
Ceramics
High Temperature Materials
Silicon Nitride
Silicon Carbide
Non-Destructive Tests
Mechanical Properties

ABSTRACT

The demonstration of uncooled brittle materials in structural applications at 2500°F is the objective of the "Brittle Materials Design, High Temperature Gas Turbine" program. Ford Motor Company, the contractor, will utilize a small vehicular gas turbine while Westinghouse, the subcontractor, will use a large stationary gas turbine. Both companies had in-house research programs in this area prior to this contract.

A significant achievement in the vehicular turbine project was the successful engine test, 175 hours at 1930°F, of a silicon nitride stator. Durability testing on a nose cone was extended to 246 hours, equalling the previously demonstrated durability of 245 hours on 1st and 2nd stage rotor tip shrouds. A "Refel" silicon carbide combustor previously demonstrated 171 hours durability, crack-free, including 20 hours at 2500°F. Two additional combustors of the same material were tested for 10 hours each. Eight hours of testing the stationary ceramic flowpath at 2500°F were accumulated, non-catastrophic cracks occurred in the nose cone and stator after surviving three hours crack-free. Two stator vanes survived 1000 cycles to 2500-2600°F plus 3720 cycles to 2900°F in the thermal shock rig. A poor quality partially bladed duo-density silicon nitride turbine rotor was tested for two hours with excursions to 1920°F and 33,600 rpm before failure. Two ceramic rotors with short blades were successfully proof spun to 64,000 rpm, cold, as part of a program to test ceramic rotors with phased increases in blade height. One of seven hot pressed rotor hubs, spun to determine material strength, achieved 111,800 rpm before failure.

A concentrated effort on turbine rotor fabrication development was initiated. Improvements in the rotor fabrication processes have been made. Reduction of the MgO content increased the hot strength of the hot-pressed silicon nitride rotor hub material. Over 500 rotor blade rings were fabricated using the injection molding process and some high density rotor blade rings were also fabricated by slip-casting. The lower stressed Design D' rotor blade ring injection molding tooling was received and checkout initiated. Improvements in the nitriding cycle and injection molding process produced 2.7 gm/cm^3 test bars with a characteristic 4 point bend strength of 44.3 ksi with a Weibull slope of 6.8, this represents a considerable improvement over the 17,000 psi strength of 2.3 gm/cm^3 silicon nitride developed earlier in the program. A stress rupture test on 2.7 gm/cm^3 injection molded material was suspended without failure after 1159 hours at 2300-2400°F and stresses in 4 point bending of up to 35 ksi. This is a significant improvement over a previous creep test on 2.55 gm/cm^3 material when failure occurred at 35 ksi at 2300°F.

The goal of the stationary turbine project is to demonstrate ceramic stator vanes operating at a maximum temperature of 2500°F for 100 cycles simulating peaking service conditions. The original goal to accomplish this in an advanced gas turbine engine was revised to complete the demonstration in a static test rig. Sixty cycles have been completed in the static test rig with the total time at temperature (2500°F) approaching three hours and three of the original eight vanes remain crack-free. Twenty-eight tapered-twisted silicon nitride airfoils and 24 end caps of the 3rd generation (advanced turbine) design were received for the 2500°F static rig test. Physical properties of the boron nitride insulators are reported. A tensile creep test of NC-132 silicon nitride was suspended without failure after 10,000 hours at 2100°F and 10,000 psi. The effect of static oxidation in the 2000-2500°F range on the high temperature strength of NC-132 was determined. Several CVD coatings were applied to NC-132 to reduce the strength degradation observed due to oxidation; preliminary results are presented. Experimental silicon nitride billets hot-pressed with yttria showed negligible weight gains at 1800 and 2500°F in an oxidizing atmosphere for periods up to 300 hours. High purity alpha silicon nitride powder of low oxygen content can now be produced at the rate of 8-9 kg/month.

Army Materials and Mechanics Research Center
Watertown, Massachusetts 02172

AD ____________

BRITTLE MATERIALS DESIGN
HIGH TEMPERATURE GAS TURBINE

Arthur F. McLean, Robert R. Baker, Ford
Motor Company, Dearborn, Michigan 48121
Raymond J. Bratton, Donald G. Miller,
Westinghouse Electric Corporation, Pittsburgh,
Pennsylvania 15235

Technical Report AMMRC CTR 76-12, April, 1976
168 pages, 110 illus., 27 tables, 18 references.
Contract DAAG 46-71-C-0162, ARPA Order Number
1849 Ninth Interim Report, July 1, 1975 to
December 31, 1975.

Key Words

Gas Turbine Engine
Brittle Design
Ceramics
High Temperature Materials
Silicon Nitride
Silicon Carbide
Non-Destructive Tests
Mechanical Properties

ABSTRACT

The demonstration of uncooled brittle materials in structural applications at 2500°F is the objective of the "Brittle Materials Design, High Temperature Gas Turbine" program. Ford Motor Company, the contractor, will utilize a small vehicular gas turbine while Westinghouse, the subcontractor, will use a large stationary gas turbine. Both companies had in-house research programs in this area prior to this contract.

A significant achievement in the vehicular turbine project was the successful engine test, 175 hours at 1930°F, of a silicon nitride stator. Durability testing on a nose cone was extended to 246 hours, equalling the previously demonstrated durability of 245 hours on 1st and 2nd stage rotor tip shrouds. A "Refel" silicon carbide combustor previously demonstrated 171 hours durability, crack-free, including 20 hours at 2500°F. Two additional combustors of the same material were tested for 10 hours each. Eight hours of testing the stationary ceramic flowpath at 2500°F were accumulated; non-catastrophic cracks occurred in the nose cone and stator after surviving three hours crack-free. Two stator vanes survived 1000 cycles to 2500-2600°F plus 3720 cycles to 2900°F in the thermal shock rig. A poor quality partially bladed duo-density silicon nitride turbine rotor was tested for two hours with excursions to 1920°F and 33,600 rpm before failure. Two ceramic rotors with short blades were successfully proof spun to 64,000 rpm, cold, as part of a program to test ceramic rotors with phased increases in blade height. One of seven hot-pressed rotor hubs, spun to determine material strength, achieved 111,800 rpm before failure.

A concentrated effort on turbine rotor fabrication development was initiated. Improvements in the rotor fabrication processes have been made. Reduction of the MgO content increased the hot strength of the hot-pressed silicon nitride rotor hub material. Over 500 rotor blade rings were fabricated using the injection molding process and some high density rotor blade rings were also fabricated by slip-casting. The lower stressed Design D' rotor blade ring injection molding tooling was received and checkout initiated. Improvements in the nitriding cycle and injection molding process produced 2.7 gm/cm^3 test bars with a characteristic 4 point bend strength of 44.3 ksi with a Weibull slope of 6.8, this represents a considerable improvement over the 17,000 psi strength of 2.3 gm/cm^3 silicon nitride developed earlier in the program. A stress rupture test on 2.7 gm/cm^3 injection molded material was suspended without failure after 1159 hours at 2300-2400°F and stresses in 4 point bending of up to 35 ksi. This is a significant improvement over a previous creep test on 2.55 gm/cm^3 material when failure occurred at 35 ksi at 2300°F.

The goal of the stationary turbine project is to demonstrate ceramic stator vanes operating at a maximum temperature of 2500°F for 100 cycles simulating peaking service conditions. The original goal to accomplish this in an advanced gas turbine engine was revised to complete the demonstration in a static test rig. Sixty cycles have been completed in the static test rig with the total time at temperature (2500°F) approaching three hours and three of the original eight vanes remain crack-free. Twenty-eight tapered-twisted silicon nitride airfoils and 24 end caps of the 3rd generation (advanced turbine) design were received for the 2500°F static rig test. Physical properties of the boron nitride insulators are reported. A tensile creep test of NC-132 silicon nitride was suspended without failure after 10,000 hours at 2100°F and 10,000 psi. The effect of static oxidation in the 2000-2500°F range on the high temperature strength of NC-132 was determined. Several CVD coatings were applied to NC-132 to reduce the strength degradation observed due to oxidation; preliminary results are presented. Experimental silicon nitride billets hot-pressed with yttria showed negligible weight gains at 1800 and 2500°F in an oxidizing atmosphere for periods up to 300 hours. High purity alpha silicon nitride powder of low oxygen content can now be produced at the rate of 8-9 kg/month.

Army Materials and Mechanics Research Center
Watertown, Massachusetts 02172

AD ____________

BRITTLE MATERIALS DESIGN
HIGH TEMPERATURE GAS TURBINE

Arthur F. McLean, Robert R. Baker, Ford
Motor Company, Dearborn, Michigan 48121
Raymond J. Bratton, Donald G. Miller,
Westinghouse Electric Corporation, Pittsburgh,
Pennsylvania 15235

Technical Report AMMRC CTR 76-12, April, 1976
168 pages, 110 illus., 27 tables, 18 references.
Contract DAAG 46-71-C-0162, ARPA Order Number
1849 Ninth Interim Report, July 1, 1975 to
December 31, 1975.

Key Words

Gas Turbine Engine
Brittle Design
Ceramics
High Temperature Materials
Silicon Nitride
Silicon Carbide
Non-Destructive Tests
Mechanical Properties

ABSTRACT

The demonstration of uncooled brittle materials in structural applications at 2500°F is the objective of the "Brittle Materials Design, High Temperature Gas Turbine" program. Ford Motor Company, the contractor, will utilize a small vehicular gas turbine while Westinghouse, the subcontractor, will use a large stationary gas turbine. Both companies had in-house research programs in this area prior to this contract.

A significant achievement in the vehicular turbine project was the successful engine test, 175 hours at 1930°F, of a silicon nitride stator. Durability testing on a nose cone was extended to 246 hours, equalling the previously demonstrated durability of 245 hours on 1st and 2nd stage rotor tip shrouds. A "Refel" silicon carbide combustor previously demonstrated 171 hours durability, crack-free, including 20 hours at 2500°F. Two additional combustors of the same material were tested for 10 hours each. Eight hours of testing the stationary ceramic flowpath at 2500°F were accumulated; non-catastrophic cracks occurred in the nose cone and stator after surviving three hours crack-free. Two stator vanes survived 1000 cycles to 2500-2600°F plus 3720 cycles to 2900°F in the thermal shock rig. A poor quality partially bladed duo-density silicon nitride turbine rotor was tested for two hours with excursions to 1920°F and 33,600 rpm before failure. Two ceramic rotors with short blades were successfully proof spun to 64,000 rpm, cold, as part of a program to test ceramic rotors with phased increases in blade height. One of seven hot-pressed rotor hubs, spun to determine material strength, achieved 111,800 rpm before failure.

A concentrated effort on turbine rotor fabrication development was initiated. Improvements in the rotor fabrication processes have been made. Reduction of the MgO content increased the hot strength of the hot-pressed silicon nitride rotor hub material. Over 500 rotor blade rings were fabricated using the injection molding process and some high density rotor blade rings were also fabricated by slip-casting. The lower stressed Design D' rotor blade ring injection molding tooling was received and checkout initiated. Improvements in the nitriding cycle and injection molding process produced 2.7 gm/cm^3 test bars with a characteristic 4 point bend strength of 44.3 ksi with a Weibull slope of 6.8, this represents a considerable improvement over the 17,000 psi strength of 2.3 gm/cm^3 silicon nitride developed earlier in the program. A stress rupture test on 2.7 gm/cm^3 injection molded material was suspended without failure after 1159 hours at 2300-2400°F and stresses in 4 point bending of up to 35 ksi. This is a significant improvement over a previous creep test on 2.55 gm/cm^3 material when failure occurred at 35 ksi at 2300°F.

The goal of the stationary turbine project is to demonstrate ceramic stator vanes operating at a maximum temperature of 2500°F for 100 cycles simulating peaking service conditions. The original goal to accomplish this in an advanced gas turbine engine was revised to complete the demonstration in a static test rig. Sixty cycles have been completed in the static test rig with the total time at temperature (2500°F) approaching three hours and three of the original eight vanes remain crack-free. Twenty-eight tapered-twisted silicon nitride airfoils and 24 end caps of the 3rd generation (advanced turbine) design were received for the 2500°F static rig test. Physical properties of the boron nitride insulators are reported. A tensile creep test of NC-132 silicon nitride was suspended without failure after 10,000 hours at 2100°F and 10,000 psi. The effect of static oxidation in the 2000-2500°F range on the high temperature strength of NC-132 was determined. Several CVD coatings were applied to NC-132 to reduce the strength degradation observed due to oxidation; preliminary results are presented. Experimental silicon nitride billets hot-pressed with yttria showed negligible weight gains at 1800 and 2500°F in an oxidizing atmosphere for periods up to 300 hours. High purity alpha silicon nitride powder of low oxygen content can now be produced at the rate of 8-9 kg/month.

UNCLASSIFIED
SECURITY CLASSIFICATION OF THIS PAGE (When Data Entered)

REPORT DOCUMENTATION PAGE

READ INSTRUCTIONS
BEFORE COMPLETING FORM

1. REPORT NUMBER
AMMRC CTR 76-12

2. GOVT ACCESSION NO.

3. RECIPIENT'S CATALOG NUMBER

4. TITLE (and Subtitle)
Brittle Materials Design, High Temperature Gas Turbine

5. TYPE OF REPORT & PERIOD COVERED
Interim Report Number 9
7/1/75 to 12/31/75

6. PERFORMING ORG. REPORT NUMBER

7. AUTHOR(s)
A. F. McLean, Ford Motor Company
R. R. Baker, Ford Motor Company
R. J. Bratton, Westinghouse Elec. Corp.
D. G. Miller, Westinghouse Elec. Corp.

8. CONTRACT OR GRANT NUMBER(s)
DAAG 46-71-C-0162

9. PERFORMING ORGANIZATION NAME AND ADDRESS
Ford Motor Company, Dearborn, Mi 48121

10. PROGRAM ELEMENT, PROJECT, TASK AREA & WORK UNIT NUMBERS
D/A Project: ARPA Order 1849
AMCMS Code:
Agency Accession: DA OD 4733

11. CONTROLLING OFFICE NAME AND ADDRESS
Army Materials and Mechanics Research Center
Watertown, Massachusetts 02172

12. REPORT DATE
April, 1976

13. NUMBER OF PAGES
168

14. MONITORING AGENCY NAME & ADDRESS (if different from Controlling Office)

15. SECURITY CLASS. (of this report)
Unclassified

15a. DECLASSIFICATION/DOWNGRADING SCHEDULE

16. DISTRIBUTION STATEMENT (of this Report)
Distribution limited to U.S. Government agencies only: Test and Evaluation data; April, 1976. Other requests for this document must be referred to the Director, Army, Materials and Mechanics Research Center, ATTN: AMXMR-PL, Watertown, Massachusetts 02172

17. DISTRIBUTION STATEMENT (of the abstract entered in Block 20, if different from Report)

18. SUPPLEMENTARY NOTES

19. KEY WORDS (Continue on reverse side if necessary and identify by block number)
Gas Turbine Engine
Brittle Design
Ceramics
High Temperature Materials
Silicon Nitride
Silicon Carbide
Non-Destructive Test
Mechanical Properties

20. ABSTRACT (Continue on reverse side if necessary and identify by block number)

(See reverse side)

DD FORM 1 JAN 73 1473 EDITION OF 1 NOV 65 IS OBSOLETE

UNCLASSIFIED
SECURITY CLASSIFICATION OF THIS PAGE (When Data Entered)

ABSTRACT

The demonstration of uncooled brittle materials in structural applications at 2500°F is the objective of the "Brittle Materials Design, High Temperature Gas Turbine" program. Ford Motor Company, the contractor, will utilize a small vehicular gas turbine while Westinghouse, the subcontractor, will use a large stationary gas turbine. Both companies had in-house research programs in this area prior to this contract.

A significant achievement in the vehicular turbine project was the successful engine test, 175 hours at 1930°F, of a silicon nitride stator. Durability testing on a nose cone was extended to 246 hours, equalling the previously demonstrated durability of 245 hours on 1st and 2nd stage rotor tip shrouds. A "Refel" silicon carbide combustor previously demonstrated 171 hours durability, crack-free, including 20 hours at 2500°F. Two additional combustors of the same material were tested for 10 hours each. Eight hours of testing the stationary ceramic flowpath at 2500°F were accumulated; non-catastrophic cracks occurred in the nosecone and stator after surviving three hours crack-free. Two stator vanes survived 1000 cycles to 2500-2600°F plus 3720 cycles to 2900°F in the thermal shock rig. A poor quality partially bladed duo-density silicon nitride turbine rotor was tested for two hours with excursions to 1920°F and 33,600 rpm before failure. Two ceramic rotors with short blades were successfully proof spun to 64,000 rpm, cold, as part of a program to test ceramic rotors with phased increases in blade height. One of seven hot pressed rotor hubs, spun to determine material strength, achieved 111,800 rpm before failure.

A concentrated effort on turbine rotor fabrication development was initiated. Improvements in the rotor fabrication processes have been made. Reduction of the MgO content increased the hot strength of the hot-pressed silicon nitride rotor hub material. Over 500 rotor blade rings were fabricated using the injection molding process and some high density rotor blade rings were also fabricated by slip-casting. The lower stressed Design D' rotor blade ring injection molding tooling was received and checkout initiated. Improvements in the nitriding cycle and injection molding process produced 2.7 gm/cm^3 test bars with a characteristic 4 point bend strength of 44.3 ksi with a Weibull slope of 6.8; this represents a considerable improvement over the 17,000 psi strength of 2.3 gm/cm^3 silicon nitride developed earlier in the program. A stress rupture test on 2.7 gm/cm^3 injection molded material was suspended without failure after 1159 hours at 2300-2400°F and stresses in 4 point bending of up to 35 ksi. This is a significant improvement over a previous creep test on 2.55 gm/cm^3 material when failure occurred at 35 ksi at 2300°F.

The goal of the stationary turbine project is to demonstrate ceramic stator vanes operating at a maximum temperature of 2500°F for 100 cycles simulating peaking service conditions. The original goal to accomplish this in an advanced gas turbine engine was revised to complete the demonstration in a static test rig. Sixty cycles have been completed in the static test rig with the total time at temperature (2500°F) approaching three hours and three of the original eight vanes remain crack-free. Twenty-eight tapered-twisted silicon nitride airfoils and 24 end caps of the 3rd generation (advanced turbine) design were received for the 2500°F static rig test. Physical properties of the boron nitride insulators are reported. A tensile creep test of NC-132 silicon nitride was suspended without failure after 10,000 hours at 2100°F and 10,000 psi. The effect of static oxidation in the 2000-2500°F range on the high temperature strength of NC-132 was determined. Several CVD coatings were applied to NC-132 to reduce the strength degradation observed due to oxidation; preliminary results are presented. Experimental silicon nitride billets hot-pressed with yttria showed negligible weight gains at 1800 and 2500°F in an oxidizing atmosphere for periods up to 300 hours. High purity alpha silicon nitride powder of low oxygen content can now be produced at the rate of 8-9 kg/month.